

Integrating wind turbines with highway infrastructures

Chrysochoidis-Antsos, N.

DOI

[10.4233/uuid:2d790875-d244-4d55-9e4e-1b20de52fefb](https://doi.org/10.4233/uuid:2d790875-d244-4d55-9e4e-1b20de52fefb)

Publication date

2024

Document Version

Final published version

Citation (APA)

Chrysochoidis-Antsos, N. (2024). *Integrating wind turbines with highway infrastructures*. [Dissertation (TU Delft), Delft University of Technology]. <https://doi.org/10.4233/uuid:2d790875-d244-4d55-9e4e-1b20de52fefb>

Important note

To cite this publication, please use the final published version (if applicable). Please check the document version above.

Copyright

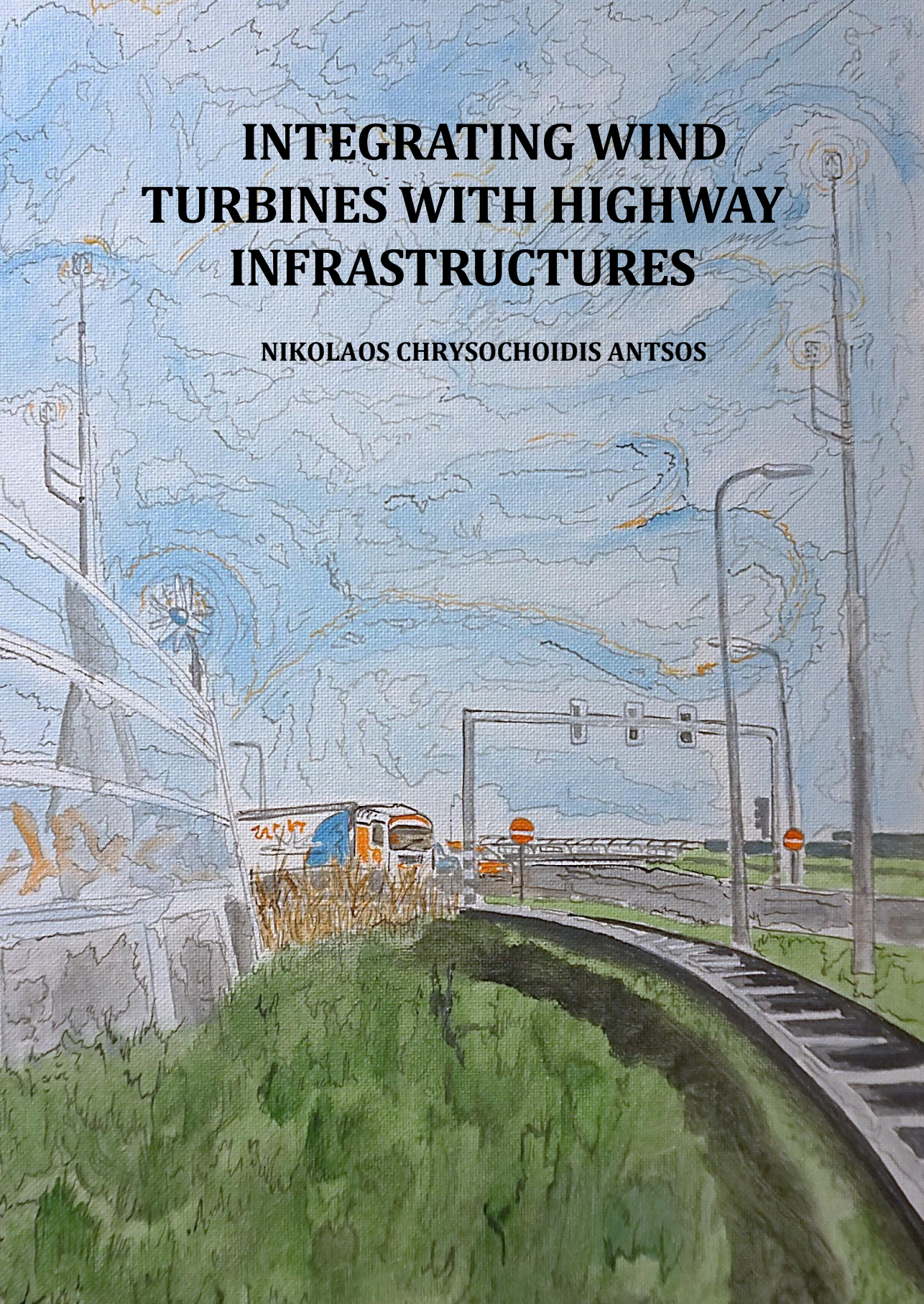
Other than for strictly personal use, it is not permitted to download, forward or distribute the text or part of it, without the consent of the author(s) and/or copyright holder(s), unless the work is under an open content license such as Creative Commons.

Takedown policy

Please contact us and provide details if you believe this document breaches copyrights. We will remove access to the work immediately and investigate your claim.

INTEGRATING WIND TURBINES WITH HIGHWAY INFRASTRUCTURES

NIKOLAOS CHRYSOCHOIDIS ANTOS



Integrating wind turbines with highway infrastructures

DISSERTATION

for the purpose of obtaining the degree of doctor
at Delft University of Technology
by the authority of the Rector Magnificus, Prof. dr. ir. T.H.J.J. van der Hagen
chair of the Board for Doctorates
to be defended publicly on
Monday 23 September 2024 at 12.30 o'clock

by

Nikolaos CHRYSOCHOIDIS ANTSOS

Master of Science in Sustainable Energy Technology,
Technical University of Delft, The Netherlands
born in Thessaloniki, Greece.

This dissertation has been approved by the promotor.

Composition of the doctoral committee:

Rector Magnificus, chairperson

Em. prof. dr. A.J.M. van Wijk, Delft University of Technology, promotor

Em. prof. dr. ir. G.J.W. van Bussel, Delft University of Technology, promotor

Independent members:

Prof. dr. K. Blok, Delft University of Technology

Prof. dr. ir. Z. Lukszo, Delft University of Technology

Prof. ing. D. Micallef, University of Malta, Malta

Dr.ir. C.P.W. Geurts, TNO, The Netherlands

Prof. dr. D.A. von Terzi, Delft University of Technology

The project is financed by NOW (former STW) with a grant number 12728 under the acronym Duct4U



Cover by: Stelios Stavrou (painting) and Nikolaos Chrysochoidis Antsos (original photo)

Copyright © 2024 by Nikolaos Chrysochoidis Antsos

ISBN: 978-94-6366-910-8

An electronic copy of this dissertation is available at <http://repository.tudelft.nl/>

To my partner Eirini

CONTENTS

CONTENTS	1
SUMMARY	5
SAMENVATTING	9
ACRONYMS.....	13
Introduction	17
1.1 Research context.....	18
1.2 Scope and novelty of research	20
1.3 Aims, objectives and research questions	22
1.4 Brief description of research methods.....	23
1.5 Overview of structure	24
1.6 References.....	27
Wind resource characteristics and energy yield for micro wind turbines integrated on noise barriers – An experimental study.....	29
2.1 Introduction.....	30
2.2 Set-Up Description.....	33
2.2.1 Noise Barrier Set-Up.....	34
2.2.2 Wind Tunnel Set-Up	38
2.3 Results.....	39
2.3.1 Influence of noise barrier on mean wind speed	39
2.3.2 Influence of the noise barrier on inflow angle	42
2.3.3 Influence on Turbulent Intensity	45
2.3.4 Annual Energy Production sensitivity analysis and results	47
2.4 Discussion.....	54

2.4.1	<i>Wind resource characteristics</i>	54
2.4.2	<i>Economic analysis and energy yield</i>	55
2.2.5	Conclusions.....	57
2.5	Recommendations – Future Studies.....	59
2.6	References.....	60

Performance Characteristics of a Micro Wind Turbine Integrated on a Noise Barrier		65
3.1	Introduction.....	66
3.2	Materials and Methods	71
3.2.1	<i>Wind Tunnel Experiment</i>	71
3.2.2	<i>Field Experiment</i>	76
3.3	Results.....	78
3.3.1	<i>Flow Misalignment Losses</i>	78
3.3.2	<i>Electrical System Losses</i>	83
3.3.3	<i>Optimal Power Control Performance</i>	91
3.3.4	<i>Starting behaviour and idling fatigue</i>	95
3.4	Discussion.....	99
3.5	Conclusions	100
3.6	References.....	102

Technical potential and application of micro wind turbines integrated on noise barrier acoustic screens in the Netherlands using GIS ...		107
4.1	Introduction.....	108
4.1.1	<i>Renewable energy applications on noise barriers</i>	108
4.1.2	<i>Wind energy potential estimation at urban level with GIS</i>	109
4.1.3	<i>Novelty – Motivation – Outline</i>	111
4.2	Nationwide wind energy potential estimation for acoustic screen noise barriers in the Netherlands	112
4.2.1	<i>Suitable noise barriers for micro wind turbine applications</i>	112

4.2.2	<i>Weather station time series translation to the noise barrier site</i>	117
4.2.3	<i>Noise barrier influenced Annual Energy Production Potential</i>	124
4.2.4	<i>Uncertainties to consider for the potential estimation</i>	129
4.3	Noise barrier renewable energy utilisation in an integrated energy system	130
4.3.1	<i>Integration with PVNB and grid interconnection proximity</i>	130
4.3.2	<i>Connection to future hydrogen demand and street lighting</i>	134
4.4	Conclusions	141
4.5	References.....	143

Techno-economic evaluation of turbine-solar PV systems integrated on a noise barrier 149

5.1	Introduction.....	150
5.2	Literature Review	150
5.2.1	<i>kW scale wind turbines integrated near highways</i>	151
5.2.2	<i>Electricity pathways for a wind and solar power noise barrier</i>	154
5.2.3	<i>Techno-economic analysis of small-scale wind energy systems</i>	154
5.3	System design and input data.....	156
5.3.1	<i>Brief system design</i>	156
5.3.2	<i>Technoeconomic analysis and methodology</i>	156
5.3.3	<i>Electricity production</i>	158
5.3.4	<i>Costs</i>	160
5.3.5	<i>Summary Cost Figures</i>	168
5.4	Results of levelised cost of electricity	169
5.5	Conclusions	173
5.6	References.....	174

Technical potential of on-site wind powered hydrogen producing refueling station in the Netherlands 181

6.1	Introduction.....	182
-----	-------------------	-----

6.1.1	<i>Hydrogen roadmaps worldwide and in the Netherlands</i>	182
6.1.2	<i>Hydrogen Refuelling stations in the Netherlands</i>	183
6.1.3	<i>GIS and technical potential of hydrogen production</i>	184
6.1.4	<i>Outline</i>	186
6.2	Amount of suitable fuelling stations	186
6.2.1	<i>Methodology</i>	186
6.2.2	<i>Results</i>	193
6.3	Wind powered hydrogen production potential at suitable fuelling stations 195	
6.3.1	<i>Methodology</i>	195
6.3.2	<i>Results</i>	198
6.4	Case study to assess the possibility for Natural Gas Grid Interconnection	200
6.5	Discussion.....	202
6.6	Conclusions	203
6.7	References.....	204
Conclusions – Recommendations.....		211
7.1	Answers to the Research Questions.....	212
7.2	Recommendations for Future Research	215
LIST OF PUBLICATIONS		219
CURRICULUM VITAE.....		221
ACKNOWLEDGEMENTS		222

SUMMARY

The country of the Netherlands has set targets to increase its renewable energy generation. For onshore wind renewable capacities are required to meet the climate targets. However, achieving additional onshore wind generation is limited by issues related to land availability, zoning and grid congestion. Therefore new locations to install more wind capacity need to be found. Highway infrastructures are a place which offers possibilities to integrate onshore wind turbines at different capacities. For example, micro wind turbines could be structurally integrated with acoustic screen noise barriers which offer a solid foundation and support. While at the MW scale, wind turbines could be installed next to highway fuelling stations to provide electricity and hydrogen for the mobility sector by production locally at the station.

This Dissertation aims to investigate two concepts and their nationwide implementation in the country of the Netherlands:

1. Micro wind turbines integrated in highway structures for electricity production
2. MW wind turbines integrated at fuelling stations for hydrogen production.

The research is focussed on the main question: “What is the technical and economic potential of integrating wind turbines with highway infrastructures?”. To answer this question for both concepts the following activities were conducted. Initially, wind tunnel and field experimental campaigns are planned and executed to understand the wind resource potential and the performance for the concept of micro wind turbines on top of noise barriers along with a technical and economic analysis. It was understood that to determine the potential for the Netherlands, a nationwide analysis using GIS datasets would be needed. Therefore, GIS analyses were then conducted by using the results from the experimental campaigns and applied for all noise barriers in the Netherlands. Finally, the GIS analysis was further expanded to the second concept of MW scale wind turbines collocated with fuelling stations.

In particular, the dissertation starts with the experimental campaigns. Specifically in Chapter 2, a wind resource assessment experimental campaign is performed on top of a noise barrier, located at the intersection of N470 road and A13 motorway in South Holland, with the use of sonic anemometers. Some parameters were compared with a reference measurement next to the noise barrier. The parameters assessed are wind speed, inflow angle and turbulence intensity. It is found that wind speed is increased in perpendicular flows while decreases in parallel flows to the noise barrier. The range of difference in wind speed can be between 80 – 140 %. These parameters are included in sensitivities analysis to measure the Annual Electricity Production of noise barrier in different orientations and heights of installation. It was found that the range of total annual electricity production including the noise barrier effects on wind flow could result between 60 – 150% of a reference case without noise barrier influence on the flow.

In Chapter 3, results are presented from an experimental campaign of several micro wind turbine rotors and inverters in a wind tunnel to determine the idealised performance of those turbines in similar conditions as experienced on top of the noise barrier. Tests are further extended to a field experiment of a micro wind turbine on top of the noise barrier. It was found that the turbine is under-performing for most of time in comparison to wind tunnel conditions (42% from the reference value in wind tunnel), attributed to its inverter related losses, yaw misalignment and controller effectiveness. It is recommended to find further ways to increase and optimize efficiencies of micro wind turbines especially when integrated with structures which expose turbines to skewed flows.

In Chapter 4, the micro wind turbine integrated on noise barrier concept is assessed for nationwide implementation in the country of the Netherlands. This is done by using noise barrier GIS and wind speed datasets from weather stations in combination with mesoscale models and wind energy corrections from the aforementioned experiments. Suitable noise barrier sites were identified to amount for a total of 17MW micro wind installed capacity. Statistical analysis was performed from national to provincial level to achieve the wind energy potential at wind turbine noise barriers. An average 150m noise barrier is found representative to have installed ~9kW of micro wind electricity. It was found that overall the noise barriers can potentially increase slightly the wind energy potential due to their influence by increasing the wind speed on top of the barrier resulting in a nationwide capacity factor of 11.7%. Furthermore, it is shown that noise barriers are located near grid interconnection networks and other types of future electricity demand, which will result in low grid integration cost.

Chapter 5 dives into the economics of this integrated micro wind turbine system. It explores also the economics for a combination with a photovoltaic system integrated on the same noise barrier. Multiple configurations are assessed to understand the cost variability within the country of the Netherlands. The cost variability is shown for different noise barrier orientations, wind sites with different wind profiles, losses, corrections and sensitivities on economic parameters (capital and operational expenditures, cost of capital). The results show a very wide range of micro wind electricity levelised cost of electricity, between 0.25 – 2.5 €/kWh. When combining and integrating 9kW of micro wind turbines and 90kW of photovoltaic systems on the Dutch average noise barrier length of ~150m, the levelised cost of electricity turns out to range between 0.15 – 0.24 €/kWh, as the more economical PV generation contributes between 80 – 96% of the total electricity generation.

In Chapter 6, the research is expanded to the integration of MW-scale wind turbines being collocated next to a refuelling station for hydrogen production and refuelling. Several databases are used in a Geographical Information System (GIS) software to define the suitability of all fuelling stations in the Netherlands to host a wind turbine next to them. The analysis uses built-up area, infrastructure and environmental

zoning criteria to define the suitability and hence the potential. Using further statistical analysis in a National and Provincial level assuming a fuel cell vehicle demand, the total hydrogen demand coverage could be estimated. It was found that 4.6% of current fuelling station can host a turbine next to them with a capability of producing between 24 – 104 kgH₂per kW installed wind capacity. These stations could produce 23400 tonnes of hydrogen annually covering 2.3% of total hydrogen demand in a 30% FCEV penetration scenario for the country of the Netherlands.

The main conclusion is that the integration of wind turbines with highway infrastructures is possible and that there is indeed potential for both concepts for the country of the Netherlands, but with some remarks. For micro wind turbines, it was found overall that noise barriers have a positive effect on wind energy as wind speed is increased on top of noise barriers. However, this only happens in certain wind to noise barrier relative direction and combinations of local wind resource and noise barrier orientation. It was also found that micro wind turbines have a very limited performance on top of the noise barrier due to several factors. Additionally, even though there are benefits of investment cost reductions from the integration, the micro wind turbine electricity turns out to be more expensive than other sources of electricity. And at a national scale there is limited contribution to the renewable electricity targets. However, for the MW scale wind turbine next to fuelling station it was found that nationwide implementation is appealing. When these wind turbines produce hydrogen, the integrated wind turbines can cover a considerable part of the total national fuel cell electric vehicle (FCEV) hydrogen demand.

Recommendations are provided to further research the micro wind turbine technologies in order to improve their performance in the field and especially when integrated with noise barriers. Finally, it is highlighted that GIS analyses is a powerful tool to assess at a nationwide scale the effectiveness of integrated systems from generation to consumption such as the wind turbine powered hydrogen refuelling stations.

SAMENVATTING

Nederland heeft doelen gesteld om de opwekking van duurzame energie te vergroten. Voor wind op land is hernieuwbare capaciteit nodig om aan de klimaatdoelstellingen te voldoen. Het realiseren van extra opwekking van windenergie op land wordt echter beperkt door problemen die verband houden met de beschikbaarheid van land, zonering en congestie van het elektriciteitsnet. Daarom moeten er nieuwe locaties worden gevonden om meer windcapaciteit te installeren. Snelweginfrastructuren bieden mogelijkheden om windturbines op land met verschillende capaciteiten te integreren. Zo zouden microwindturbines structureel kunnen worden geïntegreerd met geluidsschermen die een stevig fundament en voldoende hoogte bieden. Op MW-schaal zouden windturbines naast tankstations langs de snelweg kunnen worden geïnstalleerd om elektriciteit en waterstof voor de mobiliteitssector te leveren door lokaal op het station te produceren.

Dit proefschrift heeft tot doel twee concepten en hun landelijke implementatie in Nederland te onderzoeken;

1. Microwindturbines geïntegreerd met constructies langs snelwegen voor elektriciteitsproductie

2. MW-windturbines naast tankstations voor waterstofproductie.

Het onderzoek beperkt zich tot de hoofdvraag: “Wat is het technische en economische potentieel van het integreren van windturbines met snelweginfrastructuren?”. Om deze vraag voor beide concepten te beantwoorden, is het volgende onderzoek uitgevoerd. Windtunnel- en veldexperimenten zijn gepland en uitgevoerd om inzicht te krijgen in het potentieel aan windbronnen en de prestaties van microwindturbines bovenop geluidsschermen. Vervolgens is een technische en economische analyse uitgevoerd. Het werd duidelijk dat, om het potentieel voor Nederland te bepalen, een landelijke analyse met behulp van GIS-datasets nodig zou zijn. Daarom zijn vervolgens GIS-analyses uitgevoerd op basis van de resultaten uit de experimentele campagnes en toegepast op alle geluidsschermen in Nederland. Ten slotte werd de GIS-analyse verder uitgebreid naar het tweede concept van windturbines op MW-schaal naast tankstations.

Het proefschrift begint met de beschrijving van de experimentele campagnes. Zo wordt in Hoofdstuk 2 een experimentele campagne voor het beoordelen van windenergie uitgevoerd bovenop een geluidsscherm, gelegen op het kruispunt van de N470 en de A13 in Zuid-Holland, met behulp van sonische anemometers. Enkele parameters zijn vergeleken met referentiemetingen naast het geluidsscherm. De belangrijkste gemeten parameters zijn windsnelheid, instroomhoek en turbulentie-intensiteit. Het blijkt dat de windsnelheid toeneemt bij loodrechte stromingen, terwijl deze afneemt bij parallelle stromingen ten opzichte van de geluidsbarrière. Het verschil in windsnelheid kan tussen 80 – 140% liggen. Deze parameters zijn opgenomen in de

gevoelighedenanalyse om de jaarlijkse elektriciteitsproductie van geluidsschermen in verschillende oriëntaties en installatiehoogtes te meten. Er is vastgesteld dat de totale jaarlijkse elektriciteitsproductie inclusief de effecten van de geluidsbarrière op de windstroming tussen 60 en 150% oplevert ten opzichte van een referentie situatie zonder invloed van de geluidsbarrière op de stroming.

In Hoofdstuk 3 worden de resultaten van een experimentele campagne gepresenteerd van verschillende micro-windturbinerotoren en omvormers in een windtunnel. Dit om de geïdealiseerde prestaties van die turbines te bepalen onder vergelijkbare omstandigheden als ervaren bovenop de geluidsbarrière. De experimenten zijn verder uitgebreid met een veldexperiment waarbij een microwindturbine bovenop de geluidswal is geplaatst. Er is vastgesteld dat de turbine het grootste deel van de tijd ondermaats presteert in vergelijking met windtunnelomstandigheden (42% van de referentiewaarde in de windtunnel), wat wordt toegeschreven aan de verliezen die verband houden met de omvormer, verkeerde uitlijning van de krui-hoek en de effectiviteit van de controller. Het verdient aanbeveling om naar meer manieren te kijken om de efficiëntie van microwindturbines te vergroten en te optimaliseren, vooral wanneer ze worden geïntegreerd in constructies waarbij de turbines worden blootgesteld aan scheve aanstroming.

In Hoofdstuk 4 wordt het concept van een op een geluidsscherm geïntegreerde microwindturbine onderzocht voor landelijke implementatie in Nederland. Dit wordt gedaan door gebruik te maken van geluidsscherm-GIS en windsnelheidsdatasets van weerstations in combinatie met mesoschaalmodellen en windenergiecorrecties uit de bovengenoemde experimenten. Er zijn geschikte locaties voor geluidsschermen geïdentificeerd die een totaal geïnstalleerd vermogen van 17MW micro-windenergie kunnen opleveren. Er zijn statistische analyses uitgevoerd van nationaal tot provinciaal niveau naar het windenergiepotentieel van geluidsschermen met windturbines. Een gemiddelde geluidsbarrière van 150 meter blijkt representatief te zijn voor de installatie van ~9kW aan micro-windenergie. Gebleken is dat de geluidsschermen in totaal het windenergiepotentieel enigszins kunnen vergroten vanwege hun invloed van de windsnelheid bovenop het scherm, wat resulteert in een landelijke capaciteitsfactor van 11,7%. Bovendien wordt aangetoond dat geluidsschermen zich in de buurt van interconnectie-netwerken en andere vormen van toekomstige elektriciteitsinfrastructuur bevinden, wat resulteert in lage netintegratiekosten.

Hoofdstuk 5 duikt in de economische aspecten van dit geïntegreerde micro-windturbinesysteem. Het onderzoekt ook de economische aspecten van een combinatie van micro-windturbines met een fotovoltaïsch systeem geïntegreerd in dezelfde geluidsbarrière. Er worden meerdere configuraties beoordeeld om inzicht te krijgen in de kostenvariabiliteit binnen Nederland. De kostenvariabiliteit wordt weergegeven voor verschillende oriëntaties van de geluidsschermen, windlocaties met verschillende windprofielen, verliezen, correcties en gevoeligheden op economische parameters (kapitaal- en operationele uitgaven, kapitaalkosten). De resultaten laten een zeer breed

scala aan micro-windenergie-genivelleerde elektriciteitskosten zien, tussen 0,25 – 2,5 €/kWh. Bij het combineren en integreren van 9 kW aan microwindturbines en 90 kW aan fotovoltaïsche systemen op de Nederlandse gemiddelde lengte van de geluidsbarrière van ~150 meter, blijken de genivelleerde elektriciteitskosten tussen de 0,15 en 0,24 €/kWh te liggen, aangezien de goedkopere PV-opwekking tussen de 0,15 en 0,24 €/kWh bedraagt en 80 – 96% van de totale elektriciteitsopwekking verzorgt.

In Hoofdstuk 6 wordt het onderzoek uitgebreid naar de integratie van windturbines op MW-schaal die naast een tankstation worden geplaatst voor de productie en het bijtanken van waterstof. Er worden verschillende databases gebruikt in een Geografisch Informatie Systeem (GIS)-software om de geschiktheid van alle tankstations in Nederland te bepalen om er een windturbine naast te plaatsen. In de analyse wordt gebruik gemaakt van bebouwde oppervlakte-, infrastructuur- en milieuzoneringscriteria om de geschiktheid en daarmee de potentie in kaart te brengen. Met behulp van verdere statistische analyses op nationaal en provinciaal niveau, waarbij wordt uitgegaan van een vraag naar brandstofcelvoertuigen, kan de totale dekking van de vraag naar waterstof worden geschat. Er werd vastgesteld dat 4,6% van de huidige tankstations een turbine ernaast kan huisvesten die tussen de 24 en 104 kgH₂ per kW geïnstalleerd windvermogen kan produceren. Deze stations zouden jaarlijks 23.400 ton waterstof kunnen produceren, waarmee 2,3% van de totale waterstofvraag kan worden gedekt in een FCEV-penetratiescenario van 30% voor Nederland.

De belangrijkste conclusie is dat de integratie van windturbines met snelweginfrastructuur mogelijk is en dat er inderdaad potentieel is voor beide concepten voor Nederland, maar met enkele kanttekeningen. Voor microwindturbines werd over het geheel genomen vastgesteld dat geluidsschermen een positief effect hebben op de windenergie, aangezien de windsnelheid bovenop geluidsschermen toeneemt. Dit gebeurt echter alleen bij bepaalde relatieve richtingen tussen wind en geluidsscherm en bij combinaties van lokale windkracht en oriëntatie van het geluidsscherm. Ook werd vastgesteld dat microwindturbines vanwege verschillende factoren zeer beperkte prestaties leveren bovenop de geluidsbarrière. Bovendien blijkt de elektriciteit uit microwindturbines duurder te zijn dan andere elektriciteitsbronnen, ook al zijn er voordelen verbonden aan de verlaging van de investeringskosten als gevolg van de integratie. En op nationale schaal is er een beperkte bijdrage aan de doelstellingen voor hernieuwbare elektriciteit. Voor de windturbine op MW-schaal naast het tankstation bleek echter dat landelijke implementatie aantrekkelijk is. Wanneer deze windturbines waterstof produceren, kunnen deze geïntegreerde windturbines een aanzienlijk deel van de totale nationale waterstofvraag voor brandstofcel-elektrische voertuigen (FCEV) dekken.

Er worden aanbevelingen gedaan om de micro-windturbinetechologieën verder te onderzoeken om hun prestaties in het veld te verbeteren, vooral wanneer ze worden geïntegreerd met geluidsschermen. Ten slotte wordt benadrukt dat GIS-analyses een

krachtig hulpmiddel zijn om op landelijke schaal de effectiviteit van geïntegreerde systemen, van opwekking tot verbruik, te beoordelen, zoals de door windturbines aangedreven waterstoftankstations.

ACRONYMS

3D	Three-Dimensional
A13	National Motorway in the Netherlands
AC	Alternating Current
AEP	Annual Electricity Production
AHP	Annual Hydrogen Production
AME	Annual Mean Error
CAPEX	Capital Expenditures
CBS	Centraal Bureau voor de Statistiek (Central Agency for Statistics) in the Netherlands
CFD	Computational Fluid Dynamics
CORINE	Coordination of information on the Environment (Land Use and Land Cover Database part of European Union's Copernicus Land Monitoring Service)
CRS	Coordinate Reference System
DAWT	Diffuser Augmented Wind Turbine
DC	Direct Current
DEMO	Dienst Electronische en Mechanische Ontwikkeling (Electronic and Mechanical support Division in TU Delft)
DSO	Distribution System Operator
Duct4U	Acronym for the grant number
EPSG	European Petroleum Survey Group
FCEV	Fuel Cell Electric Vehicle
GIS	Geographic Information System
HAWT	Horizontal Axis Wind Turbine
IEEE	Institute of Electronic and Electrical Engineers
JRC PV GIS	Joint Research Center's Photovoltaic Geographic Information System Online Tool

KNMI	Koninklijk Nederlands Meteorologisch Instituut (Royal Dutch Meteorological Institute)
kW	kilowatts
kWh	kilowatt-hour
LCOE	Levelised Cost of Electricity (or Energy)
LED	Light Emitting Diode
LV	Low Voltage
MATLAB	Acronym for Matrix Laboratory (Simulation Software)
MPPT	Maximum Power Point Tracker
MSc	Master of Science
MV	Medium Voltage
MVLV	Medium to Low Voltage Station
MW	Megawatts
MWh	Megawatt-hour
N470	Regional Road in the Netherlands
NaN	Not a Number
NB	Noise Barrier
NOABL	Numerical Objective Analysis of Boundary Layer Database
NPV	Net Present Value
NWO	Nederlandse Organisatie voor Wetenschappelijk Onderzoek (Netherlands Organisation for Scientific Research)
OJF	Open Jet Facility wind tunnel in TU Delft
OPEX	Operational Expenditures
OSM	Open Street Maps
P	Power
PEM	Proton Exchange Membrane
PIV	Particle Image Velocimetry
PMSG	Permanent Magnet Synchronous Generator
PPE	Polypropylene
PV	Photovoltaic
PVC	Polyvinylchloride
PVNB	Photovoltaic Noise Barrier
QGIS	Quantum Geographic Information System (open-source software)

RES	Regional Energy Strategies
RMS	Root Mean Square
RPM	Rotations per Minute
RVO	Rijksdienst voor Ondernemend Nederland (The Netherlands Enterprise Agency)
SEST	Smart Energy Systems and Technologies
TI	Turbulence Intensity
TNO	Nederlandse Organisatie voor Toegepast-Natuurwetenschappelijk Onderzoek (Dutch Organization for Applied Scientific Research)
TSR	Tip Speed Ratio
TU	Technical University
UK	United Kingdom
USA	United States of America
VAWT	Vertical Axis Wind Turbine
WACC	Weight Averaged Cost of Capital
WASP	Wind Atlas Analysis and Application Programme
WT	Wind Turbine

1

Introduction

*“New-found wealth sits on the shelf of yesterday”
— Ian Anderson (lyrics from “North Sea Oil” song)*

This chapter prepares the reader for the content of this dissertation. It introduces the context of the research, defines the scope, aim, objectives and the research questions and provides the outline of the thesis.

1.1 Research context

World is under serious problems arising from climate change and resource depletion. Climate change is factually happening and the global community is making efforts to tackle it while limiting global warming. Starting from the scientific international efforts and the several synthesis reports from the Intergovernmental Panel for Climate Committee (IPCC [1]) and to the ratifications of several Nations (195 out of 198 parties) for the Paris Agreement [2]. These are all translated into concrete actions like National Determined Contributions (NDCs). The European Union has formulated since the European Climate Law which sets the goal of the European Green Deal with an intermediate target to reduce greenhouse gas emissions by at least 55% by 2030 (compared to 1990 levels) and to achieve net zero emissions by 2050. One of the means to reduce greenhouse gas emissions is to increase the share of renewable (sustainable) energy resources. The current work aims to investigate novel ways to increase the share of renewable energy generation in the overall system where limitations in further increase start to arise.

This is a case for densely populated areas, where limitations start to arise for increasing the share of sustainable energy generation. A good example is the country of the Netherlands where land availability is already decreasing to install more solar and wind capacity. As a matter of fact in the Netherlands, recently an agreement was made to no longer permit solar farms in agricultural and natural land areas (with some exemptions) but to rather investigate installations in existing infrastructures (building, facades, parking lots etc.) [3]. Another problem is the expensive grid reinforcements at both transmission and distribution level which are required to transfer additional amounts of electricity from remote areas to demand centers [4] with numerous sites being already congested as shown in Figure 1-1 below.

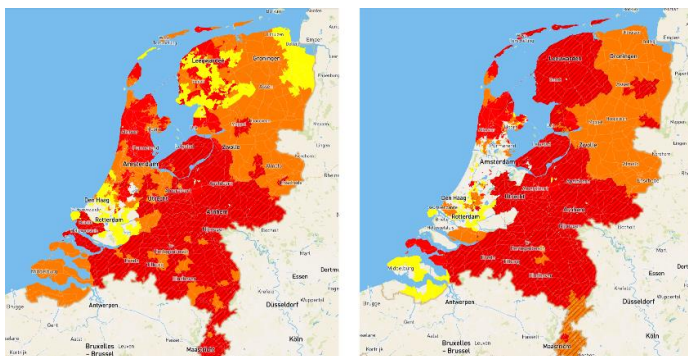


Figure 1-1: Grid capacity maps of the Netherlands with (left) grid import capacity, (right) grid export capacity. Colors represent the following (red) No transport capacity available: congestion management cannot be applied, (orange) No transport capacity available for the time being pending outcomes of congestions management studies, (yellow) Limited transport capacity and (transparent) Transport capacity available

Introduction

For all those reasons, the integration of renewable energy systems with existing built infrastructure has emerged as a crucial avenue for achieving a cost-effective increase of sustainable generation. Some examples of built infrastructure are road and highway networks, canals and navigable waterways, airports and ports, water management systems (sewage, drainage, irrigation etc.) and buildings. From those examples, road and highway infrastructure is one interesting case as it spans along large distances providing a potential for integrating renewable energy systems. Road and highway networks contain several structures like bridges, tunnel, noise barriers and specialized facilities like fueling stations which could be ideal for integrating additional renewable energy systems. For the European Union, the Alternative Fuels Infrastructure Regulation has recently published new targets for the specific deployment of electric vehicle charging stations (every 60km of the trans-European network) and hydrogen refuelling stations (every 200km along the trans-European core network) [5]. These could be as well good candidate offtakers for renewable electricity produced along highways beside grid feed-in.

Between solar and wind systems, the concept of infrastructure integrated systems is already demonstrated for solar generation. For example, the PV industry has progressed into designing and installing building integrated photovoltaic systems [6] or even PV systems integrated with canal networks [7]. For the highway infrastructures, photovoltaic noise barriers (PVNBs) have been developed which can be ideally placed near urban areas [8]. The benefit of PV systems is its versatile and modular design of $\sim 1.5 \text{ m}^2$ modules which can be integrated in a number of surfaces. Integrating wind energy with existing infrastructures presents different challenges than PV as wind turbines are available in different sizes and are usually not designed for modular implementation. Smaller turbines could be structural integrated with buildings or other structures while larger turbines can only be mounted on dedicated bottom fixed structures. The integration with infrastructures is further complicated by permitting processes related to noise, safety and other aspects, especially for large-scale wind turbines (megawatt sizes) when installed near urban areas and small turbines (kilowatt sizes) when aggregated in rooftop installations. Therefore, it is needed to identify new ways to effectively integrate wind turbines with infrastructures as the ones shown in Figure 1-2. One novel way is to integrate wind turbines with highway infrastructures, for example small turbines can be integrated with noise barriers which span across urban areas in countries while large turbine can be installed next to fueling stations. Those interesting concepts are studied in the current dissertation in order to unravel challenges and opportunities via scientific methods from a conceptual level up to a nationwide implementation with a focus on wind turbines.



Figure 1-2: (left) photovoltaic noise barrier PVNB, (middle) micro wind turbine noise barrier (MWTNB), (right) wind powered hydrogen producing refuelling station concepts

1.2 Scope and novelty of research

The integration of wind turbines near urban areas has so far mainly been focused on roof mounted installations of micro wind turbines. For the case of highway infrastructures, a very small part of research has focused on integrating wind turbines next to highways. The concepts of integration are mainly on light poles and the median of the highway thus using the wind generated by traffic. Despite the large set of literature on the integration of photovoltaic systems with noise barriers little is known on the integration on wind turbines with noise barriers. Noise barriers could provide a solid structural support for wind turbines as shown in Figure 1-3 below, thus eliminating tower and foundations cost.

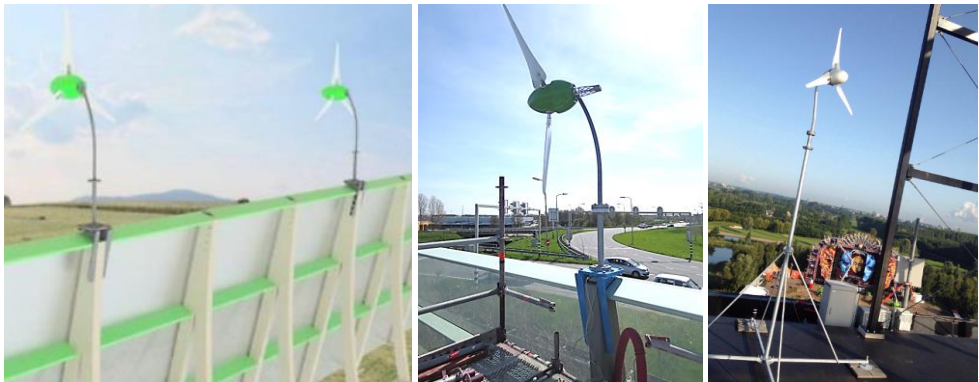


Figure 1-3: The concept of a noise barrier integrated wind turbine (left) as realised in the field test conducted near TU Delft, showing the blue flange (middle) which could eliminate costs related to additional tower and foundations or tripods as shown on the WindChallenge rooftop installation (right)

Literature also shows that wind velocity, on top of similar objects to noise barriers, could be increased thus potentially increasing the energy yield [9]. Even though there are several wind flow assessments on top of similar objects as shown in Figure 1-4

Introduction

below, little is known about the wind flows and turbine performance on top of sharp-edged objects like noise barriers. This is therefore one of the main scopes of this research.



Figure 1-4: Concepts and research of wind energy along highways and turbines integrated with highway infrastructures (left) light pole mounted horizontal axis wind turbine next to a road, (middle) vertical axis wind turbine installed on top of a median of a highway and (right) experimental set-up of wind energy generation along North Carolina's highways

Another part of highway infrastructure where large amounts of energy are being consumed (via means of fuel for mobility) are the fueling stations. An interesting and upcoming concept is hydrogen production at those refuelling station. Even though there are studies for nationwide implementation of those concepts, little is known when planning and zoning limitations are being applied to define the technical potential. Therefore, current study's scope aims as well to quantify the technical potential of wind turbines when collocated and integrated with highway refuelling infrastructure.

Finally, the 2 concepts that this dissertation will focus are illustrated in Figure 1-5 below.

Introduction

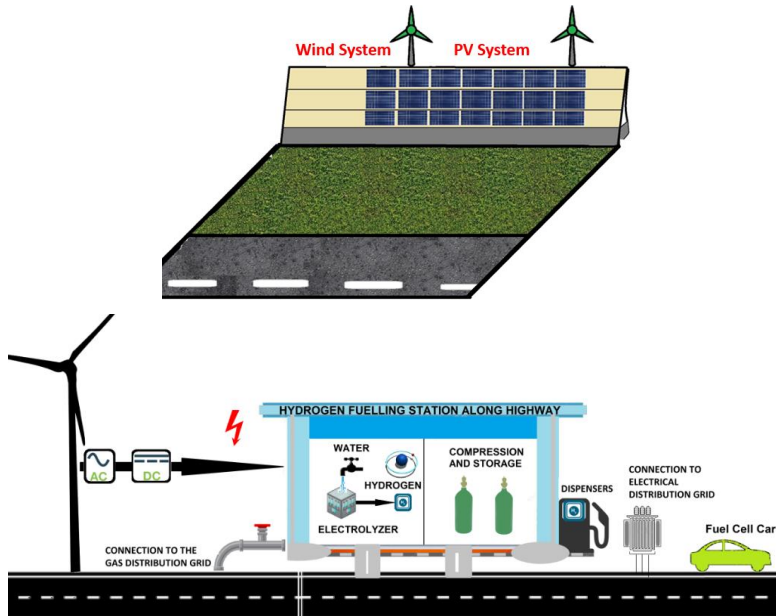


Figure 1-5: Concepts of wind turbines integrated with highway infrastructure, wind turbine integrated with noise barriers and photovoltaic panels (above), wind turbines integrated with highway hydrogen refuelling stations (below)

1.3 Aims, objectives and research questions

The main aim of this dissertation is to find out how wind turbines can be effectively integrated with highway infrastructures and assess the potential when nationally applied. This aim is further narrowed down to specific objectives which helped to formulate the different parts of work for this research. In particular, the following objectives were identified:

- To investigate the challenges and benefits of integrating wind turbines with highway infrastructures like noise barriers
- To measure the wind flow on top of noise barriers and the performance of integrated wind turbine noise barrier system
- To quantify the cost of electricity that is expected from this integration
- To assess the technical potential of this integrated wind turbine noise barrier concept for the case of the Netherlands
- To evaluate other wind turbine integration concepts with highway infrastructures

The aims, objectives and scope of this research, were translated into a research questions package.

The main research question is

“What is the technical and economic potential of integrating wind turbines with highway infrastructures?”.

This main question is broken into the following research questions:

- What is the wind resource that micro wind turbines will experience when integrated on top of noise barrier highway infrastructures?
- What is the performance of a micro wind turbine integrated on top of a noise barrier?
- What is the nationwide technical potential of micro wind turbine noise barriers in the Netherlands?
- What is the levelised cost of electricity of noise barrier integrated wind turbines?
- What is the nationwide technical potential of wind turbines integrated with fuelling stations in the Netherlands for hydrogen production?

1.4 Brief description of research methods

Several research methods have been applied to answer the research questions. In particular, it started with an experimental campaign of a 1-year wind resource data collection at a noise barrier site with several sonic anemometers placed in different heights and locations above and near the noise barrier to scan the wind fields. The findings from the wind resource assessment that directly influence the wind turbine performance such as wind speed, inflow angle and skewed flow parameters were then used to assess a prospect turbine’s performance in a wind tunnel. Once this was done, the wind turbine was then set-up on top of a noise barrier. To do this, the set-up was realized by designing the integrated concept and finally realizing the installation of the wind turbine on top of the barrier. Several performance parameters were then monitored and analysed via a campaign. Figure 1-6 below presents a compilation of highlights from the experimental campaigns aforementioned.

The next part was to implement findings in a nationwide scale to determine the potential of micro wind turbines on noise barriers for the country of the Netherlands. This was conducted via an extensive Geographical Information Systems (GIS) study by using noise barriers datasets and applying wind resource findings. Additionally, an economic analysis on the levelised cost of electricity for the micro wind turbine on top of the noise barrier is performed including also an integration with photovoltaic systems on noise barriers. As part of a wider understanding of the technical potential of integrating wind turbines with highways infrastructures, a GIS study was conducted for the concept of wind turbines producing hydrogen when collocated and integrated next to a fuelling station. The nationwide potential of this concept was evaluated with a suitability analysis of all existing fuelling stations in the Netherlands by applying several zoning criteria which could limit the installation of wind turbine in the vicinity.

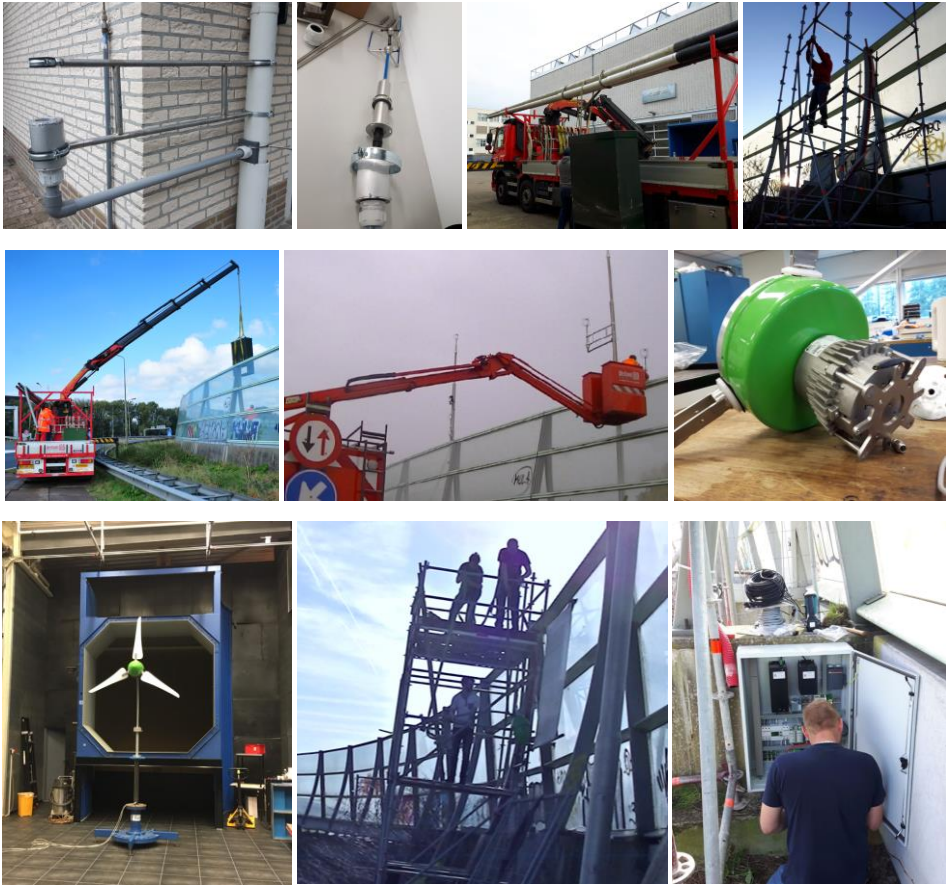


Figure 1-6: Compilation of experimental campaign photos with text flow logical order, (i) sonic anemometer bracket design, (ii) sonic anemometer, (iii) loading of truck with 3 light poles for the installation of anemometers and grid connection cast, (iv) scaffold installation, (v) crane installation of the electricity cast, (vi) sonic anemometer installation, (vii) custom design of measurement devices on the wind turbine's hub, (viii) wind tunnel experiment, (ix) wind turbine installation with scaffold and (x) installation of turbine sensor box

1.5 Overview of structure

The thesis structure is first focussing on how a particular noise barrier is influencing the wind flow and potential energy yield. Following to the wind turbine system aspects and then assessing the energy potential for this particular system in a nationwide case. The study includes also the cost aspects of this concept when combined with other integrated systems such as PV. Next to this also another concept

Introduction

of wind energy integration with highway infrastructures is assessed, the wind turbine integration with fuelling stations. The thesis research themes and methodology is outlined in a Chapter structure shown in Table 1 – 1 below.

Table 1- 1: *Thesis Research Themes and Methodology Structure*

<p><u>CHAPTER 2</u> Wind Resource Assessment</p>	<p>Experimental campaign and analysis whereby:</p> <ul style="list-style-type: none"> - High resolution wind time series are produced - Analysis of time series with relevant turbine characteristics
<p><u>CHAPTER 3</u> Wind Turbine Performance</p>	<p>Experimental campaign and analysis which:</p> <ul style="list-style-type: none"> - tests the turbine in a wind tunnel by emulating the results of wind resource assessment - Identifies critical system parameters - Analyses the field performance of the turbine to identify technological gaps
<p><u>CHAPTER 4</u> Nationwide concept potential for micro wind turbines</p>	<p>Desktop GIS study defining the technical potential of wind turbine noise barriers in the Netherlands by:</p> <ul style="list-style-type: none"> - Filtering suitable noise barrier and combining findings related to performance on top of noise barriers - Making estimates on nationwide implementation
<p><u>CHAPTER 5</u> Wind electricity cost and integration with PV</p>	<p>Desktop technoeconomic analysis of wind turbine and PV noise barrier which:</p> <ul style="list-style-type: none"> - Takes into account integration costs - Makes sensitivity analysis on different configurations
<p><u>CHAPTER 6</u> Nationwide potential evaluation of integrating wind turbines with fuelling stations</p>	<p>Desktop GIS Study which defines the technical potential of MW scale wind turbines to be integrated with refuelling stations by making a suitability analysis on fuelling stations because of wind turbine limiting regulations</p>

The different chapters contain the following:

- The 2nd Chapter presents the design, methods (monitoring, collection, analysis) and results of a 1-year wind resource assessment (experimental campaign) for a noise barrier located near the TU Delft. This chapter is entitled as “Wind resource

Introduction

characteristics and energy yield for micro wind turbines integrated on noise barriers – An experimental study” and has been published in the Journal of Wind Engineering and Industrial Aerodynamics (Elsevier) [11]

- The 3rd Chapter presents the design, methods and results of the performance assessment of the turbine that was placed in the noise barrier site. Micro wind turbines were also tested in a wind tunnel set-up before the installation of one at the noise barrier set-up. This chapter is entitled as “Performance characteristics of micro wind turbine integrated on a noise barrier” and has been published in the Journal Energies of MDPI [12]
- The 4th Chapter presents the methods and results of the national potential of wind turbine noise barriers. This is done by using publicly available GIS datasets which are corrected from the experimental results from previous chapters. This chapter is entitled as “Technical potential and application of micro wind turbines integrated on noise barrier acoustic screens in the Netherlands using GIS”.
- The 5th Chapter includes a techno-economic sensitivity analysis, where the concept of an electricity producing noise barrier by wind turbines and photovoltaic systems is shown. This chapter is entitled as “Techno-economic evaluation of wind turbine and solar PV systems integrated on a noise barrier”. This work uses cost models built from the work entitled “On-site wind powered hydrogen refuelling stations – From national level to a case study in Germany” published in Conference Proceedings of the International Conference on Smart Energy Systems and Technologies (SEST) from the Institute of Electrical and Electronics Engineers (IEEE) [13]
- The 6th Chapter presented the method and results of the assessment of the nationwide implementation of wind powered hydrogen refuelling stations. Building upon the concept of integrating wind turbine with highway infrastructures. This chapter is entitled as “Technical potential of on-site wind powered hydrogen producing refuelling stations in the Netherlands “and has been published in the International Journal of Hydrogen Energy (Elsevier) [14], [15]
- The 7th Chapter includes the conclusion of this study, hence the answers to the main research question and the sub-questions, while it provides recommendations relevant to the topic of this Thesis and proposes future research work.

1.6 References

1. IPCC. *AR6 Synthesis Report, 2023*. <https://www.ipcc.ch/report/ar6/syr/>
2. United Nations. *Paris Agreement - Status of Ratifications, 2023*. <https://unfccc.int/process/the-paris-agreement/status-of-ratification>
3. Netbeheer Nederland. Solar panels on agricultural and natural areas. Available online at: <https://www.netbeheernederland.nl/nieuws/-nee-tenzij-voor-zonnepanelen-op-landbouw-en-natuurgronden-1702>
4. Netbeheer Nederland. *Position Paper voor het Rondetafelgesprek over het Electriciteitsnet, 2022*. [https://www.netbeheernederland.nl/upload/Files/Rondetafel Elektri citeitsnet 03-02-2022 Inbreng Netbeheer Nederland 242.pdf](https://www.netbeheernederland.nl/upload/Files/Rondetafel%20Elektricit%20net%2003-02-2022%20Inbreng%20Netbeheer%20Nederland%20242.pdf)
5. EU Council. Alternative fuels infrastructure: Council adopts new law for more recharging and refuelling stations across Europe. 2023.
6. Sara Freitas, Teresa Santos and Miguel C. Brito. Impact of large scale PV deployment in the sizing of urban distribution transformers. *Renewable Energy* **2018**, 119, doi:10.1016/j.renene.2017.10.096.
7. N. Chrysochoidis-Antsos and C. Chrysochoidis. Benefits from PV system integration with irrigation and drainage infrastructures : Case study for Thessaloniki-Imathia-Pella plain. 2017 In Proceedings of 33rd European Photovoltaic Solar Energy Conference and ExhibitionAt: Amsterdam (The Netherlands).
8. E. De Schepper, S. Van Passel, J. Manca and T. Thewys. Combining photovoltaics and sound barriers - A feasibility study. *Renewable Energy* **2012**, 46.
9. Xiaoxu Wu, Xueyong Zou, Chunlai Zhang, et al. The effect of wind barriers on airflow in a wind tunnel. *Journal of Arid Environments* **2013**, 97, doi:10.1016/j.jaridenv.2013.05.003.
10. Rijkswaterstaat. GIS data for Noise Barriers and Highways. Available online at: <https://www.rijkswaterstaat.nl/kaarten/geluidregister.aspx?cookieload=true>
11. Nikolaos Chrysochoidis-Antsos, Andrea Vilarasau Amoros, Gerard J. W. van Bussel, Sander M. Mertens and Ad J. M. van Wijk. Wind resource characteristics and energy yield for micro wind turbines integrated on noise barriers – An experimental study. *Journal of Wind Engineering and Industrial Aerodynamics* **2020**, 203, doi:<https://doi.org/10.1016/j.jweia.2020.104206>.

Introduction

12. Nikolaos Chrysochoidis-Antsos, Gerard J.W. van Bussel, Jan Bozelie, Sander M. Mertens and Ad J.M. van Wijk. Performance Characteristics of A Micro Wind Turbine Integrated on A Noise Barrier. *Energies* **2021**, *14*.
13. N. Chrysochoidis-Antsos, C. Liu and A. van Wijk. On-site wind powered hydrogen refuelling stations - From national level to a case study in Germany. 2018 In Proceedings of 2018 International Conference on Smart Energy Systems and Technologies (SEST), 10-12 Sept. 2018; pp. 1-6.
14. Nikolaos Chrysochoidis-Antsos, Miguel Rodríguez Escudé and Ad J. M. van Wijk. Technical potential of on-site wind powered hydrogen producing refuelling stations in the Netherlands. *International Journal of Hydrogen Energy* **2020**, *45*, doi:<https://doi.org/10.1016/j.ijhydene.2020.06.125>.
15. Nikolaos Chrysochoidis-Antsos, Ad van Wijk. Could wind turbines fuel up our future hydrogen refuelling stations? A GIS-based methodology. 2016 In Proceedings of Wind Europe - Wind Resource Assessment, Edinburgh (Scotland).

2

Wind resource characteristics and energy yield for micro wind turbines integrated on noise barriers – An experimental study

“Small is beautiful”

—*British Economist Ernst Friedrich Schumacher (title from book)*

*This **chapter** provides an understanding of the wind resource characteristics that occur on top of noise barriers and would affect the performance of micro wind turbines and introduces the concept of micro wind turbine noise barriers.*

*The **main question answered** in this chapter is:*

“What is the wind resource that micro wind turbines will experience when integrated on top of noise barrier highway infrastructures?”

This chapter is published as “Wind resource characteristics and energy yield for micro wind turbines integrated on noise barriers – An experimental study” by N. Chrysochoidis-Antsos, A. Vilarasau Amoros, Ad van Wijk, Gerard van Bussel and Sander Mertens (2020) in the “Journal of Wind Engineering and Industrial Aerodynamics” published by © Elsevier.

2.1 Introduction

The concept of structural integration of wind turbines with noise barriers could lead to cost reduction and energy yield increase. Potential higher winds on top of the noise barrier might lead to higher wind energy yields. This hypothesis in combination with the strong need for energy yield increase motivated further investigation of the wind resource properties of this concept through an experimental study for urban wind flows and an energy yield assessment.

This concept exists in patents in China [1], [2] and in Korea for a vertical axis wind turbine integrated with a sound barrier while there is a concept of a velocity sensor [3] as well as with horizontal axis turbines [4]. Finally, a real world experimentation is finished near TU Delft in the Netherlands and the results are presented in the next Chapter [5]. Results of this chapter are important for noise barrier wind turbine concepts as the safe, reliable and efficient operation of wind turbines in the highly turbulent built environment near noise barriers are located, is challenging [6].

There are as well economic challenges. Micro wind turbines installed within urban environments have low energy payback ratios [7], low energy output with low (average of 4%) capacity factors [8] and the high capital expenditures ranging from 6700-10900 €/kW (2017 equivalent from US Dollars) [9] while PV is ranging 2500-6700 €/kW (2017 equivalent from US Dollars) [10]. All this result to high levelised cost of electricity (LCOE) up to 1.20 €/kWh [11] while solar can be as low as 0.25 €/kWh for the same rated power capacities. This means that small wind costs are somewhere in between 3.5-4.5 times higher than PV.

Focussing further out 590 km of noise barriers are found in the Netherlands with potentially suitable foundations for wind turbines [12]. Placing 1 turbine every 10 meters equals to 59.000 turbines along highway infrastructures. Assuming a 0.375 kW for micro wind turbines (1.5m diameter), like the Dutch-made WindChallenge [13], then 17.700 kW of micro-wind turbines could be installed. However, the energy yield of these systems is unknown. This lack of knowledge of how the noise barriers affect the wind flow for micro-wind turbine application has led to perform this study. The vision of this study is animated in Figure 2 - 1 below. Finally, in this Chapter the subsequent change in energy yield for the noise barrier is estimated and together with an assumed cost reduction the changes in LCOE are observed.



Figure 2 - 1: Visualization of micro wind turbines integrated on a noise barrier

To understand the relevant wind resource parameters, a literature review has been performed for wind speed, skewed inflow angle, turbulence and energy yield on top of obstacles which is relevant for the acoustic screens that are investigated in this study. These are non-porous fences, 10 m high, with a gradient of 10° .

Wind Speed

In general wind speed related literature reaches consensus on wind speed increase on top of obstacles. In particular, the wind tunnel work of [14] with 0% permeable fences showed speed-up at $1.5H-2H$ on top of the noise barrier and $1H-4H$ at the wake of the fence. Wind speed increase is also shown on porous and solid fence experiments in wind tunnel conditions with fence heights ranging (5-16cm). A wind speed increase of 10-20% between heights of $1.24H$ and $1.60H$ and in the leeward direction of the windbreak is shown in [15] plotting data of [16]. Wind speed increase ranging from 20-50% on top of windscreen for normal flow to the wind screen is shown in wind tunnel validated 3D wind flow simulations behind porous fence [17]. In [18] increase in wind speed for different types of roofs and directions was found with Computational Fluid Dynamics (CFD) simulations. Increases ranged from 9.3% to 53%. [19] identified as well 10% wind speed increase for perpendicular flow to a screen ($0.25H$ leeward from barrier) and at $1.50H$ on top of it. Finally, [20] made an extensive lidar-based analysis of the shelter effects of porous and non-porous effects with subsequent effects on the wind speed.

There is also work that examines flow over ridges, escarpments and other topographic features. Whilst not perfectly analogous, there is a larger focus on the flow above these structures and there are studies that consider the impact of wind direction and the inclination angle. Amplified wind flow from 1-1.5 times the upstream velocity was observed in wind tunnel and field tests of [21] for wind flow in the edge of cliffs. In

the wind tunnel study of [22] up to 20% speed-up was observed on top of a cliff obstacle exposed into yaw angles $0^\circ - 40^\circ$ at locations from 0-2H on top of the edge. Turbulence intensity was affected as well. Cliff is a different obstacle to noise barrier spanning 48h downstream, while noise barrier are thin slices of few centimetres. The effect of ruggedness was also assessed in [23]. Finally, the effects of a cliff on the flow for wind turbine operation are assessed in [24], where small speed-up is observed when a flow is perpendicular to the cliff for a turbine placed nearly 3H downstream of the cliff side. Most of obstacles above are not similar to noise barrier in terms of aspect ratio but still is an attempt to utilize similar effects as the ones present in flow acceleration on top of windbreaks (noise barriers).

Skewed Flow Angle

The skewed flow angle is the angle from the horizontal and vertical components of wind and is important for the performance of micro wind turbines. [25] examined with CFD the effect of skewed flow on vertical and horizontal axis wind turbines on rooftops. For horizontal axis wind turbines (HAWT) the skew angle had negative effect while for vertical axis wind turbines (VAWT) positive, for skew angles $0^\circ - 40^\circ$. [26] also examined turbine's performance in yawed flow situations in with theoretical estimation and Particle Image Velocimetry (PIV) measurements and found that for yawed flow the power coefficient of the wind turbine is dropping significantly. Finally, [27], observed in experimental data that with skew angle increase, the rotor's C_P (power performance coefficient) is decreasing.

Turbulence Intensity

Turbulence intensity can affect the energy yield and the performance of the wind turbine. Specifically, [28] presents the anomalous behaviour of power curve for different turbulence intensities. Power curves vary more when turbulence intensities increase. Also, [29] concludes that increase of turbulence intensity decreased the power output of a multi-bladed Savonius rotor in an experiment with a constant wind speed of 8 m/s. [30] observed that the performance of a bare and a diffuser augmented micro wind turbines showed decrease in performance due to turbulence intensity increase. [31] observed that the kinetic energy at a specific site for small wind turbines can vary by 20% depending on the levels of T.I. In [32] a theoretical approach shows increase in power in low wind speeds and decrease in power at high wind speeds with high TI and a correction curve is presented only for wind speeds from 7-8 m/s. Also, from field test in [33] author suggests decrease in performance due to turbulence intensity. A Zephyr turbine was used and 20% decreased power was observed with respect to the manufacturer power curve a turbulence levels of 70%.

Energy Yield

In terms of energy yield, [18] found for various roof cases and different wind direction the increase in power for wind energy. In [34] a higher wind power coefficient was found for a cross-flow wind turbine integrated above a porous 60% geometric shielding rate windbreak fence examined in a wind tunnel. Finally, [35] agree that urban areas are considered poor sites for micro wind turbine installation and little work has been done for optimizing the placement of the turbines. Thus, current work expands prior art with wind time series annual energy yield estimation for a particular noise barrier near Delft and a sensitivity analysis by rotating the wind rose in increments.

Research Gap

As discussed above, several publications exist for wind flows on top of porous and non-porous obstacles and cliffs. However, for noise barriers there is need for real-world dataset with wind properties to be collected and analysed. This will bring more insight on wind energy applications. Current research adds upon the prior knowledge with the addition of results for multiple orientations assessed due to the large dataset given [36]. Emphasis is given on wind speed on top of the structure and not upstream or downstream. The skewed inflow angle is used as well for estimating the energy yield. The results are translated through a real-world micro wind turbine application into energy yield and cost terms.

Novelty

The objective of this Chapter is to propose the integration of micro wind turbines with noise barrier structures and assesses its potential benefits in terms of energy yield and cost reduction. The assessment combines an experimental wind resource study results, together with a wind tunnel power performance study in an energy yield sensitivity assessment for micro wind turbines installed on top of a noise barrier.

Outline

The outline of this work started with the literature review in Section 2.1, followed by a detailed description of the set-up in Section 2.2, presentation of Results in Section 2.3, discussion of main outcomes in Section 2.4 and finishes with Conclusions and Recommendations.

2.2 Set-Up Description

Two set-ups are realized. An outdoor set-up where all wind flow properties at the noise barrier site are measured and a wind tunnel power curve measurement test. Both explained below.

2.2.1 Noise Barrier Set-Up

A set-up with 8 sonic anemometers placed on 2 poles on top of the noise barrier and 1 pole as a reference point has been designed and built near a road with a 50 km/h speed limit. The site is on the north side of the ring road that intersects the N470 (regional Dutch road) and the A13 (Dutch National Motorway). A dataset of 3-dimensional wind speeds has been collected during the period in 2016-2017 and can be accessed online [36]. 10-minute averaging is used for statistical means. Further, binning methodologies are applied in order to classify the effect of the noise barrier on the wind flow properties per direction of the wind flow relative to the barrier. The documented effects are utilized in a case study for the particular barrier to identify the potential wind turbine energy extracted by the wind turbine model and an LCOE cost change is assessed. For an artistic impression of the wind turbine envisioned, refer to Figure 2 - 1.

Equipment selection

Gill Wind Master 3D sonic anemometers are used to record all wind components. A calibration and measurement validation test was performed for each anemometer, in various angles in all 3 planes (2 horizontal and 1 vertical) as [37] suggests. A correction factor of 1.16 for the vertical velocity component was implemented, as advised by the manufacturer of the sonic anemometers (which was assessed and validated through wind tunnel testing) [38]. All results should be treated with the accuracy of the sensors (1.5%RMS at the reference of 12 m/s).

Set-up installation

Dimensions of the set-up and the wind vector reference system are given in Figure 2 - 2. Eight sonic anemometers are installed on 3 measurement poles with brackets. There is a reference pole away from the noise barrier, and two poles behind the noise barrier. All sonic anemometers have cables that guide the signals through underground pipelines to the main electrical cabinet, where the data are recorded.

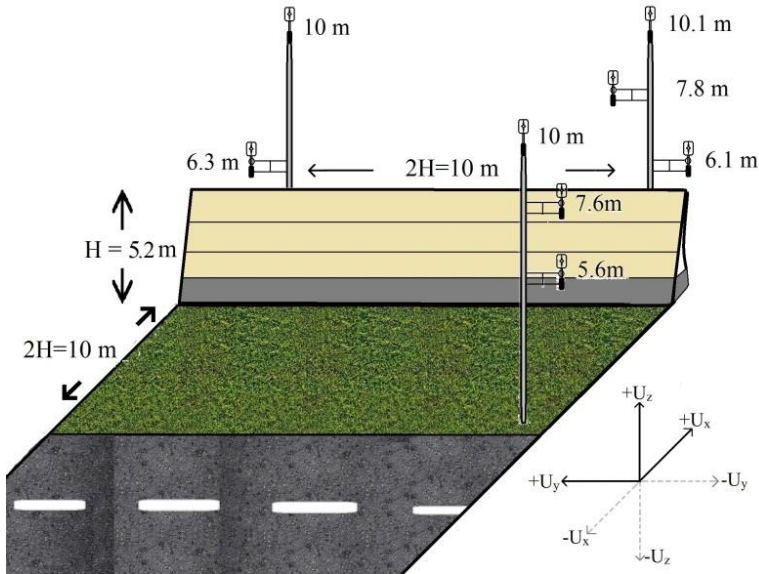


Figure 2 - 2 : Schematic of the placement of the poles of the set-up together with the sonic anemometer corresponding heights and the wind speed reference system

Some parameters are taken into account for the design of the set-up. These are summarized below:

- The anemometers are placed at distance of 10 times the pole diameter to avoid the **aerodynamical blockage of the cylindrical pole** [39]. This is also validated by comparing experimental results from various orientations with respect to the position of the bracket.
- Poles are fixed in the soil by 1.5 m for **structural integrity and avoidance of oscillations** that might affect the measurements from the relative motion of the tower.
- **Passing vehicle effects on wind speed and turbulence** are considered negligible for current set-up, placed on a road passage with a speed limit of 50 km/h . This is 30 km/h less than the experiment in [40], with vehicle fleet passing with 80 km/h from a highway. In this they found that for a distance of 15 m away from the road a minimal difference in wind speed of 0.1 m/s (at heights of 5 meters) and 0.06 m/s (at heights of 10 meters).
- **Reference pole is at a distance of 2 times the height of the noise barrier** as seen in Figure 2 - 2. [41] suggested that flow is undisturbed in front of small buildings at a distance of $2H$. For shelterbelt obstacles such as the noise barrier there are some guidelines but based on empirical assessments. The presence of a road, in Figure 2 - 3, limited as well the installation of the reference pole more than 2 times the height from the noise barrier.

Wind Data characteristics

Data are collected with “WindView” software and processed with MATLAB. During the 13-month period of November 2016 until November 2017, a total of 3066 hours were recorded. This is the 32% of all that period resulting in 18396 10-minute datasets. The rest was not recorded due to remote connection issues and other limitations. For the recorded datasets, a 10-minute median wind direction is used. Only windward datasets are considered and classified (coming from the arc from -90° to 0° to $+90^\circ$ in Figure 2 - 3). These datasets are relevant for the study as the effect on windward flow properties is examined. Outliers are removed (circuitry failure, power outages, bird interference and ice formation) to avoid uncertainty on results. Even if 1 anemometer contained error values then this specific time-series 10-minute dataset is excluded. 1.03% of datasets was removed. Finally, the total amount of 10-minute periods that are examined is 11.335 (20% of a full year).

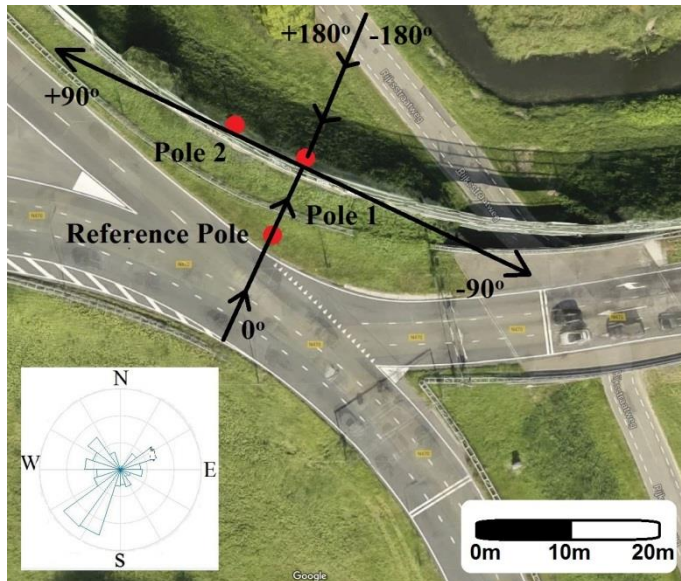


Figure 2 - 3 : Top view of the studied noise barrier (bottom left) Wind orientation rose (red circles filled in black) Poles with the sonic anemometers (black lines and arrows) The reference system used in this study. Coordinates (51°59'50.4"N 4°23'24.8"E)

Sampling frequency

Data were logged with sampling frequencies of 1Hz (54% of datasets), 2Hz (13% of datasets), 4Hz (32% of datasets) and 5, 8 and 16Hz for the rest 1% of datasets. Even though the selection seems arbitrary it does not influence the results. Literature presented that different sampling rates of the same recorded period (10Hz, 4Hz and 1Hz) do not significantly influence the values of turbulence intensity and power spectral density. In particular, changing the sampling rate from 10Hz to 1Hz changed the characteristic turbulence intensity by at most 0.25% of the reference value [42].

Similarly mean wind speed and inflow angle as well would not be influenced for the purpose of this Chapter which is not to capture turbulent structures of flow, but to use results for micro wind turbine energy yield. Therefore, a comparison between 1Hz and 4Hz datasets is performed (~80% of all datasets). The standard deviation of wind speed for sampling frequencies of 1 Hz and 4 Hz can be seen in Figure 2 - 4. This was done for the anemometer placed on the top of the reference pole (see Figure 2 - 3). Sampled points (10-minute standard deviation) per wind direction φ ($^{\circ}$) are less for 4Hz than for 1Hz. But some observations can be made with the help of the grid lines. For wind speeds 0-2 m/s (red dots) and for both datasets with different sampling frequency the standard deviation is between 0-1. Same applies for all other wind speed bins where standard deviation is within similar ranges for different sampling frequency datasets. Finally, a periodogram (power spectral density) is also presented of 4Hz and 1Hz (which was resampled from 4Hz). Again, no significant differences are observed. Therefore, all datasets of different sampling frequencies are used in the statistical analysis.

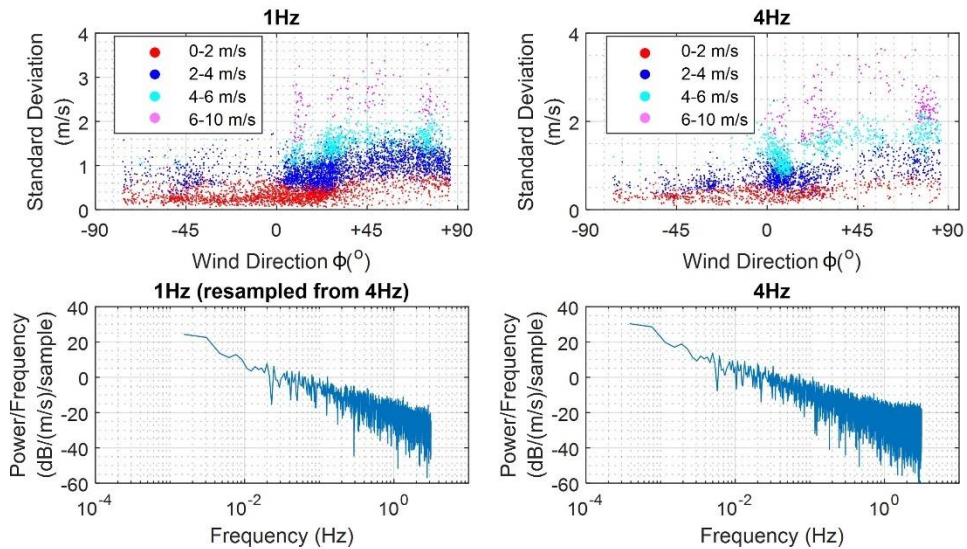


Figure 2 - 4 : (top) Scatter plots of the standard deviation σ_u of wind speed for different wind direction φ ($^{\circ}$) and wind speed bins (see legend) and different sampling frequencies of 1Hz and 4Hz (bottom) Periodogram of 4Hz and 1Hz dataset (resampled from 4Hz)

Estimation of wind resource parameters

A comparison between the data on top of the noise barrier and the data on the reference pole is done for the reference domain. Wind speed U (m/s), wind direction φ ($^{\circ}$) and inflow angle θ ($^{\circ}$) are calculated in each measurement point for each time sample. Input data are the 3 vectors of each anemometer averaged in 10-minute periods. Turbulence intensity TI (%) is based on this period. 10-minute averaging is common for wind energy analysis as many handbooks and international standards

suggest [43]. Shorter averaging periods of 5 and 1 minutes is also used in order to compare the results with the 10 minutes averaging but as no great deviations were found, they were not considered.

Wind Direction: Results are binned for wind directions. Vector arctangent function is applied for the horizontal wind components U_x (m/s) and U_y (m/s) and the median value of 10-minute dataset is selected, thus solving the discontinuity of the degrees (0° - 360°) [37]. Finally, the wind direction is expressed relative to the noise barrier with 0° being the perpendicular line as seen in Figure 2 - 3.

Comparison of different pole wind data

Exponential fit is used on 10-minute averaged values to estimate wind properties on heights of comparison on the reference pole. For example, in Figure 2 - 5 below, the reference anemometer near the road (see Figure 2 - 2 as well) is at a height of 5.6 meters while on Pole 1 at 6.1 meters. With 3 data points before the noise barrier and exponential fitting, the resulting wind speed is calculated at the projected height of 6.1 meters for the reference pole for the sake of comparison.



Figure 2 - 5 : Noise barrier set-up photo from Google Earth

2.2.2 Wind Tunnel Set-Up

Calculation of the wind turbine energy yield is done using an experimentally derived power curve of a commercial downwind micro wind turbine. The experiment is performed in the Open Jet Facility of TU Delft (Low Wind Speed tunnel 0-35 m/s) in Figure 2 - 6. The micro wind turbine is placed in a distance of 3 meters from the 2.85mx2.85m nozzle of the wind tunnel, where the control wind speed is calibrated and corrected for blockage effects [44]. Power is recorded with specialized electro-technical

equipment (voltage and current measurements) which are further processed in order to derive the power produced (5% error margin). The power fed to the grid is measured including inverter, generator and other losses [45]. Figure 2 - 16 indicates the average power values recorded for several wind speeds including the 5% error margin of the sensors. Wind speed sweeps were performed and the average values of Power (W) per wind speed (m/s) are fitted in the curve below. Wind speed is measured with a Pitot-tube placed inside the wind tunnel nozzle and corrected for the distance of the wind turbine from the nozzle.

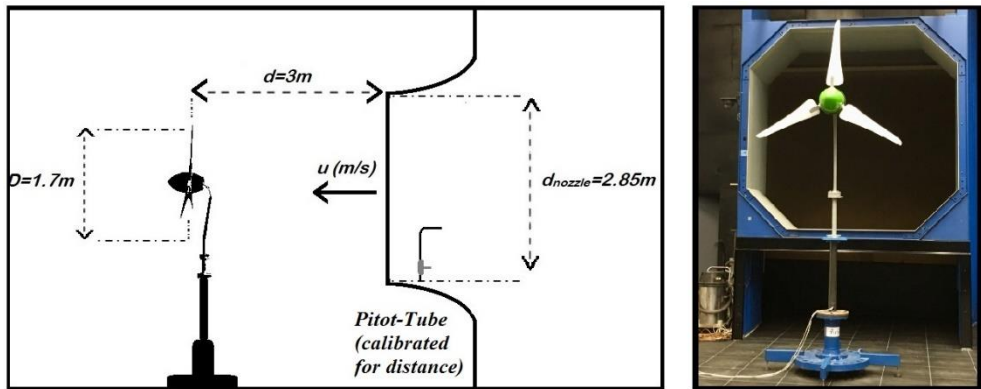


Figure 2 - 6 : (right) Micro wind turbine placed in front of the nozzle of Open Jet Facility in TU Delft (left) plan drawing of the distances

2.3 Results

The following section presents the equations and the results for all properties assessed

2.3.1 Influence of noise barrier on mean wind speed

2.3.1.1 Methodology

Sonic anemometers provide 3-dimensional wind velocity components. Mathematical equations are applied to estimate the metrics for assessing the wind flow conditions. In current case, U_x (m/s) horizontal wind speed component is perpendicular to the noise barrier, U_y (m/s) horizontal wind speed component is 90 degrees left and U_z (m/s) is the vertical wind speed component (see legend in Figure 2 - 2 and Figure 2 - 7).

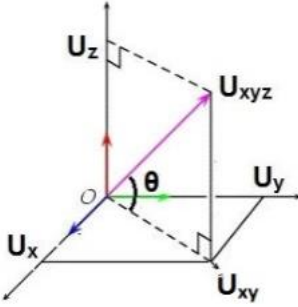


Figure 2 - 7 : The 3 components of wind speeds (m/s) U_x , U_y and U_z . The horizontal wind vector U_{xy} and the U_{xyz} resultant vector for the magnitude of wind speed together with the inflow angle $\theta(^{\circ})$

Wind speed U_{xyz} (m/s) is derived from all the U_x , U_y and U_z components recorded from the sonic anemometers, see Figure 2 - 7. Then these values are averaged with $n_{samples}$, which are the number of samples within 10-minutes (depending on sampling frequency) as seen in equation 2.1.

$$\overline{U_{xyz}} = \frac{\sum_{i=0}^{i=n_{samples}} \sqrt{U_{x_i}^2 + U_{y_i}^2 + U_{z_i}^2}}{n_{samples}} \quad (2.1)$$

Wind speed vector magnitudes are used to estimate the speed. Then wind speed magnitudes are compared at the height h (m) on top of the noise barrier ($U_{xyz,NoiseBarrier}$) with the reference pole at similar height ($U_{xyz,REFERENCE}$). Exponential fitting is used for the sonic anemometers not in same height of comparison. Wind speed magnitude is used later for energy yield calculations of micro-wind turbine installed on top of the noise barrier. Equation 2.2 shows the relative wind speed change ΔU_{xyz} (-).

$$\Delta U_{xyz}(h) = \frac{U_{xyz,NoiseBarrier}}{U_{xyz,REFERENCE}} \quad (2.2)$$

2.3.1.2 Results

A scatter plot of all the 10-minute averaged values is shown in Figure 2 - 8 for the sonic anemometer that is right above the noise barrier at 1.17H height (6.1 meters from ground). The wind speed bin from 0-1.5 m/s has a very large spread. Higher than 1.5 m/s a trend can be observed with wind speed reductions towards -90° and $+90^{\circ}$ which are parallel wind flow in respect to the barrier. When flow is nearly perpendicular to the noise barrier (-30° until -15°) a maximum increase is observed.

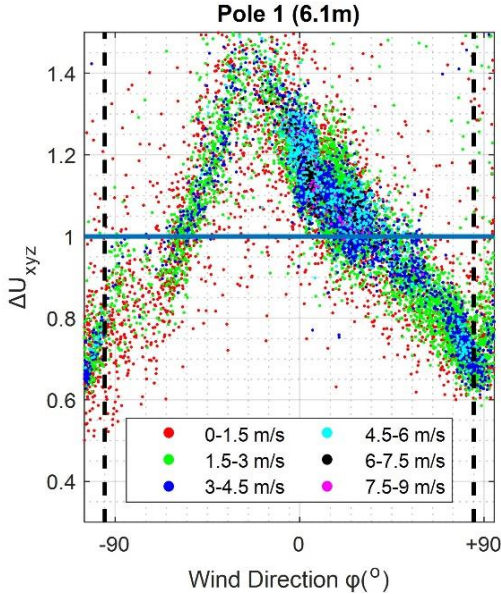


Figure 2 - 8 : Scatter plot of wind speed relative change (ΔU_{xyz}) for the sonic anemometer places at $1.17H$ (Pole 1 at 6.1 meters) on top of the noise barrier. All coloured dots represent different wind speed bins (see legend) with 0° being perpendicular

In Figure 2 - 9, the plot shows the wind speed differences for different heights. The data are categorized for 10° increments from -90° until $+90^\circ$, which is the windward side of the barrier. The most positive increase is observed in perpendicular flows (-30° until 0°) while it decreases in parallel flows in the edges of the graphs. The right part of both graphs is less steep while the left part is steeper, this might be attributed to the localized terrain.

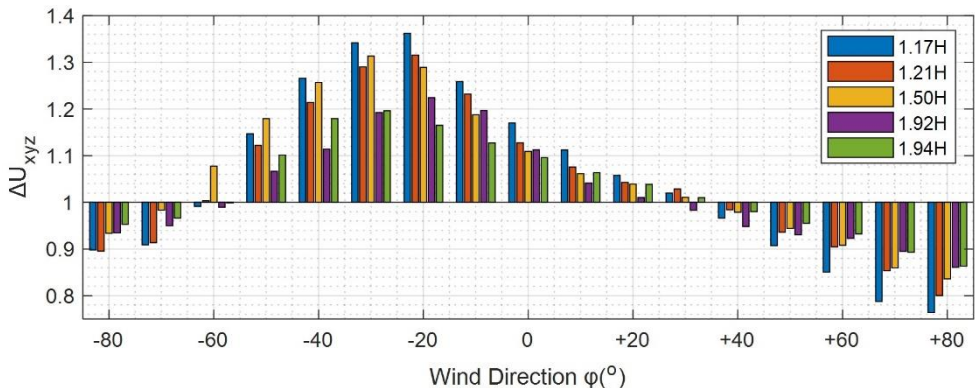


Figure 2 - 9 : Bar plot of wind speed relative changes for different directions and heights for the reference arc (-90° until $+90^\circ$) with 0° being perpendicular

The positive change is higher rather than negative with maximum of 1.35 (-20°) and minimum of 0.75 (+80°). In Figure 2 - 9, it is observed that the maximum changes do not occur in a perfectly perpendicular flow at 0° but at -20°. Similarly, at +20° there are no changes ($\Delta U_{xyz} \sim 0$), but when moving to more parallel flows relative to the barrier then a wind speed reduction is observed for both sides. These lead to recheck the calibration and positioning of the sensing equipment as well as the methods to assess the orientation of the barrier but no abnormalities were found. Therefore, a hypothesis is made that pressure reduction due to the presence of the bridge shown in Figure 2 - 3 (at direction -40° until -10°) might lead to this shift of the localized maxima. Results of Figure 2 - 9 for the wind direction of 0° match well the references presented in Section 2.1, where most authors observed increases from 5%-35% in wind speed on top of windbreaks.

2.3.2 Influence of the noise barrier on inflow angle

2.3.2.1 Methodology

Inflow angle $\theta(^{\circ})$ is used to estimate the wind turbine's rotor flow misalignment losses. The $\theta_i(^{\circ})$ inflow angle for the time step(i) is calculated using the resultant vector U_{xy} of the horizontal wind components U_x and U_y (equation 2.3) and the vertical wind component U_z with the arc tangent function in equation 2.4. When every angle is estimated for the 10-minute period then an averaging is performed.

$$U_{xy_i} = \sqrt{U_{x_i}^2 + U_{y_i}^2} \quad (2.3)$$

$$\theta_i = \arctan\left(\frac{U_{z_i}}{U_{xy_i}}\right) \quad (2.4)$$

Several studies have been conducted that investigate the flow misalignment effects (mostly from yaw misalignment) in loads, power performance just like in [46] where it is found that power losses can be as much as 30% at 30° misalignment. Therefore, inflow angle describes the flow misalignment of a potential installed rotor on top of the barrier and it used to estimate the affected energy yield. Micro wind turbines have usually a tip vane or are designed to self-align with the flow in order to minimize the yaw misalignment losses but when the inflow angle varies in the vertical component there is not such a mechanism to allow the rotor to align. Thereby, the vertical component is estimated in order to derive the losses resulting from the inflow angle θ° as in Figure 2 - 10. The energy yield is further estimated with the magnitude of the U_{xyz} (m/s) and the effect of inflow angle $\theta(^{\circ})$ as a misalignment loss.



Figure 2 - 10 : Wind speed $U_{xyz}(m/s)$ magnitude vector and the inflow angle θ ($^{\circ}$), illustrated for a perpendicular flow indicating the presence of sonic anemometers with red stars in different heights for Pole 1

2.3.2.2 Results

Inflow angle θ ($^{\circ}$) when skewed affects the power performance of the micro wind turbine. Figure 2 - 11 presents a time series of 2 seconds (4Hz sampling) of the flow field between the reference pole and Pole 1. [47] and [48] have visualized the effects on wind flow in front of wall structures with an emphasis as well on the periodic swell and shed in front of the noise barrier as well as the separation bubble behind the noise barrier. The intention here is different as data are presented only at the installation height of micro wind turbines and do not focus on more specific flow properties related to turbulence behaviour studies.

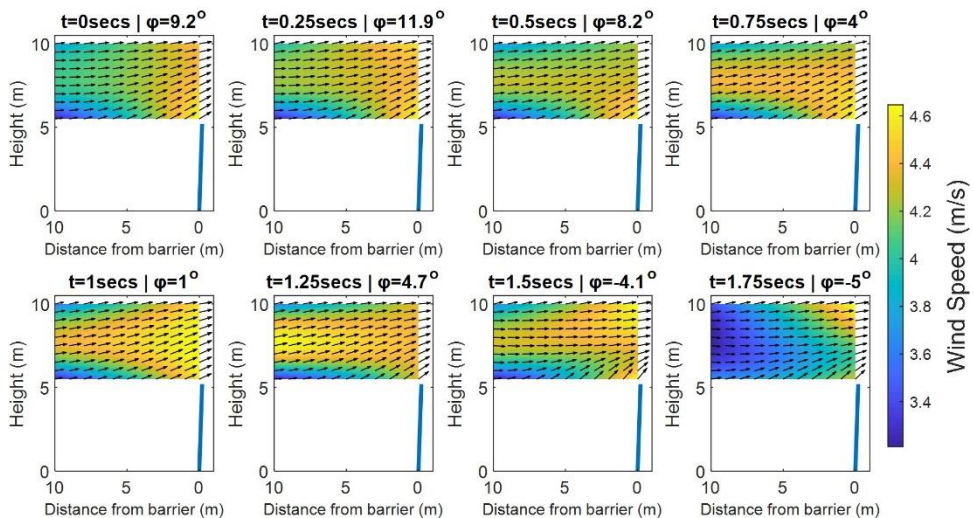


Figure 2 - 11 : Time series (2 secs - 4Hz) of wind field contour (blue-yellow) and quiver plot (black arrows) for the noise barrier near-perpendicular flows $\varphi = (-5^{\circ}+10^{\circ})$. Distance from barrier is 0 at reference and 10 on top of the barrier.

Contour and arrows are constructed using 6 points (Reference Pole and Pole 1 anemometer height locations in Figure 2 - 11). First, vertical exponential fit is performed for the wind shear and second a horizontal fit between poles. Blue towards yellow contour on the back represents instantaneous wind speed U_{xyz} (m/s). Black arrows overlaid represent inflow angle. The representation is questionably oversimplified and neglects many wind flow phenomena happening between the 2 poles such as vortexes, especially in front of the noise barrier. It simply illustrates the averaged flow parameters. In particular, wind speeds increase (blue contour becomes yellow) in perpendicular wind directions to the barrier ($\varphi=-5^\circ$ until $\varphi=10^\circ$). Inflow angles θ (black arrows) have a tendency to move upwards and surpass the barrier thus high inflow angles. Finally, the variability of wind speed and the stochastic nature of wind can be seen in these time series.

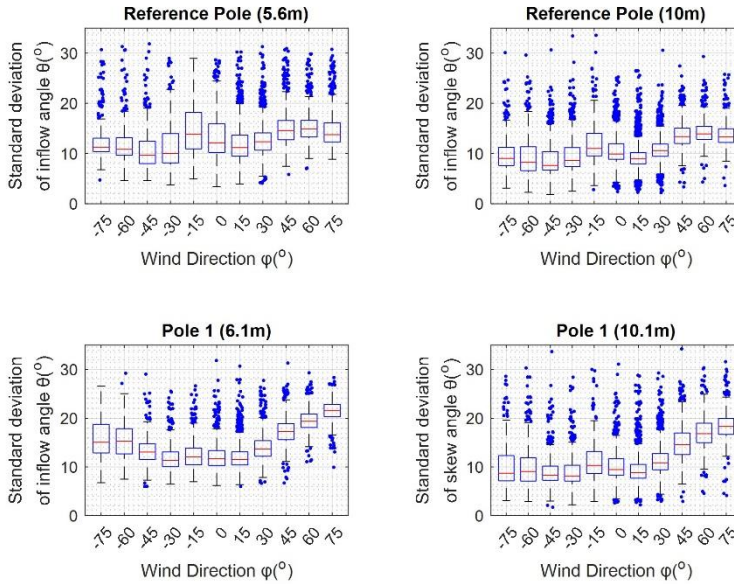


Figure 2 – 12 : Box plots indicating the 10-minute standard deviation of the skewed inflow angle θ ($^\circ$) for the sonic anemometers placed (top) on the reference pole (bottom) and noise barrier at pole 2 at different heights

Large variations in inflow angle mean more variations in power due to the more frequent misalignment of the rotor with the skewed flow leading to lower aerodynamical performance coming from the reduction of the $\cos^3\theta$ rule [49]. Therefore, it is worthwhile presenting the standard deviation of the inflow angle.

Figure 2 – 12 shows that standard deviation of inflow angle θ ($^\circ$) increases at the edges of the box plots for Pole 1 which represents the parallel to the barrier flows. Also, in perpendicular flows (near 0°) a decrease of the standard deviation is observed for Pole 1 comparing with the Reference Pole for all heights. Boxes represent the values in

between the 25th and 75th percentile of each data bin. The line in between the boxplot is the median value. The whiskers include all values that are in between 1.5 times the interquartile range, while the outliers are plotted using a spatial randomization with Jitter function for better visuals.

Figure 2 - 13 presents the 10-minute averaged inflow angle for 3 heights h (m) and different wind direction φ ($^{\circ}$) bins. For 1.17H a maximum of 22° is observed at -15° wind direction. For 1.50H inflow angle has a maximum of 17° and for 1.94H it is 8° . This result could be compared with the wind tunnel experiment and CFD study [50] which similarly showed increase in inflow angle on the tip of the barrier. A trend is observed that in parallel flow (close to -90° and $+90^{\circ}$) inflow angle decreases and especially near the -90° region. Due to this drop, a comment is made that the terrain next to the installed poles as in Figure 2 - 3 and the complex road topology with a small bridge and an air-hang noise barrier segment might be factors of lower wind angles present for both poles above the barrier, similarly as with the shift of localized maxima for wind speed.

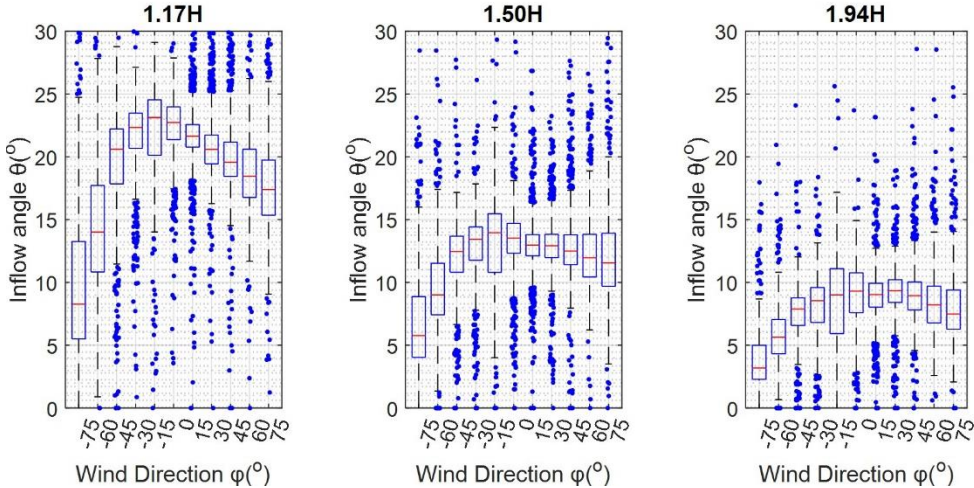


Figure 2 - 13 : Box plots of 3 different heights of the 10-minute averaged inflow angle θ ($^{\circ}$) for different wind directions φ ($^{\circ}$)

2.3.3 Influence on Turbulent Intensity

2.3.3.1 Methodology

Turbulence intensity TI_{xyz} (%) of the U_{xyz} (m/s) magnitude is determined using the ratio of the 10 min. average mean magnitude of U_{xyz} (m/s) (as shown in equation 2.1) and the Standard Deviation $\sigma_{u_{xyz}}$ (m/s) of each 10-min dataset as shown in equation 2.5.

$$TI_{U_{xyz}} = \frac{\sigma_{U_{xyz}}}{U_{xyz}} \quad (2.5)$$

2.3.3.2 Results

In Figure 2 - 14, a comparison is made between the turbulence intensities of 2 sonic anemometers. It ranges between 20-40% for perpendicular (-30° until +15°) and 40-60% for parallel flows (-75° until -60° and +60° until +75°). Spread of TI is greater for wind speeds (<2 m/s). Box plots are used and their property interpretation is found in section 2.3.2.2. Parallel flows at the tip of the noise barrier exhibit increases in turbulence intensities. Flow mixing on top of the barrier might lead into more turbulent flow structures. Decrease of turbulence intensity happens in perpendicular flows. A hypothesis is that large pressure difference before and after the noise barrier leads to increased wind mass flow (thus increase in wind speed) and thereby decreases the turbulence intensity as its value depends on the average mean wind speed on the denominator.

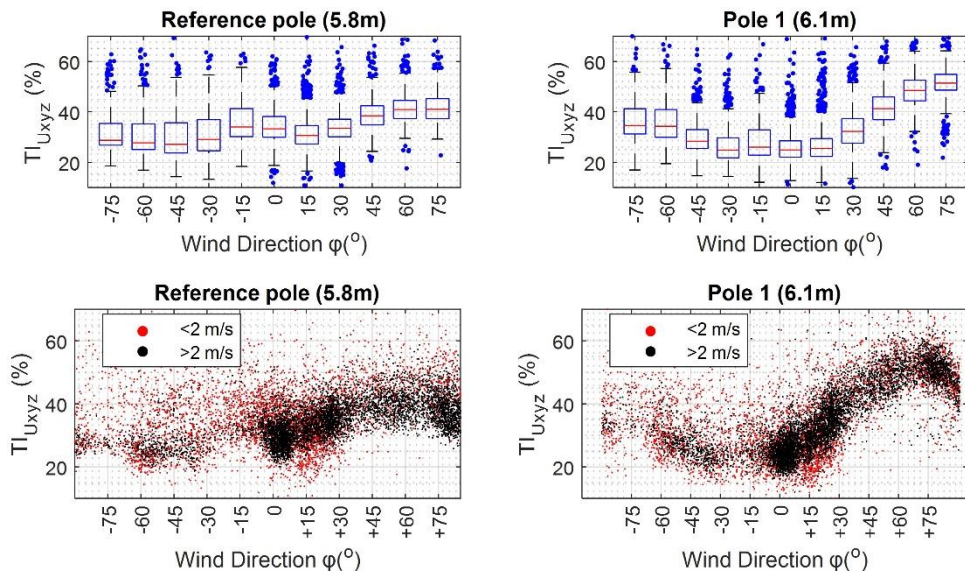


Figure 2 - 14 : Box plots of the turbulence intensity TI (-) of the lowest sonic anemometers (5.8m and 6.1m) for the reference pole and the noise barrier (Pole 1) (box area is 25th and 75th percentile)

As discussed in Section 2.3.3, turbulence might lead to power variations. Positive effect of high turbulence could occur in lower wind speeds, leading to greater power and more chances for the rotor to continue idling thus increasing the chances of reconnecting and generating useful power. Turbulence intensity is a factor to take into account as urban environment wind speeds tend to be rather low. However, these are not used in the energy yield estimation as more detailed modelling approach would be required to correct the power performance of the wind turbine for certain ranges of turbulence intensity.

2.3.4 Annual Energy Production sensitivity analysis and results

Literature identifies wind resource assessment as very important as current tools could overestimate the energy yield of wind turbines [35]. A sensitivity analysis for the wind turbine yield is performed using the corrections from the results of the assessment on wind speed and inflow angles for the energy yield.

2.3.4.1 Sensitivity analysis parameters

The Annual Energy Production (AEP) in kWh is estimated for 3 different heights above the noise barrier (1.94H, 1.55H and 1.17H) based on the heights of the anemometers on Pole 1. The annual time series wind rose is rotated in steps of 20° for a full 360° rotation by keeping the noise barrier still as in Figure 2 - 15, where δ ($^\circ$) is the rotation angle that is applied in each time step of the annual time series. Therefore, for each wind field rotation angle δ ($^\circ$) only the relative wind direction φ_i ($^\circ$) with respect to the noise barrier would change and the effects on the total Annual Energy Production are estimated.

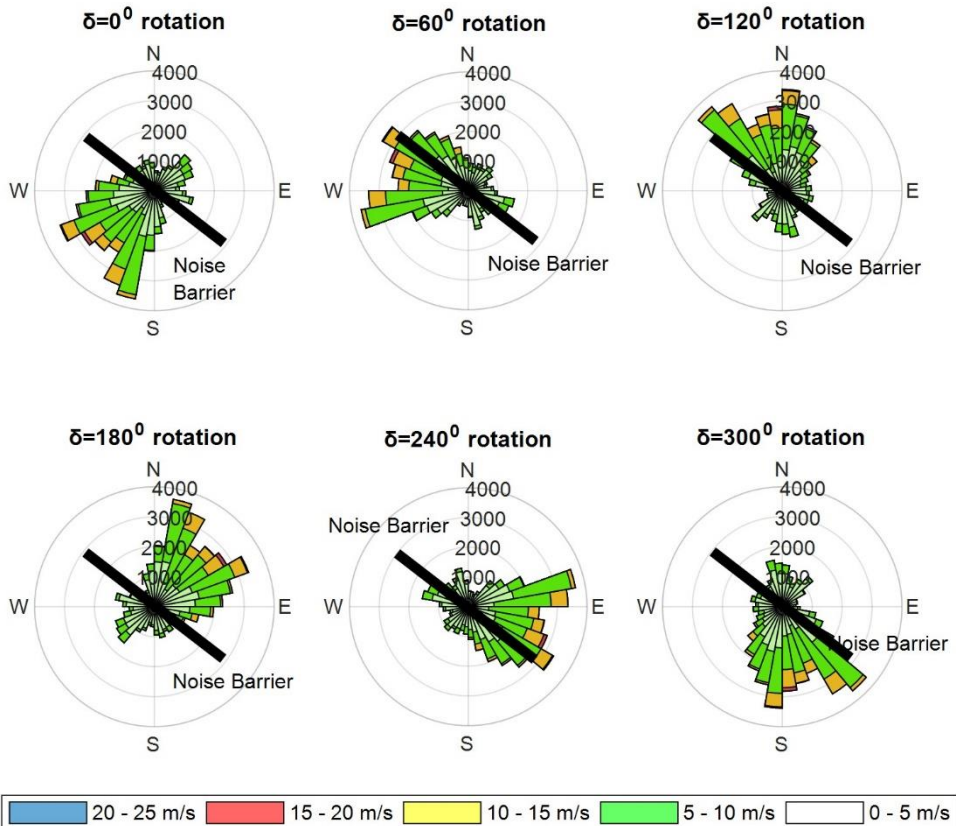


Figure 2 - 15 : Binned wind speed rose rotation by angle δ (clockwise) for the sensitivity analysis. Black line indicates the noise barrier. Legend indicates the wind speed bins

2.3.4.2 Methodology

The baseline Annual Energy Production (AEP) of a micro wind turbine on top of the noise barrier is calculated with a 12-month 10-minute wind speed and direction record from Rotterdam Airport resulting in 52560 entries [51]. Wind speed correction is applied for the differences in surface roughness between the two locations, resulting in wind time series at the reference pole U_i (m/s). Another correction for effects of the noise barrier on wind speed and inflow angle is used. Finally, through a look up table is used to find the energy yield of a reference micro wind turbine (375 Watts) for each time step that corresponds to the corrected wind speed. Energy yield of the wind turbine is based on wind tunnel measured power curve. Wake losses are excluded as the evaluation of the performance is done for a single turbine rather many installed on top of noise barriers. Finally, all time steps values are summed to derive the Annual Energy Yield (AEP) in kWh.

The annual free stream energy yield, AEP_0 (kWh) at a height h (m) from ground is without the influence of noise barrier and is used as a reference for comparison, shown in equation 2.6. For the sum of those 52560 10-min entries the corrected wind speed U_i (m/s) at the height h (m) of turbine installation are used.

$$AEP_0(h) = \sum_{52560}^{i=1} E_i(U_i(h)) \quad (2.6)$$

The AEP (kWh) is then corrected for speed-up associated effects from the noise barrier. The wind speed factor ΔU_{xyz} (-) is then applied from section 2.3.1. This varies as a function of the relative wind direction φ_i ($^\circ$) and is applied to the wind speed U_i (m/s). The resulting annual energy yield is AEP_1 (kWh), which includes noise barrier wind speed magnitude ΔU_{xyz} effects and assumes an aligned rotor with the skewed incoming flow on top of the noise barrier. In reality this is not true, but with this variable the effects can be isolated due to skewed angle flow misalignment and the relative change in wind speed due to the noise barrier. AEP_1 (kWh) is estimated for different heights h (m) and different wind field rotation angles δ ($^\circ$) as part of the sensitivity analysis, shown in equation 2.7.

$$AEP_1(h, \delta) = \sum_{52560}^{i=1} E_i(\Delta U_{xyz}(h, \delta, \varphi_i) \cdot U_i) \quad (2.7)$$

Finally, AEP_2 (kWh) contains the additional correction for misalignment losses due to the skewed inflow angle. This is done applying the $\cos^3\theta$ correction at each time step. This is mostly used for yaw misalignment [49] but in this case it is applied for the skewed flow misalignment.[52] found $\cos^3\theta$ as a good approximation for normalized power but it slightly underestimates power while the $\cos^2\theta$ theory slightly

overestimates power. In the approach the more conservative yaw correction $\cos^3\theta$ law is used. AEP_2 (kWh) is estimated for different heights h (m) and different wind field rotation angles δ ($^\circ$) as part of the sensitivity analysis, shown in equation 2.8.

$$AEP_2(h, \delta) = \sum_{52560}^{i=1} (E_i(\Delta U_{xyz}(h, \delta, \varphi_i) \cdot U_i) \cdot \cos^3 \theta_i) \quad (2.8)$$

The relative impact on AEP of speed-up associated with the noise barrier can be expressed as: $\eta_{aligned}$ (-), which is the ratio that describes the influence of the noise barrier to the wind speed vector magnitude expressed in energy terms, shown in equation 2.9.

$$\eta_{aligned}(h, \delta) = \frac{AEP_1(h, \delta)}{AEP_0(h)} \quad (2.9)$$

Similarly, the relative impact of flow misalignment due to the inflow angle is expressed as: $\eta_{misaligned}$ (-), which is the ratio that describes the losses in energy due to the misalignment of the rotor with the incoming skewed flow, shown in equation 2.10.

$$\eta_{misaligned}(h, \delta) = \frac{AEP_2(h, \delta)}{AEP_1(h, \delta)} \quad (2.10)$$

Finally, the overall impact on AEP is expressed as: $\eta_{nbttotal}$ (-), which is the ratio that describes the total influence of the noise barrier, taking into account both the influence to the wind speed but also accounting for the skewed flow misalignment effects. See equations 2.11 and 2.12.

$$\eta_{nbttotal}(h, \delta) = \frac{AEP_2(h, \delta)}{AEP_0(h)} \quad (2.11)$$

$$\eta_{nbttotal} = \eta_{aligned} \times \eta_{misaligned} \quad (2.12)$$

In order to derive all above-mentioned variables, the measured power curve in the wind tunnel is used.

Power Curve:

Below you can see the measured power curve in the wind tunnel and the validation with the manufacturer's data. Whiskers indicate error margins of the sensor

equipment and different measurements performed. Power curve is used as a look-up table for the Annual Energy Production (AEP) estimations.

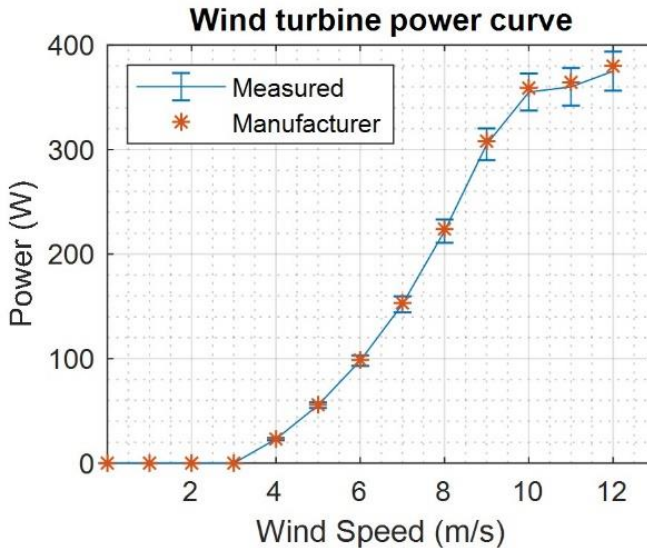


Figure 2 - 16 : Power curve of the WindChallenge micro wind turbine recorded in the OJF wind tunnel experiment and compared with manufacturer's

Wind speed corrections

Corrections are applied based on local roughness (the site is 3 kilometres away from the weather station) in order to translate it for the noise barrier case before applying corrections for the noise barrier. First, the weather station time series wind speed of time step i is translated to a blending height and then to the height of the reference pole.

- The wind speed dataset from the airport is translated to a blending height of 60 meters with log wind law in equation 2.13. Local roughness parameters are being taken into account. Rotterdam airport weather station is placed on flat terrain area without presence of obstacles and therefore the roughness length is assumed to be 0.03 [53] while zero-displacement is 0. Blending height h_2 (60m) and weather station height h_1 (10m) are used.
- Wind speed at blending height is then translated to the three hub heights of Pole 1 at the noise barrier. Table 2 – 1 presents zero-displacement height d and roughness length z_0 which have been determined with an empirical approach from wind gradient data of the reference pole for the windward side in Figure 2 - 3. For the downwind side of the barrier as seen in Figure 2 - 3 they were determined by the elevation, the terrain and the surrounding landscapes taking into account the [53] classifications because of lack of reference data from measurements.

$$U_i = U_{ref} \times \frac{\ln\left(\frac{h_2 - d}{z_0}\right)}{\ln\left(\frac{h_1 - d}{z_0}\right)} \quad (2.13)$$

Table 2 - 1: Surface parameters of the study area as a function of wind direction sector. Empirical data from -90° until +90°. For data with asterisk * [53] classification used.

Sector(°)	d(m)	z ₀ (m)
(-180°) to(-150°)*	2.30	0.20
(-150°) to(-120°)*	2.00	0.19
(-120°) to(-90°)*	2.60	0.26
(-90°) to(-60°)	3.00	0.75
(-60°) to(-30°)	2.00	0.16
(-30°) to(0°)	3.10	0.09
(0°) to(+30°)	3.00	0.08
(+30°) to(+60°)	2.30	0.22
(+60°) to(+90°)	1.70	0.15
(+90°) to(+120°)*	1.90	0.18
(+120°) to(+150°)*	2.00	0.20
(+150°) to(+180°)*	2.20	0.18

Noise barrier correction factors

Corrections on wind speed due to noise barrier are applied based on results in section 2.3.1. Wind speed is multiplied at each time step with ΔU_{xyz} for the corresponding relative wind direction φ_i with the barrier which depends on the wind direction from the dataset used [51]. Effects for the downwind side of the noise barrier (symmetry) are “mirrored” since the effects are recorded only from the upwind side of the barrier. Despite the fact that it is a questionable assumption because the noise barrier is not erected vertically but with a given angle to the vertical, it had to be assumed because experimental data are only available for 1 side of the barrier. Thereby, the same effects are assumed on the other 180° arc behind the barrier. For example, if at a certain time step wind comes from +100° then the effect is mirrored while the correction factors are used from results that apply for +80°. Similarly, from -150° a correction is considered with results from -30°. The correction factors used are the $\Delta U_{xyz}(\varphi_i)$ for wind speed used for AEP₁ and AEP₂ and the $\theta(\varphi_i)$ for skew corrections in AEP₂. Finally, each relative wind direction φ_i is corrected with respect to the wind field rotation angle δ (°) because the wind direction relative to the noise barrier for each rotation would change according to the rotation angle and thereby the effects on wind speed would change accordingly.

2.3.4.3 Results

Energy yields in top graph of Figure 2 – 17 show the sensitivity of energy output of a wind turbine on top of a barrier for wind field (wind and direction dataset) rotations of 20° including the noise barrier effects. The misaligned energy yield (AEP_2) is always lower as they contain effects on wind speed magnitude and inflow angle. For the aligned energy yield (AEP_1), the effects only on wind speed magnitude are considered assuming that the rotor is always pointing at the resultant wind vector. Annual energy production at $1.94H$ ranges from 400-600 kWh with some localized maximum and minimum points which depend on orientation of the noise barrier (projected from the wind field rotation). For $1.50H$ installation height, energy ranges from 300-550 kWh and for $1.17H$ ranges at 150-430 kWh. Installing the turbine closer to the barrier has more uncertainty as the ranges are more widespread. Total annual energy production is very sensitive to relative noise barrier rotation angle with the wind rose. In Figure 2 – 17 bottom graph, annual energy production is compared with the straight line (reference yield). Positive effect is mostly observed but there are cases with significant drop in energy yield (40° , 60° , 80° , 140° , 220° , 260° and 280°). Importance of site assessment is shown between 120° and 160° , where only for a range of 40° a difference from 600kWh to 400kWh is observed.

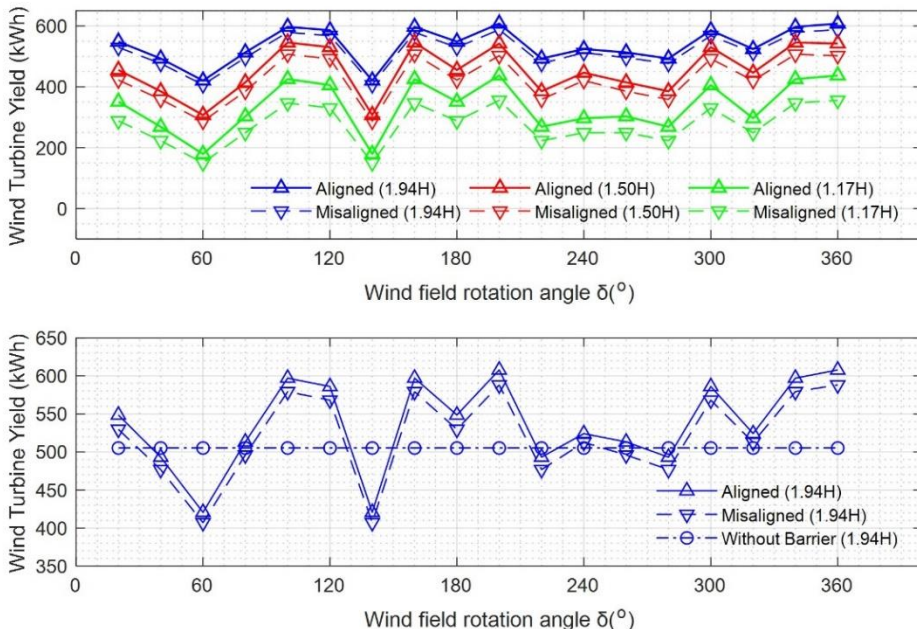


Figure 2 – 17 : (top graph) Sensitivity analysis of total annual wind turbine yield for an aligned and misaligned flow towards a micro wind turbine installed on top of a noise barrier at different heights and for 20° increments of wind field rotation (bottom graph) Without Barrier, aligned and misaligned flow total annual wind turbine yields for 20° increments of wind field rotation

In Figure 2 - 18, the dominant effect on wind energy yields for each noise barrier orientation is explained. The $\eta_{nbtotal}$ (%) is mainly affected by the wind speed magnitude changes as seen in the left graph with $\eta_{aligned}$ (%) while the flow misalignment $\eta_{misaligned}$ (%) always contributes in a negative way but to a less extent. In particular, for the effect of the wind speed magnitude and especially for installation heights of 1.17H, the energy yield could range from 60%-150% of the reference total annual energy yield. For 1.50H, the ranges are 75%-140% and for 1.94H, the ranges are 85%-120%. The effect of inflow angle leading to a misaligned rotor to the flow in middle graph of Figure 2 - 18 increases closer to the barrier as the inflow angle increases. But overall, it influences energy yield to a less extent with respect to the wind speed magnitude changes. For 1.94H, the total energy yield is $\sim 97\%$ of the reference yield while for 1.75H is $\sim 92\%$ and for 1.55H is $\sim 83\%$. Finally, the total energy yield with all the noise barrier related effects is compared with the free stream wind turbine energy yield. This is presented with the $\eta_{nbtotal}$ (%) in Figure 2 - 18. The lowest position at 1.17H noise barrier height is the less profitable attributed mainly to the flow misalignment losses. The other 2 height locations are either marginally positive or negative with ranges from 90%-120%. For the increments from 250° - 300° the performance is greatly and negatively affected at 30-60% of the free stream energy.

The conclusion from the results is that noise barrier can have both negative and positive influence on energy yield depending on its orientation to the wind field. Installers should be very careful designing such systems, paying great attention to the wind resource assessment and energy yield estimation including noise barrier effects.

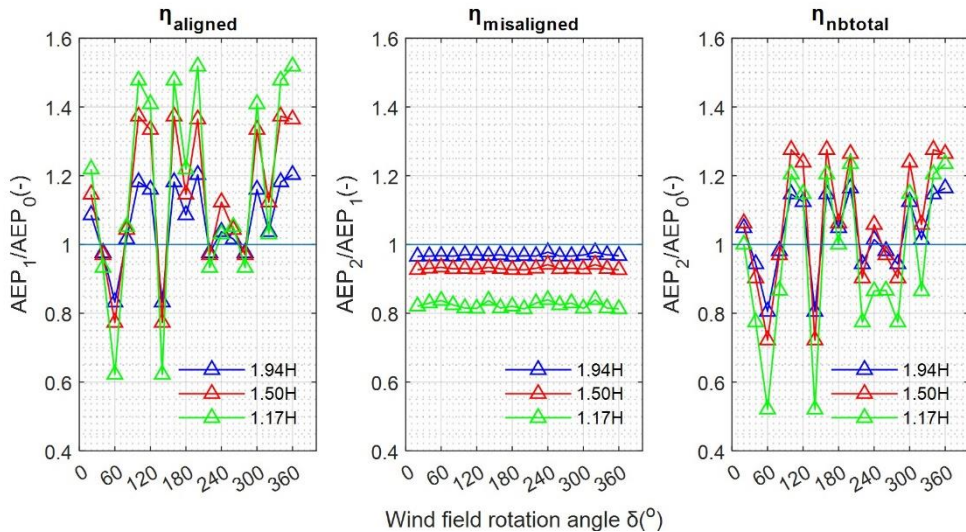


Figure 2 - 18 : (left) Change in annual energy yield (AEP) on top of the noise barrier as a function of the wind field rotation angle $\delta(^{\circ})$ (left) not taking into account skewed inflow angle $\theta(^{\circ})$. (middle) due to the skewed flow misalignment taking as a reference the energy yield of the aligned flow (right) taking into account both effects

Finally, Table 2 – 2 summarizes the results for the reference case of the existing noise barrier.

Table 2 - 2: Case study for the current noise barrier orientation

Case study of the current noise barrier (corresponding to wind field rotation angle 360°)			
	1.17H	1.50H	1.94H
Total annual energy yield without noise barrier effects (kWh)	290	395	505
η_{align} (-)	1.51	1.36	1.20
$\eta_{misaligned}$ (-)	0.81	0.92	0.96
η_{nbtot} (-)	1.22	1.25	1.15
Noise barrier Influenced Yield (kWh)	354	494	580

In Table 2 – 2, the influence of the noise barrier in the total annual wind turbine yield for all heights 1.17H, 1.50H and 1.94H is positive. An overall increase of 22%, 25% and 20% for these heights is observed respectively. Increase due to wind speed magnitude is greater than these numbers but the skewed flow misalignment with the micro wind turbine rotor leads to a slight decrease by 80%, 92% and 96% of the yield that was estimated taking into account only the wind speed magnitude increases. This case is positive but in a different noise barrier orientation with the same wind field there is possibility for negative influence of the energy yield as the case of 60° wind field rotation with the turbine producing 50%, 70% and 80% of the reference.

2.4 Discussion

Here a discussion is made relevant to the results and a discussion about the economics of micro wind turbines on noise barrier with respect to the results is made.

2.4.1 Wind resource characteristics

Some noise barriers are placed in complex topologies near highways, with elevated roundabout and other elements. [54] studied effects of such hills in wind tunnel and found that wind speeds increase when flows are perpendicular to the ridge of hills. However, expansion of wind resource assessment to cover those cases as well is needed. Finally, regarding local wind flow characteristics, the shift in localized maxima (probably explained by the presence of the bridge) is intriguing a suggestion for further wind tunnel validation along with numerical modelling and CFD calculations in order to derive a concrete model for relevant flows.

Designing turbines in different way might alleviate skewed inflow angle effects. For example, predefined wind turbine hub angles could alleviate these losses. But new loading types will start affecting the operation of the turbine (e.g. gravitational). Results in Figure 2 - 13 showed that the turbine on top of the noise barrier would be mostly exposed to skewed flow between 5°-25°. As horizontal axis wind turbines

underperform in skewed flow and vertical axis wind turbines seem to have better power performance coefficient [25]. A hypothesis is made that there is potential for further energy yield increase with vertical axis wind turbines.

Turbulence intensity (TI) decreases for perpendicular flows while wind speeds increase and vice-versa TI decreases for parallel flows while wind speeds tend to decrease. Literature suggests that increased turbulence intensity might lead to more energy production for low wind speed ranges of near ground applications and less energy production in higher wind speeds near rated. So since parallel flows have increased TI and decreased wind speed and perpendicular flows decreased TI and increased wind speed, a hypothesis could be made that the changes of the noise barrier to the Turbulence Intensity could have a positive effect in energy yield. But this would require further investigation. Finally, the impact of TI (%) in lifetime, fatigue, loading and O&M costs should be determined as well. As turbulence intensity might induce potential harmful excitations in the loading of the system and thus decrease lifetime and increase O&M costs.

2.4.2 Economic analysis and energy yield

Proper siting of turbines and local characteristics can affect greatly the energy yield. Even a slight change in the relative angle of the noise barrier with the local wind rose could have dramatic changes in the energy yield as seen in the results in Figure 2 - 19. This is very relevant for noise barriers on curved road passages where the relative wind field rotation angle could vary significantly (such as seeing from top in Figure 2 - 3). This is quite important for infrastructure designers who need to take decisions to install energy systems that are financially attractive.

Closing the economic loop in section 2.4, a preliminary estimation of the Levelised cost of electricity is conducted for a micro wind turbine on top of a noise barrier and is also compared to a reference case. It is presented in the equation 2.14 below based on [55]. An assumption of $n=20$ years lifetime is considered for the installed turbine and a discount rate $i=0.04$. The reference LCOE is estimated including the I_t investment costs (or else CAPEX) and the O&M costs spent in year t . The investment costs I_t (€) is assumed in the order of 7000 €/kW installed. Annual O&M costs are assumed 1-2% of the CAPEX [56]. The AEP_0 is the reference energy yield excluding the noise barrier. It should be noted that this is not the analytical economic analysis of this Thesis as Chapter 4 contains all the details. This analysis presented in this Section is just to present the sensitivity of cost.

$$LCOE_{reference}(h) = \frac{\sum_{t=1}^n (I_t + O \& M_t) \frac{1}{(1+i)^t}}{\sum_{t=1}^n AEP_0(h)} \quad (2.14)$$

Then the LCOE is calculated of a turbine installed at 3 different heights $h(m)$ and for various wind field rotations as used before. For the new LCOE, in equation 2.15, the annual energy yield AEP_2 is taken into account, which includes the effect of the noise barrier of each height and wind field rotation. A 20% cost reduction is assumed in the investments as $\kappa_{reduction}$, due to exclusion of foundation and allocation of other costs of electrical infrastructure, installation, permitting, transportation, logistics and other costs as defined in [56], and the findings of [57] with respect to lowering costs when retrofitting micro wind turbines on roofs.

$$LCOE(h, \delta) = \frac{\sum_{t=1}^n (I_t \cdot \kappa_{reduction} + O \& M_t) \frac{1}{(1+i)^t}}{\sum_{t=1}^n AEP_2(h, \delta)} \quad (2.15)$$

Finally, the reference LCOE is compared with each calculated one with equation 2.16.

$$LCOE_{change} = \frac{LCOE(h, \delta)}{LCOE_{reference}(h)} \quad (2.16)$$

LCOE(€/kWh) decreases in most wind field rotation cases and different heights and is between 60-90% of the reference. Even though this is an overgeneralized interpretation it is a positive result meaning that with such a cost reduction and installation on a barrier higher energy yields and lower electricity costs could be expected. However, there are still cases in Figure 2 - 19 where LCOE increases with a sensitive deviation such as between $\delta=1200$ and $\delta=1600$. Finally, the reference LCOE are 0.30€/kWh for 1.94H, 0.38€/kWh for 1.50H and 0.52€/kWh for 1.17H.

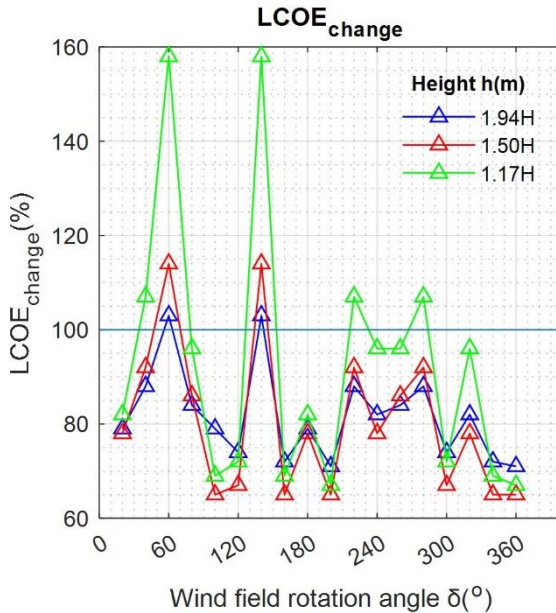


Figure 2 - 19 : LCOE change for different wind field rotation angles δ ($^{\circ}$) and heights h (m)

2.5 Conclusions

To answer the research question of “What is the wind resource that micro wind turbines will experience when integrated on top of noise barrier highway infrastructures?”, sonic anemometers were installed on top of a noise barrier and on a reference location to assess the effect of the noise barrier on the wind flow for all windward wind directions φ ($^{\circ}$). The properties of wind speed magnitude U (m/s), turbulence intensity TI (%) are assessed and compared. Additionally, the inflow angle θ ($^{\circ}$) is being assessed for its influence on the annual energy production AEP (kWh). A sensitivity assessment of the annual energy yield with a wind field rotation angle δ ($^{\circ}$) based on these results has been made for the application of a micro wind turbine installed on top of the noise barrier. Finally, the effect on the Levelised cost of electricity $LCOE$ (€/kWh) is presented.

The most important findings that answer the question are summarized in the following bullet points:

- Wind speed on top of noise barriers increases in perpendicular flows. The maximum increase of 36% is found at 1.19H and a 20% increase at 1.94H, with H representing the height of the barrier.
- Wind speed on top of noise barriers is decreasing in parallel flows with maximum decrease of 27% at 1.19H and 20% at 1.94H.

- Inflow angle is always skewed for all wind flow direction towards the barrier. The averages are in the range of 5° (at higher heights) to 25° (at lower height towards the barrier tip).
- Terrain and road network layout near a noise barrier affect the symmetry of changes that the barrier induces to approaching flows. Presence of a small bridge next to the barrier probably influences and shifts the local maxima of the changes, especially for wind speed and inflow angle.
- Turbulence intensity on top of a noise barrier for perpendicular flows (-30° until $+15^\circ$) drops with respect to the Reference Pole from 28%-40% to 22-32%. For parallel flows towards the barrier at ($+60^\circ$ until $+90^\circ$) the turbulence intensity range increases from 35-45% to 36-55%. For parallel flows (-60° until -90°) and ($+60^\circ$ until $+90^\circ$), it increases from 25%-35% to 25%-42%, with respect to the freestream reference pole turbulence intensity ranges.
- Annual Energy yields could vary greatly even within 20° of wind field rotation from 110% down to 80% and back to 115% of the reference yield value. Installers are advised to perform wind resource assessment before installing.
- Effects on wind speed magnitude have the greatest contribution in the relative change in energy yield ranging from 60%-150%. Skewed inflow angle losses should also be included as described before and range from 80%-95% as a loss.
- Different combinations of height of installation and noise barrier (potential) orientation could bring variation in energy yield from 100-600 kWh for a 0.375kW micro wind turbine

Electricity cost reduction is possible for micro wind turbines on noise barriers due to the 20% investment cost reduction from structural integration and the energy yield increase due to the noise barrier flow effects. LCOE can drop to 60%-90% of the reference value. When the wind field annual time series is rotated in order to assess the sensitivity with respect to the noise barrier orientation, it is found that LCOE can dramatically change even in 20° increments of rotation. Finally, when comparing micro wind energy projects of the like with onshore wind energy, it is clearly seen that micro wind energy is more expensive.

As presented in Figure 2 - 19, LCOE could potentially decrease considerably but is very sensitive on the noise barrier relative angle to the wind rose (expressed in rotation angle $\delta(^\circ)$). This is quite positive for micro wind energy generation. However, a potential of 17.7 MW of micro wind energy generation exists for cases on top of noise barriers in the Netherlands. This is quite a small number comparable to 6 wind turbines of ~ 3 MW, and is at a very low competitive level comparing to onshore wind prices of nearly 0.05 €/kWh [58]. Therefore it is concluded that viability of such projects is quite limited and further cost reduction is needed for example by using larger rotors along highways. However, micro wind energy is still an important part of wind energy developments where various applications may be powered.

2.5 Recommendations – Future Studies

Based on results and all insight gained from the experiment and the data analysis process, the following recommendations are proposed. Some of those recommendations are implemented in this thesis while others are for future research:

- 1) Micro-wind turbine installation on noise barrier to evaluate the behaviour and estimate the energy yield (covered in current thesis in Chapter 3)
- 2) Wind tunnel testing to assess micro wind turbine's behaviour on misaligned flow conditions (covered in current thesis in Chapter 3)
- 3) Validation with more noise barrier sites and comparison with respect to surrounding roughness factors and zero-scale displacements and different year time series to assess the sensitivity (future research recommendation)
- 4) Measuring in more detail the influence of turbulence due to passing vehicles, as the examined noise barrier is placed on low-speed limit road and other noise barriers are in higher speed limit (future research recommendation)
- 5) Experimentation, modelling, analysis and correlation of the turbulent intensity effect of micro wind turbine yields on top of noise barriers (future research recommendation)
- 6) Wake flow studies from the dataset for all other flows (future research recommendation)
- 7) Validation of CFD studies of similar obstacles for urban flows or numerical simulations. (future research recommendation)
- 8) Other measurement techniques in order to capture detailed aspects of the relevant flows on top of the noise barrier (for example, smoke visualization, LiDar etc) (future research recommendation)
- 9) Experimental or modelling assessment of different turbine rotor sizes (pico/micro/small) and types, such as Vertical Axis Wind Turbines (VAWTs) or Diffuser-Augmenter Wind Turbines (DAWTs) (future research recommendation)
- 10) Discussion with local authorities for regulations regarding turbine installation next to highways. (future research recommendation)
- 11) Modelling of turbulence intensity impact on fatigue, loading, lifetime and O&M costs of the micro wind turbine integrated on top of a noise barrier. (future research recommendation)
- 12) Detailed economic analysis and survey with installation companies in order to identify installation, operation and maintenance costs of micro wind turbines integrated on noise barriers (covered to some extent in Chapter 5 of current thesis)
- 13) Wake losses in multiple turbines installation on noise barriers (future research recommendation)

2.6 References

1. Luo W., Lei X. and Wang Z. Wind energy utilization type load reduction sound barrier. 2016.
2. Luo W., Lei X. and Wang Z. Wind energy utilization type subtracts a year sound barrier. 2017.
3. S. C. Gi Sound proof wall having wind power generating function. 2009.
4. K. Changsoo Sound proof wall having wind power generating function. 2013.
5. (Province of South Holland) PZH. Miniwindturbine op geluidsscherm aan de N470 - Mini wind turbine on a noise barrier at N470 regional road. Province of South Holland: 2018.
6. G.J.W. van Bussel and S.M. Mertens. Small wind turbines for the built environment. 2005 In Proceedings of 4th European & African Conference on Wind Engineering, Prague, 11-15 July.
7. S. R. Allen, G. P. Hammond and M. C. McManus. Energy analysis and environmental life cycle assessment of a micro-wind turbine. *Proceedings of the Institution of Mechanical Engineers Part a-Journal of Power and Energy* **2008**, 222, doi:DOI: 10.1243/09576509jpe538.
8. Encraft. *Warwick Wind Trials Report*, Encraft, **2009**.http://www.microwindturbine.be/Rapportering_files/Warwick+Wind+Trials+Final+Report+%281%29.pdf
9. A. Orrell, N. Foster, S. Morris, et al. *2017 Distributed Wind Market Report*, U.S. Department of Energy/Office of Energy Efficiency and Renewable Energy/Wind Energy Technologies Office, 2017.<https://www.energy.gov/sites/prod/files/2018/09/f55/2017-DWMMR-091918-final.pdf>
10. R. Fu, D. Feldman, R. Margolis, M. Woodhouse and K. Ardan. *U.S. Solar Photovoltaic System Cost Benchmark: Q1 2017*, National Renewable Energy Laboratory (NREL), 2017; p vi.<https://www.nrel.gov/docs/fy17osti/68925.pdf>
11. K. Sunderland, M. Narayana, G. Putrus and M. Conlon. Levelised cost of energy analysis: A comparison of urban (micro) wind turbines and solar PV systems. In Proceedings of 51st International Universities Power Engineering Conference (UPEC); pp. 1-6.
12. Rijkswaterstaat. GIS data for Noise Barriers and Highways. Available online at: <https://www.rijkswaterstaat.nl/kaarten/geluidregister.aspx?cookieLoad=true>
13. WindLeaf. WindLeaf turbine specifications. Available online at: <https://windchallenge.com/the-windleaf/#specs>
14. J.K. Raine. *Modelling the Natural Wind : Wind Protection by Fences*. 1974.

Chapter 2

15. G. M. Heisler and D. R. Dewalle. Effects of Windbreak Structure on Wind Flow. *Agriculture Ecosystems & Environment* **1988**, 22-3, doi:DOI: 10.1016/0167-8809(88)90007-2.
16. Woodruff N. P., Read R. A. and Chepil W. S. *Influence of a field windbreak on summer wind movement and air temperatures*; 1959; pp. 24.
17. G. H. Chen, W. W. Wang, C. F. Sun and J. L. Li. 3D numerical simulation of wind flow behind a new porous fence. *Powder Technology* **2012**, 230, doi:DOI: 10.1016/j.powtec.2012.07.017.
18. I. Abohela, N. Hamza and S. Dudek. Effect of roof shape, wind direction, building height and urban configuration on the energy yield and positioning of roof mounted wind turbines. *Renewable Energy* **2013**, 50, doi:DOI: 10.1016/j.renene.2012.08.068.
19. W. Dierickx, W. M. Cornelis and D. Gabriels. Wind tunnel study on rough and smooth surface turbulent approach flow and on inclined windscreens. *Biosystems Engineering* **2003**, 86, doi:DOI: 10.1016/S1537-5110(03)00120-X.
20. A. Pena, A. Bechmann, D. Conti and N. Angelou. The fence experiment - full-scale lidar-based shelter observations. *Wind Energy Science* **2016**, 1, doi:DOI: 10.5194/wes-1-101-2016.
21. A. J. Bowen and D. Lindley. A wind-tunnel investigation of the wind speed and turbulence characteristics close to the ground over various escarpment shapes. *Boundary-Layer Meteorology* **1977**, 12, doi:DOI: 10.1007/bf00121466.
22. J. Rowcroft, D. Burton, H. M. Blackburn and J. Sheridan. Siting wind turbines near cliffs - the effect of wind direction. *Wind Energy* **2016**, 19, doi:DOI: 10.1002/we.2004.
23. J. Rowcroft, D. Burton, H. M. Blackburn and J. Sheridan. Siting Wind Turbines Near Cliffs: The Effect of Ruggedness. *Journal of Fluids Engineering-Transactions of the Asme* **2019**, 141, doi:DOI: 10.1115/1.4041231.
24. R. J. Barthelmie and S. C. Pryor. The impact of wind direction yaw angle on cliff flows. *Wind Energy* **2018**, 21, doi:DOI: 10.1002/we.2227.
25. F. Balduzzi, A. Bianchini and L. Ferrari. Microeolic turbines in the built environment: Influence of the installation site on the potential energy yield. *Renewable Energy* **2012**, 45, doi:DOI: 10.1016/j.renene.2012.02.022.
26. M. Bastankhah and F. Porte-Agel. Experimental and theoretical study of wind turbine wakes in yawed conditions. *Journal of Fluid Mechanics* **2016**, 806, doi:DOI: 10.1017/jfm.2016.595.
27. S. J. Schreck and J. G. Schepers. Unconventional Rotor Power Response to Yaw Error Variations. *Journal of Physics: Conference Series* **2014**, 555, doi:<https://doi.org/10.1088/1742-6596/555/1/012001>.

28. A. Honrubia, A. Viguera-Rodríguez and E. Gómez-Lázaro. The Influence of Turbulence and Vertical Wind Profile in Wind Turbine Power Curve. *Progress in Turbulence and Wind Energy Iv* **2012**, 141.
29. B. Loganathan, I. Mustary, H. Chowdhury and F. Alam. Effect of turbulence on a Savonius type micro wind turbine. *1st International Conference on Energy and Power, Icep2016* **2017**, 110, doi:10.1016/j.egypro.2017.03.183.
30. B. Kosasih and H. S. Hudin. Influence of inflow turbulence intensity on the performance of bare and diffuser-augmented micro wind turbine model. *Renewable Energy* **2016**, 87, doi:DOI: 10.1016/j.renene.2015.10.013.
31. B. Cochran. *The influence of atmospheric turbulence on the kinetic energy available during small wind turbine power performance testing*, CEDER-CIEMAT, 2002
<http://citeseerx.ist.psu.edu/viewdoc/download?doi=10.1.1.61.4472&rep=rep1&type=pdf>
32. K. Kaiser, W. Langreder, H. Hohlen and J. Hojstrup. Turbulence Correction for Power Curves. 2004.
33. T. Rogers and S. Omer. Yaw analysis of a micro-scale horizontal-axis wind turbine operating in turbulent wind conditions. *International Journal of Low-Carbon Technologies* **2012**, 8, doi:10.1093/ijlct/cts009.
34. T. Kiwata, H. Nakata, T. Kuratani, et al. Study of a performance of a cross-flow wind turbine located above a windbreak fence and the associated flow field. 2011 In Proceedings of 21st National Symposium on Wind Engineering.
35. D. R. Drew, J. F. Barlow and T. T. Cockerill. Estimating the potential yield of small wind turbines in urban areas: A case study for Greater London, UK. *Journal of Wind Engineering and Industrial Aerodynamics* **2013**, 115, doi:DOI: 10.1016/j.jweia.2013.01.007.
36. N. Chrysochoidis-Antsos, *Sonic anemometer wind speed field for urban wind flows around a noise barrier (acoustic screen) and weather station supplementary dataset (temperature, wind, solar)*. 2019,
37. ISO. ISO 16622 - Meteorology - Sonic anemometers/thermometers - Acceptance test methods for mean wind measurements. International Organization for Standardization: **2002**.
38. . Gill Instruments. WindMaster and WindMaster PRO - User Manual. Gill Wind Instruments.
39. B. H. Bailey and S. L. McDonald. *Wind Resource Assessment Handbook - Fundamentals of conducting a Successful Monitoring Programme*; 1997.
40. R. E. Eskridge and S. T. Rao. Measurement and Prediction of Traffic-Induced Turbulence and Velocity-Fields near Roadways. *Journal of Climate and Applied*

Chapter 2

- Meteorology* **1983**, 22, doi:DOI: 10.1175/1520-0450(1983)022<1431:Mapoti>2.0.Co;2.
41. H. Wegley, J. Rammsdell, M. Orgill and R. L. Drake. *A siting handbook for small wind energy conversion systems*; Pacific Northwest Laboratory: 1980.
 42. A. B. Tabrizi, J. Whale, T. Lyons and T. Urmee. Rooftop wind monitoring campaigns for small wind turbine applications: Effect of sampling rate and averaging period. *Renewable Energy* **2015**, 77, doi:<https://doi.org/10.1016/j.renene.2014.12.037>.
 43. T. Burton, D. Sharpe, N. Jenkins and E. Bossanyi. *Wind Energy Handbook*; John Wiley and Sons Ltd.: 2001.
 44. A. Krynytzky, Ewald, B. *AGARDograph 336 - Wind Tunnel Wall Corrections*; North Atlantic Treaty Organization (NATO): 1998.
 45. IEC. IEC 61400-12-1:2005(E) (Wind Turbines - Part 12-1: Power Performance measurements of electricity producing wind turbines). 2005.
 46. C. Schulz, P. Letzgus, T. Lutz and E. Kramer. CFD study on the impact of yawed inflow on loads, power and near wake of a generic wind turbine. *Wind Energy* **2017**, 20, doi:DOI: 10.1002/we.2004.
 47. M. Kiya and K. Sasaki. Free-Stream Turbulence Effects on a Separation Bubble. *Journal of Wind Engineering and Industrial Aerodynamics* **1983**, 14.
 48. J. F. Largeau and V. Moriniere. Wall pressure fluctuations and topology in separated flows over a forward-facing step. *Experiments in Fluids* **2007**, 42, doi:DOI: 10.1007/s00348-006-0215-9.
 49. J.F. Manwell, J.G. McGowan and A.L. Rogers. *Wind Energy Explained - Theory, Design and Application*, Second ed.; John Wiley & Sons Ltd.: 2009.
 50. G. S. W. Hagler, W. Tang, M. J. Freeman, et al. Model evaluation of roadside barrier impact on near-road air pollution. *Atmospheric Environment* **2011**, 45, doi:<https://doi.org/10.1016/j.atmosenv.2011.02.030>.
 51. KNMI. Rotterdam The Hague AP (Wind Data) - Station ID: 915096001. KNMI (Koninklijk Nederlands Meteorologisch Instituut): 2015.
 52. U. Ciri, M. A. Rotea and S. Leonardi. Effect of the turbine scale on yaw control. *Wind Energy* **2018**, 21, doi:DOI: 10.1002/we.2262.
 53. WMO. *Guide to Meteorological Instruments and Methods of Observation*, World Meteorological Organization, 2010. https://library.wmo.int/pmb_ged/wmo_8_en-2012.pdf
 54. W. D. Lubitz and B. R. White. Wind-tunnel and field investigation of the effect of local wind direction on speed-up over hills. *Journal of Wind Engineering and Industrial Aerodynamics* **2007**, 95, doi:DOI: <https://doi.org/10.1016/j.jweia.2006.09.001>.

Chapter 2

55. Magdi Ragheb. Chapter 25 - Economics of Wind Power Generation. In *Wind Energy Engineering*, Letcher, T.M., Ed. Academic Press: 2017; DOI: [https://doi.org/10.1016/B978-0-12-809451-8.00025-4pp. 537-555](https://doi.org/10.1016/B978-0-12-809451-8.00025-4pp.537-555).
56. A.C. Orrell and E.A. Poehlman. *Benchmarking U.S. Small Wind Costs*, PNNL, September 2017, 2017. https://wind.pnnl.gov/pdf/Benchmarking_US_Small_Wind_Costs_092817_PNNL.pdf
57. D. Udell, D. Infield and S. Watson. Low-cost mounting arrangements for building-integrated wind turbines. *Wind Energy* **2010**, 13, doi:<https://doi.org/10.1002/we.386>.
58. IRENA. *Renewable Power Generation Costs in 2018*, Abu Dhabi, 2019. https://www.irena.org/-/media/Files/IRENA/Agency/Publication/2019/May/IRENA_Renewable-Power-Generations-Costs-in-2018.pdf

3

Performance Characteristics of a Micro Wind Turbine Integrated on a Noise Barrier

“Negative results are just what I want. They’re just as valuable to me as positive results. I can never find the thing that does the job best until I find the ones that don’t.”

— Thomas A. Edison

*This **chapter** describes the experimental procedures, methodologies, analysis and presents results for the concept of micro wind turbines installed on top of noise barriers. A number of performance characteristics that influence ultimately energy yield and thus overall economic performance are examined.*

*The **research question** answered in this Chapter is:*

“What is the performance of a micro wind turbine integrated on top of a noise barrier?”

This chapter is published as “Performance Characteristics of a Micro Wind Turbine Integrated on A Noise Barrier” by Nikolaos Chrysochoidis-Antsos, Gerard J.W. van Bussel, Jan Bozelie, Sander M. Mertens and Ad J.M. van Wijk (2021) in “Energies” published by © MDPI

3.1 Introduction

Micro wind turbines have a potential to be utilized for energy production in the urban environment. In order to reduce electricity production costs, they can be installed on buildings or on infrastructure. This has already been demonstrated at an affordable cost for photovoltaics in the urban environment. The challenge is also indicated in a cost comparison of free-standing micro wind turbines ranging from 6700 to 10900 €₂₀₁₇/kW (2017 equivalent from US dollars) [1], while photovoltaic (PV) systems range from 2500–6700 €/kW (2017 equivalent from US dollars) [2]. Therefore, research is needed to find ways to reduce costs for micro wind turbines and optimize the performance characteristics, thus lowering electricity production costs.

For micro wind turbines, there are numerous claims, showing a wide range of energy efficiencies and a wide range of costs, which are caused by an unregulated market without proper standardization. Also, their operating performance differs largely per wind turbine system and site of installation, hence more research is needed to identify all possible issues. The poor performance of numerous systems is shown in [3] where capacity factors were found extremely low up to an average of 0.85% when taking into account electrical standby losses and 4.15% when not. The ranges of the capacity factors of the various examined sites in England were between 1%–20%. This means that it is a difficult task for installers to select a proper micro wind turbine system for a particular site. This chapter addresses some of the above issues as they have been found through experiments both in a wind tunnel and from a field experiment on a noise barrier.

The micro wind turbine system that is examined in this work is structurally integrated with noise barriers as seen in Figure 3 - 1. Noise barriers are part of many highway infrastructures passing through populated areas and reduce the noise produced by the passing vehicles. If micro wind turbines are structurally integrated with noise barriers, then a part of the structural costs of the micro wind turbines is reduced due to the use of its heavy support foundations that these barriers can provide to locate these turbines (multiple infrastructure use). The tower costs for micro wind turbines can vary from 13%–31% of the total investment cost [4] and if replaced instead by a simple flange as in Figure 3 - 1 in blue, the electricity cost could be reduced. A similar integration has been demonstrated in [5] for roof- and wall-mounted micro wind turbine applications on buildings.



Figure 3 - 1: Micro wind turbine integrated on top of the noise barrier.

In current work, a number of performance characteristics are investigated and a state-of-the-art literature review is presented below. The intention is to aggregate the most relevant aspects that determine the performance of a micro wind turbine in an urban environment. The relevant characteristics are summarized as:

- (1) Flow misalignment in open air experiments
- (2) Electrical power conversion losses under dynamic external conditions
- (3) Starting behaviour of micro wind turbines in a varying wind speed environment
- (4) Optimal power control of micro wind turbines in urban wind conditions

The first performance characteristic of current work refers to the misalignment of the flow with respect to the rotor. Wind flows passing through the rotor of micro wind turbines installed in urban environments, such as on noise barriers are not always perpendicular with the rotor. This misalignment effect can be observed under two different operational conditions. The first condition is when the wind flows are affected by urban obstacles such as a noise barrier, thus resulting in a skewed flow towards the rotor. In the second condition is the misalignment of the rotor with the flow due to the inadequate yaw response of the micro wind turbine's hub with the rapidly occurring wind variations at low heights.

The first operational condition has been examined in [6] where it was shown that flow on top of noise barriers is constantly misaligned with a range from +5 to +25

degrees for all wind flow directions towards the barrier. This constant flow misalignment was shown to lower the performance. The performance assessment was theoretically modelled with $\cos^3\theta$ law that predicted power under skewed flow. The intention of the current work is twofold. First to observe the validity of those theories with wind tunnel experiments presented in the Section 3.1.1 and second to apply the theory and wind tunnel results for observations from the field experiment.

Regarding the different theories for prediction of power in misaligned flows, much literature is presented. For example, in [7], a rotor power measurement under yawed conditions was performed in a wind tunnel. It was found that there were anomalies from model predictions regarding rotor power responses to yaw error variations in experimental data. The conclusion was that higher accuracy prediction of wind turbine power performance under yaw conditions required a more complete understanding of rotor and blade aerodynamics. In [8], large eddy simulations were performed for yawed rotors of large wind scale turbines. The authors found that the $\cos^2\theta$ and $\cos^3\theta$ power decay laws respectively over and underestimate the power production in the experimental datasets for an inflow with shear. In [9] and [10], the maximum power production versus the tip speed ratio (TSR) was found to vary approximately like $\cos^3(\theta)$, where θ is the yaw angle in this case. The turbine used in this experiment was rather small with a diameter of 0.15 m and placed at a height of 0.125 m from the floor of the closed-loop tunnel. The power was extracted with a small Direct Current (DC) generator. Even though the $\cos\theta$ law was applicable for this small turbine, care should be taken because the airfoils of such a small turbine operate in very viscous flow and as a consequence the behaviour will be different from a larger turbine with airfoils that operate at higher Reynolds numbers. In [11], yaw misalignment was studied for the MEXICO rotor with Computational Fluid Dynamics (CFD) for three wind speeds at 30° yaw angle with respect to aerodynamic performance for a 4.5 m diameter. In [12], wind turbine power performance was also investigated, showing drops up to 40% in the power coefficient C_P with an increasing inclined flow (towards 40°) for a 75-kW system. Finally, in [13] a drop in the thrust coefficient C_T and therefore in C_P was observed for micro wind turbines in wind tunnel experiments for measurements of wakes from yawed flow from 0–45 degrees. In current chapter, a comparison of the $\cos\theta$, $\cos^2\theta$ and $\cos^3\theta$ laws was performed with experimental data from several wind turbine configurations and at different yaw position. These theoretical approximations are based on the momentum theory in steady yaw, the Glauert momentum theory model, and the vortex cylinder model, which seem to be applicable for large scale wind turbines [14].

Beside flow misalignment losses, which were part of the noise barrier structural integration, there were electrical losses that made the system inefficient. These were further classified in generator losses and power conversion losses. In this study, the focus lies on the power conversion losses with the point of measuring efficiency right after the generator and before the inverter. Also, the inverter efficiency was determined

during the operation of the wind turbine. Nevertheless, some notable studies on efficiencies also including generator losses were referred to as well. The conversion of mechanical power to electrical within the generator for a miniature wind-turbine was observed in [15], where a micro wind turbine of 0.15 m diameter was tested in a wind tunnel with various DC generators. Performance of the generator was also assessed in [16] for a miniature wind turbine. These studies presented losses between 60%–80% for DC generators. In the present study, a PMSG generator was used for which better efficiencies were achieved up to 95% [17]. But as said, the aim was not to study the generator losses but to focus on power conversion losses.

Power conversion related losses occurred in the conversion of the generator's Alternating Current (AC) to Direct Current (DC) for boosting up then back to fixed frequency AC for grid connection. Most commercial micro wind turbines have a Permanent Magnet Synchronous Generator (PMSG) that produces a three-phase power which is rectified to DC and then depending on the voltage level of the generator a buck-boost converter brings it to each AC grid country compatible frequency. The instantaneous loss was dependent on the different electronic components and configurations and could be between 20%–40% [18]. These losses accumulate in the total power performance and can vary greatly depending on rectifier topology [19–21]. The literature also indicated other electrical losses that should not be neglected as it might lead to considerable reduction in cumulative energy yield. These are, for example, the standby losses of the inverter connected to the turbine. Such losses are hardly ever taken into account in commercial micro wind turbine manufacturer websites and brochures. The standby losses depending on the inverter can contribute to a considerable amount of energy lost. The field trials from Energy Savings Trust 2009 report indicated that in some cases, micro wind turbine installations were found to become net-consumers of electricity due to the power consumption of the inverter taking its power (~10 W continuously) from the mains supply even when the turbine is connected but is not generating [22]. Similarly, [23] indicates that most small wind turbines have system electronics that run in standby mode or monitoring mode if the turbine is not generating. Depending on how much the wind turbine operates, these are additional losses for the micro wind turbine system. Due to lack of outdoor data in the literature, this is unfortunately hard to quantify upfront.

In the current work, the above phenomena will be observed through the wind tunnel experiments in which different inverters will be tested. The results will be then used to quantify the annual energy yield and standby losses for 9 location cases in the Netherlands with accenting wind speed. Finally, the performance of the inverter, for the experiments where the micro wind turbine is integrated on noise barrier structure, will be presented.

The starting and idling behaviour of the micro wind turbines is another important performance aspect not to be neglected. The low wind speeds in combination with the highly turbulent wind environment at low heights will certainly influence performance

and knowing the turbine's behaviour at low wind speeds is important. Most micro wind turbines need a gust to overcome cogging torque and to complete the starting sequence at low wind speeds, quite often about 4 m/s [24]. Even when starting, the wind turbine might spend much time in idling mode until the inverter is able to boost the generator voltage to an acceptable level where it can be inverted to AC. Only then sufficient voltage is built up from the controllers in order to connect to the grid. Cogging torque is important and in [25] researchers tried to minimize it. But looking at the greater picture, the effect of the idling and starting behaviour can significantly influence the overall energy yield. During the experiments that will be presented in this chapter, the starting behaviour of micro wind turbines is observed for various yaw positions and wind regimes. After that, a quantification of the time that turbine would be in idle, stop, or operation is presented for different wind speeds.

Finally, the performance aspect of controlling a micro wind turbine is crucial for identifying the maximum power performance point. Wind turbines have an optimal operating rotational speed for each wind speed. This rotational speed gives the best aerodynamic power extraction from the given wind flow [26]. The system's controller should ideally control the power electronics in order to find the optimum rotational speed in rotations per minute (RPM) at all times for all wind speeds. If such controller is badly designed then a potential micro wind turbine project can turn into a financial and/or technical disaster. There are numerous studies on control of micro and small wind turbines and on how to assess and define the performance metrics such as power coefficient C_P and tip speed ratio (TSR or λ) curve for micro wind turbines.

In [27], the authors address the importance of the C_P - λ curve for micro wind turbine operation and how power electronic converters are currently programmed with power and speed curves, which do not effectively optimize the power generation. For compensating the high costs and complexity of wind tunnels, authors designed an emulator to assist the development of controllers of small wind turbines. In the present study, data are analysed and shown with respect to the C_P - λ curve response of the turbine. Additionally, a qualitative presentation of the results of the controller performance in the field experiment is shown to address the importance of the maximum power performance controller operating in a highly turbulent environment.

All aforementioned studies mentioned here present performance characteristics. The motivation for the current study is generated by the fact that numerous individual issues are addressed regarding the performance, but an overall holistic understanding of those characteristics with respect to the overall power production performance is lacking. The novelty in the present work is hence found in a holistic approach to present and discuss the results of the experiments. One set of experiments conducted in a wind tunnel and used as a comparison basis for the other set of field experiment, where the performance of micro wind turbines integrated with highway infrastructures such as noise barriers is recorded. The chapter does not address the fundamentals of the aerodynamic, electrical, and control performance of the systems described, but rather ad-

dresses the key aspects that result in an energy efficient system. All the performance characteristics addressed with respect to the field experiment are classified and quantified for a 22-minute dataset. However, the results can be also interpreted in a qualitative manner and inspire the research community to investigate further those aspects in a combined holistic effort.

This chapter is organized as follows. In Section 3.1, a literature review and scope are presented. In Section 3.2, a detailed set-up description is presented of the wind turbine systems examined as well as the methodology used. In Section 3.3, results are presented for each key performance characteristic. In Section 3.4, a discussion on the obtained results can be found. Finally, in Section 3.5, the conclusions are presented.

3.2 Materials and Methods

To provide a quantitative and qualitative assessment of the performance characteristics of the micro wind turbines for installation on noise barriers, the following experimental set-ups, methods, hardware, and equations are used. The experiments are done in a wind tunnel under controlled conditions, in order to have a properly calibrated environment where micro wind turbine performance aspects can be determined. An outdoor field experiment with a micro wind turbine installed on top of a noise barrier will also be presented in order to understand the “real-world” conditions and how such outdoor conditions can affect the performance of the micro wind turbine. Numerous wind tunnel experiments inspired the methods of this work in many ways [16,28–31].

The methods and experimental conditions for both the wind tunnel tests and the field experiment are subsequently presented in the following subsections.

3.2.1 *Wind Tunnel Experiment*

The experiments were conducted in the Open Jet Facility (OJF) of TU Delft. This is a closed-circuit open jet wind tunnel with a jet diameter d_{nozzle} of 2.85 meters. Wind speed was measured with a pitot tube placed inside the wind tunnel’s nozzle and was calibrated for the distance from the exit of nozzle in which all micro wind turbines are placed as seen below in Figure 3 - 2. Even though some literature suggests that blockage corrections are necessary even for small wind turbines like in [32] and [33], this is mainly the case for experiments in closed test sections. Since the current test object is exposed to an open jet flow (in a room with height of 8 meters and length of 13m) in significantly larger diameter with an area ratio of 3.5 between OJF nozzle and the turbine’s rotor, the blockage effects were considered negligible. Open jet blockage corrections were typically one order of magnitude smaller and of opposite sign compared to closed tunnel sections with similar diameter [34]. The use of open jet sections was a well-known setup for reducing blockage effects [35,36]. The Open Jet

Facility tunnel in TU Delft was used before with success for many aero-dynamic studies on blunt body loads as well for small scale wind turbine rotors like in [37].

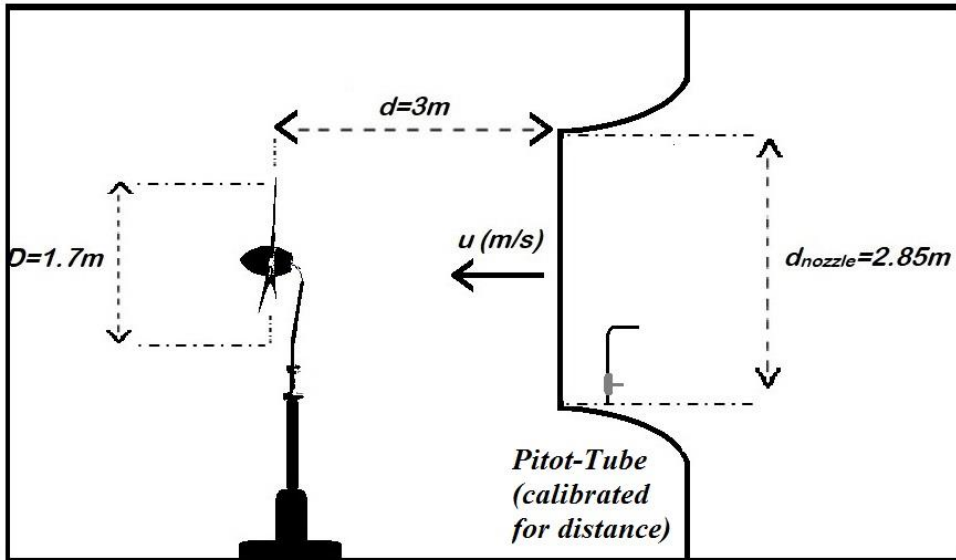


Figure 3 - 2 : Diagram of installation of micro wind turbine in the Open Jet Facility (OJF) and wind speed pitot-tube.

Two commercial wind turbine hubs are used in the experiments, the DOD Electric and the WindChallenge. For the DOD Electric, 3 different rotors were used. The standard commercial 5 bladed rotor from the manufacturer, an American 5 bladed rotor, and an American 3 bladed rotor. All these rotors had a blade radius of 0.83–0.87 m. WindChallenge was a 3 bladed downwind turbine with blade radius of 0.86 m. All hubs had a permanent magnet synchronous generator with a rated power of 375 watts. All the turbine rotors were installed at the same distance from the wind tunnel's jet exit.

To study the losses of the inverter and the loss due to the skewed flow misalignment, the generator was directly connected to a grid-tied inverter before all energy was fed to the grid. This configuration is depicted in Figure 3 - 3. The nacelle of the wind turbine, see Figure 3 - 3, was locked at several yaw misalignment positions θ degrees with a tightening bolt. In that way, the effect of flow misalignment was calibrated and hence potential detrimental effects of the yawed and skewed flow of a micro wind turbine installed on a noise barrier can be identified.

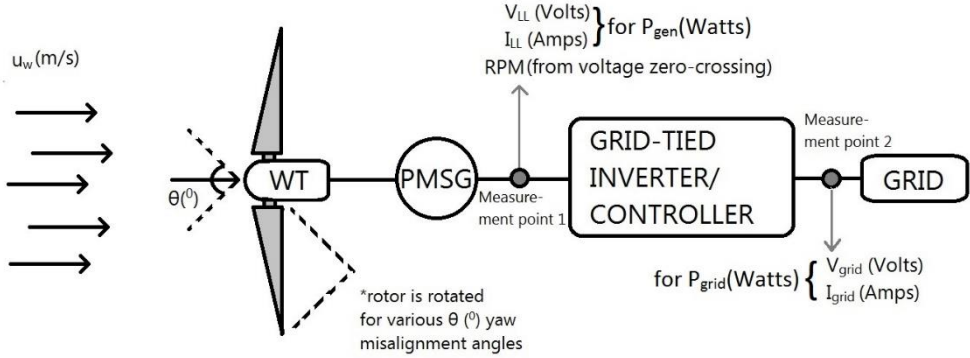


Figure 3 - 3 : Schematic of configuration of skewed flow losses experiments and inverter losses for the wind turbine (WT) and its permanent magnet synchronous generator (PMSG), together with all relevant measured parameters

In order to assess the energy losses, different measurement points were defined for each configuration, as seen in Figure 3 - 3. with measurement Point 1 and 2 before and after the inverter. The measurements were recorded in a DEWETRON data acquisition computer. Line-to-line voltage V_{LL} (Volts) and line-to-line current I_{LL} (Amps) in each phase were measured with a 10 kHz sampling frequency. Voltage was measured with DAQP-V-B and DAQP-V-HV modules and current were measured with Fluke clamp meters. For the calculations, the root-mean-square (RMS) values were considered, while the rotational speed (RPM) was estimated from the voltage zero-crossing. From those, the 3-phase power produced from the micro wind turbine right after the generator P_{gen} (Watts) was derived using equations 3.1. Grid voltage V_g (volts) and grid current I_g (Amps) measurements were also considered at the grid side and power P_{grid} (Watts) was estimated with equation 3.2.

$$P_{gen} = \sqrt{3} V_{LL} I_{LL} \quad (3.1)$$

$$P_{grid} = V_g I_g \quad (3.2)$$

These power values were later processed in order to find the efficiency of the inverter, but also to compare the power values for different yaw misalignment angles θ ($^\circ$). Especially for yaw misalignment angles, a comparison of the experimentally recorded power at the measurement points with the theoretical estimation was considered. Equation 3.3 is used to estimate the theoretical power P (watts) using P_{gen} (watts) at each angle θ ($^\circ$).

$$P(\theta=\theta_i) = P_{\text{gen}}(\theta=\theta^0) \times \cos\theta \quad (3.3)$$

For the C_p - λ study, the 3 phases of the generator are connected to a DC bridge rectifier and then to a DC controllable load unit on which a constant voltage could be set as seen in Figure 3 - 4. By setting up different voltages, the rotational speed of the rotor can be set. In that way, the performance of the micro wind turbine is assessed for different tip speed ratios TSR (see equation below). TSR is the ratio of the rotational speed ω (rad/s) times the rotor radius R (m) divided by the incoming wind speed u_w (m/s), shown in equation 3.4. Further analysis of the equation to use the RPM measured from the equipment is shown in the equation.

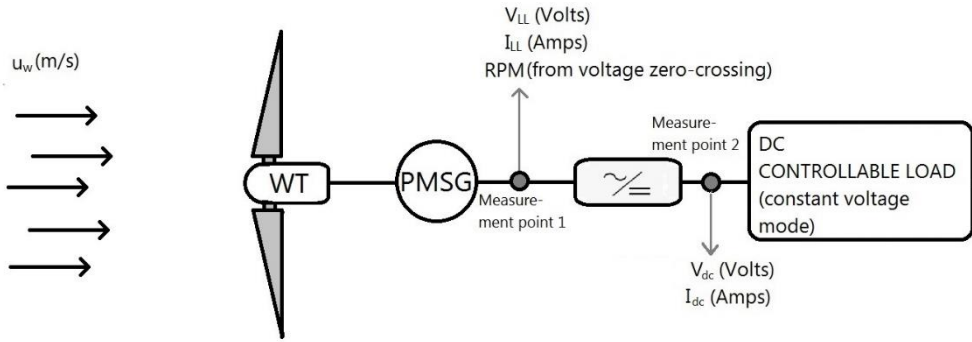


Figure 3 - 4 : Configuration of DC-controllable load tests in wind tunnel.

Studying the TSR and generated power at each instance is important since this can confirm if the commercial MPPT (Maximum Power Point Tracker) inverters used were operating in the maximum performance possible. This configuration is visualized in Figure 3 - 4.

$$\text{TSR}(-) = \frac{\omega \times R}{u_w} = \frac{2\pi}{60} \times \text{RPM} \times R_{\text{rotor}} \quad (3.4)$$

The summary of all equipment that was used for the wind tunnel experiments can be found in Table 3 - 1.

Table 3 - 1: Wind tunnel experimental equipment and relevant descriptions.

Equipment	Description
Wind tunnel facility	Open jet Facility (TU Delft) Wind speed ranges 0-30 m/s Jet diameter 2.85 m.
Turbine generator(s)	Both are 3 phase PMSG $P_{rated} = 375 \text{ W}$
Rotors used	3 bladed upwind ($R = 0.87 \text{ m}$) 5 bladed upwind ($R = 0.86 \text{ m}$) 5 bladed upwind large ($R = 1.06 \text{ m}$) 3 bladed downwind ($R = 0.85 \text{ m}$)
Grid-tied inverters	DF-SUN500-GWAL Custom-made for WindChallenge
DC bridge rectifier	3 phase bridge rectifier Zhejiang Jing Tai Electronics (MDS60-16)
DC controllable load	KIKUSUI (PLZ1004 W)
Data loggers	DEWETRON (DEWE-5000) National Instruments (cRio9063 with relevant modules)
Voltage measurement	(before inverter) - DAQP-V-B module (DEWETRON) with 0.05% accuracy (after inverter) - DAQP-HV module (DEWETRON) with 0.05% accuracy
Current measurement	Fluke i30 (current clamp) with Accuracy <1% Chauvin Arnoux MN38 (current clamp) with Accuracy <1%

In Figure 3 - 5, a compilation of photos is presented showing all the experimental geometries tested in the jet of the OJF wind tunnel.

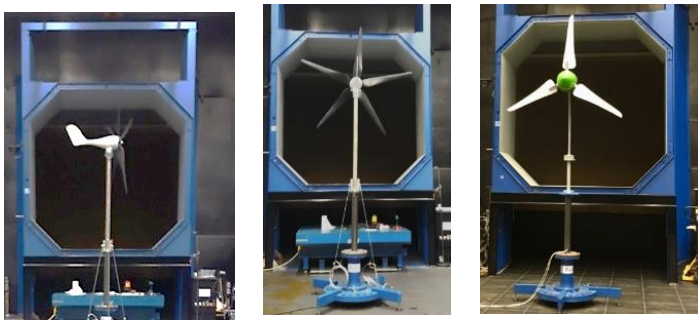


Figure 3 - 5 : Photo-compilation of the micro wind turbines installed in front of the nozzle of the Open Jet Tunnel, (left photo) 5 bladed upwind in skewed flow configuration, (middle photo) 5 bladed upwind turbine in 0° skew angle and (right photo) 3 bladed downwind turbine.

3.2.2 Field Experiment

Finally, field experiments are performed using the WindChallenge downwind micro wind turbine integrated on top of a noise barrier. The noise barrier is located at the road intersection of N470 – A13 near TU Delft in the Netherlands. The micro wind turbine is situated on top of the noise barrier with the hub 2 m above the noise barrier. A special flange was fabricated in order to allow the micro wind turbine be attached on the noise barrier, as seen in the left part of Figure 3 - 6. The micro wind turbine is connected to its dedicated designed inverter and is grid connected similar to the sketch in Figure 3 - 3. The power measurements, calculations, and equations are as explained in Figure 3 - 3. in the previous subsection. For the measurement of the hub's yaw direction, a digital compass is designed and integrated with the hub of the turbine as in Figure 3 - 1.

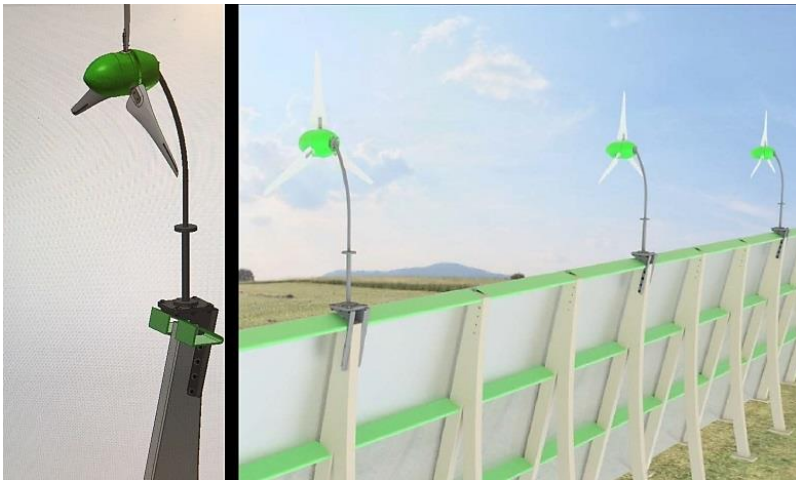


Figure 3 - 6 : Visualization of the micro wind turbine structural integration with the noise barrier.

The observed directional data are then compared to the wind direction measured from the sonic anemometers next to the wind turbine as can be seen in Figure 3 - 7. The rotational speed of the micro wind turbine (RPM) is measured via a magnetic pulse counter installed on the hub's shaft. The RPM measured in combination with the local wind speed was used to define the tip speed ratio (TSR) of the micro wind turbine. The yaw orientation is also measured with the digital compass installed on the hub of the generator. Finally, the power was measured before and after the inverter similar to the wind tunnel set-up but with different data acquisition equipment and power, voltage, and current sensors of similar accuracy.



Figure 3 - 7 : Micro wind turbine integrated on noise barrier field experiment. The 6 sonic anemometers are visible on the right located on two masts on three heights. The scaffolding behind the barrier is for access purposes and does not influence the incoming flow over the barrier.

Finally, Table 3 - 2 below describes the equipment used.

Table 3 - 2 : Field experimental equipment and relevant descriptions.

Equipment	Description
Noise barrier	Height =5.2 m
Wind turbine	3 phase PMSG - $P_{rated} = 375$ W
Rotor	3 bladed downwind ($R = 0.85$ m)
Grid-tied inverters	WindChallenge
Current sensor (after inverter)	CR4200 (accuracy +/-2% below 0.5 A and +/-0.5% above it)
Current and voltage sensor (before inverter)	EM24 DINAV53DM1X (Energy Meter before inverter with accuracy +/-0.5% rdg)
Data loggers	National Instruments (cRio9063 with relevant modules)
Digital compass	A magnetometer with that measures 0-360° the orientation of the turbine. Sampling rate 15 Hz and stored at 10 Hz
RPM meter	Hall effect sensor with magnets placed inside the turbine's hub

3.3 Results

The following section includes the results relating to the performance characteristics addressed in the introduction with the experiments described in Section 3.2. Each subsection addresses each performance characteristic measured in the wind tunnel or the field test and relevant discussions address the importance with respect to the overall performance. The overall performance is addressed extensively with a post analysis in the Discussion section.

3.3.1 Flow Misalignment Losses

As presented in the Introduction, flow misalignment losses can play a detrimental role into the overall lifetime performance of the micro wind turbines. In this part, experimental results from wind tunnel tests of different rotors in different yaw angles are compared with the theoretical approaches. Finally, these theories are projected to potential losses due to inadequate yaw response of micro wind turbines on a noise barrier.

3.3.1.1 Skewed Flow Losses

The theories regarding skewed flow were compared with wind tunnel observations for different wind turbine configurations. Rotors were tested in different skewed flow angles with respect to the wind tunnel free stream. The difference of P_{gen} (watts) generated power before the inverter of 3 different rotors and the reference power P_{gen} at a skew angle $\theta = 0$ degrees is presented in *Figure 3 - 8*. The result is shown as the ratio η_{yaw} (-) between the measured power and the reference power at zero skew angle, shown in equation 3.5.

$$\eta_{yaw(\theta_i)} (-) = \frac{P_{gen}(\theta_i)}{P_{gen}(\theta=0^\circ)} \quad (3.5)$$

The results for the DOD-Electric micro wind turbine in the 5-bladed and 3-bladed upwind rotor configurations are shown for yaw angles of 22° and 45° in *Figure 3 - 8*. For angles of 22°, the difference was between 80%–95% of the reference power for all tested wind speeds. For 45 degrees, it dropped significantly to 35%–65% for the 5-bladed rotor and to 20%–35% for the 3-bladed rotor. These differences might be attributed due to the blade aerodynamic performance and the controller. A decrease in the relative difference of power at higher wind speeds than 10 m/s was observed.

For the 3-bladed downwind turbine, see in *Figure 3 - 8*, the different skew angles considered were 15°, 30°, and 40°. There were no specific reasons for this difference with the other rotors. For 15°, the generated power was between 94%–100% of the

reference power. For 30° it drops to 85%–95% and for 40° to 75%–85%. This turbine seemed to have a better aerodynamic skewed flow performance than the other rotors, which could also be attributed to its controller and blade aerodynamic design.

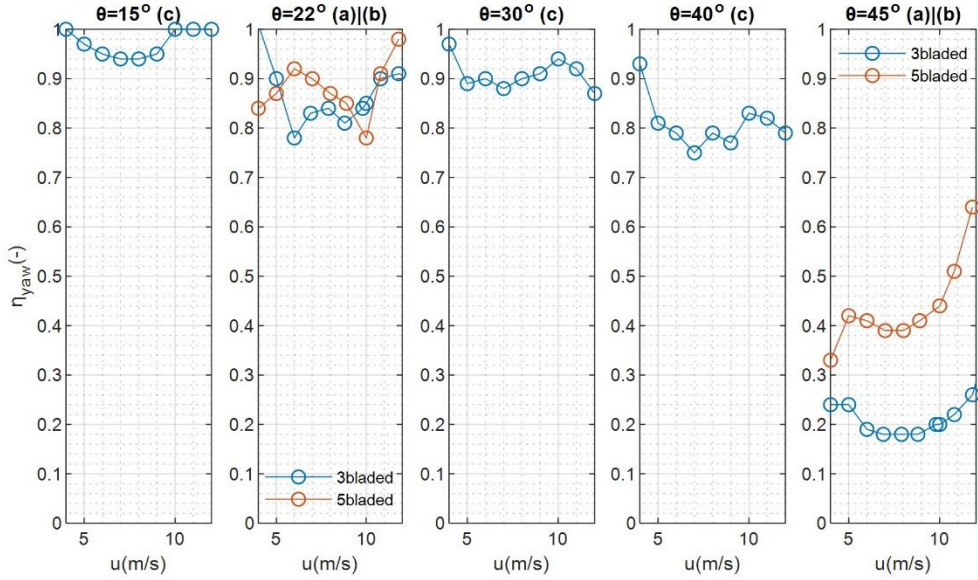


Figure 3 - 8 : Ratio of experimentally measured power to the reference power at $\theta = 0^\circ$ expressed as $\eta_{yaw}(-)$ at different skew angles θ (15°,22°,30°,40°,45°) for (a) 5 bladed upwind, (b) 3 bladed downwind, and (c) 3 bladed downwind configurations.

Next, the theoretical approximations for yawed flow power were compared with the experimental data of the 3 different turbine configurations. The results are shown in Figure 3 - 9. The comparison was made with the $\cos\theta$, $\cos^2\theta$, and $\cos^3\theta$ theories, which were presented in the introduction of the chapter. Each theoretical generated power is presented in equation 3.6 below. These theories were coming mostly from rotor aerodynamics and thus do not include generator losses; however, the generator losses were assumed constant for any yaw angle $\theta(^{\circ})$ to be compared. Thus $P_{\text{theoretical}}$ (watts) is estimated from the P_{gen} (watts) power at the reference angle $\theta=0^\circ$.

$$\begin{aligned}
 P_{\text{gen}}(\theta=0^\circ) \times \cos\theta_i \\
 P_{\text{theoretical}}(\theta_i) = P_{\text{gen}}(\theta=0^\circ) \times \cos^2\theta_i \quad (3.6) \\
 P_{\text{gen}}(\theta=0^\circ) \times \cos^3\theta_i
 \end{aligned}$$

To assess the validity of each theory using the experimental data, the following ratio η_{theory} was used, shown as equation 2.7.

$$\eta_{\text{theory}} = \frac{P_{\text{theoretical}}(\theta_i)}{P_{\text{gen}}(\theta_i)} \quad (3.7)$$

For the 15° yaw angle in Figure 3 - 9, the theoretical estimations were between 90%–105% of the experimentally recorded values for the 3 bladed downwind turbine. The $\cos\theta$ theory seemed to be the one closer to the reference value 1.

For the 22° yaw angle in Figure 3 - 9, the theories give an approximation between 80%–120% of the reference value for both upwind rotor configurations (3 bladed and 5 bladed). For both rotors the $\cos^2\theta$ seemed to have better approximation. For different wind speeds, different approximations observed were probably attributed to the rotor aerodynamics and controller.

For the 30° yaw angle and the 3-bladed downwind rotor in Figure 3 - 9, the theories gave an approximation between 70%–98% of the reference value. All theories seem to underestimate the power generated from the rotor. The closest approximation was the $\cos\theta$ theory.

For the 45° yaw angle and the 3-bladed and 5-bladed upwind rotor configurations in Figure 3 - 9, all theories seemed to fail dramatically in predicting the generated power. Especially for the 3 bladed rotor, all three theoretical models greatly over predicted the power production from values of 150%–200% for $\cos\theta$ up to 250%–300% for $\cos^2\theta$. For the $\cos^3\theta$ model, the overprediction was even out of the range doubling the value reaching 400%. For the 5-bladed configuration, the theories were somewhat between 60%–200% of the theoretical values. In high wind speeds, the $\cos^2\theta$ and $\cos^3\theta$ theories under predicted power and in lower wind speeds, where the $\cos\theta$ and $\cos^2\theta$ theories are over predicting power. The $\cos^3\theta$ theory seemed to be the most promising model. However, the large deviations in the results leads to conclude that all the cosine theories failed to predict greatly above 40 degrees skew angle.

Finally, it was also observed that the ratio between measured power and theoretical power for the skewed angle experiments varied with increasing wind speed. This can most probably be attributed to the non-optimal control strategies of the turbines.

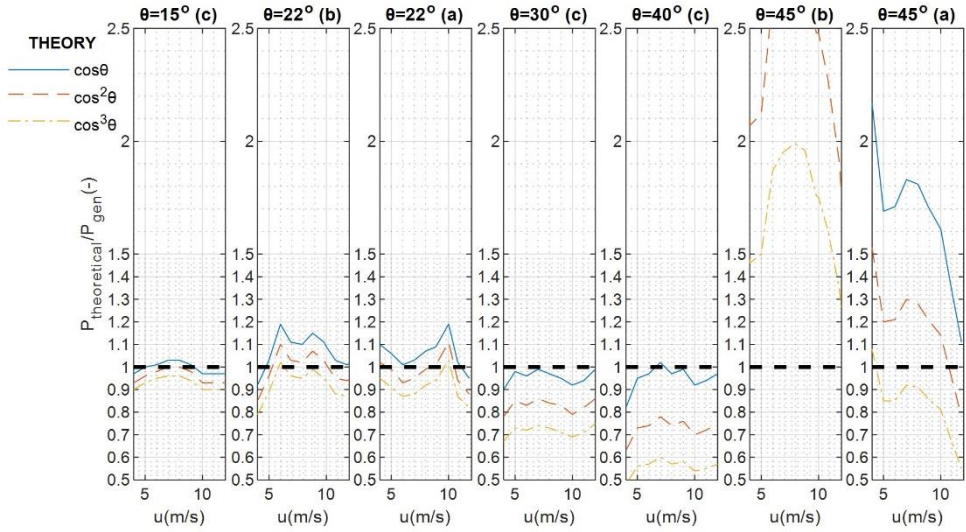


Figure 3 - 9 : Ratio of theoretical power estimation from 3 different yaw misalignment theories at different skew angles θ_0 ($15^\circ, 22^\circ, 30^\circ, 40^\circ, 45^\circ$) with the experimentally derived generated power at these skew angles for (a) 5 bladed upwind, (b) 3 bladed upwind, and (c) 3 bladed downwind configurations.

At this point, the findings, highlights and conclusions with respect to the theories that predict the flow misalignment losses will be discussed below:

1. It is evident from Figure 3 - 8 that when any rotor configuration was exposed to a misaligned flow, the power performance dropped. This drop of power production due to misalignment for micro wind turbines on top of noise barriers is of importance to assessing the overall performance.
2. $\cos\theta$, $\cos^2\theta$, and $\cos^3\theta$ theories for skewed flow did not manage to accurately reproduce the measured wind turbine power performance in wind tunnel conditions for micro wind turbines for all wind speeds and yaw angles. The hypothesis was that aerodynamics of the various rotors plus the control scheme that each turbine had, influenced the power output of the wind turbine in this skewed conditions in a non-linear way resulting in large deviations.
3. The $\cos\theta$ theory seemed to work quite well for the (c) configuration which was also the one that will be used in the field experiment. Thereby, this theory is used to estimate potential losses in the next sub-section.
4. For all the other cases, both theories can lead to great deviations of the actual estimation of the power output. Thus, such theories must be treated carefully to accurately estimate wind energy yield on top of noise barrier, or any wind turbine installation point where flow was skewed by 15° and more (e.g., rooftops) and if

the wind turbine to be installed did not have its own custom-made inverter, or was intentionally designed for highly complex turbulent environments.

3.3.1.2 Inadequate Yaw Response Losses

The yaw response is the turbine's hub effort to align at any point of time with the wind direction. The wind turbine's hub was a free-moving mass on top of a bearing that should align with the wind flow in order to extract the wind energy available in the most efficient way. If the hub does not respond fast enough in these changes, then the wind turbine runs the risk of extracting less energy that it is able to. Downwind turbines have a weight displaced far from the centre of rotation. The downwind position allowed them to align with the flow, but the displacement of the weight (and the spinning rotor) led to a large inertia that was slowing down the yaw tracking of the rotor. In this study observations were made in order to approximate the losses due to this configuration. The effect was clearly demonstrated in the 2-minute example dataset shown in Figure 3 - 10. The dataset was sampled with 10 Hz for the wind speed, hub's yaw angle, and wind direction. It was clear that there was a mismatch between the alignment of the turbine's head with the upcoming wind direction, which gets larger in lower wind speeds. Nearly all the time it was shown that the turbine's hub was not aligned with the incoming flow.

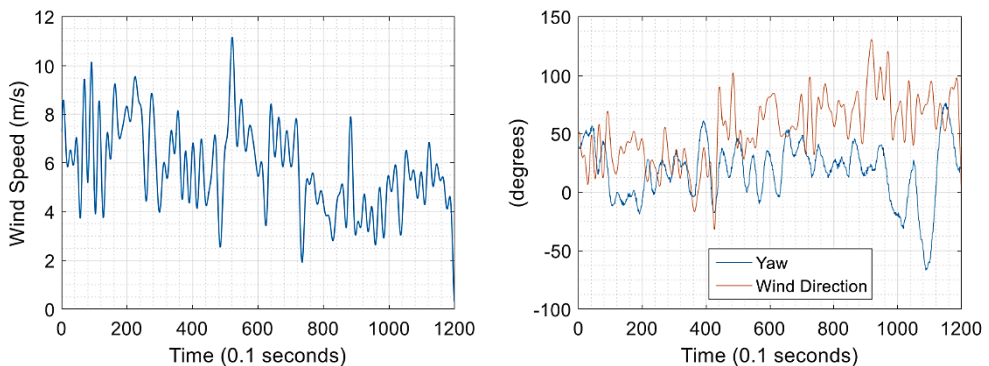


Figure 3 - 10 : Data measured for a period of 2 minutes with 10 Hz sampling frequency, (left graph) Wind speed measured at hub height and 6 meters next to the micro wind turbine, (right graph) Yaw angle of the micro wind turbine and wind direction (0° is North and 90° is East) for WindChallenge turbine.

This yaw misalignment error was estimated for a dataset of 22 minutes with an average wind speed of 6.5 m/s. A duration curve of the mismatch of the flow and the yaw orientation is presented. This error was translated to a drop in power using the $\cos\theta$ theory. The average potential power performance decrease in all this dataset due to inadequate yaw response was -37%. The average recorded power performance coefficient C_p of the turbine for this 22-minute dataset was 0.20. If the turbine was able

to follow the wind flow at all times, then the power performance would increase to an average of 0.273 rather than 0.20, which is a substantial difference. From the power duration curve, in

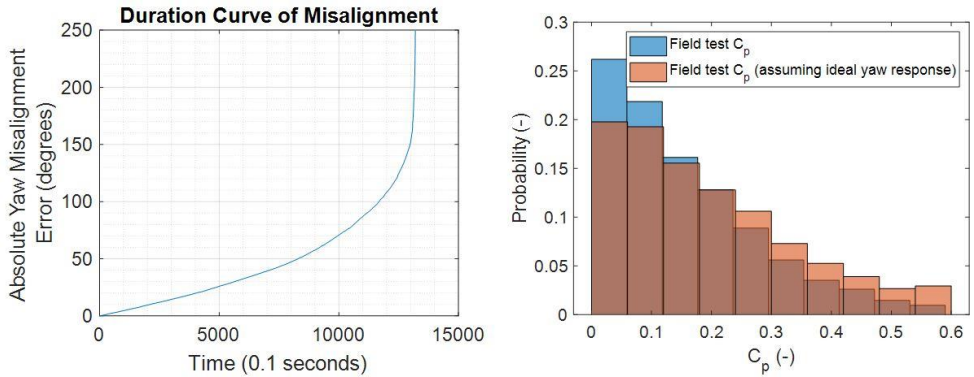


Figure 3 - 11 (left graph), it can be seen that for about 500 seconds the misalignment was less than 30 degrees. This also means that over the remaining 820 seconds, so about 62% of time, the misalignment was large, which results in serious power losses. This calls for much more emphasis on dedicated yaw system designs for small urban wind turbines.

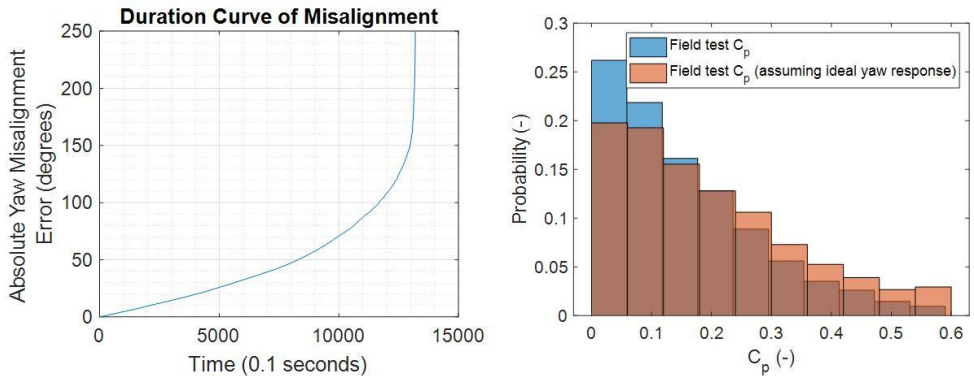


Figure 3 - 11 : (left graph) Duration curve of the absolute yaw misalignment error (degrees), (right graph) histogram of probability of occurrence for C_p values assuming ideal yaw response and comparison with actual measured from the 22-minute dataset obtained in the field.

3.3.2 Electrical System Losses

The power available in the wind extracted by the micro wind turbine significantly reduced due to the aerodynamic performance of the rotor and the generator's losses, power drops as shown in Figure 3 - 12 when comparing the red with the green curve. Next, the inverter and control caused the power to drop further (blue curve).

Up to 10 m/s, the aerodynamic and generator losses dominated. In the region above 10 m/s, the inverter conversion losses started to increase, while at the same time, the loss in power was also due to aerodynamics (stall or pitch control) and/or the controller function to limit current from generator by means of electrical resistance.

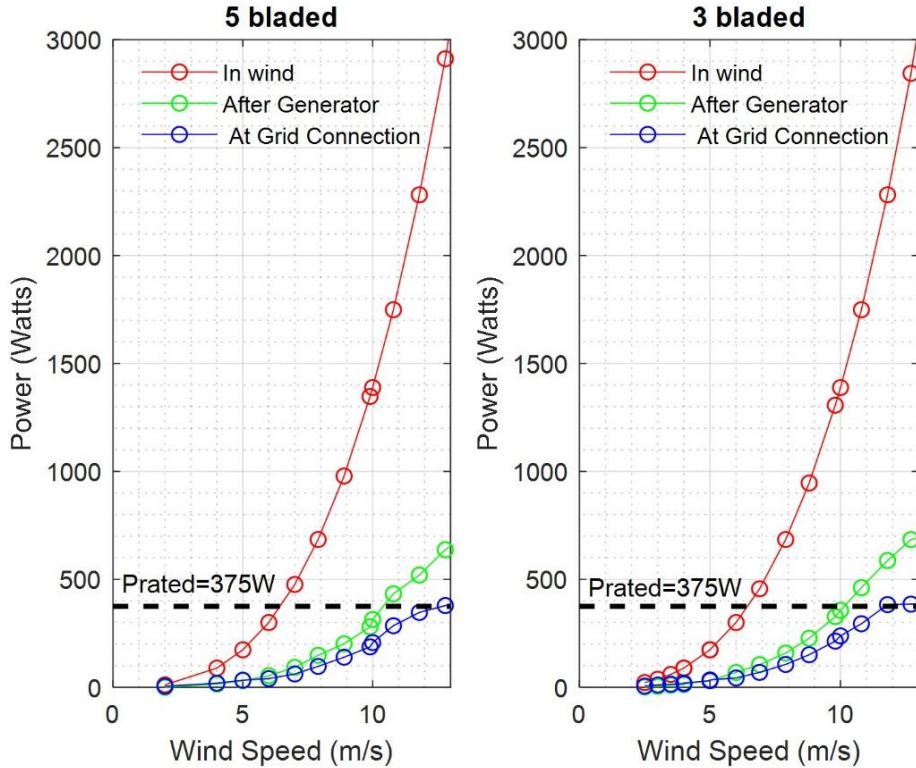


Figure 3 - 12 : Available wind power (red), generated power (green), and delivered power to the grid (blue).

During the experiments, the inverter efficiencies were recorded for the power conversion together with the standby power consumption losses. These were losses in order to keep the controller running, light indications, anti-islanding relays, and other isolation units.

These losses were divided into two main components:

1. Inverter operating efficiency
2. Standby power consumption losses

3.3.2.1 Inverter Operating Efficiencies

Inverter operating efficiency is crucial in order to convert the power in an efficient and reliable manner to bring to grid quality standards (for example 230 volts at 50 Hz

frequency for Europe). The inverter efficiency was calculated from the ratio of P_{grid} (watts) and P_{gen} (watts) with equation 3.8. Results for 2 different inverters are shown in Figure 3 - 13.

$$\eta_{\text{inverter}} (-) = \frac{P_{\text{grid}}}{P_{\text{gen}}} \quad (3.8)$$

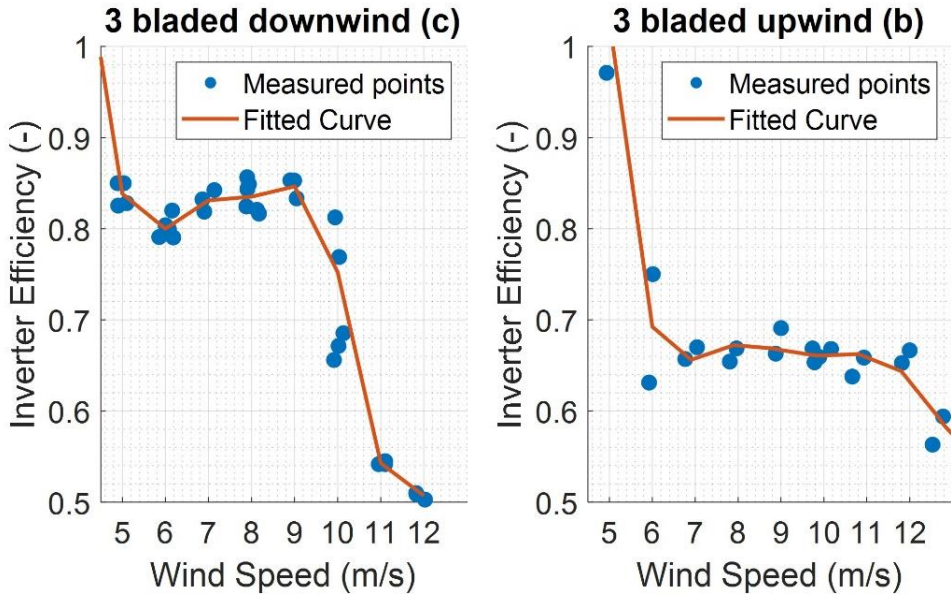


Figure 3 - 13 : Wind tunnel measured inverter operating efficiencies as a function of wind speed for (left graph) the (c) configuration of 3-bladed downwind and (right graph) the (b) configuration of 3-bladed downwind configurations.

These losses should be part of the performance characteristics of a micro wind turbine project as they might greatly influence the final total annual energy yield that a potential micro wind turbine could deliver. The experiments indicated that a wind turbine with a PV MPPT inverter performs less than a micro wind turbine with a dedicated designed inverter. Finally, a note shall be made on the drop of performance after 10 m/s, which is an intentional measure of the control system in order to regulate the large in-crease in power and rotor over-speeding.

The inverter efficiency is shown in Figure 3 - 14 from the field experiment. It can be concluded that the inverter was performing as in the wind tunnel setting, by comparing with Figure 3 - 13 above with some deviations around the fitted line.

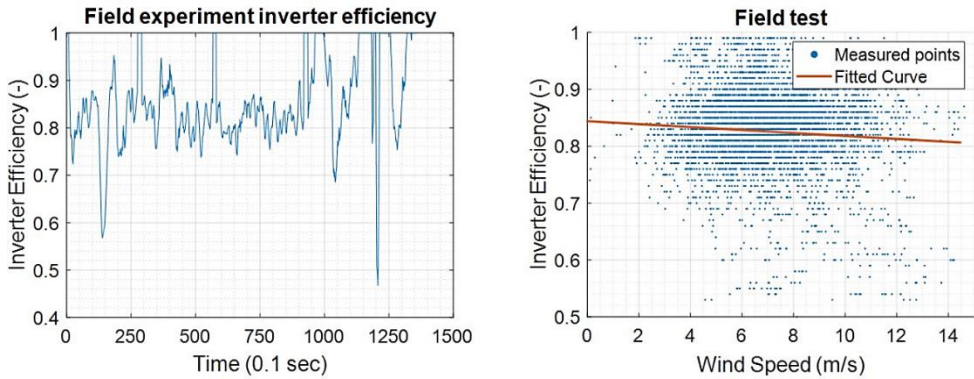


Figure 3 - 14 : (left graph) Time series plot of a 2-minute dataset (right graph) Scatter plot of field test for a 22-minute dataset of measured inverter operating efficiencies for WindChallenge downwind turbine with average wind speed of 6 m/s.

3.3.2.2 Standby Losses Assessment

Another type of losses are standby losses. These typically reflect the electrical consumption of the inverter during standstill or idling conditions.

Measurements were made for different rotors and generators, for several inverters in the wind tunnel experiment and for one inverter for the field experiment. It was found that each inverter had an average constant loss during idling or full stop. The losses during idling of standby conditions were 2, 4, and 22 watts for (a), (b), and (c), respectively (see definition in Figure 3 - 9 for (a), (b), (c)).

The standby losses were used in annual energy calculations. For these annual yields, wind speed hourly datasets were used from the Royal Netherlands Meteorological Institute (KNMI) [38]. Several locations in the Netherlands were chosen (near coastal, inland etc.) as a production sensitivity parameter. All data from each station were evaluated on their validity and quality. Some datasets were neglected whenever there were Not a Number (NaN) values, outliers, or other errors (due to weather station issues). The period of data acquisition assessed was from 01 January, 2018 until 31 December, 2019. The annual energy production estimations were made by interpolating the grid power output of the wind turbine's measured power curve with the query points of hourly wind speed for each location. This was a rough approach since at low wind speeds close to the standby loss point, typically, turbulence intensities are higher and might lead to a slight increase in instantaneous power output [39]. However, this increase was considered minimal in this experiment case since micro wind turbine were not able to follow all fluctuations in an instantaneous fashion without moving away from the optimal point of operation. The intention of this case study was to provide insight into how losses can increase when standby losses are taken into account or not.

Thereby, a power curve look-up table was used with the hourly wind speed u_t (m/s) for each hourly time step t translated to an hourly energy output E (kWh), presented in equation 3.9. During the moments that power generation from the turbine was zero, the standby losses that were found in the wind tunnel experiments were subtracted. In that way, the influence of the standby losses on the Annual Energy Production AEP (kWh) was taken into account.

$$E(u_t) = \begin{cases} -P_{\text{standbyloss}}, & \text{if } (P(u_t)=0) \\ P(u_t)=P(u_t), & \text{if } (P(u_t)>0) \end{cases} \quad (3.9)$$

Once $E(u_t)$ is defined for each time step, the annual energy production AEP (kWh) is then the sum of each hourly time step with equation 3.10.

$$\text{AEP(kWh)} = \sum_{t=0}^{8760} E(u_t) \quad (3.10)$$

The influence of standby losses on the total annual wind electricity production is presented for 3 locations in the Netherlands (De Bilt, Rotterdam, and IJmond) with mean wind speeds of 3.36, 4.13, and 6.97 m/s, respectively. For these calculations, the power curve of the downwind 3-bladed WindChallenge micro wind turbine is used, which was rated at 375 watts. A calculation is made for different inverter standby losses (2, 4, and 22 watts) for fully aligned flow conditions. The first bar presented in *Figure 3 - 15* below is the reference generated power excluding the standby losses. For low wind speed sites (3.3 m/s), the standby losses are of a considerable amount (5%, 10%, and 50%). When average wind speed increased, the losses dropped significantly. The amount of standby loss also play a role.

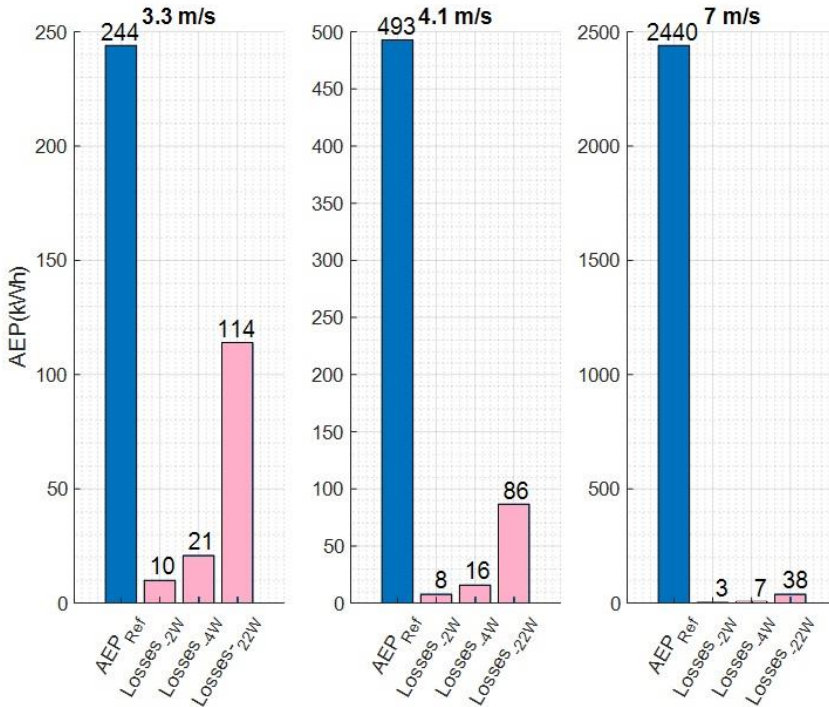


Figure 3 - 15 : Annual Energy Production (AEP) for 3 sites with different annual mean wind speed (left=3.3m/s, middle=4.1m/s, right=7m/s) assessing the losses for 3 different inverter standby losses (2, 4, and 22 W) compared to the reference AEP.

3.3.2.3 Site Assessment Feasibility with Electrical Losses and Skewed Flow

A more detailed assessment is conducted for 9 sites in the Netherlands from inland to nearly coastal wind climate conditions with increasing mean wind speeds of 2.7–5 m/s, measured at 10 meters height, whose details are found in Table 3 – 3 below. This was relevant because micro wind turbines usually are installed at such heights and will experience these mean wind speeds. The site characteristics are presented in the table below. This assessment is a sensitivity analysis for the effect of yaw misalignment and inverter standby losses (assuming 6 watts). It is assumed that whenever the turbine was not producing any power, a consumption of standby loss was occurring. The site that was the nearest to the noise barrier location of the field test was R'dam (Rotterdam) measured in an open field at an airport. The noise barrier site is located 10 kilometres away from that measurement point. By extrapolating the results for the standby losses shown in Figure 3 - 15, about 24 kWh of losses are expected from a 493-kWh reference AEP. This is a ~5% decrease in AEP due to the standby losses.

Chapter 3

Table 3 - 3 : Wind Site characteristics including the Weibull lambda and k parameters that describe the wind regime for 9 locations.

Station	Arce n	De Bil t	Ell	Eindhove n	Maastrich t	R' da m	Voorschote n	Schipho l	R'dam Geulhave n
U_{mean} (m/s)	2.7	3.3	3. 3	3.5	3.7	4.1	4.3	4.7	5
λ (scale)	3.0	3.8	3. 7	4	4.2	4.6	4.8	5.4	5.7
k (shape)	1.6	1.9	1. 6	1.8	2.0	1.8	1.8	1.9	2.2

The results for the assessment of the 9 sites are presented in the curves in Figure 3 -16. In particular the annual energy production is plotted versus the increasing wind speed per site, The conclusions derived are:

1. Energy yield is higher for higher mean wind speeds.
2. The annual energy production (AEP) standby losses are lower at higher mean wind speed as the wind turbine produces more time and stays less time inactive, consuming standby power.

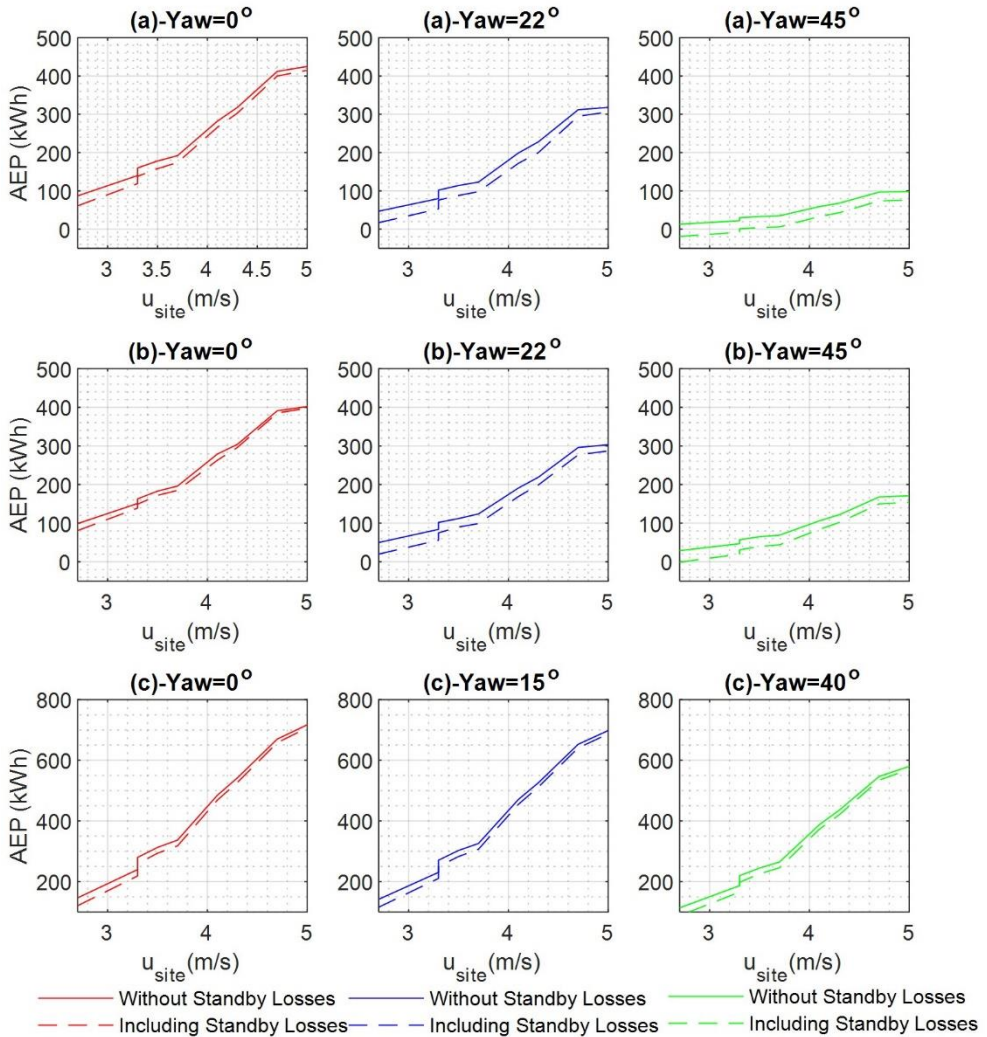


Figure 3 - 16 : Annual Energy Production AEP (kWh) without and including standby losses for an increasing mean wind speed per different site and different yaw angles for (a) 5-bladed upwind, (b) 3-bladed upwind, and (c) 3-bladed downwind configurations.

Figure 3 - 17 shows the ratio of AEP (kWh) with and without the standby losses. It was clear how much overestimation of predicted power can occur especially in the low wind speed regions. Another important finding is that there are cases where the combination of low site average wind speed, large average yaw angle that the rotor is exposed, and a specific rotor can lead to even a net consumer wind turbine system

rather than producing one overall a year. This is seen well for the 3-bladed upwind turbine in the left graph and for yaw angles of 45° .

It is also clear that some wind rotors have much more beneficial production, such as 3-bladed downwind, which is due to better aerodynamic performance in yawed flow, better controllers, and possibly lower grid connection wind speed leading to less losses.

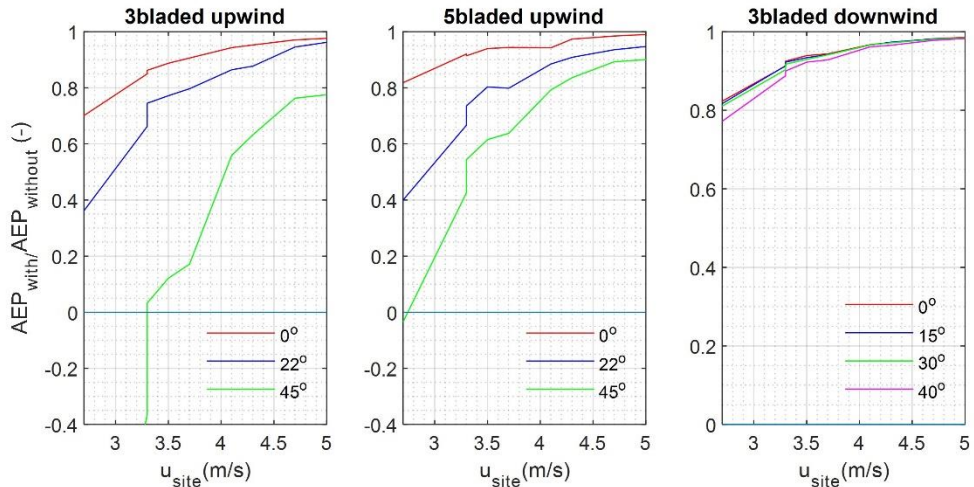


Figure 3 - 17 : Ratio of Annual Energy Production with and without the standby losses plotted for increasing mean wind speed $u_{site}(m/s)$ per different site and different yaw angles $\theta(^\circ)$.

3.3.3 Optimal Power Control Performance

Micro wind turbines have an aerodynamic maximum operating point at which they harvest maximum power from the available wind power. However, when placed in the field there are a number of factors that might lead to deviations from those optimal points. These factors have to do with the micro wind turbine design, the turbulent nature of wind speed at low heights, and the control system of the wind turbine. Observations from a wind tunnel experiment are presented showing the best operating point and the corresponded tip speed ratios and performance coefficients for micro wind turbines and then are compared with real-field measurements in order to give an impression of the micro wind turbine's behaviour on the field and identify the room for improving the performance characteristics of micro wind turbines.

3.3.3.1 C_P and Tip Speed Ratio Measurements in a Wind Tunnel

A test was performed by using the DC load set-up where the RPM of the generator could be controlled through voltage and thus the maximum aerodynamic power coefficient of this particular rotor was found. Figure 3 - 18 below presents the results for 2 rotor configurations with 5 blades (a smaller and a larger rotor diameter). For

both rotor diameters it was found that the maximum performance was between a tip speed ratio (TSR) of 4–6. Also, as wind speed increased, the optimum C_P was found in higher Tip Speed Ratios (TSR). Also, the C_P slightly decreased with increasing wind speeds. The C_P equation 3.11 below was based on the ratio of aerodynamic power P_{aero} (watts) (equation 3.12) and P_{gen} (watts). P_{aero} (watts) was based on the air density ρ_{air} (kg/m³), rotor radius $R_{turbine}$ (m) and wind speed u_w (m/s).

$$C_P = \frac{P_{gen}}{P_{aero}} \quad (3.11)$$

$$P_{aero} = 0.5 \times \rho_{air} \times \pi \times R_{turbine}^2 \times u_w^3 \quad (3.12)$$

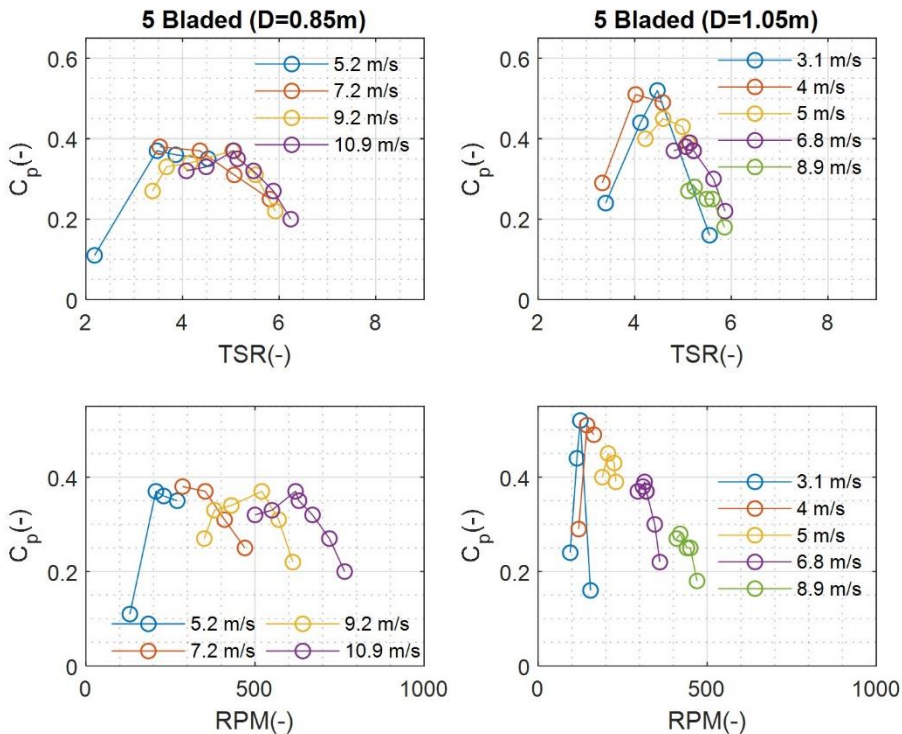


Figure 3 - 18 : Wind tunnel results of generator's C_P - λ (top) and C_P -RPM (down) curves of different rotor diameter 5 bladed upwind rotor configurations (left graphs for 0.85m diameter and right graphs for 1.05m diameter) based on $P_{gen}(W)$ power after the generator for different wind speeds (see legend).

For the 3-bladed downwind micro wind turbine used in the field experiment, unfortunately a detailed C_P - λ assessment was unfortunately not available. But data were extracted from the power curve characterization test including the RPM of the generator, thus the optimal operating point of the wind turbine for each wind could be found. The C_P and TSR characteristic data for all wind speeds are presented below in *Table 3 - 4*. This shows the power performance of the micro wind turbine for ascending wind speeds.

Table 3 - 4 : C_P -TSR characteristic curve for the 3-bladed downwind turbine configuration derived from wind tunnel test.

Wind Speed (m/s)	RPM	C_P	TSR
3.00	190.00	0.40	4.97
4.00	240.00	0.40	4.71
5.00	300.00	0.35	4.71
6.00	360.00	0.34	4.71
7.00	430.00	0.34	4.82
8.00	490.00	0.30	4.81
9.00	560.00	0.31	4.88
10.00	690.00	0.29	5.42
11.00	770.00	0.33	5.50
12.00	880.00	0.30	5.76
13.00	963.00	0.28	5.82

3.3.3.2 Performance of the Controller in the Field

A 22-minute dataset was collected from the field experiment. An analysis was performed for the wind speed U (m/s), Tip Speed Ratio (TSR), power performance (C_P), and rotational speed (RPM), which were recorded with 10 Hz sampling frequency. By comparing the scatter plots in Figure 3.19 with the experimental results in Table 4, it was understood that there were significant mismatches with respect to the optimal performance measured in the controller wind tunnel conditions. In particular, by looking at the histogram of TSR, nearly 37% of time the TSR was between 2–4, while 24% of time the TSR was between 4–6, which was the optimal range determined in the wind tunnel experiments. Looking at power performance coefficient consequently, a poor performance was also observed, with the turbine operating most of time not close to 30%–40% (as determined in the wind tunnel experiment).

This was also observed in the scatter plots where most data points co-exist for low TSR and low C_p (bottom right scatter plot). The results were also assessed with a lower sampling frequency of 1 Hz (with resampling), which presented no deviations for TSR with mean values being 3.48 (at 10 Hz) and 3.49 (at 1 Hz). But for the result C_p , an overestimation of the value was found with 20.7% (at 10 Hz) and 21.4% (at 1 Hz). Therefore, it is concluded that lower sampling rate overestimated power performance coefficients.

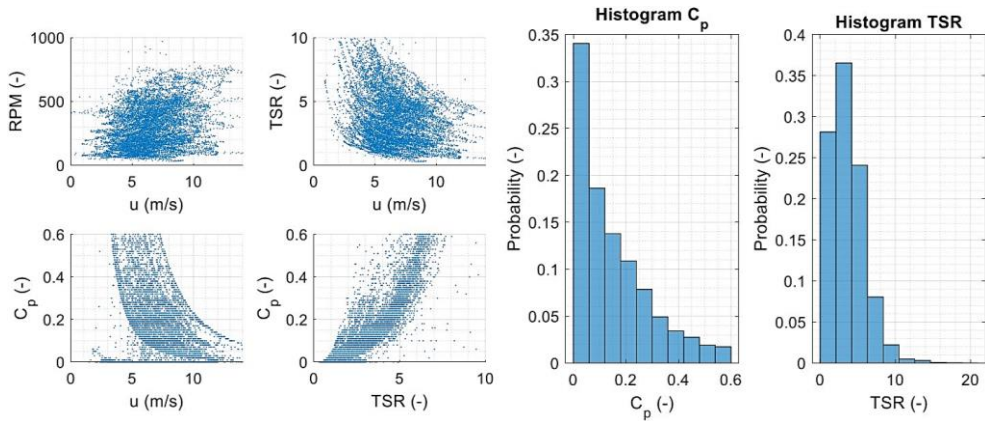


Figure 3 - 19 : (left 4 graphs) scatter plots of the 22-minute dataset for wind speed u (m/s), tip speed ratio, rotational speed (RPM), and coefficient of power performance C_p (right 2 graphs) histogram of probability of occurrence for the power performance coefficient C_p and tip speed ratio (TSR).

The results as such did not indicate a potential solution to this mismatch but rather addressed this issue. Control strategies differ per micro wind turbine manufacturer. It was understood that control systems were giving a flexibility on the micro wind turbine to operate in the near ground low wind speed and turbulent environment. Technically this is done by allowing the voltages to rise more, in order to keep the micro wind turbine spinning. At low wind speeds, manufacturers tend to let the micro wind turbines operate at a higher tip speed ratio (with the price of less efficiency) in order to avoid a full stop of the micro wind turbine, while in higher wind speeds, they allow the turbine to operate at lower tip speed ratio to allow better control. This is evidently shown in the top-right scatter plot of figure above. It is hard to classify in which conditions of the field experiment, the controller allowed on purpose to lower or higher tip speed ratios to find the optimal point of operation. But the dynamics of the controller response and ability to follow the turbulent nature of wind together with the inertial responses of the turbine could definitely be a next step into research.

3.3.4 *Starting behaviour and idling fatigue*

This section presents the findings of the starting and idling behaviour of the micro wind turbine from the wind tunnel and field experiment. The micro wind turbine behaviour was classified according to the following states:

1. Complete Stop
2. Idling
 - a. Rotor comes to idling condition from complete stop
 - b. Rotor comes to idling from generation
3. Generation
 - a. Coming from stop condition
 - b. Coming from idling condition

These states are further described below:

During the complete stop phase, if the hub's yaw angle is misaligned with respect to the flow, then the flow acts as a force to align the hub to the flow. The force acting on the rotor should be enough to rotate the hub to the direction needed. Figure 3 - 20 below shows results for different rotors tested in a wind tunnel from different yaw conditions. A 5-bladed and 3-bladed rotor with similar aerodynamic properties was exposed to an incremental wind speed increase in the wind tunnel starting from 90° yaw misalignment until the point the rotor started aligning fully with the flow (refer to the left image in Figure 3 - 5). It is clear that the 5 bladed rotor with higher solidity needs higher wind speed to start the flow alignment. Also, another finding was that while the tail-vane of the micro wind turbine assisted the rotor to start rotating from the perpendicular mis-aligned position in lower wind speeds, it took slightly higher wind speeds for the rotor to align with the flow (observe the region between 2–3 m/s).

Once the alignment is successful, then the rotation of the turbine starts leading to either idling state or generating state, described below.

While idling, the rotor does not produce any power but is in a standby mode where the controller boosts the voltage to connect to the grid by, for example allowing higher rotational speed to generate sufficient inertia in the system and then boosting voltage to connect to the grid side. This mode can happen from either a complete stop of the rotor or a rotating turbine that generates power. These two possibilities are explained below:

During the point where the rotor comes to idling condition from complete stop, the rotor is aligned with the incoming flow and the aerodynamical power is enough to allow the rotor to spin up to a point that it has overcome the cogging torque of the generator. However, there's not sufficient voltage boost to connect to the grid. The wind speed resource and its turbulence characteristics in combination with the power do not allow for sufficient rotational speed to be built up and thus voltage to connect to the grid. A final remark on this state, is that a combination of low wind speed with high

turbulence and some small magnitude gusts are needed to bring the rotor to this condition.

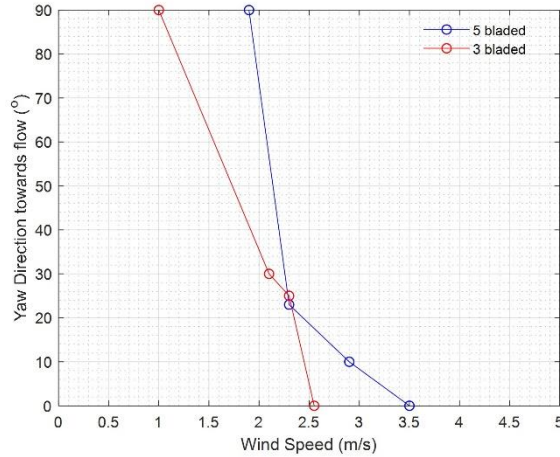


Figure 3 - 20 : Experiment where rotor alignment with the flow is assessed from a complete stop and a 90° misalignment and by increasing the wind speed until the rotor becomes fully aligned at 0°.

In the stage when the rotor comes to idling from generation, the turbine was connected to the grid and generating while the wind speed dropped significantly. Therefore, there was still inertia in the rotor, thus allowing for it to rotate up to a point that the voltage is not sufficient for grid interconnection. However, the aerodynamic wind speed power is enough to allow rotational movement by overcoming the generator's cogging torque.

While in generation mode, the turbine's generator voltage is sufficiently high to connect to the grid and the power electronics assure that the turbine is connecting to the grid and delivering power with the appropriate grid quality (typically 220 volts and 50 Hz). The turbine can reach this state either from a period where the rotor was at full stop or a period where the wind regime was such to allow the turbine only to idle. These are described below:

In the stage of coming from stop condition, the rotor reaches rotational speed that is sufficient to build the sufficient voltage in order to connect to the local grid conditions from a complete stop. Current is now flowing effectively and the power electronics make their work to deliver power to the grid. A combination of a previous stage of complete stop due to low wind speeds and a sudden increase in wind speed with gust behaviour might have allowed for this.

The stage of coming from idling condition, is similar to the previous step, but the rotor is already rotating, thus it is easier for it to connect to the grid with a slight increase to the mean wind speed.

This behaviour is quantified with a case study where the complete stop (State Zero), the idling mode (State One), and the generating mode (State Two) are assessed. This is quite important as during idling mode the wind turbine basically is not providing power while increase the overall cumulative fatigue to its components even though it is still in low rotational speeds. An algorithm was developed to assess this for 10-minute wind speed data for the place of Delft. The logic is quite simple and it considers 4 important wind speeds for the turbine, depicted from the explanations before.

These are described below and presented in Figure 3 - 21 below:

1. **Starting Speed u_{start} (m/s)**, this happens when the rotor starts rotating and has to be monitored through the wind tunnel experiments.
2. **Stopping Speed u_{stop} (m/s)**, when rotor comes to a full stop.
3. **Cut-In Speed u_{cut-in} (m/s)**, when the generator connects to the main grid coming from a complete stop condition.
4. **Disconnecting Speed u_{dis} (m/s)**, for which the turbine was still rotating before but in an idling condition.

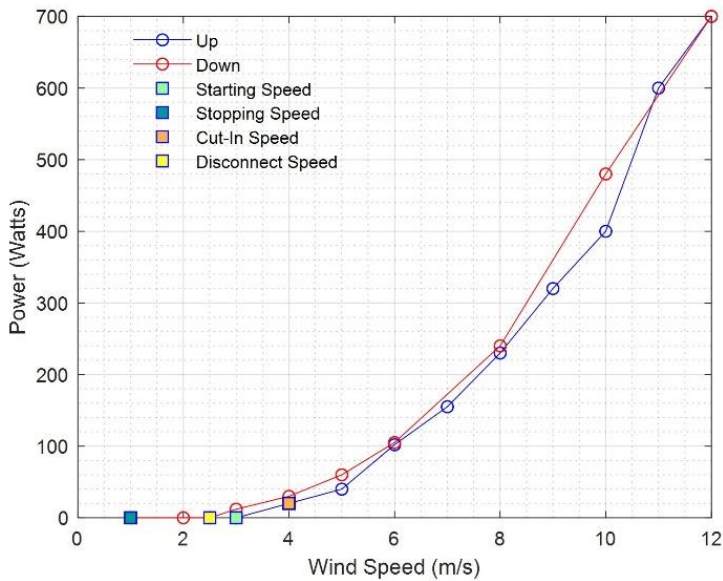


Figure 3 - 21 : Power curve recordings with an increasing (up) wind speed and then decreasing (down) wind speed. Characterizing wind speeds are noted in the legend box.

Using an annual wind speed dataset from Rotterdam airport's weather station, the different wind turbine states were determined along the logic scheme plotted in Figure 3 - 22. Thus, the amount of time was quantified when the turbine is actually generating, idling, or being at a full stop. This happens by assessing the previous state of the turbine

in each time step. The region between 2.5–4 m/s is quite important as the turbine might come from either a generating point or a full stop point. The logic is described below.

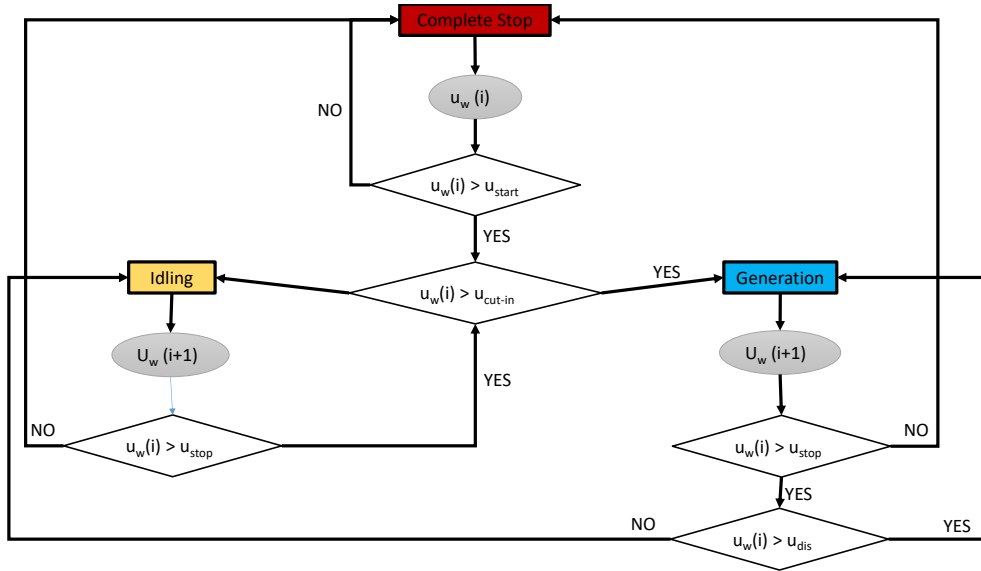


Figure 3 - 22 : Flow diagram for idling state assessment.

The results from this case study are presented in Figure 3 - 23, where State One represents the idling stage for this particular site and accounts for 15% of time, while complete stop (State Zero) is for 22% of time and generation (State Two) is at 63% of time.

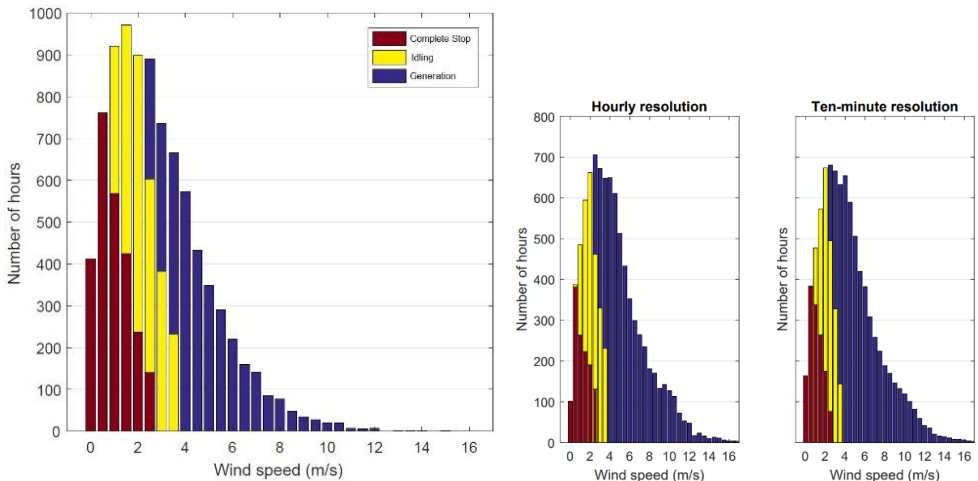


Figure 3 - 23 : (left graph) Case study for different wind turbine states in legend: (State Zero) rotor at complete stop and turbine not generating, (State One) rotor is idling and

not generating, and (State Two) rotor is rotating and generating. (middle and right graph) Different time resolutions.

Table 3 - 5 presents the distribution between stop, idling and generating for three different wind speed. When the mean wind speed of a site increases the idling states decreases and generation increase. For example, between 3 to 5 m/s idling reduces from 29% to 22% while generation increase from 41% to 57%.

Table 3 - 5 : Distribution of different wind turbine states for different sites mean wind speeds.

Mean Wind Speed (m/s)	3	4	5
State Zero (complete stop)	30%	23%	21%
State One (idling)	29%	28%	22%
State Two (generating)	41%	49%	57%

3.4 Discussion

This experimental study, inspired by the large number of articles that examine the performance of micro wind turbines, has cross validated many of the claims for their different performance characteristics. From the theoretical and experimental research work on flow misalignment, to the electrical system losses with a great emphasis on the standby losses, which are typically neglected, and from the control system losses to the findings on turbine idling state. All these results are very relevant for the noise barrier application, but could very well be projected to any urban micro wind turbine system. The results indicate the necessity for micro wind turbine designers to redesign many of the subsystems in order to more efficiently capture the available urban wind energy. Finally, from an installer's point of view, the combination of the poor performance characteristics with the rather expensive cost of micro wind energy systems (compared to the more mature PV systems) and the particularly low wind speed regimes near ground, makes the techno-economic evaluation of a micro wind energy system challenging. All these uncertainties increase the financial risks for a profitable system installation. Another characteristic not addressed in this current work is the maintenance demand of such a rotating electromechanical system, which could also affect the cost of electricity and it is proposed to be included in the future for further assessment.

To conclude this chapter in a holistic way, a final post-analysis of the results was made to picture the overall performance of the micro wind turbine in the field presented in Table 3 - 6. To understand where there could be points of improvement, the ideal power production was estimated by interpolating the wind speed

measurements for the 22-minute dataset with the idealized wind tunnel measured power curve before the inverter. Then the ideal energy productions are summed for each timestep from the wind turbine. This was the basis to estimate all the next ratios.

The measured actual power production data from the 22-minute dataset, right after the inverter and including standby losses, were summed and divided with the ideal production. It was found that the actual production was only 42% of the ideal one, which means that there were significant losses of ~58%.

These 58% losses were further classified into 3% for the standby losses and 5% for the inverters power conversion losses. The next loss presented was due to the inadequate yaw response resulting in flow-rotor misalignment. This was estimated by multiplying in each time step the potential drop of power with the ideal power production before the inverter, then summing up and diving with the ideal one. It was found that 18% of these losses might be attributed to the inadequate yaw response. Finally, the remaining 33% of losses must be attributed to the poor controller performance and other losses.

Table 3 - 6 : Breakdown of ratio of energy measurements related to performance characteristics at field test with respect to the ideal performance in wind tunnel.

Energy Measurements (Production or Losses)	Ratio of Energy Production or Losses with the Ideal Performance in Wind Tunnel
Net actual power production	42%
Standby losses	3%
Inverter losses	5%
Losses from Inadequate Yaw Response	18%
Controller performance losses (or other)	33%
Ideal Power Production before inverter (measured from wind tunnel)	100%

The Table 3 - 6 presented above for the 22-minute dataset for the average wind speed of 6.5 m/s brings up a conclusion that there is still room for improvement for the micro wind turbines on noise barriers. Therefore, the installation of the examined wind turbine at the particular noise barrier is not yet a mature choice to be made.

3.5 Conclusions

This chapter aimed to answer the research question of “What is the performance of a micro wind turbine integrated on top of a noise barrier?”. Therefore a wind tunnel and field test of a micro wind turbine on noise barrier were conducted. The key conclusion is that the actual performance on the noise barrier in terms of energy yield

was 42% from the ideal power production measured before the inverter in the wind tunnel. Eight percent of losses were due to the inverter and standby losses, 18% were due to inadequate yaw response to the wind flow, while the remaining 33% of losses were linked to poor controller performance. These results mean that there is still room to achieve the ideal performance as recorded in a controlled wind tunnel environment.

The key conclusions per performance category are summarized here.

Flow Misalignment

1. Power performance drops significantly with the increase of the flow skewed angle for which micro wind turbine's rotor is exposed on the noise barrier.
2. $\cos\theta$, $\cos^2\theta$, and $\cos^3\theta$ decay laws do not accurately reproduce the actual power for different yaw angles and wind speeds.
3. The micro wind turbine installed on top of the noise barrier presented a considerable flow misalignment for a 22-minute dataset (average wind speed of 6.5 m/s) resulting in an overall drop of C_P

Power conversion performance

4. Inverter performance measured at the wind tunnel was fairly reproduced in the field experiment with small deviations.
5. Standby losses from the inverter are not typically considered in Annual Energy Production estimations, but their importance should be addressed as in some case studies examined in current work, the combination of high standby losses and low wind speed regimes resulted in a net-consumer turbine.

Starting and idling of turbine

6. The idling state of the micro wind turbine, which might result in increased fatigue without any useful generation, could occur between 20%–30% of a full year as it was assessed for sites with annual average wind speeds of three to five meters per second.

Optimal Control

7. Wind tunnel measurements of different rotors indicated that power performance coefficients were optimum for tip speed ratios between four to six for the tested turbines.
8. These optimum points were achieved minimally in the field. A 20-minute dataset post analysis indicated that 40% of time the TSR was between two to four, thus in an inefficient region, resulting in nearly 70% to operate at power performances below 20%.

3.6 References

1. Orrell, E.P. Benchmarking U.S. Small Wind Costs; PNNL: Richland, WA, USA, 2017.
2. Ran Fu, D.F.; Margolis, R.; Woodhouse, M.; Ardan, K.U. Solar Photovoltaic System Cost Benchmark: Q1 2017; National Renewable Energy Laboratory (NREL): Golden, CO, USA, 2017.
3. Encraft. Warwick Wind Trials Report; Encraft: Delhi, India, 2009.
4. CarbonTrustUK. Small-Scale Wind Energy—Policy Insights and Practical Guidance; The Carbon Trust: London, UK, 2008.
5. Udell, D.; Infield, D.; Watson, S. Low-cost mounting arrangements for building-integrated wind turbines. *Wind. Energy* 2010, 13, 657–669, doi:10.1002/we.386.
6. Chrysochoidis-Antsos, N.; Amoros, A.V.; Van Bussel, G.J.; Mertens, S.M.; Van Wijk, A.J. Wind resource characteristics and energy yield for micro wind turbines integrated on noise barriers—An experimental study. *J. Wind. Eng. Ind. Aerodyn.* 2020, 203, 104206, doi:10.1016/j.jweia.2020.104206.
7. Schreck, S.J.; Schepers, J.G. Unconventional Rotor Power Response to Yaw Error Variations. *J. Phys. Conf. Ser.* 2014, 555, 012001, doi:10.1088/1742-6596/555/1/012001.
8. Ciri, U.; Rotea, M.A.; Leonardi, S. Effect of the turbine scale on yaw control. *Wind. Energy* 2018, 21, 1395–1405, doi:10.1002/we.2262.
9. Bastankhah, M.; Porté-Agel, F. A wind-tunnel investigation of wind-turbine wakes in yawed conditions. *J. Phys. Conf. Ser.* 2015, 625, 625, doi:10.1088/1742-6596/625/1/012014.
10. Bastankhah, M.; Porté-Agel, F. Experimental and theoretical study of wind turbine wakes in yawed conditions. *J. Fluid Mech.* 2016, 806, 506–541, doi:10.1017/jfm.2016.595.
11. Qian, Y.; Zhang, Z.; Wang, T. Comparative Study of the Aerodynamic Performance of the New MEXICO Rotor under Yaw Conditions. *Energies* 2018, 11, 833, doi:10.3390/en11040833.
12. Pedersen, T.F. On wind turbine power performance measurements at inclined airflow. *Wind. Energy* 2004, 7, 163–176, doi:10.1002/we.112.
13. Haans, W. Wind Turbine Aerodynamics in Yaw—Unravelling the Measured Rotor Wake; TU Delft: Delft, The Netherlands, 2011.

14. Tony, B.; David, S.; Nick, J.; Ervin, B. *Wind Energy Handbook*; John Wiley and Sons Ltd.: Hoboken, NJ, USA, 2001.
15. Bastankhah, M.; Porté-Agel, F. A New Miniature Wind Turbine for Wind Tunnel Experiments. Part II: Wake Structure and Flow Dynamics. *Energies* 2017, 10, 923, doi:10.3390/en10070923.
16. Hirahara, H.; Hossain, M.Z.; Kawahashi, M.; Nonomura, Y. Testing basic performance of a very small wind turbine designed for multi-purposes. *Renew. Energy* 2005, 30, 1279–1297, doi:10.1016/j.renene.2004.10.009.
17. Verde, A.; Lastres, O.; Hernández, G.; Ibañez, G.; Vereá, L.; Sebastian, P. A new method for characterization of small capacity wind turbines with permanent magnet synchronous generator: An experimental study. *Heliyon* 2018, 4, e00732, doi:10.1016/j.heliyon.2018.e00732.
18. Chub, A.; Husev, O.; Blinov, A.; Vinnikov, D. Novel isolated power conditioning unit for micro wind turbine applications. *IEEE Trans. Ind. Electron.* 2017, 64, 5984–5993, doi:10.1109/tie.2016.2645890.
19. Kristina, B.; Friedrich, W.F. Power Losses of Three Phase Rectifier topologies in small wind turbines. In *Proceedings of the PCIM Europe 2015; International Exhibition and Conference for Power Electronics, Intelligent Motion, Renewable Energy and Energy Management, Nuremberg, Germany, 19–20 May 2015*.
20. Alvis, S.; Linards, G. Front-End Converter Choice Considerations for PMSG-based micro-wind turbines. In *Proceedings of the 56th International Scientific Conference on Power and Electrical Engineering of Riga Technical University (RTUCON), Riga, Latvia, 14 October 2015*.
21. Whaley, D.M. *Low-Cost Small-Scale Wind Power Generation*. Ph.D. Thesis, University of Adelaide, Adelaide, Australia, 2009.
22. James, P.; Bahaj, A.S.; Anwar, A.; Myers, L. *Location, Location, Location: Domestic Small Scale Wind Field Report*; Energy Saving Trust: London, 2009; pp 2-3.
23. Shawn, S.; Rowen, A.; Beavers, D.; Korn, D. *Status Report on Small Wind Energy Projects Supported by the Massachusetts Renewable Energy Trust*; The Cadmus Group Inc.: Waltham, MA, USA, 2008.
24. Ebert, P.; Wood, D. Observations of the starting behaviour of a small horizontal axis wind turbine. *Renew. Energy* 1997, 12, 245–257, doi:10.1016/s0960-1481(97)00035-9.

25. García-Gracia, M.; Romero, Á.J.; Ciudad, J.H.; Arroyo, S.M. Cogging Torque Reduction Based on a New Pre-Slot Technique for a Small Wind Generator. *Energies* 2018, 11, 3219, doi:10.3390/en11113219.
26. Bukala, J.; Damaziak, K.; Kroszczyński, K.; Krzeszowiec, M.; Malachowski, J. Investigation of parameters influencing the efficiency of small wind turbines. *J. Wind. Eng. Ind. Aerodyn.* 2015, 146, 29–38, doi:10.1016/j.jweia.2015.06.017.
27. Martínez-Márquez, C.I.; Twizere-Bakunda, J.D.; Lundback-Mompó, D.; Orts-Grau, S.; Gimeno-Sales, F.J.; Seguí-Chilet, S. Small Wind Turbine Emulator Based on Lambda-Cp Curves Obtained under Real Operating Conditions. *Energies* 2019, 12, 2456, doi:10.3390/en12132456.
28. Loic, Q.; Clement, J.; Christian, E.C. Measuring the power curve of a small-scale wind turbine: A practical example. In *Proceedings of the 1st International e-Conference on Energies*, online, Switzerland, 14–31 March 2014.
29. Wegley, H.; Ramsdell, J.; Orgill, M.; Drake, R. *Siting Handbook for Small Wind Energy Conversion Systems*; Battelle Pacific Northwest Labs.: Richland, WA, USA, 1980.
30. ISO. ISO 16622—Meteorology—Sonic Anemometers/Thermometers—Acceptance Test Methods for Mean Wind Measurements; International Organization for Standardization: Geneva, Switzerland, 2002.
31. Predescu, M.; Bejinariu, A.; Nedelcu, A.; Mitroi, O.; Nae, C.; Pricop, M.V.; Craciunescu, A. Wind tunnel assessment of small direct drive wind turbines with permanent magnets synchronous generators. *Renew. Energy Power Qual. J.* 2008, 1, 306–311, doi:10.24084/repqj06.287.
32. Eltayesh, A.; Hanna, M.B.; Castellani, F.; Huzayyin, A.S.; El-Batsh, H.M.; Burlando, M.; Becchetti, M. Effect of Wind Tunnel Blockage on the Performance of a Horizontal Axis Wind Turbine with Different Blade Number. *Energies* 2019, 12, 1988, doi:10.3390/en12101988.
33. Chen, T.; Liou, L. Blockage corrections in wind tunnel tests of small horizontal-axis wind turbines. *Exp. Therm. Fluid Sci.* 2011, 35, 565–569, doi:10.1016/j.expthermflusci.2010.12.005.
34. NATO. *Wind Tunnel Wall Corrections*; Ewald, B.F.R., Ed.; NATO: Brussels, Belgium, 1995.
35. Grant, I.; Mo, M.; Pan, X.; Parkin, P.; Powell, J.; Reinecke, H.; Shuang, K.; Coton, F.; Lee, D. An experimental and numerical study of the vortex filaments in the wake of an operational, horizontal-axis, wind turbine. *J. Wind. Eng. Ind. Aerodyn.* 2000, 85, 177–189, doi:10.1016/s0167-6105(99)00139-7.

Chapter 3

36. Sicot, C.; Devinant, P.; Loyer, S.; Hureau, J. Rotational and turbulence effects on a wind turbine blade. Investigation of the stall mechanisms. *J. Wind. Eng. Ind. Aerodyn.* 2008, 96, 1320–1331, doi:10.1016/j.jweia.2008.01.013.
37. Lignarolo, L.; Ragni, D.; Krishnaswami, C.; Chen, Q.; Ferreira, C.S.; Van Bussel, G. Experimental analysis of the wake of a horizontal-axis wind-turbine model. *Renew. Energy* 2014, 70, 31–46, doi:10.1016/j.renene.2014.01.020.
38. KNMI. Uurgegevens Van Het Weer in Nederland—Hourly Data of Weather in the Netherlands. Available online: <https://www.knmi.nl/nederland-nu/klimatologie/uurgegevens> (accessed on 3 April 2019).
39. Kaiser, K.; Langreder, W.; Hohlen, H.; Højstrup, J. *Turbulence Correction for Power Curves*; Springer International Publishing: Berlin/Heidelberg, Germany, 2007; pp. 159–162.

4

Technical potential and application of micro wind turbines integrated on noise barrier acoustic screens in the Netherlands using GIS

“GIS is waking up the world to the power of geography, this science of integration, and has the framework for creating a better future”

— Jack Dangermond (American businessman and environmental scientist)

*This **chapter** provides a methodology to assess in a national scale the technical potential of micro wind turbines structurally integrated on top of noise barriers. The method uses GIS databases, wind energy models and corrections derived from the experimental work in previous Chapters.*

*The **research question** answered in this chapter is:*

“ Is there nationwide technical potential of micro wind turbine noise barriers in the Netherlands?”

This chapter uses the GIS methodologies that were developed as presented in Chapter 6.

4.1 Introduction

There is a strong tendency of utilizing urban energy towards the sustainable energy transition goals. While solar energy technologies are already implementing numerous concepts of integrating with infrastructures and buildings, micro wind energy is still under progress and development. An interesting concept of integration is to place structurally integrated micro wind turbines on top of noise barriers thereby avoiding support structure and foundation costs leading to an electricity cost reduction. This has been proposed and applied already for photovoltaic systems with the PVNB (Photovoltaic Noise Barrier). One of the major challenges though is to assess which would be the technical potential of micro wind energy systems on noise barriers. The availability of datasets of noise barriers, as well as wind resource datasets from weather stations and land cover maps, has made it possible to study the wind energy potential of micro wind turbines on noise barriers in the Netherlands. The combination of these datasets in a GIS tool together with the application of already existing wind resource models to translate wind speed time series to each noise barrier location and the results of the influence of noise barriers on wind flow properties, has given the opportunity to examine this on a national level. Additionally, the availability of GIS datasets in terms of infrastructures (electrical and gas networks) can be used to estimate the interconnection capabilities of such noise barriers. Current work examines bottom-up, the technical potential of integrating micro wind turbines on all existing noise barriers in the Netherlands and discusses potential power applications.

4.1.1 *Renewable energy applications on noise barriers*

Renewable energy potential on top of noise barriers could be from solar or wind energy. Much research has been done already on photovoltaic modules integrated with noise barriers but little has been done for micro wind turbines on noise barriers at least on the technical potential. The physical integration of photovoltaics on noise barriers has the potential to reduce costs and the same holds for micro wind turbines due to the structural integration with also the potential increase in energy production as found in [1] as a bonus.

Regarding solar energy barriers, an early European study identified the technical potential [2] of photovoltaic noise barriers (PVNB). A case study for mass deployment of photovoltaic noise barriers has been done as well with combination of GIS datasets for US [3]. Also in the Netherlands a monitoring programme was concluded on a motorway to identify the performance characteristics of PVNB [4]. This research and demonstration study of PVNB has identified the benefits of PVNB and resulted in governmental incentives in the Netherlands to promote solar panel physical integration with civil traffic highway infrastructures [5].

Urban energy roadmaps in the Netherlands indicate that renewable energy production and direct utilization should be increased in urban environments, in order to fulfil climate targets. These targets are presented in the Climate Agreement (Klimaatakkoord), but a specific mention of physical integration of micro wind energy with highway infrastructures is not made. Therefore, the present research findings could identify the merits pros/cons towards the long-term climate goals.

However, there has been some guidance regarding micro wind energy installation. At a European-wide level there is a report for micro wind turbines [6], where the deployability of those systems is assessed. It was found that small wind turbines could either directly sell electricity to the grid and get a premium or simply they lower the expenses of the electricity bill of the owner of the micro wind turbines. Around the same time, a report was published in the Netherlands from RvO (The Netherlands Enterprise Agency) regarding placement of micro wind turbines in urban environments. This report is a guideline for interested municipalities who want to install micro wind turbines [7]. However, there is not any holistic strategic approach on the real amounts of micro wind energy to be installed. The 2019 Dutch Climate Agreement (Klimaatakkoord) emphasizes the role of the different regions into promoting renewable energy projects in order to achieve a total target of 35TWh renewable electricity production on land by 2030. This electricity production refers to installations of wind turbines on land or PV greater than 15kW, thus more than a single micro wind turbine unit [8]. This goal is also described in Regional Energy Strategies [9] but there is not any mention, classification or description with respect to micro wind electricity. It is even mentioned that the smallest turbine installation is rated at 3.6 MW and an installation height of 80m. This is quite different from micro wind turbine scales, which are typically in order of a few kilowatts and a few meters from the ground. This could be interpreted as those smaller systems than 15kW (namely domestic solar and urban wind) are seen as a contribution to reduce the domestic energy consumption rather than contributing to National Renewable Energy Targets.

But since the hypothesis is that a large scale potential in wind turbine integrated noise barrier systems exist, therefore a nation-wide study assessment of the potential together with a feasibility study towards potential applications is necessary. Knowing the potential of the concept may assist authorities for identifying new non domestic possibilities for micro wind energy physical integration projects. But to do this, modelling at a national level of the potential is important. The next sections show different methods that have inspired this study to assess this technical potential.

4.1.2 Wind energy potential estimation at urban level with GIS

The use of GIS for the estimation of the energy potential of urban renewable energies has been researched by many. For the case of solar energy on noise barriers a list of test set-ups together with the European wide potential is presented in [2]. Authors combine meteorological data together with noise barrier data to find the total

potential for Europe. Another useful study in Italy uses GIS data for financial feasibility of roof-top mounted wind turbines in [10]. A GIS-based decision support model is configured using data from weather stations, an urban canopy meshed grid and a link to equations related to estimation of wind energy potential and Annual Energy Production (AEP). For this case a 3kW turbine was used. Interestingly land lease values were also used for the estimation of profitability of the system. Another holistic approach is the GIS use for energy estimation of solar noise barriers in the USA presented in [3]. The power and energy potential of mass-scale deployment of photovoltaic noise barriers (PVNB) was estimated. GIS software was used in which noise barrier characteristics (orientation, location) in combination with irradiation data were combined to determine the potential. Losses related to solar energy potential such as soiling of panels was also included. GIS was also used to assess the impact of large scale building integrated PV deployment in the sizing of urban transformers in [11]. Solar extension modules in GIS software estimate the power needed and then relate it to the existence of transformers. In that manner, GIS are very powerful in strategic planning of urban infrastructural developments, especially for the energy transition to happen in urban centres with increasing amounts of renewable energy. GIS has been used as a decision support tool for evaluating renewable energy in [12]. Urban wind turbines and PV deployment potential has been examined as well for the city of Sydney in [13] with the use of GIS. Finally, another interesting method is presented in [14] where the wind resource is mapped in the UK. For the UK the Numerical Objective Analysis of Boundary Layer database (NOABL) is widely used for urban wind resource assessment having a 1km² resolution of annual wind speed without the effect of surface roughness [15]. Hence the NOABL dataset overestimated the wind resource available. The study in [16] addressed the surface roughness for wind resource assessments in a case study for London. The surface roughness is plotted like a GIS plot. One of the results, relevant for the concept described here, is that micro wind turbines placed at city outskirts, where typically a noise barrier would be installed, present a larger capacity factor than the central locations of cities. This effect, even though not studied within the current study, shows that micro wind turbines on noise barriers in outskirts of cities would be the preferred location.

GIS clearly provides a large number of data, as well as with information and tools to combine geospatial parameters for the energy potential estimation. For the present study, the inclusion of wind resource models is crucial in order to estimate accurately the potential on top of the noise barriers. Estimating the wind speed for micro wind turbine sites can be costly and expensive if done through a wind resource assessment [15]. Therefore, several techniques have been proposed to assess wind speeds by combining existing datasets from weather stations. Several models exist that estimate the local energy potential for wind resources using weather stations. Regarding the quantification of wind energy resources, one of the methods is to “translate” historical measured data from weather stations nearby to the site of interest. An early study in

[17] presents a method to translate wind data in the Netherlands from a weather station upward to a blending height, which produces a representative mesoscale wind speed for an area block of $5 \times 5 \text{ km}^2$. After that wind speeds are translated to the macro wind level taking into account the surrounding roughness. Finally, these are interpolated for regional smoothing and then translated back to the desired site. The method has been used as well by the Royal Dutch Meteorological Institute (KNMI) [18]. This method produces representative wind speed statistical estimates (e.g., Weibull parameters, mean wind speed wind direction). However, this method was questioned in [19], and concluded that spatial interpolation methods with mesoscale level wind produce better results than macroscale level wind in Flanders in Belgium. A method of bias was used to compare the data for some weather stations. To determine the wind potential, roughness lengths for the different wind directions are essential, as typically used in the log-wind model. The estimation of such roughness lengths has as well been subject of research. In [20] a numerical study is presented for the area-averaged roughness lengths for estimation of wind potential. Another study used the WASP software's (Wind Atlas Analysis and Application Programme) roughness model with wind direction sector weighted roughness length for each site [21]. Averaging roughness length scale in directional sectors from GIS datasets with land cover classes was performed trying to represent the roughness of each sector. In this study four test cases are made, a land cover based roughness length map, a corrected land cover-based roughness length map, a constant roughness length map and a custom digitized roughness map. This directional roughness length is needed for the estimation of sectorial wind speed time series. The aerodynamic roughness length is direction-dependent due to the various roughness elements within the source area [22]. This was as well examined in an open field experiment of 1000 meters length and 500m width. Roughness length sectorial parameters were estimated by spatial average roughness lengths for each direction. The footprint model which weighs the contribution of each parcel of land in the upwind direction of different sectors has been used. This approach is useful as well for the present study.

Finally, once the wind speed is translated to the noise barrier site then barrier related corrections are needed. In current case the corrections come from the study presented in chapter 2 on wind resource characteristics on top of noise barriers through an experimental campaign that took place in 2017 near the city of Delft in the Netherlands [1].

4.1.3 Novelty – Motivation – Outline

In the introduction of the chapter, the need of a nationwide approach to assess the potential of novel micro scale renewable energy projects and in particular micro wind energy projects, is emphasized. Additionally, various methods of wind resource assessment are presented as well as how the reproduction of wind time series from nearby sites is possible whenever there is a weather station and a roughness map.

Finally, it is shown that a combination of GIS and wind estimation models is needed in order to answer questions related to the available technical potential for those sites. This chapter presents results for micro wind turbine integrated on top of noise barriers including the corrections determined from a test site. The chapter is structured accordingly: it has an Introduction, followed by the second section where the nationwide potential estimation methodology and results are presented and classified per provincial level. Then a discussion section is presented in order to match the electricity potential with demand clusters and finally a conclusions section highlights the major findings.

4.2 Nationwide wind energy potential estimation for acoustic screen noise barriers in the Netherlands

This section presents the methodology and results for the Dutch nationwide wind energy potential for micro wind turbines on noise barriers. In section 4.2.1, an explanation of the way the datasets of the noise barriers were handled is presented along with the suitability of certain noise barriers for this study. In section 4.2.2, the methodology to estimate the localized wind resource at the noise barrier is presented along with the complexities to translate wind speed time series from nearby weather stations. And finally, in Section 4.2.3, the estimation of the Annual Energy Production (AEP) together with the classification per province in the Netherlands is presented and discussed.

4.2.1 Suitable noise barriers for micro wind turbine applications

GIS datasets provided by Rijkswaterstaat [23] showed that the Netherlands has 6138 segments of noise barriers with a total length of 1071 kilometres. These noise barriers are initially classified in three types. These are the earth embankments, the acoustic screens and the combination of both when a screen is installed on top of an earth embankment. Examples are shown in Figure 4 - 1.



Figure 4 - 1: Different types of noise barriers (left) earth embankment type of Photovoltaic Noise Barrier [24] (middle) acoustic screen type of micro wind turbine noise barrier (right) combination of an earth embankment photovoltaic noise barrier with an acoustic screen [25]

In the current study the focus is on the acoustic screen type for reasons explained below. These represent 622 kilometers (58% out of the total length). These screens are suitable for structural integration with micro wind turbine as they have a rigid support structure. The selection to investigate this type of noise barriers is also based on the availability of experimental dataset for wind flow corrections on such types, while for the other two there were not available. Therefore, the other 2 categories are excluded from the analysis as explained below.

Specifically, the earth embankments, which represent 343 kilometers (32% of the total length), are excluded from the analysis. Earth embankments are inclined parts of land (similar to landfills) and could be suitable for PV farm installation. They do not have rigid support structures where the micro wind turbines can be integrated. Instead, micro wind turbines would require a support structure (tower and foundations) which increases the overall cost of integration. The focus of this study is to investigate the noise barriers on which structural integration is possible as it significantly reduces the cost of micro wind energy. Therefore, earth embankments are not included.

Finally, also the noise barrier types which are a combination of both earth embankments and screens are not taken into account. These represent 114 kilometers (10% of the total). The reason for not including those hybrid noise barriers is that, as the methodology will indicate, wind speed and direction corrections will be applied to estimate the wind energy potential on top of acoustic screen type of noise barriers. These are the only evidence possessed for the blockage effects that these noise barriers' structure will impose to the localized wind flow. These corrections are based in the current study in experimental data that were collected from a wind resource assessment [1] for acoustic screen type of noise barrier. Since the combination of earth embankment and acoustic screen will have a different effect on the flow, the corrections applied in the current methodology would not be applicable. Hence the analysis is reduced to only the acoustic screen type of noise barriers.

For the selected acoustic screens, a further classification is applied based on material suitability and the tilt angle of the barrier. The material suitability is relevant due to the installation of a rotating electromechanical equipment on top of the noise barrier which should be qualified for structural integrity, strength and vibration mitigation. A detailed technical assessment has not been performed to select the most appropriate materials but rather a suggestion based on qualitative assumptions is made. Finally, for the tilt angle criterion, a simplistic selection of noise barriers that have the most similar configuration to the experimental set-up in [1] is made.

Regarding the noise barrier acoustic screen material suitability, a dataset has been used provided by Directorate-General for Public Works and Water Management (Rijkswaterstaat) [23]. The dataset classifies noise barrier with 2 general material categories. The first category is the construction material which is typically the foundation, the main support structure of the noise barrier and the frame. The second

category is referred to as the primary material of the noise barrier which refers to the sound absorbing panels which the support structures hold.

Regarding the construction material category, a qualitative structural integrity assumption was made that wood type construction material barriers are the unsuitable ones. The total lengths that these represent are classified into:

- Concrete (32km – 162 segments with average length of 200m)
- Wood (1.2km – 11 segments with average length of 116m),
- Metal (381km – 2674 segments with average length of 142m)
- Not Available (207km – 1409 segments with average length of 147m)

The second filtering is based on the primary materials of the noise barriers. The ones based on vegetation, brick, wood and gabion basket material (58km in total) are assumed not suitable for micro wind turbine installations based on the assumed qualitative criterion for structural integrity as explained before. Therefore, the following primary materials are assumed suitable for micro wind turbine structural integration at the noise barrier:

- Concrete (211km – 1527 segments with average length of 138m)
- Glass, Plastic, Composite² (187km – 1449 segments with average length of 129m)
- Wood-fibre reinforced concrete (91km – 460 segments with average length of 199m)
- Metal (67km – 41 segments with average length of 166m)

Finally, another classification is based on the tilt angle of the barrier. About 12km in total of noise barrier is tilted towards the road while all the rest of the barriers are either positioned vertical or have a tilt backwards of the road.



Figure 4 - 2: Photo examples of noise barrier tilt orientation (left) noise barrier with a forward tilt towards the road [24] (right) noise barrier with a backwards tilt towards the road

² Glass Plastic Composite material category aggregates all glass or (reinforced) plastic types of material in a single category. An example could be the PPE or Perspex or PVC plastic materials.

This information is important as part of the further modelling corrections which use wind speed corrections for a noise barrier measured from [1] with a backward tilt angle of 5-10 degrees. Therefore, both 0- and 10-degree barrier segments are selected for the analysis.

The following classes have been defined:

- 0 degrees (vertical) (275km – 1890 segments with average length of 145m)
- 10 degrees (253km – 1784 segments with average length of 142m)
- 20 degrees (22km – 137 segments with average length of 164m)
- 30 degrees (9km – 62 segments with average length of 159m)

On the suitable noise barriers, it is assumed that 0.375 kW micro wind turbines of 1.7 m rotor diameter will be installed. These wind turbines are placed with a 5D clearance between each other in order to avoid wake effects. This is a standard practise for large scale wind farms and in this case, this clearance is assumed in order to get the order of magnitude estimates necessary. Therefore, the total length of each noise barrier is divided by 5 times the diameter (1.7m) of the rotor = 8.5 meters in order to get an estimate about the amount of micro wind turbines that can be located on the noise barriers.

This results in a total of 53600 micro wind turbines to be installed on suitable noise barriers with a total installed capacity of 20114 kW in a total length of ~554km. This means that 50% of the total length of noise barriers in the Netherlands is potentially suited for micro wind turbine installation. The average amount of micro wind turbines per noise barrier segment is 11 resulting in an average installed power per segment of 3.3kW. The histogram in Figure 4 - 4 presented in next pages shows that 2000 noise barrier segments are less than 10 turbines (3.3 kW). This is an important finding towards the nationwide implementation of such concept, provided it makes sense both financially and energy-wise.

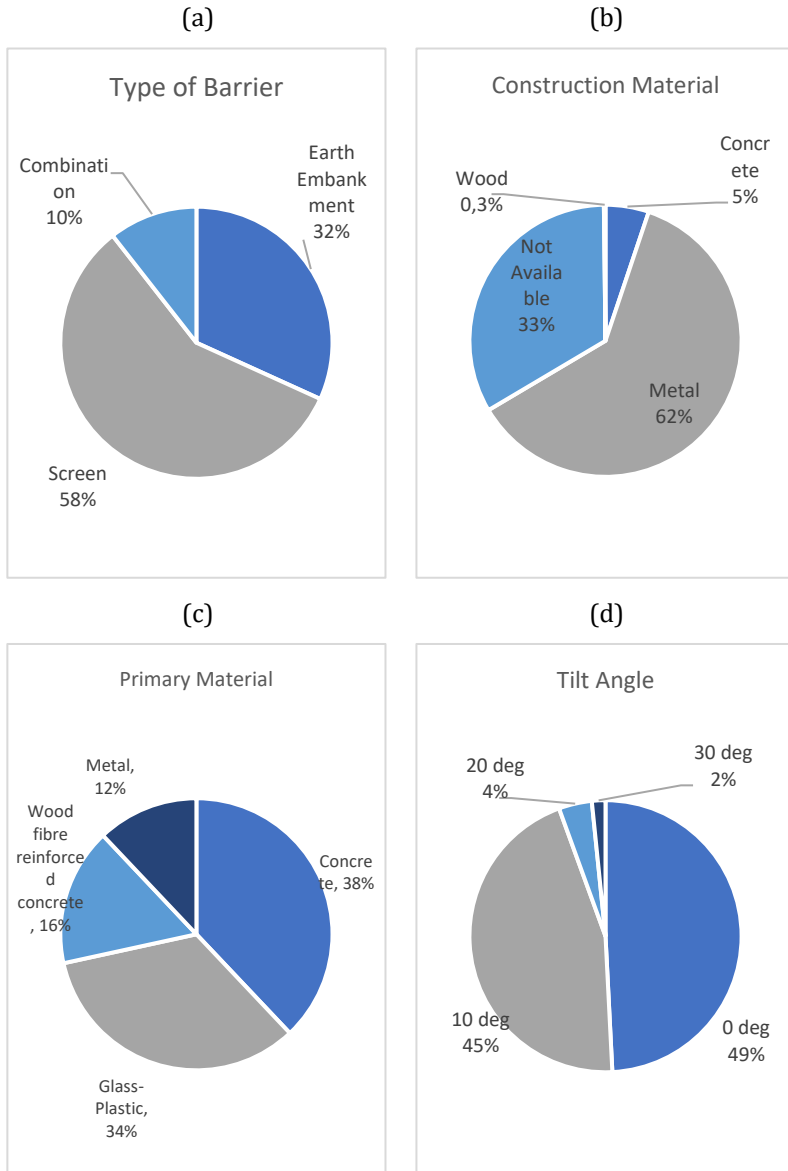


Figure 4 - 3: Noise barrier filtering and classification results based on (a) type of barrier, (b) construction material, (c) primary material and (d) tilt angle

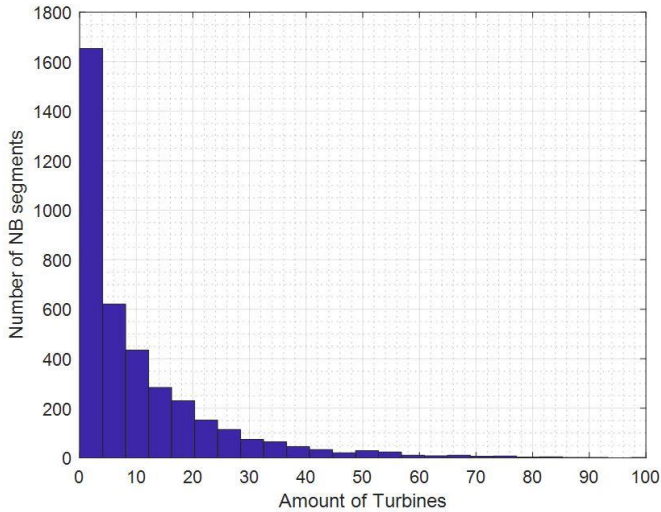


Figure 4 - 4: Histogram showing number of noise barrier segments that can host a given amount of installed micro wind turbines

4.2.2 Weather station time series translation to the noise barrier site

With the suitable noise barrier segments known from the previous section, the wind resource available to each noise barrier site can be estimated. This is composed by the following steps:

- Identification of the closest and suitable weather station to each noise barrier
- Translation of the wind speed time series of the weather station to the particular noise barrier site

KNMI has 42 weather stations around the Netherlands, where 10 minutes wind speed and direction time series are aggregated, from which 1-hour average values are composed. Those stations are usually placed in open fields (for example airports) where the roughness length around the anemometers is not affecting the wind regime. After each 10-minute average measurement the values are corrected for the roughness length valid for the respective wind direction, in order to create a uniform roughness data base. These KNMI stations are related to each noise barrier segment with a Nearest Neighbour Analysis tool available in GIS software. The weather stations are indicated with stars in Figure 4 - 5 and the noise barriers are depicted with green dots.

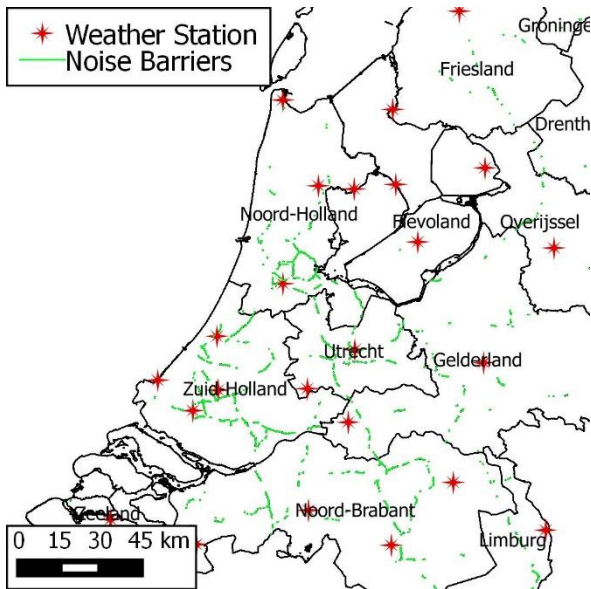


Figure 4 - 5: Weather stations (red stars) and noise barrier segments (green dots) in the Netherlands

The distribution of the distances from the midpoint of the line geometry of all the suitable noise barrier segments to the weather stations is shown in Table 4 - 1 below. These distances are used later for validation purposes. It is concluded that ~85% of noise barrier segment midpoints are within a 20km range from a KNMI weather station. A zoomed in example of the distances is also shown in Figure 4 - 6.

Table 4 - 1: Distribution of noise barriers distance range from nearest weather station

Distance Range	Number of segments
0-10 km	1181 (38%)
10-20 km	1424 (45%)
20-50 km	511 (16%)

As described above the wind speed time series are translated to the noise barrier sites. This is done by using the interpolating method for wind speed normal from [17] where all the wind speed time series are projected to a blending height of 60 meters, suitable for the flat lands of the Netherlands. Instead of statistical normal mean, blended time series are used to estimate the local wind speed time series at the noise barrier location. The second step of translation to macroscale level wind is omitted as a more recent study for Flanders in Belgium [19], identified that transforming the surface wind

to mesoscale levels yields into better results for wind resource mapping than the macroscale level for wind speed estimation.

Initially wind speed time series are translated to the blending height of 60 meters above the weather station. This is shown in equation 4.1 below. For each hourly time step t_i the weather station wind speed u_{WS} (m/s) at the elevation height at of the weather station location h_{EL_WS} (m) is translated to the wind speed u_{BLEND} (m/s). This wind speed is at the mesoscale blending height h_{BLEND} (m) of 60 meters. The local roughness length z_{SECTOR_WS} (m) surrounding the weather station at each wind direction dir ($^\circ$) sector is used to correct. This approach is the so-called log-law of wind speeds.

$$u_{BLEND}(t_i) = u_{WS}(t_i) \times \frac{\ln\left(\frac{h_{BLEND} - h_{EL_WS}}{z_{SECTOR_WS}(dir(t_i))}\right)}{\ln\left(\frac{h_{WS} - h_{EL_WS}}{z_{SECTOR_WS}(dir(t_i))}\right)} \quad (4.1)$$

The roughness lengths corrections for both the weather station time series and the noise barrier site are important because they represent the effects from the surrounding landscape on the potential wind flow. These variables, z_{SECTOR_WS} (m) and z_{SECTOR_NB} (m), are determined using data for 10° directional segments around the nearest weather station of each noise barrier. The method of determination of sector roughness lengths was presented in [17] with weighted averages of the surrounding local surface roughness lengths of the weather station. The same method is also presented in [26] in which a circle of 3km radius is used with 3 concentric circles of 1, 2 and 3km distance from the point of interest. A method to apply weighting factors dependent on the distance of the roughness length class of the concentric circles was used in [27]. Unfortunately, this method was not validated by comparing with site measurements. Therefore, no weighting factors are applied in the presented methodology for the sectorial roughness lengths. Instead, the values for the 3 points, for each kilometre at each 10° roughness length sector, are averaged. The 3-point concentric method can be found in Figure 4 - 6.

The roughness lengths assigned for each geospatial place are derived from the classifications in the CORINE's (Coordination of information on the Environment) Land Use and Land Cover database [28] and their assigned roughness length are explained in [21]. This database classifies the Netherlands with 9805 shapes of area. The shapes of area are enclosed multiline areas within which a specific land use or cover category exist which has a specific roughness length. These shapes have for the Netherlands a median area of 0.7 km², while 98% of the classified area shapes are below 25km². Therefore this database is suitable for the analysis since it is within the ranges of areas

presented in the method for blending height in [17]. The CORINE database for an application in South Spain proved to be an updated database which takes into account urban use areas which are very important for the current study [29]. In particular, this method provided good estimates in comparison with measured wind speeds and directions due to the good representation of land-use variability around the weather station. Therefore, this roughness length database is used in the current method for the translation of wind speed time series to each noise barrier site.

The roughness length is assigned for each point and sector around the weather stations and the noise barriers with the following steps, applied in a GIS software:

- Define the central point of the noise barrier (midpoint) and the weather station through the GIS Geoprocessing Tools
- Create a multi-ring around the central point with a maximum diameter of 3000 meter with 1000 meter segments, similarly as in [26], through the GIS Geoprocessing Tools
- For each point around the centre of the weather station or noise barrier (see the red or green 36 points in each multi ring with 10° segments in Figure 4 - 6):
 - o Estimation of the azimuthal orientation with respect to the central point of the noise barrier or the location of the weather station via the x and y position of the point and the centre as equation 4.2

$$azimuth = \arctan\left(\frac{x_{point} - x_{center}}{y_{point} - y_{center}}\right) \quad (4.2)$$

- o Assign the roughness length (Land Cover classes) of the area with which each point coincides, through the “Join Attribute” tool from the Vector data management Tools of QGIS software.

This method allows to have a more refined representation of the roughness lengths surrounding the noise barrier and weather station, which is very important especially for the low heights assessment of exploiting urban wind energy.

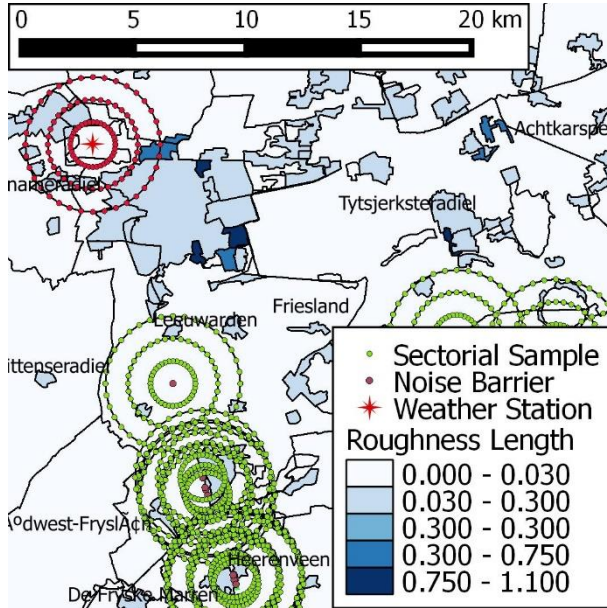


Figure 4 - 6: Weather station and noise barrier concentric 10° segment roughness length sample points

After the translation of the weather station time series to the blending height, these time series are translated to the noise barrier wind turbine installation height $h_{install}$ (m) in equation 4.3. The installation height of the turbine on top of the noise barrier is found from the top height of the noise barrier H_{nb} available in the GIS databases for noise barriers in the Netherlands [23], the turbine's hub distance from the tip of the noise barrier for the wind turbine used is H_{tur} 1.8 m, as can be seen in Figure 4 - 7. Finally, the heights are corrected by the local elevation height h_{EL_LOCAL} (m).

$$h_{install} = H_{nb} + H_{tur} \quad (4.3)$$

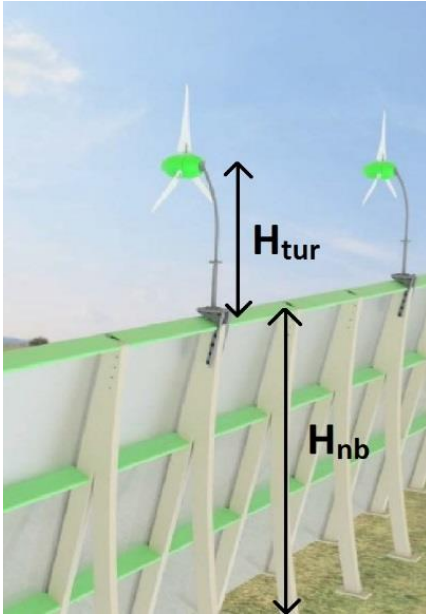


Figure 4 - 7: Noise barrier and micro wind turbine height

The sectorial roughness length z_{SECTOR_NB} (m) for the location of the noise barrier is used as explained before. The roughness length is different for each particular segment and each direction of the wind speed due to the highly rough area surrounding the barriers. The log-wind equation 4.4 is used for the u_{NB} (m/s) for each hourly time step t_i . The same wind direction $dir(^{\circ})$ time series from the weather station are used as well here and are assumed equal.

$$u_{NB}(t_i) = u_{BLEND}(t_i) \times \frac{\ln\left(\frac{h_{install}}{z_{SECTOR_NB}(dir(t_i))}\right)}{\ln\left(\frac{h_{BLEND} - (h_{EL_NB} - h_{EL_WS})}{z_{SECTOR_NB}(dir(t_i))}\right)} \quad (4.4)$$

Figure 4 - 8 summarizes the method for translating the wind speed time series from the weather station to the noise barrier location. The wind speed time series are translated first for a case assuming micro wind energy production without the presence of a noise barrier and the following step is with a micro wind turbine integrated with the noise barrier.

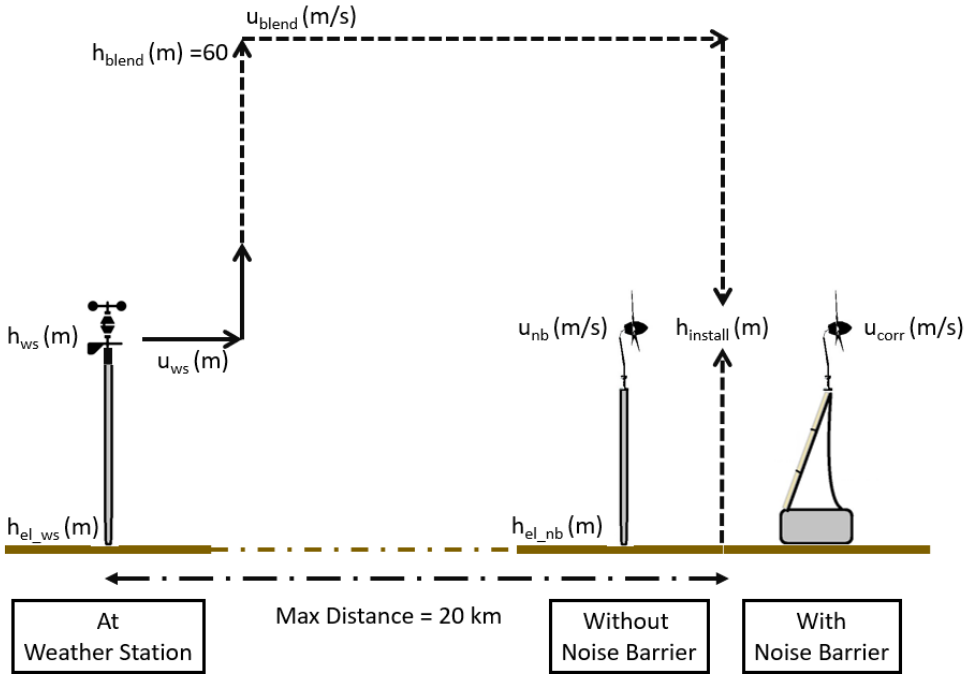


Figure 4 - 8: Schematic summarizing the methodology to translate the wind time series from the weather station location at the left up to location of the noise barrier.

The method analysed above to translate time series from weather station to the noise barrier is complemented by an error analysis. An annual mean error analysis is performed by comparing pairs of KNMI weather stations which have a distance smaller than 20 kilometres to the noise barrier segment. 85% of noise barrier segments are placed within a 20-kilometre distance from a KNMI station as indicated in Table 4 - 1 earlier. The Annual Mean Error (AME) (shown in equation 4.5) is estimated from the difference of the predicted value from Station 1 with the KNMI measured hourly time series of Station 2. The Annual Mean Error (m/s) is found from the following equation, similarly as in [19], where $u_{ws_prediction}$ is the wind speed time series prediction and $u_{ws_measured}$ (m/s) is the reference measured time series of the weather station. Below, in Table 4 - 2, the annual mean error is presented for the 5 suitable weather station pairs that are in a distance of less than 20km. The average median error is around -0.77 m/s, and this must be taken into account in the energy analysis estimates.

$$AME(m/s) = \frac{1}{8760} \sum_{i=1}^{8760} [u_{ws_PREDICTION}(t_i) - u_{ws_MEASURED}(t_i)] \quad (4.5)$$

Table 4 - 2: Annual Mean Error for the weather station pairs below 20km distance.

Distance	Station 1 (time series used for prediction)	Station 2 (reference measured time series)	Annual Mean Error (m/s)
19.9km	215	344	-0.61
13.2km	248	249	-0.48
15.4km	248	258	-1.39
17.1km	330	343	0.87
19.9km	343	344	-0.67
19.5km	348	356	-0.63

4.2.3 Noise barrier influenced Annual Energy Production Potential

Once the annual wind speed time series for each noise barrier segment are identified, the annual energy production $AEP_{reference}$ (kWh), excluding the influence of the noise barrier, is calculated first. Next corrections are applied to estimate the influence of the noise barrier on the total energy yield. The annual energy production is estimated from the sum of the hourly wind turbine power production values. For each hour, the wind speed estimated is used as an input for a look-up table function of the power curve for the wind turbine used. The reference power curve of this 0.375 kW turbine has been measured in [1]. The reference $AEP_{reference}$ (kWh) (shown in equation 4.6) of the micro wind turbine for each noise barrier segment is multiplied by for the total amount of installed wind turbines per segment. This is done by dividing the length of the noise barrier segment $L_{barrier}$ (m) with the turbine spacing parameter of 5 times the diameter of the turbine $D_{turbine}$ (m). Whenever this number is a decimal, it is rounded downwards to an integer.

$$AEP_{reference} (kWh) = \sum_{i=1}^{8760} P(u_{NB}(t_i)) \times \left\lfloor \frac{L_{barrier}}{5 \times D_{turbine}} \right\rfloor \quad (4.6)$$

Once the total $AEP_{reference}$ (kWh) is estimated for each noise barrier segment, the hourly wind speed time series are corrected for the noise barrier influence. These corrections are based on the experimental results measured in the field experiment in [1]. There are two types of wind speed corrections applied. First, the changes in wind speed magnitude when flow is misaligned with the fixed azimuth of the noise barrier expressed as wind speed magnitude change η_{wsf} (%). At each time step, the relative flow

angle is found with respect to the azimuth of the noise barrier and the corresponding wind speed factor change is assigned to the wind speed. The wind speed change with respect to the relative wind flow angle is presented with the left graph in Figure 4 - 9.

Secondly, the changes in wind speed due to the flow misalignment with the turbine's rotor due to the vertically skewed flow on top of the barrier are applied. The skewed flow angles, that correspond at each incoming wind flow angle relative to the fixed noise barrier azimuth, are shown in the right graph in Figure 4 - 9. These results were experimentally determined in [1]. It is clear that in any direction the flow is skewed between 8-13 degrees. This correction is applied by using the yaw misalignment $\cos\theta$ theory. At each time step the relative flow angle is estimated for which a specific skew angle was measured. This skew angle is added as the θ angle in the $\cos\theta$ theory.

Since the corrections presented in Figure 4 - 9 were measured only for the upwind side of the noise barrier in [1], an assumption has to be made for the corrections for wind flows coming towards the downwind side of the noise barrier. Therefore a "mirrored" symmetry of the corrections is assumed. Even though this is questionable assumption because the noise barrier is not erected vertically but with a given angle to the vertical, it had to be assumed because experimental data are only available for 1 side of the barrier. Thereby, the effects are assumed equal on the other 180° arc behind the barrier. The performance characteristics of the turbine as measured in Chapter 3 are not taken into account into the technical potential estimations as different turbines are expected to make up the total of the national potential which would thereby have different losses and different system designs. Finally, the noise barrier corrected wind speed u_{CORR_NB} (m/s) is estimated in each time step t_i taking into account the different losses aforementioned in equation 4.7 described below:

$$u_{CORR_NB}(t_i) = u_{NB}(t_i) \times \left[1 + \eta_{wsf}(azimuth(t_i)) \times \cos\theta_{skew}(azimuth(t_i)) \right] \quad (4.7)$$

The experimental results used in this study come from a typical noise barrier located in Delft with a backward tilt angle of 10° and a height of 5 meters [1]. There will certainly be deviations for each particular noise barrier case but the generalized approximation of equation 4.8 will help to sketch the bigger picture of the national energy potential of wind power on top of noise barriers.

The corrected wind speed time series can now be used in the AEP calculations. The corrected annual energy production $AEP_{corrected}$ (kWh) is estimated for each noise barrier segment with equation 4.8. All the estimated annual energy productions that are determined either for the reference or the corrected case can then be aggregated to make nationwide conclusions, which are presented later.

$$AEP_{corrected} (kWh) = \sum_{i=1}^{8760} P(u_{CORR_NB}(t_i)) \times \left(\frac{L_{barrier}}{5 \times D_{turbine}} \right) \quad (4.8)$$

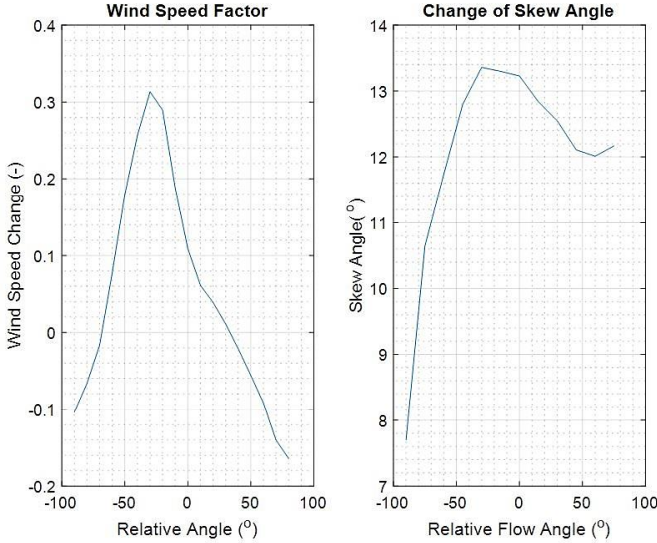


Figure 4 - 9: Noise barrier wind speed corrections (left) wind speed percentage change factor due to noise barrier (right) change of skew angle

Another important metric which shows the performance of the micro wind turbine on the noise barrier is the capacity factor cf (%). The following equations are used to estimate the capacity factor at the noise barrier site, both for the reference (equation 4.9) and the corrected AEP (kWh) in equation 4.10. This factor is the ratio of the total potential energy produced within a year divided by the potential energy production if the turbine would be operating at its rated power. With this metric, the utilization of the wind turbine can be determined.

$$cf_{reference} (\%) = \frac{AEP_{reference}}{8760 \times P_{RATED}} \quad (4.9)$$

$$cf_{corrected} (\%) = \frac{AEP_{corrected}}{8760 \times P_{RATED}} \quad (4.10)$$

After the determination of each noise barrier segment's capacity factor, a statistical analysis can present the overall national picture. In Figure 4 - 10, the capacity factor probability histogram is presented for all potential micro wind turbine

installations in the Netherlands. The left graph shows the capacity factor distribution assuming no influence from the noise barrier on the wind flow, therefore using the $AEP_{reference}$ as a basis for the calculation. The right graph shows the distribution taking into account the corrected $AEP_{corrected}$. For both cases nearly 80% of all noise barrier segments have a capacity factor in between 0-15%. The influence of the barrier shows a clear positive shift of the capacity factor compared to the case without a barrier. It is found that the average capacity factor for a micro wind turbine installed on a noise barrier increases from 11.4% to 11.7%, which is a positive result.

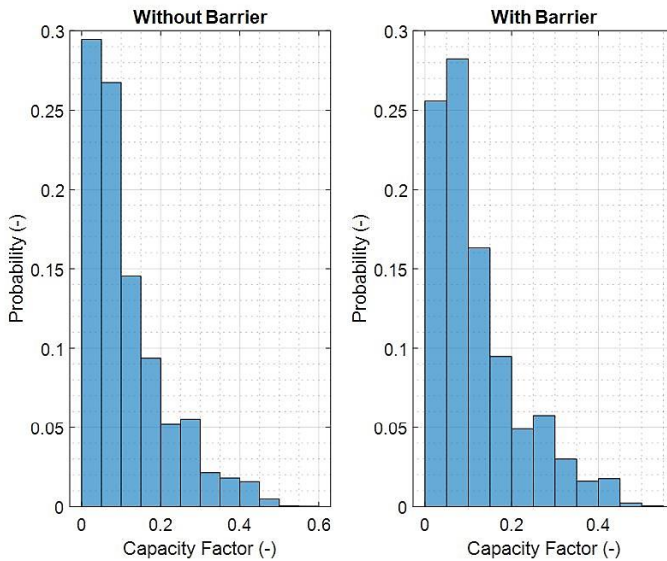


Figure 4 - 10: Capacity Factor probability histogram for all the suitable micro wind energy noise barriers in the Netherlands

Aggregating the $AEP_{reference}(kWh)$ and $AEP_{corrected}(kWh)$ of all noise barrier segments is needed for assessing the national and provincial level potential.

Table 4 - 3 below presents the national level findings. The sum of potential electricity production of all suitable noise barrier segments with a micro wind turbine installed on top, is 3% higher than the hypothetical reference potential electricity of the turbines at the noise barrier without the noise barrier wind flow effects taken into account. This is determined by the ratio of the sum of all corrected AEP values and divided with the sum of all reference values, as shown in equation 4.11.

$$\eta_{sum_nb}(\%) = \frac{\sum_{i=1}^{n_{segments}} AEP_{corrected}}{\sum_{i=1}^{n_{segments}} AEP_{reference}} \quad (4.11)$$

Averaging the influence of each individual noise barrier summing up each segment's individual influence and dividing by the total amount of suitable segments $n_{segments}$, then it corresponds to 6.5% energy yield increase, as calculated in equation 4.12 . This result is different from the national total 3% increase, because it takes into account the installed capacity and length of each individual element.

$$\eta_{average_nb}(\%) = \frac{\sum_{i=1}^{n_{segments}} \frac{AEP_{corrected}}{AEP_{reference}}}{n_{segments}} \quad (4.12)$$

Table 4 - 3: Micro wind energy on noise barrier results for all suitable noise barriers in the Netherlands

Variables	
Total Wind Power Installed on Noise Barriers (kW)	20,114
Total Reference Annual Energy Production on noise barriers (GWh)	20.11
Total Corrected Annual Energy Production on noise barriers (GWh)	20.77
Total Noise Barrier Influence (%)	103.3
Average Noise Barrier Influence (%)	106.5
National averaged Reference Capacity Factor cf (%)	11.4
National averaged noise barrier corrected capacity Factor cf (%)	11.7

After the national level aggregations of the potential values in Table 4 - 3, it would be useful to present the findings classified per provincial level in Table 4 - 4. These results are of importance to policy makers and energy infrastructure planners. Capacity factors differ per province as the wind resource differs. For the coastal regions of North-Holland, South-Holland and Friesland the largest capacity factors are observed. Most of the energy is produced in the most densely populated Provinces of South-Holland and North-Holland, where most micro wind turbines can be installed. The average noise barrier influence per Province is as well presented. It can be

Chapter 4

observed that in some Provinces a larger influence occurs, and this can be to a large extent explained by a combination of wind resource and azimuth of noise barrier.

Table 4 - 4: Micro wind energy on noise barrier metrics for each Dutch Province.

Province	Total NB Length (m)	Amount Of Noise barrier segments	Installed Power (kW)	Reference Capacity Factor (%)	Noise barrier Capacity Factor (%)	Total Reference AEP (MWh)	Total NB AEP (MWh)	Average Noise Barrier Influence (%)	Mean Elevation (m)
Drenthe	8023	82	268	6.8%	7%	153	156	102%	10
Flevoland	17	1	2.6	12%	12.9%	7.49	7.57	107%	0.06
Friesland	9821	97	661.5	11.97%	11.92%	703	699	99.7%	5.5
Gelderland	47558	220	1167	8.6%	9.1%	921	981	110.8%	17.6
Groningen	14053	131	676	5.5%	5.6%	316	323	117.7%	6.9
Limburg	48878	315	1611	9.5%	9.8%	1294	1344	105.4%	45
North-Brabant	108288	622	3284	6.8%	7.3%	2093	2238	108.9%	16.6
North-Holland	90081	750	4075	19.5%	19.9%	6841	7014	104.2%	7.5
Overijssel	13310	159	733	6.2%	6.4%	437	450	102.8%	14.7
Utrecht	56159	419	2359	6.7%	7.3%	1370	1492	114.3%	10.2
Zeeland	2821	33	172	9.1%	9.2%	107	108	93%	2.3
South-Holland	155790	1038	5064	13.2%	13.5%	5836	5932	105.2%	5.7

4.2.4 Uncertainties to consider for the potential estimation

Below uncertainties are presented that should be taken into account when using the results of this study:

- 1) Wind speed time series translation from weather stations to noise barriers was found to have an average median annual mean error of -0.77 m/s which can lead to power estimation deviations. Therefore, even more detailed methods should be developed and validated to minimize the error. However, realising that there's a

negative annual mean error, this means that the energy production numbers calculated for this study are underestimated.

- 2) Wind flow properties' correction factors from a single noise barrier measurement are used for the purpose of this study but in reality, each noise barrier, has each own particularities with respect to construction and local terrains which may have an effect on the wind flow pattern on top of the noise barrier
- 3) The extent to which the car-induced effects are present. For the examined noise barrier, the car speed limit was 50 km/hour while a lot of noise barriers are placed near highway environment which can possibly affect the wind potential. A study indicated, for a vehicle fleet passing with 80 km/h from a highway, a minimal difference in wind speed of 0.1 m/s (at heights of 5m and a distance of 15m away from the road) and 0.06 m/s (at heights of 10 m) [30]. But Netherlands has many highways which could reach from 100-130 km/hour, where the effect is unknown.

Finally, as discussed in Section 4.2, there are more types of noise barriers such as the Earth Embankments and the Combination of Earth Embankments and Acoustic Screens. Only the 55% of the noise barriers of the Netherlands are examined due to availability of experimental data for a previous study for Acoustic Screen type barriers. Therefore, the total potential wind electricity production by micro wind turbines on noise barriers will be higher when these were also taken into account.

4.3 Noise barrier renewable energy utilisation in an integrated energy system

In this section of this study, the integration of micro wind turbines with noise barriers is assessed with respect to combination with photovoltaic noise barriers, interconnection to electrical networks, interconnection to gas networks and combination with urban related demands. GIS datasets are used again in order to assessed different characteristics such as distance from infrastructure and demand.

4.3.1 *Integration with PVNB and grid interconnection proximity*

Photovoltaic noise barriers (PVNB) have a larger potential installed power density than micro wind turbines on noise barriers. Therefore, it makes sense to combine both systems to make use of the same infrastructure for power conversion and transmission. Micro wind turbines having a clearance of 5 diameters of the rotor of the turbine ($5 \times 1.7\text{m} = 8.5\text{m}$), result in an installed wind turbine power of 375 Watts per 8.5m (45 Watts per meter of noise barrier). Regarding the PV, the potential power installed is different. In this discussion it is assumed that most noise barriers in the Netherlands have a height of 5 meters which allows 3 rows of solar panels to be installed. The panels typically have width of 1 meter and a typical length of 1.5 meter and are rated at 300 Watts. Therefore, 900 Watts per 1.5 meter of noise barrier could be installed (~600

Watts/m). This means that PV power density potential is much larger (~13x more than micro wind turbines) due to the surface it could potentially cover. This raises the idea of combining both systems to benefit from the structural integration with available noise barrier infrastructures to generate larger amounts of renewable urban energy (~645 W/m). This is discussed later when the potential demand of power from noise barriers is assessed.



Figure 4 - 11: Illustrations of a combined wind and solar photovoltaic noise barrier

The noise barriers could be interconnected to the nearby electrical networks. Therefore, a proximity analysis is performed. A note shall be made on the classification of the noise barriers attributes as provided from the dataset of Rijkswaterstaat. Noise barriers have a single unique ID number and each ID number is composed of segments. This identification is used to examine interconnection possibilities. Table 4 - 5 below shows potentially installed power capacity distribution and statistics of the noise barrier IDs and segments for either wind only noise barriers or wind and solar photovoltaic noise barriers.

The power capacity installed bands indicate where an energy generation system will be connected according to the Dutch legislation [31]. The three categories are explained below:

- Between 0-60kVA of installed power, the system is connected at the low voltage network (LV) cabling of the distribution system operators.
- Between 60-300kVA, the system is connected on the low voltage side of the nearest medium voltage to low voltage (MVLV) station. These stations typically transform medium voltage power to lower voltage so that it is transmitted through the low voltage network cables.
- Between 300-3000kVA, the system is connected on the medium voltage (MV) network cabling. Thus, providing sufficient electrical power to be further transmitted to any medium voltage network.

The distribution of the amount of segment and ID's interconnected to each category is presented in Table 4 - 5. As expected, noise barrier segments are mostly connected

to the lower bands of power capacity installed as their length is smaller. The addition of PV on the noise barrier increases power significantly, thereby affecting the statistical distribution of all noise barriers with respect to which interconnection category they comply.

Table 4 - 5: Distribution of noise barrier IDs and segments for 3 different electrical power capacity installed bands, wind only and combined wind with photovoltaic noise barriers. Last rows of table provide maximum, average and median values for each category.

Power Capacity Installed (kVA)		Segments		ID	
		Wind NB	Wind + PV NB	Wind NB	Wind + PV NB
Lower Band	Upper Band	Counts (%)	Counts (%)	Counts (%)	Counts (%)
0	60	3851 (99.6%)	2106 (54.5%)	1067 (93.4%)	191 (16.7%)
60	300	15 (0.4%)	1528 (39.5%)	75 (6.6%)	558 (48.9%)
300	3000	0 (0.0%)	233 (6.0%)	0 (0.0%)	392 (34.3%)
Maximum (kVA)		115	1715	230	3400
Average (kVA)		6.2	94	21.5	320
Median (kVA)		3.4	51	13.5	200

Following this classification, a proximity analysis is presented. Publicly available GIS datasets are collected from DSO's [32-36]. The layers used and processed are for the low voltage networks, medium (to low voltage) voltage stations and medium voltage networks in the Netherlands. Figure 4 - 12 illustrates a buffer zone of 100m in purple around the highlighted green noise barrier. The green (low voltage) and red (medium voltage) lines represent the cabling network while the red (low voltage) and black (medium voltage) rectangles represent the stations. Noise barriers would be interconnected in any of those points and lines depending on the power capacity of each segment or ID.

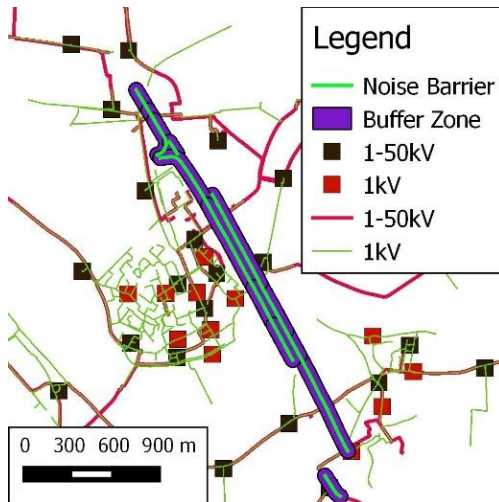


Figure 4 - 12: GIS example of the proximity of noise barrier to distribution electrical networks (lines) and stations (rectangles). Proximity is indicated as well with a 100m buffer zone in purple.

The example in Figure 4 - 12 above is for a particular location and given the existence of the GIS datasets, a proximity analysis is performed for each noise barrier ID and segment in order to understand qualitatively if significant increase in interconnection infrastructure (e.g., cabling) would be needed to make a nationwide implementation of wind turbine and photovoltaic noise barriers. The nearest neighbour analysis was performed by estimating the distance of the midpoint of a noise barrier segment or ID from the nearest station or network for each power capacity category, thus the results are not optimized for each noise barrier. The results are presented in Table 4 - 6. Each segment and each ID are classified based on the interconnection type they fit. The total installed power for each of these categories is presented together with the average and median power. The total noise barrier length per category is mentioned as well. The distance statistics are broken into the maximum, average and median interconnection distance from the nearest interconnection point. While the total cable length needed (assuming a straight line from the noise barrier midpoint to the network connection) are presented. These numbers show that it makes much more sense to aggregate the noise barriers with respect to their ID's, which have a higher distribution towards the MV Network, and would need a total cabling length of 1670 km. While interconnection of segments, which have a higher distribution towards MVLV Stations, need a lot more cabling length (10195km) due to the numerous small segments. In many cases where the cabling required is too much, there could be ways to decouple the noise barriers from the electrical grids and produce other energy vectors such as hydrogen, to avoid unnecessary and costly electrical network expansions.

Table 4 - 6: Characteristics of the “combined wind turbine and solar photovoltaic integrated noise barriers IDs and Segments” for the (upper highlighted border rows) power and length, (lower highlighted border rows) distance and proximity statistics from the nearest LV Network, MV to LV Station and MV Networks.

	Segments			ID		
	LV Network	MVLV Station	MV Network	LV Network	MVLV Station	MV Network
Total Installed Power (kVA)	44632	207900	109172	5763	87075	268908
Average Power (kVA)	21.2	136	468	33	165	690
Median Power (kVA)	50.3	50.3	50.3	34	160	555
Total NB Length (km)	69	322	169	9	135	416
Max Distance from Interconnection (km)	48	37	43.1	43.2	33.3	42.9
Average Distance (km)	4.2	0.436	2.5	2.9	0.66	2
Median Distance (km)	0.098	0.195	0.145	0.033	0.162	0.058
Total Cable Length (km)	8940	666	589	510	351	809

4.3.2 Connection to future hydrogen demand and street lighting

The distribution networks, to which the noise barriers IDs or segments would connect, face more and more limitations to expand their capabilities within the Dutch electrical system. This is addressed by several DSOs of the Netherlands, which state that they have insufficient room available to let energy generation units to be coupled at their networks. Some DSOs (Liander and Enexis including Coteq and Rendo) have published maps which indicate the scarcity of available connection points. Regarding STEDIN network the situation is better potentially due to the already reinforced infrastructure available attributed to the large population density requirements [37-39]. All these issues mean that some noise barriers might simply not be able to interconnect to the distribution networks as they are congested already. This rises incentives to decouple the noise barrier from the network and interconnect to different types of local demand or energy systems and networks. The concept for hydrogen production and street lighting is presented in this study.

Regarding hydrogen, the potential production is estimated and related to urban mobility and urban hydrogen demand. Additionally, a proximity analysis is performed for the urban mobility demand and the available gas networks. Finally, a demand coverage analysis is done for scooters within certain proximity to the barriers over the appropriate regions of the Netherlands.

Hydrogen Scooter Mobility

The Netherlands has a large number of scooters on the road. This amongst others has to do with the large population density and hence a large probability of cueing when using a car. The scooter mobility trends indicate that electrification is increasing. Electric powered scooters purchasing trends from last years are within the 3 to 6% of new purchases [40]. Nearly all these new scooters are battery electric powered. However, the concept of fuel cell powered scooters, which require hydrogen fuel, is also increasing attention [40-43]. Hydrogen is a promising energy vector announced in numerous studies in the Netherlands. These studies however, focus on large-scale deployment especially in combination with offshore wind energy. In the current study the emphasis is given on hydrogen mobility be it for smaller scale urban projects closer to the community. Therefore, there are potentially raising chances regarding quicker social acceptance and first experiments. This is the reason why it is assumed that neighbourhoods near noise barriers will adopt and will have incentives to have a 100% fuel cell scooter fleet for the locations in the proximity to noise barriers. The number of scooters and its classification and aggregation per neighborhood, municipality or region are found in the GIS datasets from the Statistics Bureau of the Netherlands (CBS) [44]. In this study, the noise barriers are assumed to generate the electricity needed to produce the amount of hydrogen needed for future scooters, either with off-grid electrolysis systems or with limited grid interconnection.

The assessment starts with a proximity analysis on whether the noise barrier locations are within the 2.5km daily average distance that scooters are driving in the Netherlands A. It is assumed that scooters refuel at a hydrogen production and the refuelling point consumes the electricity produced from the noise barrier. A nearest neighbour analysis is made for each noise barrier segment. The results are shown in Table 4 – 7 below. All noise barrier segments are within 2.5km daily distance as expected, since noise barriers are protecting neighbourhoods from highway noise.

Table 4 - 7: Proximity distribution of the noise barrier midpoint from the centroid of neighbourhoods which have scooters in the Netherlands

Distance of noise barrier from neighbourhood (meters)		
Bin Low	Bin High	Counts (-)
-0.1	500	3637 (94%)
500	1000	163 (4%)
1000	1500	26 (1%)
1500	2000	39 (1%)
2000	2500	2 (0.01%)
Maximum	2154.12	-
Average	94.95	-

Under the assumption of a 100% fuel cell scooter scenario for locations close to the barrier, the next step is to identify the electricity needed to cover its demand. With a 2.5km scooter's daily mileage (912.5km per year) and an average consumption of 45 grams of hydrogen for a 25km range with a city mode driving cycle [45,46], within one year a scooter would require 1.64 kgH₂. In order to produce this an electricity of 90.34 kWh per year would be required assuming a production efficiency of 55kWh per kgH₂ [47].

To assess, whether noise barriers can provide this amount of electricity, a simple approach based on annual capacity factors is used. Regarding the micro wind turbines, the detailed modelling approach in the previous section showed that in the Netherlands the average capacity factor for the investigated micro wind turbines on noise barriers is 11.7%.

The capacity factor of PV is also needed in order to make the electricity calculations. PV on noise barriers, shall be mostly installed with a tilt angle of 80 degrees due to the inclination of the barrier as it was shown in Section 4.2. Additionally, PV will face in different orientations. It was found that there is an equal distribution of noise barrier's orientation for four equal bins of 90 degrees starting from North East. Therefore, it is assumed that the average PV on noise barrier capacity factor is calculated by averaging the potential PV capacity factors for North, East, West and South orientation. These are shown in Table 4 - 8 below and are estimated for the aforementioned configuration from the toll available at the Joint Research Centre's Photovoltaic Geographical Information System webpage (JRC PV GIS) [48]. The assumed location to extract the solar irradiance data is within the "Randstad" where most of the barriers are located. The Randstad is the area comprising four major cities (Amsterdam, The Hague, Rotterdam and Utrecht). It got its name (Edge city) to express the conurbation of the four cities and their suburban's in central-western edge of the Netherlands. The average annual capacity factor for photovoltaics at any noise barrier configuration is assumed, with large simplifications, to be 6.41%. Shading losses are not taken into account in this simplistic approach but it is advised incorporate them in future optimization studies.

Table 4 - 8: PV Capacity factor distribution in the Netherlands for different orientation ranges

Orientation Range	NE - NW	NW - SW	SW - SE	SE - NE
Annual Capacity Factor (%)	2.68	6.57	9.52	6.87

It is assumed that 45 W/m of micro wind turbine with national average capacity factor of 11.7% and 600 W/m of PV with national average capacity factor of 6.41% are installed. These gives a combined weighted-average system capacity factor of 6.77% for a 645 W/m. And it results in 382 kWh/m produced annually. Assuming a hydrogen

conversion efficiency of 55 kWh/kgH₂ [47], it means that 6.9kgH₂ can be produced annually for each meter of a noise barrier. With a total of 560km of noise barriers with both PV panels and wind turbines integrated in them, this means that ~3892000 kgH₂ can be potentially be produced annually in the Netherlands. The average annual scooter demand was estimated previously at 1.64 kgH₂. The total amount of scooters in the Netherlands is about 650,000. This means that a demand of 1.066,000 kgH₂ would be required assuming an extreme scenario of 100% fuel cell scooter fleet in the Netherlands. Therefore, it is concluded that noise barriers with wind turbines and PV theoretically generate ~4x the demand of scooters. But this result does not mean that there should be a direct physical coupling of this demand with the noise barrier. In reality, this is predominantly possible for the noise barriers that are within the 2.5km average daily mileage proximity to this demand, as shown before in Table 4 - 7.

. The remaining scooter fleet will cover its hydrogen demand from other refuelling infrastructure points. Noise barrier will contribute virtually by injecting hydrogen into the local gas networks. In fact, the data shows that 754 out of the 12822 neighbourhoods registered for the Netherlands are located within proximity of 2.5km from noise barrier segments. The total number of scooters registered in those neighbourhoods is 46970 (77000 kgH₂ annual demand) while 3892000 kgH₂ (~50x more) could be produced near those neighbourhoods.

Since the demand coverage is extremely high comparing to the nearby neighbourhoods, an assessment is made per regional level assuming a full 100% fuel cell scooter scenario as the extreme scenario. The Netherlands has great ambitions to make its regions more sustainable. The Regional Energy Strategy (RES) programme kicked off as part of the agreements in the Climate Agreement of the Netherlands. These RES agreements are about investigations on where and how best renewable energy generation on land (wind and sun) can be realised [49]. In that context, the analysis for all the regions and the scooter mobility is presented in Figure 4 - 13 showing that 7 out of 30 RES regions cannot fully cover a 100% fuel cell scooter fleet hydrogen demand virtually with noise barriers. However, the remaining 23 regions exceed this significantly. This is especially seen for the intense green regions and it can lead up to 16 times the demand. This map may inspire regional authorities towards noise barrier related infrastructure developments related to scooter mobility.

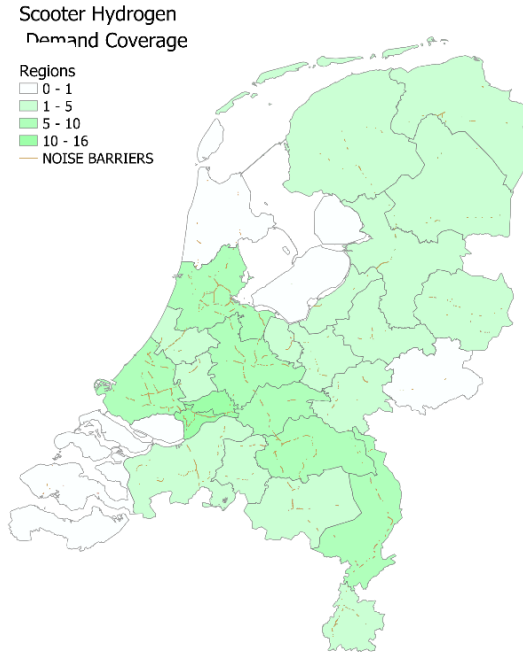


Figure 4 - 13: Hydrogen scooter demand coverage ratio from noise barrier (wind and solar) electricity for the 30 Dutch Regions.

Urban hydrogen demands via gas networks

Both the results discussed above for the neighbourhood coverage and the potential for the regions are leading to the idea that this potential hydrogen supply can also be fed or injected in the local gas networks.

The results presented demonstrate a feasible way for not having simply a stand-alone hydrogen producing noise barrier but even directly feeding in the local hydrogen networks to cover nearby future urban hydrogen demands. A TNO report indicates that the future hydrogen demand in the built environment will have a minor role in the Netherlands with $\sim 34\text{PJ}$ required per year [50]. This is nearly equivalent to $\sim 240,000,000$ kg of hydrogen. As discussed earlier all the noise barriers together can produce $\sim 3,900,000$ kgH₂, which is 1.6% of the expected built environment hydrogen demand.

If this amount of hydrogen is produced then it can be distributed via pipelines to the existing network which provides inherent flexibility. The proximity of the noise barriers to existing low pressure gas distribution networks is shown in the case example in Figure 4 - 14.

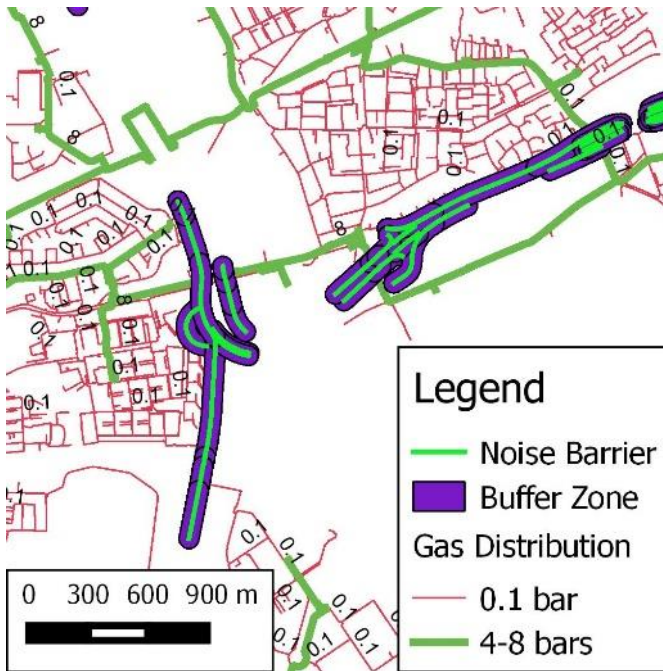


Figure 4 - 14: GIS example of proximity of noise barriers with micro wind turbines and PV from existing gas distribution grids

Based on the gas distribution network GIS data from the DSOs, a nearest neighbour proximity analysis has been performed, to identify the potential interconnection points with the hydrogen producing noise barriers. This idea significantly reduces the interconnection capacities to the electrical networks thus reducing electric grid congestion for the network operators. It is expected that this has a significant impact in the regions-provinces-borders of network operator where significant congestion problems are identified (e.g., Liander and Enexis). The binned results of the distances are presented in Table 4 - 9. The proximity analysis shows that noise barriers have a median distance from a nearby low-pressure gas network of 81 meters. The total pipeline length needed to interconnect all noise barriers within a 5km proximity with future gas networks (on which hydrogen is assumed to be injected in pure form or in blended form) is 581km.

Table 4 - 9: Distribution of proximity from the low-pressure gas networks in the Netherlands.

Distances from Gas Networks (m)			
Bin Low (m)	Bin High (m)	Counts (segments)	Total Pipeline Length (km)
0	100	2275 (60%)	102
100	200	913 (24%)	128
200	500	450 (12%)	129
500	1000	61 (2%)	43
1000	5000	63 (2%)	178
5000	40000	105 (3%)	1602
Max distance (m)	36863.16	-	
Median distance (m)	81	-	

Street lighting networks

If noise barrier IDs or segments do not have a significant techno-economic potential to be interconnected to an electricity network or produce hydrogen and feed it to a nearby gas grid, then the last idea to cover energy demand comes with street lighting networks. These are typically low voltage networks. Some interesting concepts have been described in the past in literature [51-57], where power generated next to highways can be utilized for highway lighting. Public lighting accounted for 1.5% of all electric lighting produced in 2014 [58] and can be reduced by using LED lighting and by other sustainable electrification means. Micro wind turbines integrated on noise barriers and noise barrier PV systems can potentially contribute to a small fraction of this energy demand. The integration with circuits for electric lighting posts is an obvious choice since they are typically close to noise barriers as can be seen in *Figure 4 - 15*.

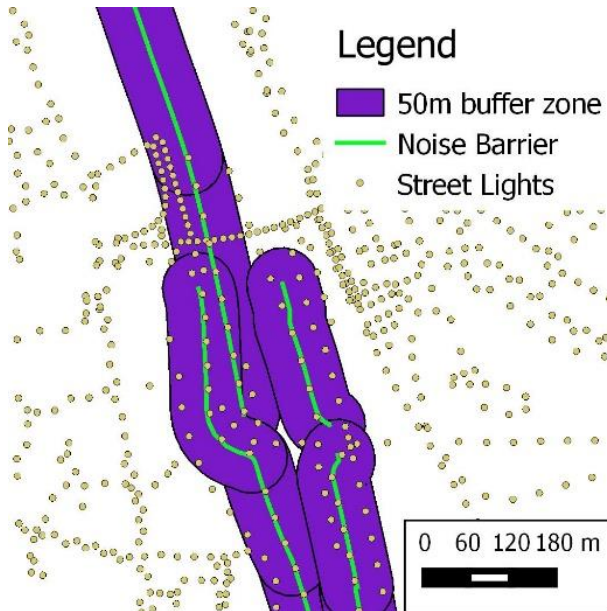


Figure 4 - 15: GIS example of proximity of noise barriers to street lighting

4.4 Conclusions

This Chapter aimed to answer the research question “Is there nationwide technical potential of micro wind turbine noise barriers in the Netherlands?”. With the use of several wind and infrastructure GIS datasets, the wind energy potential production on top of noise barriers for the country of the Netherlands was estimated. Several steps were required in order to translate the hourly wind speed time series from weather stations to the noise barrier location. Correction factors were applied due to the noise barrier influence on wind flow. Annual energy production metrics were determined and classified per provincial level. Finally, a qualitative and a quantitative discussion on wind turbine and solar panel integrated noise barriers’ interconnection to energy networks, proximity to energy demands and demand coverage potential are presented. The key conclusions from the study are summarised below:

- The Netherlands has 3785 noise barrier segments with a total length of 561 km with an average length of 156 meters which are suitable for installing micro wind turbines (assumed qualitatively on material structural compatibility criteria). This is 55% of the total length of noise barriers and equals to a total of ~25MW of installed micro wind power.
- About 85% of the suitable noise barrier segments to install a micro wind turbine are within a 20km proximity to a KNMI weather station.
- A mesoscale translation of wind speed time series data from a weather station to a point of interest such as the noise barrier was assessed. This is done by testing the

method on 2 weather stations with a 20km proximity, taking into account their surrounding roughness lengths. The roughness lengths were sampled from GIS datasets with 10° segments of 3 concentric circles around the points of interest (weather station and midpoint of a noise barrier segment). Annual mean error analysis resulted in an annual mean error of -0.77 m/s for locations within 20kms from the measuring station. This method was used to assess the Annual Energy Production (AEP) per noise barrier segment.

- It is found that noise barriers can contribute in a positive way to the deployment of micro wind turbines by increasing their yield due to both their influence on the wind flow and the potential reduction of investment cost (due to structural integration). The effect of locating wind turbines on each noise barrier segment, when comparing to the reference case, resulted in an increase of 6.5% in energy yield.
- The sum of all energy yields of micro wind turbines installed on top of suitable noise barriers in the Netherlands is 3% higher, compared to the energy yield of the micro wind turbines if there were no noise barriers at those particular locations.
- The average noise barrier micro wind turbine capacity factor increases from 11.4% to 11.7% when comparing with the reference case. However, this is only valid for the tested commercial 0.375 kW micro wind turbine which was used as the basis for the calculations.
- The classification per province shows that coastal and more densely populated regions have most of the wind energy produced. Specifically, the provinces North-Holland and South-Holland can provide 62% of the total national energy noise barriers potential (20.77GWh).
- The total technically possible micro wind installed power on noise barriers for the Netherlands amounts to roughly ~25MW. Noise barriers wind power potential (25 MW) is quite small when compared to the national energy plan perspective. There 6000 to 9000 MW is foreseen for large scale onshore wind power by 2030 and 11,400MW offshore wind power planned to be installed in the North Sea by 2030. The potential can hence slightly be increased using the combination of micro wind turbines with PV systems on noise barriers as well.
- Noise barriers which combine micro wind turbines and photovoltaic systems having an installed capacity of 645W/m can lead to a total 360MW installed power (equivalent to half the size of a typical offshore wind park in the Netherlands) but leading to less GWh produced due to the capacity factors.
- All suitable noise barriers, whether classified in terms of their ID or their segments, will be interconnected in the Low Voltage Network, the Medium to Low Voltage Stations or the Medium Voltage network. Significantly less cabling will be used if there is a single connection point for each noise barrier ID rather than Segment.

- The proximity to all categories of electrical networks shows a median range (33-195 meters), an average range (430-4200 meters) and maximum distance of 42900 meters.
- Noise barriers can produce locally hydrogen for mobility applications. Assuming 100% fuel cell scooter mobility either for neighbourhoods nearby the noise barrier (50x more) or even for all 30 Dutch regions (4x more), shows that a full hydrogen demand coverage is largely possible and most times with a lot of excess. However, this does not mean that the physical coupling is always possible.
- Hydrogen can be directly feed-in the local future hydrogen grids, realised by retrofitting/reusing the existing natural gas grids future gas grids. A potential of covering ~1.6% of the future built environment hydrogen demand is found.
- The total pipeline length needed to interconnect all noise barriers within a 5km proximity with future gas networks (on which hydrogen is assumed to be injected in pure form or in blended form) is 581km.
- Noise barrier renewable energy can also be used for street lighting as a feasible alternative.

4.5 References

1. Nikolaos Chrysochoidis-Antsos, Andrea Vilarasau Amoros, Gerard J. W. van Bussel, Sander M. Mertens and Ad J. M. van Wijk. Wind resource characteristics and energy yield for micro wind turbines integrated on noise barriers – An experimental study. *Journal of Wind Engineering and Industrial Aerodynamics* **2020**, *203*, doi:<https://doi.org/10.1016/j.jweia.2020.104206>.
2. Thomas Nordmann and Luzi Clavadetscher. PV on noise barriers. *Progress in Photovoltaics* **2004**, *12*, doi:10.1002/pip.566.
3. S. R. Wadhawan and J. M. Pearce. Power and energy potential of mass-scale photovoltaic noise barrier deployment: A case study for the U.S. *Renewable & Sustainable Energy Reviews* **2017**, *80*, doi:10.1016/j.rser.2017.05.223.
4. N.J.C.M. van der Borg and M.J. Jansen. *Photovoltaic noise barrier at the A9-highway in The Netherlands - Results of the monitoring programme*, ECN, 2001.<http://resolver.tudelft.nl/uuid:a746c334-1ae1-4ffb-a85e-1cdc7caf3426>
5. RvO. *Programme lines of Urban Energy*, 2019.<https://www.rvo.nl/sites/default/files/2019/02/Programmalijnen%20Urban%20Energy%202019.pdf>
6. Jadranka Cace, Emil ter Horst, Katerina Syngellakis, et al. *Urban wind turbines - Guidelines for small wind turbines in the built environment*, 2007.http://www.urbanwind.net/pdf/SMALL_WIND_TURBINES_GUIDE_final.pdf
7. RenCom. *Praktische toepassing van mini-windturbines - Handleiding voor gemeenten (Practical application of mini turbines - A guide for municipalities)*,

- 2010.<https://www.rvo.nl/sites/default/files/bijlagen/Praktische%20toepassing%20van%20mini-windturbines.pdf>
8. Klimaatakkoord. Available online at: <https://www.klimaatakkoord.nl/documenten/publicaties/2019/06/28/klimaatakkoord>
 9. RES. *Factsheet - Zon-pv en wind op land - Analyse naar opwek van hernieuwbare energie per RES-regio*, 2019. <https://www.regionale-energiestrategie.nl/bibliotheek/elektriciteit/analysekaarten++factsheets/1568811.aspx?t=Stand-van-zaken-zon-en-wind-op-land>
 10. Pierluigi Morano, Francesco Tajani and Marco Locurcio. GIS application and econometric analysis for the verification of the financial feasibility of roof-top wind turbines in the city of Bari (Italy). *Renewable & Sustainable Energy Reviews* **2017**, 70, doi:10.1016/j.rser.2016.12.005.
 11. Sara Freitas, Teresa Santos and Miguel C. Brito. Impact of large scale PV deployment in the sizing of urban distribution transformers. *Renewable Energy* **2018**, 119, doi:10.1016/j.renene.2017.10.096.
 12. D. Voivontas, D. Assimacopoulos, A. Mourelatos and J. Corominas. Evaluation of Renewable Energy potential using a GIS decision support system. *Renewable Energy* **1998**, 13, doi:[https://doi.org/10.1016/S0960-1481\(98\)00006-8](https://doi.org/10.1016/S0960-1481(98)00006-8).
 13. M.R. Rae, W.E. Lilley and L.J. Reedman. Estimating the Uptake of distributed energy in an urban setting. 2009 In Proceedings of 18th World IMACS/MODSIM Congress, Cairns, Australia.
 14. J. T. Millward-Hopkins, A. S. Tomlin, L. Ma, D. B. Ingham and M. Pourkashanian. Mapping the wind resource over UK cities. *Renewable Energy* **2013**, 55, doi:10.1016/j.renene.2012.12.039.
 15. S. L. Walker. Building mounted wind turbines and their suitability for the urban scale-A review of methods of estimating urban wind resource. *Energy and Buildings* **2011**, 43, doi:10.1016/j.enbuild.2011.03.032.
 16. D. R. Drew, J. F. Barlow and T. T. Cockerill. Estimating the potential yield of small wind turbines in urban areas: A case study for Greater London, UK. *Journal of Wind Engineering and Industrial Aerodynamics* **2013**, 115, doi:DOI: 10.1016/j.jweia.2013.01.007.
 17. J. Wieringa. Roughness-dependent geographical interpolation of surface wind speed averages. *Quarterly Journal of the Royal Meteorological Society* **1986**, 112, doi:10.1002/qj.49711247316.
 18. A. Stepek and Ine L. Wijnant. *Interpolating wind speed normals from the sparse Dutch network to a high resolution grid using local roughness from land use maps*, KNMI, 2011. <http://bibliotheek.knmi.nl/knmipubTR/TR321.pdf>

19. S. Van Ackere, G. Van Eetvelde, D. Schillebeeckx, et al. Wind Resource Mapping Using Landscape Roughness and Spatial Interpolation Methods. *Energies* **2015**, *8*, doi:10.3390/en8088682.
20. P.J. Mason. The formation of areally-averaged roughness lengths. *Quarterly Journal of the Royal Meteorological Society* **1988**, *114*.
21. J. Silva, C. Ribeiro and R Guedes. Roughness length classification of Corine Land Cover Classes. 2007 In Proceedings of Proceedings of EWEC.
22. L. Lu, S. M. Liu, Z. W. Xu, et al. The Characteristics and Parameterization of Aerodynamic Roughness Length over Heterogeneous Surfaces. *Advances in Atmospheric Sciences* **2009**, *26*.
23. Rijkswaterstaat. GIS data for Noise Barriers and Highways. Available online at: <https://www.rijkswaterstaat.nl/kaarten/geluidregister.aspx?cookieload=true>
24. H. Bendtsen. *Noise Barrier Design: Danish and some European Examples*, Danish Road Institute - Road Directorate, 2010. <http://www.ucprc.ucdavis.edu/pdf/UCPRC-RP-2010-04.pdf>
25. Carson Poe, Amy Plovnick, Tina Hodges, Aaron Hastings and Sue Dresley. *Highway Renewable Energy: Photovoltaic Noise Barriers*, U.S. Department of Transportation, 2017. <https://www.fhwa.dot.gov/environment/sustainability/energy/publications/photovoltaic>
26. R. J. Barthelmie, J. P. Palutikof and T. D. Davies. Estimation of Sector Roughness Lengths and the Effect on Prediction of the Vertical Wind-Speed Profile. *Boundary-Layer Meteorology* **1993**, *66*, doi:Doi 10.1007/Bf00705458.
27. J. P. Palutikof, J. H. Bass, J. A. Halliday and T. D. Davies. *Assessment of Wind Potential at Prospective Wind Energy Converter Sites - Final report to the department of Energy*, Department of Energy, London, London, 1989;
28. Copernicus_EU. Copernicus - Corine Land Cover 2018 (CLC). Available online at: <https://land.copernicus.eu/pan-european/corine-land-cover/clc2018>
29. F. J. Santos-Alamillos, D. Pozo-Vazquez, J. A. Ruiz-Arias and J. Tovar-Pescador. Influence of land-use misrepresentation on the accuracy of WRF wind estimates: Evaluation of GLCC and CORINE land-use maps in southern Spain. *Atmospheric Research* **2015**, *157*, doi:10.1016/j.atmosres.2015.01.006.
30. R. E. Eskridge and S. T. Rao. Measurement and Prediction of Traffic-Induced Turbulence and Velocity-Fields near Roadways. *Journal of Climate and Applied Meteorology* **1983**, *22*, doi:DOI: 10.1175/1520-0450(1983)022<1431:Mapoti>2.0.Co;2.
31. Tarievencode elektriciteit. Wettenbank, Ed.
32. STEDIN Connections - 3-phase power connections. Available online at: stedin.net/aansluiting

33. Enexis Monthly Network costs. Available online at: https://www.enexis.nl/zakelijk/aansluitingen/tarieven/tarievenoverzicht/maandelijkse-netwerkkosten?stap=Van%20welk%20product%20wilt%20u%20het%20tarief%20weten_1
34. STEDIN, *Open Data (Liggingsdata kabels en leidingen engasvervangingsdata)*, 2020, <https://www.stedin.net/zakelijk/open-data>
35. ENEXIS, *Open data*, 2021, <https://www.enexis.nl/over-ons/wat-bieden-we/andere-diensten/open-data>
36. LIANDER, *Beschikbaar Data*, 2021, <https://www.liander.nl/partners/datadiensten/open-data/data>
37. Stedin. Capacity of the electricity network. Available online at: <https://www.stedin.net/zakelijk/congestiemanagement-en-transportprognoses/beschikbare-netcapaciteit>
38. Liander. Beschikbaarheid capaciteit per gebied (Available capacity per region). Available online at: <https://www.liander.nl/transportschaarste/beschikbaarheid-capaciteit>
39. Enexis. Areas with scarcity for feeding into the energy grid. Available online at: <https://www.enexis.nl/zakelijk/duurzaam/beperkte-capaciteit/gebieden-met-schaarste>
40. Anna Petrakos. Energy Wall with Hydrogen Refuelling Stations for Fuel Cell Scooters - An Approach to Decentralised Sustainable Hydrogen Mobility in the Netherlands. TU Delft, TU Delft, 2020.
41. TU Delft. The scooter as mini Power Plant. Available online at: <https://www.tudelft.nl/en/2017/3me/the-scooter-as-mini-power-plant/>
42. Carla Robledo, Lotta van Leeuwen and Ad van Wijk. Hydrogen fuel cell scooter with plug-out features for combined transport and residential power generation. *International Journal of Hydrogen Energy* **2019**, *44*, doi:<https://doi.org/10.1016/j.ijhydene.2019.04.103>.
43. Lotta van Leeuwen. Performance of a hydrogen fuel cell scooter used for combined transport and residential power production. TU Delft, TU Delft, 2018.
44. CBS, *Wijk- en buurtkaart 2016*, 2016, <https://www.cbs.nl/nl-nl/dossier/nederland-regionaal/geografische-data/wijk-en-buurtkaart-2016>
45. APFCT - Asia Pacific Fuel Cell Technologies Ltd. Hydrogen Storage Canister. APFCT, Ed.
46. APFCT. Fuel Cell Scooter Product Specifications.
47. IEA. *The Future of Hydrogen - Seizing today's opportunities*, IEA, 2019;

48. European Commission. JRC Photovoltaic Geographical Information Systems (JRC PV GIS). Available online at: https://re.jrc.ec.europa.eu/pvg_tools/en/#PVP
49. Rijksoverheid. Nationaal Programma Regionale Energiestrategie. Available online at: <https://www.regionale-energiestrategie.nl/default.aspx>
50. R.J. Detz, F.O. Lenzmann, J.P.M. Sijm and M. Weeda. *Future role of Hydrogen in the Netherlands*, TNO, 2019. <https://repository.tno.nl//islandora/object/uuid:1505af16-46a2-4817-980a-1d35c1930ef4>
51. B. de Jong. Wind turbines along highways: Feasibility study of the implementation of small scale wind turbines along the Prins Bernardweg Zaandam to Bolswarderbaan highway in the Netherlands. TU Delft.
52. Z. Ibrahim and A. R. Asari. The development of wind power energy for lighting system in the highway. *Malaysian Journal of Industrial Technology* **2019**.
53. S. Georges and F. H. Slaoui. Case Study of Hybrid Wind-Solar Power Systems for Street Lighting. 2011 In Proceedings of 2011 21st International Conference on Systems Engineering, 16-18 Aug. 2011; pp. 82-85.
54. R. Devi and Jaspal Singh. Design and Development of Prototype Highway Lighting with Road Side Wind Energy Harvester. *International Journal of Science and Research* **2014**, 3.
55. Sachin Y. Sayais, Govind P. Salunkhe, Pankaj G. Patil and Mujahid F. Khatik. Power Generation on Highway by using Vertical Axis Wind Turbine & Solar System. *International Research Journal of Engineering and Technology* **2018**, 5.
56. Mahdi Shaneh, Hossein Shahinzadeh, Majid Moazzami and Gevork B. Gharehpetian. Optimal Sizing and Management of Hybrid Renewable Energy System for Highway Lighting. *International Journal of Renewable Energy Research* **2018**, 8.
57. D.B. Jani, Chaudhary Chetan, Ka. Patel Shivam, Patel Shivang and Baria Darshan. Highway lighting by use of wind turbine and solar energy. *International Journal of Innovative Research in Technology* **2019**, 6.
58. SWOV. Public lighting and vehicle lighting. Available online at: <https://www.swov.nl/en/facts-figures/factsheet/public-lighting-and-vehicle-lighting>

5

Techno-economic evaluation of turbine-solar PV systems integrated on a noise barrier

“Costs do not exist to be calculated. Costs exist to be reduced.”

- Taiichi Ohno

*This **chapter** analyses the techno-economic aspects of integrating micro wind turbines on top of noise barriers in combination with solar PV systems. It includes sensitivity analysis of the cost of electricity for micro wind electricity and PV electricity on noise barriers in the Netherlands.*

*The **research question** that this Chapter answers is:*

“What is the levelised cost of electricity of noise barrier integrated wind turbines?”

This chapter uses cost models built from the work entitled “On-site wind powered hydrogen refuelling stations – From national level to a case study in Germany” presented and published in Conference Proceedings of the International Conference on Smart Energy Systems and Technologies 2018 (SEST) from the Institute of Electrical and Electronics Engineers (IEEE).

5.1 Introduction

Increasing the amount of locally produced renewable electricity and use it locally as well is an urban climate change mitigation activity. This should be done in an economic way. Retrofitting highway infrastructures such as noise barriers with wind turbines and solar panels is a way to increase renewable generation at distribution grid levels and benefit from cost reductions due to integration. These systems are evaluated techno-economically, resulting in their levelised cost of electricity.

The main research question answered in this Chapter is “What is the levelised cost of electricity for wind and solar at noise barriers?”. This is followed by those sub-questions:

- Which are the concepts of integrating micro wind turbines with noise barriers?
- How much electricity could a typical noise barrier with integrated wind and/or solar systems produce?
- Which are the most important cost parameters?
- What cost reduction can be realized by integrating solar and wind in a noise barrier?

To address those questions, a literature review of different concepts of micro wind integration on highway infrastructures is conducted. Then the methodology for calculating the Levelised cost of electricity is presented. A detailed cost review and analysis of all subsystems is conducted. Finally, the results of each system are presented for a concept design as shown in *Figure 5 - 1* along with a sensitivity analysis and LCOE comparison with large scale solar and wind.

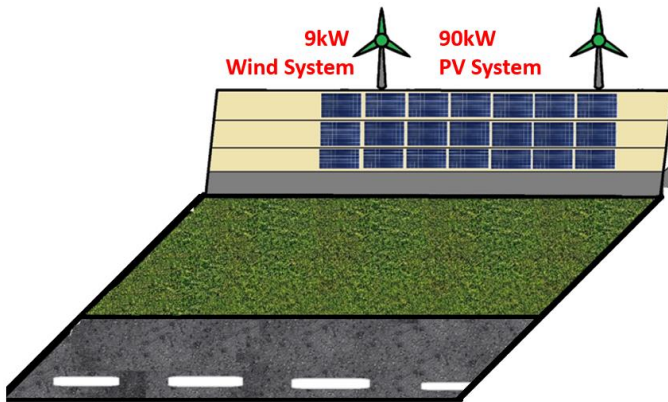


Figure 5 - 1: Sketch of the hybrid photovoltaic and wind turbine noise barrier

5.2 Literature Review

The literature review consists of 3 parts, starting with review of integration concepts of small-scale wind turbines with highway infrastructures, proceeding to a

review of challenges and opportunities of different electricity pathways for the hybrid (wind/solar) noise barrier energy systems and finally reviewing a number of techno-economic assessment literature to identify present gaps which this study will cover.

5.2.1 kW scale wind turbines integrated near highways

This chapter reviews kw scale wind turbines integrated near highways like the concepts shown in Figure 5 – 2. A classification in 4 concepts is proposed and the Table 5 – 1 below provide system description, application that the wind turbine is powering and the methodology of each reviewed work.

Wind powered concepts near highways are explored in various works from conceptual design level up to national implementation. An extensive review of the different wind turbine technologies for highway wind energy harvesting is presented in [1]. Turbines can be integrated in numerous ways with highway infrastructures. Nearly all systems in literature use vertical axis technology to be able to benefit from the highly turbulent flows as turbines are placed either in the middle or at the sides of highways. For the noise barrier study, a horizontal axis technology is explored as this technology represents around 99% of the market while Vertical Axis wind turbine (VAWT) represent a minor fraction of 1% [2]. Additionally, current study uses experimental data for the wind energy yield time series from a horizontal axis turbine integrated on a noise barrier as analysed in [3]. A proposal is made to classify turbine integration into 4 integration concepts, that are presented in Table 5 – 1.

The four proposed integrated systems are:

- Lighting pole integrated systems, where the turbine is structurally integrated on an existing lighting pole. Or micro wind turbines towers erected next to highways with integrated lighting systems.
- Highway sides or median integrated systems. These systems are erected at low heights next to highways exploiting the vehicle-induced turbulent wind energy. Vertical axis wind turbine systems are mostly used. In this category, turbines can also be placed on top of, attached or embedded on highway median strips. These could be green areas or Jersey bars.
- Tunnel integrated systems, where turbines are integrated inside tunnels or at their exits and benefit from the flows either of traffic or the natural wind flow occurring inside a tunnel due to pressure differences between the 2 exits
- Bridge integrated systems where wind energy harvesting devices can exploit the canyon wind potential to power structural health monitoring devices used in bridges or other infrastructures.



Figure 5 - 2: Concepts and research of wind energy along highways and turbines integrated with highway infrastructures (left) light pole mounted horizontal axis wind turbine next to a road, (middle) vertical axis wind turbine installed on top of a median of a highway and (right) experimental set-up of wind energy generation along North Carolina's highways

The systems often described in literature are either stand-alone or hybrid in combination systems with PV. Most examples included a form of battery storage to power the applications (e.g., street lighting). Very few are grid connected even though there are cost benefits of grid integration [4]. The urban environment presents low mean wind speeds which combined with the high costs of micro wind turbines make micro wind electricity more expensive than PV in €/kWh [5]. Combining wind and solar systems in hybrid mode can be beneficial as more energy output can be achieved with less variability, a higher of the grid interconnection capacity is achieved and reliability of overall system increases with less storage required when in off-grid operation[6]. Such hybrid systems are explored for their integration with highway infrastructures, mostly for street lighting applications.

Applications discussed in literature for highway micro wind turbines are for a very large extent be street lighting. Traffic and telecommunication signals are often described as well. Some novel applications around dust collection and health monitoring devices are also presented. Very few examples show electric vehicle charging applications.

The methods found in literature that are used to evaluate these systems are presented Table 5 – 1. The reviewed works use the methods of conceptual design, feasibility studies, experimental assessment, wind resource assessment, design of prototypes and some cost evaluations.

Chapter 5

Table 5 - 1: Review of literature of micro wind turbine integration concepts along highways

Integration Concept	System description	Application	Methodology	Reference
Lighting pole	Street lights integrated on a grid connected VAWT system pole	Street lighting Grid exports	Design and optimization	[7]
	Wind-PV-Battery integrated on a lighting pole	Street lighting	Conceptual design	[8]
	Wind-PV integrated on street lighting pole	Street lighting	Performance assessment Cost comparison stand-alone vs hybrid systems	[9]
Highway sides/median	VAWT on sides	Highway lights, traffic signals, light guide lines	Feasibility study Prototype experimental power curve determination	[10]
	Hybrid VAWT (Savonius/Darrieus) Battery	Street lighting	Design of prototype	[11]
	Linear integration along sides/medians	Street lighting/Telecommunications Signalling	Design of prototype	[12]
	Jersey blocks structural integration of horizontal axis turbines	Street lighting	Conceptual design	[13]
	VAWT on highways medians powering dust collectors	Dust and pollution particle collection	Conceptual design and feasibility	[14]
	Hybrid VAWT and PV system with battery storage	Street lighting Toll gates	Conceptual design	[15] [16]
	foldable umbrella mechanism integrated PV and Wind system on highways medians	Street lighting	Design Experimentation Feasibility	[17]
	Hybrid PV and Wind systems installed next to highways	Electric vehicle charging	Multi-objective optimization Feasibility study	[18]
Tunnel side	VAWT Tunnel side wind turbines	Tunnel lighting, pumping water	Wind resource assessment Experimental investigation Feasibility	[19]
Bridges	VAWT with piezoelectric and electromagnetic mechanisms integrated on bridges	Health monitoring devices for bridges	Resource assessment System feasibility	[20]

5.2.2 *Electricity pathways for a wind and solar power noise barrier*

Beside the specific literature on kW scale wind turbines related to highway infrastructures, literature also presents use cases of micro wind energy and solar energy. A few publications are selected to discuss potential use cases for the electricity produced from the wind and/or solar noise barrier. Literature presents several options from urban level and locally produced renewable electricity (small wind and/or solar) for several use cases. Some of the presented use cases in literature are the direct export towards distribution grids participating in electricity markets but with challenging economics due to different infrastructure configurations [21],[22],[23,24],[25]. Some considering adding batteries to such systems to benefit from grid flexibility services thus improving system economics [26]. Others focus on exporting electricity to street lighting networks but with challenges of needing to add batteries to be off-grid [7,8], [4],[27]. Some indicate an off-grid approach with private cables connected to different loads (industrial, household) [4], [28]. Others present energy storage by charging electric vehicles mainly light duty mobility vehicles (scooters, vans, small market fleets) [29], [30], [26]. While others discuss energy conversion with localized hydrogen production and refuelling for light duty electric mobility use [30], [31], [32], [33], [34], [35]. For all of those options, it is crucial to understand the economics of the electricity production on noise barriers. Therefore, this chapter analyses those techno-economic aspects.

5.2.3 *Techno-economic analysis of small-scale wind energy systems*

A literature review was performed to identify cost benchmarks, methods and sensitivity analysis parameters. This review aims to identify common techno-economic analysis methods and practices for all the relevant systems integrated on the noise barrier systems and its energy off takers. A selection of the most relevant literature is presented in Table 5 - 2 below.

The main takeaways in terms of methodology are that publications tend to use a rounded CAPEX figure for the costs of micro wind energy rather than analysing the individual sub-cost components (e.g., tower, foundations etc.), therefore in current study those costs are further investigated in order to examine the cost reduction in capital costs due to integration. Another finding is that the most common metric to benchmark with other technologies such as PV is the Levelised cost of electricity (LCOE) expressed in €/kWh. Finally, literature presents sensitivity analyses from different authors concerning varying the wind resource, the project economics (interest rates, CAPEX, OPEX), assessing combination with hybrid PV or adding batteries and other subsystems.

Some interesting findings are that the LCOE of micro wind energy is higher (0.1 – 2.7 €/kWh) than PV (0.1 – 0.3 €/kWh) especially in urban environment. At kW scale

Chapter 5

and near infrastructures, grid connection interconnected with a load, can offer benefits in terms of reliability, resilience and cost.

Table 5 - 2: Techno economic studies relevant to micro wind electricity combined with PV

Type of study	System	Key takeaways	Reference
Review of micro wind turbines aspects	(<2.5kW)	Costs/variation decrease at high wind turbine rated capacities Structure (building) mounted turbines have potential for cost decrease but installation cost factors are unknown	[36]
Techno-economic evaluation	Reference 2.4kW micro wind turbine	Mean wind speeds and interest rates significantly affect LCOE. LCOE ranges at 0.1 - 2.7 €/MWh for systems with CAPEX 1000 - 7000 €/kW and mean wind speeds 3 - 5 m/s	[37]
Cost Benefit Analysis	Turbines <1.5 kW	Turbines <1.5 kW require mean wind speeds > 5.5 m/s to achieve 15 years payback, thus unsuitable for urban environment	[38]
Hybrid with PV			
Comparison study	PV and Wind installed in Urban Environments (2.4 kW) for a case study in Dublin	LCOE (wind at 1.20 €/kWh) and (PV at 0.24 €/kWh). Difference due to energy resource potential, CAPEX and interest rates.	[5]
Techno-economic analysis for various resources and interest rates	Stand-alone 300kW PV, 2x330kW Wind system with a 200kW PWM hydrogen production/storage options and a fuel cell	Adding PV to Wind, decreases the Net Present Value (NPV) by 22% Cost of energy at 0.8 - 1 €/kWh	[39]
Grid connection aspects			
Techno-economic feasibility (HOMER)	Hybrid diesel, PV (800kW), wind (60kW) and battery for non-residential electricity consumers.	Grid-connected is 35 - 40% cheaper than battery-connected. Increased sales of electricity back to the grid	[4]
Techno-economic evaluation	On- and off-grid wind (6kW) Hydrogen production (2kW)	LCOE 0.14 - 0.3 \$/kWh at 12 - 60m hub height	[40]
Integration with hydrogen production systems			
Techno-economic analysis/optimization	Solar (2kW) + wind systems (1-15kW) + batteries for power generation and hydrogen production for typical house load demand	LCOE cheaper for batteries 0.6 \$/kWh while hydrogen production/storage and fuel cell electricity doubles cost to 1.2 \$/kWh. Overall cost of energy (electricity + hydrogen) is the lowest for the hybrid system (2kW PV + 3 turbines) at 1.4 \$/kWh	[41]

5.3 System design and input data

In this section the wind and solar noise barrier systems are described along with the modelling aspects. A brief system description is presented in Section 5.3.1. Secondly, the technoeconomic analysis modelling equations are explained with respect to LCOE in Section 5.3.2. This is followed by the electricity production scenarios assessed in Section 5.3.3. After that, the costing parameters are reviewed with a focus on the cost reduction achieved due to integration for both wind and solar systems in Section 5.3.4.

5.3.1 *Brief system design*

The concept under examination is being assessed for the cost and electricity being produced from structurally integrated micro wind turbines (9kW) and photovoltaic panels (90kW) on existing commissioned noise barriers along highways. This design has the benefit of cost reductions due to unnecessary structural systems for wind and solar systems. The solar and wind systems are assumed to share a DC or an AC bus [6] before network connection. System capacities are based on average noise barrier length (~150m) and a height (~5m) for the Netherlands. Small wind turbine systems that do not exceed a total height of 8 meters together with the noise barrier height are assumed, a boundary set by road authority rules and regulations for objects attached on noise barriers. Electricity is exported to a nearby electrical grid at distribution level at an average cable distance of 150m (found from analysis of average distance of noise barriers to distribution level transformers). The transformer costs are assumed as part of the CAPEX of the wind and solar systems, while the cabling and other costs are assumed as grid interconnection costs based on the Dutch Grid Electrical Code [42]. This system is assumed to be integrated with an existing noise barrier thus investment costs for noise barrier are excluded as well as any noise barrier maintenance costs. A graphical representation of this concept can be found in Figure 5 - 1.

5.3.2 *Technoeconomic analysis and methodology*

A model was set for benchmarking and sensitivity analysis with the metrics of Levelised cost of electricity (LCOE) [43]. The LCOE (€/kWh) of the noise barrier system (shown in equation 5.1) is the sum of the annualized costs (€) of the PV, the micro wind turbine systems integrated on the noise barriers and the grid interconnection, divided by the total annual electricity production of the noise barrier AEP_{NB} (kWh). AEP_{NB} is the sum of the Annual Electricity Production of the PV systems, AEP_{PV} (kWh) and the micro wind turbine system, AEP_{wind} (kWh). Annualized costs are the sum of the operational expenditures (OPEX) and the annual repayments to cover the investment costs. The annual repayments for the PV, the wind turbines and the grids are the product of the capital expenditures (CAPEX) with the project's capital recovery factor (CRF) [37].

$$LCOE_{NB} = \frac{[CAPEX \cdot CRF + OPEX]_{wind} + [CAPEX \cdot CRF + OPEX]_{PV} + [CAPEX \cdot CRF + OPEX]_{GRID}}{AEP_{NB}} \quad (5.1)$$

The capital recovery factor (CRF) (shown in equation 5.2) is considered to express the annual repayments to banks and investors (assuming a mixed debt-loan ratios for a low maturity investment) considering the weighted average cost of capital of the project ($WACC_{project}$) and the lifetime of the project n in years [43]. Equation 5.3 shows the weighted average cost of capital of the project ($WACC_{project}$), which is the sum of the product of debt share x_{debt} (%) with the interest rate of debt i_{debt} (%) and the product of the equity share x_{equity} (%), shown in equation 5.4, with the rate of return to equity R_{equity} (%).

$$CRF = \frac{(WACC(1+WACC))^n}{((1+WACC)^n - 1)} \quad (5.2)$$

$$WACC_{project} = x_{debt} \cdot i_{debt} + x_{equity} \cdot R_{equity} \quad (5.3)$$

$$x_{equity} = 1 - x_{debt} \quad (5.4)$$

Since the system is retrofitted on public highway infrastructures with low market maturity integration concept for photovoltaic system and very low maturity for micro wind turbines. IEA's article on cost of capital in clean energy transitions [44], provides the split between debt and equity finance for several sectors for the energy transition. The sectors relevant to noise barriers are the low-carbon generation (67% debt - 33% equity) and grids and storage (64% debt - 36% equity). Therefore, the system studied is assumed to have 65% debt and 35% equity. The cost of debt (*or interest rate*) vary per technologies and projects, with literature showing wind and solar technologies who are mature to have as low as 0.5-4% for solar projects [45],[46], and 3-7% for micro wind turbine projects [38],[47],[48],[5],[37]. Therefore, an interest rate of 4% is assumed for all systems. Regarding the rate of return (cost of equity), the same IEA report discusses the typical rate of returns that utility scale solar projects use in Europe. This is split into the revenue supported (through feed-in tariffs, contracts for difference, long term power purchase agreements or bilateral agreements) and the merchant risk (market-based revenue). Due to limited commercial maturity, it is assumed that a revenue supported category applies. The typical cost of equity (%) for utility scale solar

is 5.3 – 10.9%. Therefore, for the noise barrier project, a 7.5% cost of equity is assumed as shown in Table 5 - 3 below.

Table 5 - 3: Weighted Average Cost of Capital Structure

Factor	Value
Debt Share (%)	65
Equity Share (%)	35
Cost of Debt (%)	4
Cost of Equity (%)	7.5
WACC _{project} (%)	5

The AEP_{NB} (kWh) is the sum of all the wind and solar electricity produced in a year, shown in equation 5.5. Wind turbine electricity E_{wind} (kWh) at each time hourly step i , is estimated by interpolating the hourly wind speed time series with a small wind turbine's power curve. Since the turbine is integrated with a noise barrier, wind speed correction factors are applied to each hourly wind speed data points. The wind speed corrections come from an experimental assessment of wind speeds on top of noise barriers and are based on the wind direction and the noise barrier azimuth [49]. The solar electricity E_{solar} (kWh) at each hourly time step i , is downloaded as hourly time series from PVGIS database where a predefined azimuth and noise barrier slope can be configured to assess different sensitivities.

$$AEP_{NB} = \sum_{i=1}^{8760} (E_{wind_i} + E_{pv_i}) \quad (5.5)$$

5.3.3 Electricity production

This section dives a bit deeper on the electricity production scenarios. In order to understand the cost of electricity that the micro wind turbine noise barrier (MWTNB) and the photovoltaic noise barrier (PVNB) systems can achieve, it is important to model the electricity production in several scenarios. The scenarios are relevant in order to understand the range of costs to be expected. The scenarios are based on location, which mainly affects the average wind speed, on the azimuth of the noise barrier and its slope, which mainly affects the PV output and on the influence of the noise barrier on the wind turbine's energy yield as it was shown in [49]. The country of the Netherlands is used as a case study. Therefore wind and solar time series are used from KNMI for wind and from PVGIS for PV.

For the case of micro wind energy, wind time series are used for 3 locations with different average wind speeds (low=3.6 m/s, medium=4.1 m/s, high=4.8 m/s) at hub height of 8 meters. These locations are Eindhoven Airport, Rotterdam Airport and Schiphol Airport [50]. The met masts at those locations are similar to the typical noise barrier wind turbine height of installation, thus no corrections are applied, to simplify modelling.

Electricity production ideal micro wind turbine

The annual electricity production from the micro wind turbines AEP_{wt} (kWh) is the sum of each hourly wind electricity production $E_{wind}(i)$. Each hourly point (i) is found by interpolating the WindChallenge's micro wind turbine power curve P_{curve} with the site's wind speed $u(i)$ hourly datasets, as shown in equation 5.6. This power is not yet noise barrier corrected.

$$E_{wind}(i) = lookup\{u(i), P_{curve}[u(i)]\} \quad (5.6)$$

The AEP_{wt} (kWh) is then corrected for the noise barrier influence, with a noise barrier factor, as shown in equation 5.7. To avoid modelling extensive number of cases, the range of 60% decrease in production from the reference case (worst case) and a 63% increase from the reference case (best case), is considered. These AEP differences were calculated earlier in [49].

$$AEP_{wt} = \left[\sum_{i=1}^{8760} E_{wind}(i) \right] \times \eta_{NB} \quad (5.7)$$

Electricity production realistic micro wind turbine on noise barrier (with field experiment measured performance losses)

The AEP_{wt} (kWh) represents the energy yield per year assuming that the turbine would ideally operate as in the case of a wind tunnel. It was, however, demonstrated in [3], that a micro wind turbine is not ideally operating in the turbulent environment above the noise barrier. A number of losses were recorded related to the inverter standby power, the lack of adequate response of turbine's nacelle to follow wind direction leading to yaw misalignment losses and the controller's ineffectiveness to operate in the highest aerodynamical efficiency of the turbine system. When summing and averaging all those losses for different wind speeds and directions, these result in a turbine system operating at 42% of the actual theoretical performance, which is a substantial loss. Therefore the scenarios include, a case for the wind turbine system

where these losses are taken into account in the cost of electricity. The AEP_{wt_loss} (kWh) is then the product of AEP_{wt} (kWh) with the η_{loss} (%), shown in equation 5.8.

$$AEP_{wt_loss} = AEP_{wt} \times \eta_{wt_loss} \quad (5.8)$$

Electricity production of Solar PV on Noise Barrier

For the photovoltaic noise barrier (PVNB), the photovoltaic electricity production time series are downloaded from the PVGIS online tool [51] for the 3 locations above. PVGIS is a photovoltaic energy yield model validated from measurements performed on commercial modules at the ISO accredited Joint Research Centre's European Solar Test Facility. It is a standard tool to estimate hourly production profiles. Three azimuth cases are modelled (East=-90°, South=0° and West=+90°) and 2 noise barrier slopes (50° and 80°). These slopes are typical for noise barriers in Netherlands as analysis in Chapter 4 showed. The sensitivities in azimuth and slope are examined for the changes in the final cost of electricity. As PVNB are placed near highways, a valid question to ask is whether soiling losses are relevant as traffic dust could reduce panel output by 8%. But this is mostly for dry climates [52-54]. In weather environments such as the Netherlands, soiling in vertically placed PVNB was not found an issue. In addition, the effect of cleaning of PVNB was assessed in [55] concluding that the performance of nearly vertically placed PVs is not increased as a result of cleaning as the vertical placement in combination with rainfall avoid dust and particle accumulation on their surface resulting in soiling losses. Therefore, additional soiling losses are not assumed.

5.3.4 Costs

This section describes costs used in LCOE equation 5.1. The investigation is mainly for capital and operational expenditures concerning micro wind and PV integrated with noise barriers with a detailed cost breakdown aiming to finding potential cost reductions due to integration. Capital expenditures of systems (CAPEX) refer to one-off costs at the beginning of the project's lifetime or when hardware is replaced. They cover engineering design, construction, permitting, installation, purchase of software-hardware, interconnection to electricity grids and other investment costs. Operational expenditures (OPEX) are all costs for scheduled/unscheduled maintenance. Wind and solar systems' OPEX is typically expressed annually as a percentage of CAPEX of each system. OPEX figures could dynamically change throughout the lifetime of the system.

The study considers integration of wind and solar systems on existing and built noise barriers, hence it does not consider costs for developing new noise barrier structures. Noise barriers last 25-50 years. Costs used are exchange rate converted to € and are 2020 inflation-adjusted [56].

Wind Turbine Noise Barrier System

There is limited literature around costs for micro wind turbine systems integrated with noise barriers. The turbine sizes allowed on a typical noise barrier height of 5 meters including a 1-meter rotor clearance should have a maximum of 2 meters rotor diameter. This limitation comes from the Noise Abatement Act which does not allow the noise barrier height to exceed 8 meters including any attached objects [57]. For that reason, the study needs to consider cost breakdown of less than 2.5kW micro wind turbine systems incorporating cost changes due to integration with the noise barrier.

A literature review was conducted to identify CAPEX and OPEX shown in Table below. The CAPEX ranges greatly for small wind turbine system. Unfortunately, the Netherlands does not have a comprehensive market related literature on micro wind energy, therefore findings from other countries are presented in this costing review (USA, UK and Canada). From literature review, a large range in CAPEX figures is found (2000 – 18000 €₂₀₂₀/kW). This is due to differences in type of installation (urban, rural, building integrated), the total amount of turbines and power capacities (0.1 – 10kW) and the project complexity at the site of installation. It is therefore necessary to find a cost breakdown benchmark to base the costs for a noise barrier integrated wind turbine system as explained later in Table 5 – 5.

The OPEX in literature ranges between 1 - 3%, but this is mostly for ground mounted systems which has inherently easier access for maintenance than highways. All costs have been converted to 2020 € using historical average exchange rate data and inflation rates. The lifetime of the turbines in multiple sources and commercial brochures range from 15 up to 30 years.



Figure 5 - 3: Photos during construction of the highway experimental set-up of highway micro wind turbine noise barrier highlighting the structural integration features such as the blue flange

Table 5 - 4: Selection of cost references (CAPEX, OPEX) for micro and small wind turbine projects

Type of cost reference	CAPEX (€ ₂₀₂₀ /kW)	OPEX (%CAPEX/year)	Source	Year
Turbine owner's questionnaire (average UK installed cost)	7475	1.7%	[36]	2006
Market survey for rural and urban wind installations in UK	2150 – 18000	1%	[58]	2008
Market survey average reported installed cost in Canada	1900 – 6000	N/A	[59]	2009
Market report of installed costs of top ten small wind turbine models in US	2100 – 7350	N/A	[37]	2011
Capital costs for small wind developer's market survey (turbines <1.5kW) in UK	5450 – 7010	2%	[38]	2012
Market report for average CAPEX of 1 – 3 kW turbines at 18m height	6700	N/A	[60], [61]	2015
Market report of US Manufacturers - Average (typical) installed cost of wind turbines (<2.5kW)	3550 – 7100	1.5%	[47]	2017
Distributed Wind Market Report survey for project costs	4920 – 12770	N/A	[47]	2016
Future market scenario analysis for behind-the-meter distributed wind projects	9000	0.1 – 0.4%	[48]	2016
Small wind survey for cost benchmarking in the US	10940	~0.6%	[2]	2017
Case study using data from commercial brochure from installer for 2.4kW turbine	6350	2.7%	[5]	2016
Case studies for rural and urban installations (for a 2.4kW turbine)	3150 – 5145	1.5 – 3%	[37]	2016

To find a figure which is as close to the potential micro wind turbine noise barrier costs, the following market survey report is used which is conducted in 2017 for residential systems (<20kW) with average total cost of 9400 €₂₀₂₀/kW from a sample of 57 projects with total installed capacity of ~450kW from [61] and [2]. This report provides a detailed CAPEX breakdown which helps to demonstrate cost reductions in different CAPEX parts which will differ than a residential system installation.

The first reduction is due to the structural integration with existing noise barriers. Since the turbine is structurally integrated with the noise barrier metal support structure, a large cost reduction applies for the tower costs as the tower is replaced by a flange interconnector as shown in Figure 5 - 3. Additionally, only a very small monopole is required to support the turbine above the noise barrier of maximum 2 meters rather than a full tower. The average monopole cost of 90 €/kW/m is applied as found in the reference above. The cost of the flange interconnector is considered in the foundation costs which are as well reduced significantly by only including the flange costs. Installation costs are also reduced as no tower needs to be erected for the turbine. Costs for installation are attributed to a scaffold (shown in Figure 5 - 5), crane or cherry picker necessary to install the flange interconnector and place the turbine. The selection of equipment to install the turbines is influenced by the site access and the turbine

Chapter 5

weight characteristics. For example, the turbine shown in Figure 5 - 3 was quite heavy requiring a crane to place it (as it was more than 10-20 kgs), there are however market alternatives with less than 5 – 10 kgs of turbine which are easier to carry, place and install. Finally, installation costs can be shared with the PV system installation. Another cost reduction is due to changes in electrical infrastructure costs and the difference in permitting costs as turbines are installed next to highway environment.

Table 5 - 5: Cost breakdown of micro wind turbine projects and assumptions used to determine cost reductions for noise barrier integrated micro wind systems (all costs are converted from \$₂₀₁₇)

Cost Component	CAPEX breakdown of micro wind turbine projects (€ ₂₀₂₀ /kW)	Change due to	Costs applied in model (€ ₂₀₂₀ /kW)
Turbine	2735	Minor deviations with turbine size	2735
Tower	1310 (average cost of all projects)	Maximum 2 m monopole per 0.4kW turbine with average cost as no tilt-up tower needed	180
Customer Acquisition and Qualifications	130	No change	130
Zoning, Permitting, Interconnection (ZPII)	720	Assumed 10% reduction	640
Engineering/Design	110	Slight increase due to novel concept	140
Transportation and Logistics	205	Sharing with PV costs (50% reduction)	100
Foundation	1185	Flange interconnectors costs instead of ground foundations. Material costs will decrease but metal works required	180
Electrical Infrastructure	520	Labor/Subcontracting costs shared with PV. Equipment (power conditioning units) and material (cabling) costs can be shared with PV systems (50% reduction)	250
Installation	2230 (average figure until 20kW)	Small wind capacities (<\$1000/kW) with tilt-up tower. Labor, equipment (crane) and installation costs shared with PV (50% reduction)	450
Taxes	130	Same costs	130
Other Costs	110 (1% of total CAPEX)	Same costs	110
TOTALS	9400 €₂₀₂₀/kW	40% reduction	5100 €₂₀₂₀/kW

Based on all aforementioned cost correction due to noise barrier integration, the overall CAPEX is reduced by 40% from 9400 €/kW to 5100 €/kW. For the OPEX, a 4% of CAPEX per year is assumed as the experience from the experimentation near the highway in [3] with all the necessary permitting to perform work and the complexity of access to the noise barrier site proved that the maintenance required will be more complex than any other type of micro wind installation. The system lifetime is 20 years as most literature and manufacturers state.

Photovoltaic Noise Barrier System

Since an established market for photovoltaic noise barriers does not exist, the costs should be assumed by reviewing different sources. The main conclusion of the literature review of PVNB costs is that there is not a single cost figure that can be simply used to adequately represent the noise barrier in examination. Therefore, the most recent literature of PV systems will be used around the cost breakdown and benchmarking and some assumptions will be presented to determine the final project costs for the noise barrier. Information was found around system costs for representative rooftop, residential and commercial PV systems of sizes around 100kW. Literature also presented cost figures for photovoltaic noise barriers from case studies, commercial brochures, reports of research demonstration (such as project A9 in the Netherlands shown in Figure 5 - 4) and interviews with construction companies.



Figure 5 - 4: Compilation of PVNB photos (top row) Swiss cassette type photovoltaic noise barrier in operation and during installation (bottom row) Solar Highways Dutch experimental photovoltaic noise barrier (~240kW) during construction, installation and maintenance periods

PVNB found in literature mainly concern noise barrier panels being fabricated and laminated with solar cells as part of a single structure, these are more expensive currently than standard PV panels as the fabrication is not automated and is customized for each noise barrier. The noise barrier concept proposed in this study involves the racking of existing PV system found in market on existing noise barrier panels without the necessity to uninstall existing noise cancelling panels. OPEX costs for PV systems are generally quite low around 1% of CAPEX per year, in current project a 2% of CAPEX per year is assumed due to its novelty and concept maturity. Finally, the lifetime is 20 years.

The Table 5 – 6 below provides a general indication of what is available in literature regarding costs of PV systems and some noise barrier integrated ones. But since the projects can differ per module technology, the electrical infrastructure, structural integration and other related project costs it is important to breakdown the cost components of a PVNB project. This helps to roughly assume cost figures with uncertainties. By using a cost breakdown benchmarking reference in *Table 5 – 7* in next page, each component's costs are changed due to assumptions related to the concept described in this chapter. It is important to highlight that the noise barrier concept presented is not with glass integrated PV modules but racked modules on existing noise barrier screens thus a simpler solution and potentially more economic. All costs are converted to €₂₀₂₀. Total project baseline cost assumed in this project is 1820 €/kW of PVNB installed, which is significantly less than the other PVNB projects in Belgium and the Netherlands which assume glass laminated cassettes integrated with the noise barrier.



Figure 5 - 5: Photos of (left) Grid interconnection of the Solar Highways PVNB 240kW demonstration in the Netherlands – Copyright of Heijmans, (middle) installation of electric cast for interconnection to low voltage network for the MWTNB experiment (right) installation of the micro wind turbine on the noise barrier

Table 5 - 6: CAPEX and OPEX for generic and noise barrier integrated PV systems

Type of study	CAPEX (€ ₂₀₂₀ /kW)	OPEX (% CAPEX/year)	Source	Year
Market report in Germany	1050 – 1600 (rooftop) 30 – 170 (String Inverters <150kWp) 30 – 50 (Central Inverters >80kWp)	N/A	[62]	2022
Market Report of 10–100kW PV systems costs	2600 €/kW (balance of plant and modules)	N/A	[63]	2017
Governmental report for installation of building integrated PV	621 €/kW (>15kW until 1MW)	2%	[45]	2022
PVNB demonstration projects with installed power capacities of 55 – 220 kW in the 1990s	16000 €/kW (1989) From 7000 €/kW (2000) ¹	N/A	[64]	2004
Case Study of 430kW PVNB ² in Belgium	2800 €/kW	1% ³	[46]	2012
Commercial Brochure of PVNB ⁴	4520 \$/kW (amorphous glass PV) 1100 \$/kW (crystalline glass PV)	N/A	[65]	2021
Project report of 248kW PVNB in the Netherlands	4190 €/kW ⁵	1.5%	[55]	2020
Solar Highways Final Report for a 400m long prototype ⁶ 5m high noise barrier with 4m bifacial PV	9960 €/kW (project cost) ⁷ 6000 €/kW (planning, civil works, installation, replacement and construction of new barrier foundations).	0.8%	[66]	2020

It is assumed that values are converted to €₂₀₀₄ from authors

² No mention of integration concept (rack-mounted or integrated with noise barrier absorbing material).

³ Soiling loss maintenance not necessarily due to frequent rainfalls

⁴ Both panel technologies' costs include electrical installation

⁵ Costs are for glass PV modules, power electronics, BoP (they do not include installation and other soft costs necessary for the project developments of PVNBs)

⁶ 1600m² of PV surface with 18.5W/m² resulting in 231kW

⁷ Best offer during tender at 2.47 million € to design, construct and maintain for 1.5 year after completion (Heijmans, Scheuten, Van Campen/Bayards and Libra). Procurement costs a lot higher as custom hand-made modules were necessary to be produced. Project discusses significant cost reduction with manufacturing automation. Video in <https://www.youtube.com/watch?v=3qgAhtDsz4U> shows manually placed cells.

Grid Interconnection

Interconnection costs as stated from the Dutch law are divided into one-time costs as CAPEX (connection fees and tariff with cable extension works) and the yearly periodic costs (connection fee, fixed transport fee, capacity tariff and metering tariff). All those costs when annualized results in a range between 1200 – 3000 € for a cable length of ~150m (average length of noise barriers from transformers from analysis in chapter 4). Technical information are used for all grid operators in Wettenbank Tariff codes and in individual examples of distribution system operators (DSOs) [42,69] like

Chapter 5

STEDIN -Alliander. An important parameter in all those equations is the distance from nearby transformers which is input to the model from the average baseline distances found in the GIS analysis as well as assuming equal lifetime to the one from the project.

Table 5 - 7: Cost breakdown of PV system projects and assumptions used to determine costs for noise barrier integrated photovoltaic systems (all costs are converted to €₂₀₂₀)

Cost Component	Benchmarking Values [67] (100kW commercial project) (€ ₂₀₂₀ /kW)	Change due to	PVNB Integrated Cost (€ ₂₀₂₀ /kW)
Module	360	European module prices	360
Inverters	60 (3phase string inverter) 105 (DC power optimizer 3phase string inverter for rooftop) 255 (microinverters for rooftop)	As noise barrier could potentially experience partial shading phenomena due to on-going traffic a combination of string inverters with power optimizers are assumed String inverters in Germany 2022	130
Structural components (racking)	95(rooftop ballasted) 150 (fixed tilt ground mounted with pile foundations)	Decrease as no foundations or complex structures necessary but only racks attached on noise barrier to hook-up the panels. Also, not replacing the noise barrier panels keeps cost low.	60
Electrical components	130 (rooftop) 360 (ground mounted) (conductors, conduit and fittings, transition boxes, switchgear, panel boards and others)	Costs would be between ground and rooftop mounted ones	210
Installation (labour & equipment)	165 (rooftop) 185 (ground mounted) Indicative traffic measures (e.g. road blocking) costs for noise barrier installation activities per m of noise barrier (90 €/m) [68]	Increased value based on ground- mounted due to complexities requiring use of cranes, blocking traffic, inaccessibility and road works required due to complex landscapes around noise barriers	260
EPC Overhead	160 (rooftop) 150 (ground mounted)	Same costs	160
Permitting, Inspection & Interconnection (PII)	120 (rooftop) 90 (ground mounted)	Permitting more complex due to highway environment Inspection more complex (racking) and linear integration Interconnection complexities due to linear layout	125
Sales Tax (<i>if any</i>)	45 (rooftop) 60 (ground-mounted)	Same costs	45
Developer Overhead	315 (rooftop) 420 (ground-mounted)	Average of rooftop and ground- mounted	350
Contingencies	45 (rooftop) 50 (ground-mounted)	Increased value based on ground- mounted	70
Profit	105 (rooftop) 150 (ground-mounted)	Average of rooftop and ground- mounted	130
Totals	1600 - 1795 € ₂₀₂₀ /kW (rooftop) 2035 - 2230 € ₂₀₂₀ /kW (ground- mounted)		1820 € ₂₀₂₀ /kW

5.3.5 Summary Cost Figures

Table 5 - 8 shows the summary of all key system parameters. These include CAPEX, OPEX, lifetime, system capacities. The Table also includes design and sizing assumptions used to determine some of those figures along with additional information around the electricity production modelling.

Table 5 - 8: Initial system input data along with design and sizing assumptions for the concept

System parameters	Values and Units	Design and Sizing Assumptions	References
Micro wind turbine			
CAPEX	5100 €/kW	* production time series based on KNMI airport time series for 3 locations	[50],
OPEX	4% of CAPEX per annum	* noise barrier corrections applied (very low case – 60% AEP reduction, very high case 63% AEP increase)	[47], [59],
Lifetime	20 Years	* CAPEX based on micro wind market reports and retrofitting cost assumptions presented later	[2],
Capacity	9 kW	* total system capacity sized on average noise barrier length in the Netherlands (145m) from GIS analysis * system structurally integrated with the noise barriers with a 5D clearance (rotor diameter) to avoid wake losses * interconnected electrically with cables and share infrastructure with the photovoltaic system strings * 0.375 kW turbine size used due combined noise barrier and object height limitations (combined height of rotor and noise barrier <8 meters)	[61], [58], [70]
Photovoltaic system			
CAPEX	1820 €/kW	* production time series based on PVGIS datasets corrected for typical noise barrier inclinations and orientations	[51],
OPEX	2% of CAPEX per annum	* CAPEX based on PV system prices and retrofitting cost assumption explained in later section	[63], [45],
Lifetime	20 years	* baseline design slope is 80° (from GIS data analysis) with South facing orientation	[46]
Capacity	90KW	* sized on the average noise barrier length in Netherlands assuming 3 panels for a typical 5m high noise barrier * 0.6 kW _{PV} /m of noise barrier	
Electrical Grid and Price			
Interconnection Capacity Level	10-300 kVA	* interconnection capacity based on combined wind and solar power rating	[25],[71], [42,69]
Annual Costs	1200-3000 €/year	* connected to the low-voltage electricity distribution network according to the Grid Electrical Code	[21],[22],
Baseline Cable Distance	150 m	* range depends on distance from network and interconnection capacity which is based on GIS analysis	[72],[73]

5.4 Results of levelised cost of electricity

As a start the results section presents and discusses the LCOE ranges for all the different scenarios. The LCOE is presented for a wind only noise barrier (6 first boxes and whiskers in Figure 5 - 6), a solar only noise barrier (the next 3 boxes and whiskers) and a hybrid configuration (the last 2 boxes and whiskers). For the wind case, two cases are presented, one named as Wind_FE (in legend) which takes into account the additional field experiment (FE) performance losses as explained in Section 5.3.3 and the second named as Wind (in legend) which corresponds to an ideal theoretical performance case (as measured in the wind tunnel), see section 5.3.3. The ranges of the whiskers and boxes for the wind only noise barrier represent the most positive noise barrier influence (lowest part of whisker) and most negative influence (higher part of whisker), see also section 5.3.3. For the PV case the range represents the different configurations with south, east and west facing barriers and the slopes between 50° – 80°.

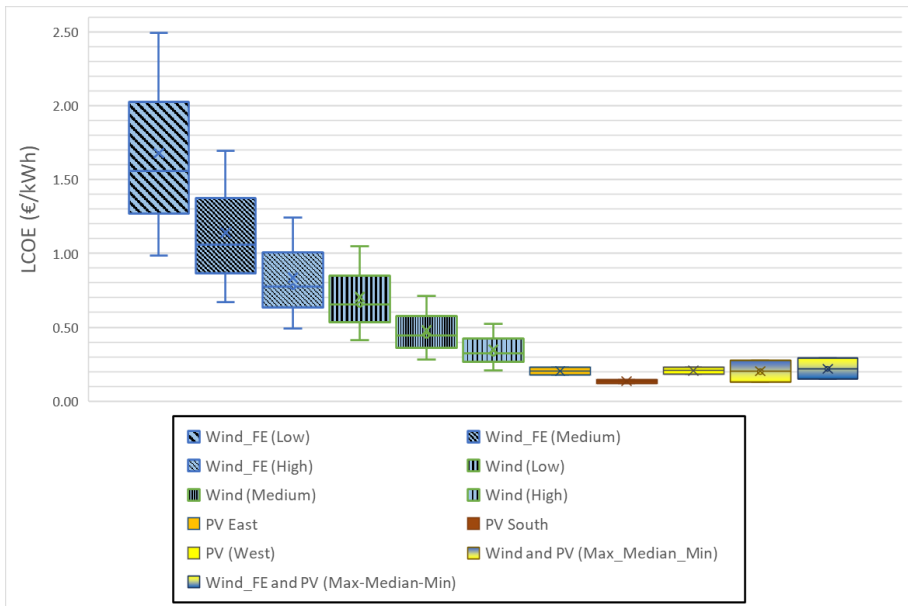


Figure 5 - 6: Levelised cost of electricity (LCOE) for various wind, solar and hybrid configurations. (striped) these represent wind system only and the ranges reflect positive and negative influence of the noise barrier in the wind yield (single colored) photovoltaic noise barrier (PVNB) system for East-South-West azimuth with ranges for slopes between 50°-80° (blue and yellow gradient) ranges of the best, median and worst combined wind and solar annual energy production yields

For the wind only case, the micro wind systems have a very wide range of levelised cost of electricity between 0.25 – 2.50 €/kWh. Especially the wind cases where

performance losses are taken into account results in a range between 0.50 – 2.50 €/kWh for all 3 locations. The ideal micro wind turbine performance cases range between 0.30 – 1.05 €/kWh. A high average wind speed results in lower costs as expected and also the cost range is decreased. Micro wind electricity is the most expensive of all systems for all cases.

For the PV only case, stand-alone PV outperforms both the wind only and hybrid cases with a LCOE range between 0.13 – 0.25 €/kWh.

For the hybrid case, the range of costs is between 0.20 – 0.30 €/kWh. The inclusion of micro wind turbines in the system slightly increases overall costs between 0.05 – 0.08 €/kWh for the ideal and limited performance case of micro wind turbine electricity.

After LCOE, the ratio of the annual electricity production (AEP) in kWh per kW installed is presented for each system. It is shown in *Figure 5 - 7* that the ideal wind system has the highest range and the best performance of all configurations while the wind system with field experiment (FE) measured losses has the lowest of all. Even though ideal micro wind presents the best energy yield case, when compared with the cost above it is still not the most economic option, which has to do with the high micro wind turbine CAPEX and OPEX costs. For the PV case, it performs a little better than the non-ideal micro wind case. Finally, the hybrid option has a little better AEP per kW than PV and the ideal wind case.

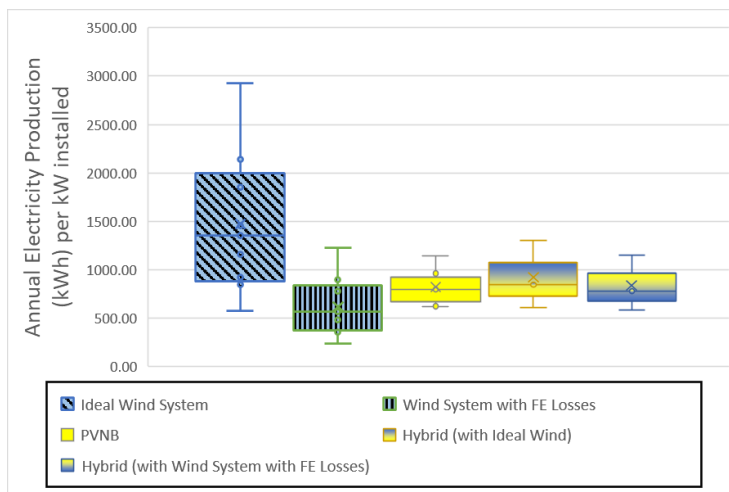


Figure 5 - 7: Annual Electricity Production (AEP) in kWh per kW of installed system

A total of 90kW PV and 9kW of wind can produce between 56 – 130 MWh per year, as presented in *Figure 5 - 8*, from the worst to best site conditions assuming an ideal or with losses performance for the wind turbine system. This AEP is equivalent to 30 – 60 homes electricity consumption. PV largely dominates electricity production between 80 – 96 % of total with wind between 4 – 20 %. This range of the results includes

sensitivities of east to south and to west for solar generation, the 3 different resource location wind profiles along with correction of the best and worst change of wind flow due to noise barriers and the ideal and poor performance micro wind turbine systems.

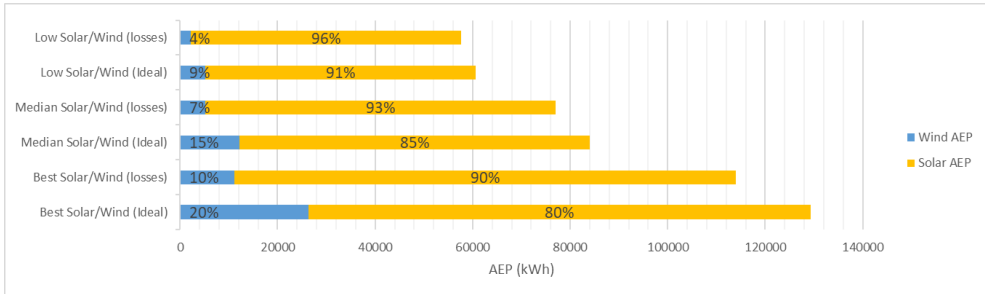


Figure 5 - 8: Annual Electricity Production (kWh) split between Solar and Wind electricity for the hybrid system (90kW solar and 9kW wind) for all possible configurations including the ideal and losses performance of the micro wind turbine systems

Figure 5 - 9 shows a waterfall diagram of the different annualized cost components of the hybrid 90kW PV system, the 9kW wind turbine system and the grid connection. It is shown that the PV costs are the highest ones with a total of 11460 € per year and for wind is 4130 € while grid is only 1300 €. It is noted however, that PV is 3.6 times cheaper per kW than wind turbine systems with ~130 €/kW/year comparing to 460 €/kW/year for wind.

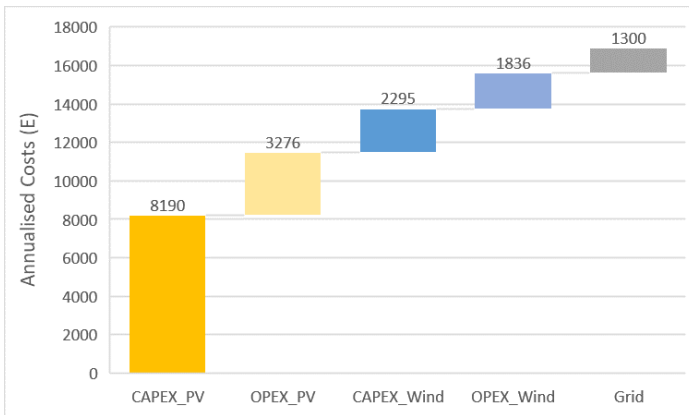


Figure 5 - 9: Annualised Cost Breakdown for a 90kW PV and 9kW micro wind turbine systems integrated on a noise barrier

In order to understand the influence of the financial parameters to the LCOE two extreme cases are compared for the wind only case by applying a sensitivity analysis on

the CAPEX, the OPEX and the WACC of the system, by varying them by 50% up and down. All those are presented in Figure 5 - 10. For these cases it is shown that CAPEX variation has the highest influence. The 2 cases are:

- the lowest wind profile location with a stand-alone wind system which is placed on a noise barrier which has the most negative influence on energy yield assuming a micro wind turbine with losses. For this case the LCOE range between 1.5 – 3.4 €/kWh.
- the best wind profile location with a standalone wind system placed on a noise barrier which achieves the most positive influence on energy yield and a turbine design is assumed that performs in an ideal manner. For this case the LCOE range between 0.13 – 0.28 €/kWh.

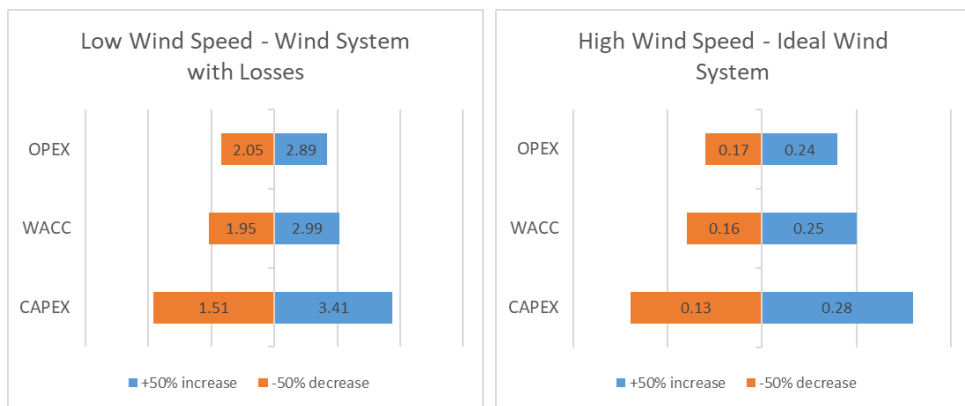


Figure 5 - 10: LCOE sensitivity analysis (€/kWh)

All the aforementioned results show that there are high uncertainties for the levelised cost of electricity (LCOE) from noise barriers integrated with solar and wind systems. The highest uncertainty in cost comes from the micro wind turbine systems as the combination of unpredictable yield and higher CAPEX costs can result in an expensive system. The systems presenting less uncertainty is the PV only systems. By combining solar with micro wind, the LCOE is slightly higher than the solar PV alone system. Unfortunately, the levelised cost of electricity for the noise barrier system in any configuration and sensitivity results in higher electricity costs than the project cost global figures for typical onshore wind 0.03 €/kWh or for offshore wind systems at 0.08 €/kWh or utility scale solar ones at 0.05 €/kWh. These figures come from the IEA's Renewable Power Generation Costs in 2022 [74] and are converted from \$₂₀₂₂ to €₂₀₂₂.

5.5 Conclusions

This Chapter aimed to answer the research question “What is the levelised cost of electricity of noise barrier integrated wind turbines?”. The conclusions of this Chapter are described here.

It was found that at present, there are very few concepts of micro wind turbines integrated with highway infrastructures. Most found in literature are integrated with highway street lighting mostly for off-grid cases. This chapter assessed the integration of micro wind turbines with PV on noise barrier structures along highways to benefit from structural component integration costs.

A detailed literature review has been conducted for the costs of micro wind turbines showing that there is a potential to reduce by 40% the CAPEX of micro wind energy on noise barriers structures (*with key reductions on tower, foundations, installation and electrical infra*). A review of photovoltaic system costs is performed, showing a potential cost breakdown for photovoltaic noise barriers (PVNB).

The energy yield of a 90 kW solar PV combined with 9 kW micro wind turbine integrated on a noise barrier ranges between 56 – 130 MWh per year. These ranges reflect production in locations with low to high average wind speeds with wind speed corrections due to the noise barrier and the additional losses (42% performance losses for micro wind turbines) as recorded in an experimental campaign. This range also includes West to South and East oriented photovoltaic noise barriers. These substantial losses are relatively small when compared to the total energy yield of a hybrid PV and wind noise barrier.

The micro wind electricity is the most expensive and sensitive to location parameters (0.25 – 2.5 €/kWh). This is due to the different resource, the influence of the noise barrier on energy yield, the poor performance of the wind turbine and the expensive CAPEX. Solar electricity LCOE is the cheapest between 0.13 – 0.24 (€/kWh) and the hybrid Solar-Wind electricity LCOE is between 0.15 – 0.24 (€/kWh).

Table 5 - 9: Levelised cost of electricity (LCOE) ranges for wind only, solar only and hybrid systems integrated with a noise barrier

System	LCOE range (€/kWh)
Micro Wind turbine noise barrier (Wind Only)	0.25 – 2.5
Photovoltaic Noise Barrier (Solar Only)	0.13 – 0.24
Hybrid System (90kW PV and 9kW Wind)	0.15 – 0.24

A sensitivity was applied for the wind only system on the CAPEX, OPEX and WACC. This resulted in a wider range of levelised cost of electricity between 0.13 – 3.41 €/kWh which is above the global average LCOE for onshore, offshore wind systems and utility

scale solar Micro wind electricity is the most expensive and does not lead to feasible projects. For the hybrid PV and wind noise barrier system performs better than the wind only system, with an LCOE between 0.2 – 0.3 €/kWh. But it is still more expensive than utility scale wind and solar systems. Therefore, the main conclusion of this study is that the researched solar and wind systems integrated with noise barrier infrastructures do not result in feasible projects.

5.6 References

1. H F Liew, I Baharuddin, Abd R Rosemizi, I Muzamir and S I S Hassan. Review of feasibility wind turbine technologies for highways energy harvesting. *Journal of Physics: Conference Series* **2020**, <https://iopscience.iop.org/article/10.1088/1742-6596/1432/1/012059>, doi:<https://iopscience.iop.org/article/10.1088/1742-6596/1432/1/012059>.
2. AC Orrell and EA Poehlman. *Benchmarking U.S. Small Wind Costs With the Distributed Wind Taxonomy*, Pacific Northwest National Laboratory, 2017. <https://www.pnnl.gov/news-media/first-its-kind-report-benchmarks-costs-us-small-wind-projects>
3. Nikolaos Chrysochoidis-Antsos, Gerard J.W. van Bussel, Jan Bozelie, Sander M. Mertens and Ad J.M. van Wijk. Performance Characteristics of A Micro Wind Turbine Integrated on A Noise Barrier. *Energies* **2021**, *14*.
4. Mehdi Baneshi and Farhad Hadianfard. Techno-economic feasibility of hybrid diesel/PV/wind/battery electricity generation systems for non-residential large electricity consumers under southern Iran climate conditions. *Energy Conversion and Management* **2016**, *127*, doi:<https://doi.org/10.1016/j.enconman.2016.09.008>.
5. K. Sunderland, M. Narayana, G. Putrus and M. Conlon. Levelised cost of energy analysis: A comparison of urban (micro) wind turbines and solar PV systems. In Proceedings of 51st International Universities Power Engineering Conference (UPEC); pp. 1-6.
6. Rashid Al Badwawi, Mohammad A. Abusara and Tapas K. Mallick. A Review of Hybrid Solar PV and Wind Energy System. *Smart Science* **2015**, *3*.
7. R Menaka., K. R. Mohan, P MuthuVijay., I. Ranjith and D. Ragul. Power Generation by Hybrid VAWT System for Highway Applications. *International Journal for Advance Research and Development* **2018**, *3*.

8. S. Georges and F. H. Slaoui. Case Study of Hybrid Wind-Solar Power Systems for Street Lighting. 2011 In Proceedings of 2011 21st International Conference on Systems Engineering, 16-18 Aug. 2011; pp. 82-85.
9. Nadwan Majeed Ali and Handri D. Ammari. Design of a hybrid wind-solar street lighting system to power LED lights on highway poles. *AIMS Energy* **2022**.
10. Ehab Hussein Bani-Hani, Ahmad Sedaghat, Mashael Al-Shemmary, et al. Feasibility of Highway Energy Harvesting Using a Vertical Axis Wind Turbine. *Energy Engineering* **2018**, 115, doi:10.1080/01998595.2018.11969276.
11. R. Devi and Jaspal Singh. Design and Development of Prototype Highway Lighting with Road Side Wind Energy Harvester. *International Journal of Science and Research* **2014**, 3.
12. Z. Ibrahim and A. R. Asari. The development of wind power energy for lighting system in the highway. *Malaysian Journal of Industrial Technology* **2019**.
13. Ali Zarkesh and Mohammad Javad Heidari. Developing a New Application for Wind Generators in Highways. *2013 Fifth International Conference on Computational Intelligence, Communication Systems and Networks* **2013**.
14. Wenyu Hu, Jiaqiang E, Feng Zhang, et al. Investigation on cooperative mechanism between convective wind energy harvesting and dust collection during vehicle driving on the highway. *Energy* **2022**, 260, doi:<https://doi.org/10.1016/j.energy.2022.124923>.
15. Sachin Y. Sayais, Govind P. Salunkhe, Pankaj G. Patil and Mujahid F. Khatik. Power Generation on Highway by using Vertical Axis Wind Turbine & Solar System. *International Research Journal of Engineering and Technology* **2018**, 5.
16. D.B. Jani, Chaudhary Chetan, Ka. Patel Shivam, Patel Shivang and Baria Darshan. Highway lighting by use of wind turbine and solar energy. *International Journal of Innovative Research in Technology* **2019**, 6.
17. Lingfei Qi, Peng Zheng, Xiaoping Wu, et al. A hybrid wind-photovoltaic power generation system based on the foldable umbrella mechanism for applications on highways. *Solar Energy* **2020**.
18. Peng Zheng, Zheng Fang, Hai Li, et al. Multi-objective optimization of hybrid energy management system for expressway chargers. *Journal of Energy Storage* **2022**, 54, doi:<https://doi.org/10.1016/j.est.2022.105233>.
19. Kamil M. Yousif, Diyar A. Bleej, Alan Ibrahim Saeed and Rezheen A. Bleej. Analysis of Wind Energy Potential Inside a Tunnel Located on the Highway. 2019.

20. Hao Cao, Xiaoping Wu, Hao Wu, et al. A Hybrid Self-Powered System Based on Wind Energy Harvesting for Low-Power Sensors on Canyon Bridges. *International Journal of Precision Engineering and Manufacturing-Green Technology* **2022**.
21. CBS, *Average electricity prices for consumers*, 2022, <https://www.cbs.nl/en-gb/figures/detail/84672ENG>
22. Kira Taylor. LEAK: Energy prices will 'remain high and volatile until at least 2023', EU Commission says. *EURAKTIV* 18 Feb 2022, 2022.
23. LIANDER. Ruigoord electricity station in Amsterdam's Westelijk Havengebied reaches maximum capacity. 2022.
24. LIANDER. Extra space for waiting entrepreneurs on full electricity grid Leeuwarden. 2022.
25. Netbeheer Nederland. *Position Paper voor het Rondetafelgesprek over het Electriciteitsnet*, 2022. [https://www.netbeheernederland.nl/upload/Files/Rondetafel Elektricitetsnet 03-02-2022 Inbreng Netbeheer Nederland 242.pdf](https://www.netbeheernederland.nl/upload/Files/Rondetafel_Elektricitetsnet_03-02-2022_Inbreng_Netbeheer_Nederland_242.pdf)
26. Ariana Ramos, Markku Tuovinen and Mia Ala-Juusela. Battery Energy Storage System (BESS) as a service in Finland: Business model and regulatory challenges. *Journal of Energy Storage* **2021**, *40*, doi:<https://doi.org/10.1016/j.est.2021.102720>.
27. Paul Jochems. The potential of PV panels near road infrastructure in the Netherlands. Technical University of Eindhoven, Eindhoven, 2013.
28. Mohamed Nasser, Tamer F. Megahed, Shinichi Ookawara and Hamdy Hassan. Techno-economic assessment of clean hydrogen production and storage using hybrid renewable energy system of PV/Wind under different climatic conditions. *Sustainable Energy Technologies and Assessments* **2022**, *52*, doi:<https://doi.org/10.1016/j.seta.2022.102195>.
29. Kristian Sevdari, Lisa Calearo, Peter Bach Andersen and Mattia Marinelli. Ancillary services and electric vehicles: An overview from charging clusters and chargers technology perspectives. *Renewable and Sustainable Energy Reviews* **2022**, *167*, doi:<https://doi.org/10.1016/j.rser.2022.112666>.
30. Weipeng Zhan, Zhenpo Wang, Lei Zhang, et al. A review of siting, sizing, optimal scheduling, and cost-benefit analysis for battery swapping stations. *Energy* **2022**, *258*, doi:<https://doi.org/10.1016/j.energy.2022.124723>.

31. Santanu Kumar Dash, Suprava Chakraborty, Michele Roccotelli and Umesh Kumar Sahu. Hydrogen Fuel for Future Mobility: Challenges and Future Aspects. *Sustainability* **2022**, 14.
32. Yvonne Ruf, Markus Kaufmann, Simon Lange, et al. *Fuel Cells and Hydrogen Application for Regions and Cities Vol. 2 - Cost analysis and high-level business case*, Roland Berger, 2017;
33. Trinomics and Ludwig Bolkow Systemtechnik. *Opportunities for hydrogen energy technologies considering the National Energy & Climate Plans, 2020*. https://www.fch.europa.eu/sites/default/files/file_attach/Brochure%20FCH%20Netherlands%20%28ID%209474122%29.pdf
34. Chunto Tso and Shih-Yun Chang. A viable niche market—fuel cell scooters in Taiwan. *International Journal of Hydrogen Energy* **2003**, 28, doi:[https://doi.org/10.1016/S0360-3199\(02\)00245-8](https://doi.org/10.1016/S0360-3199(02)00245-8).
35. Fuel cell scooters, solar hydrogen station launched in Hawaii. *Fuel Cells Bulletin* **2012**, 2012, doi:[https://doi.org/10.1016/S1464-2859\(12\)70261-4](https://doi.org/10.1016/S1464-2859(12)70261-4).
36. Stephen P Carroll. *Investigation into the Installation of Small Wind Turbines in an urban environment*, Center of Renewable Energy Systems Technology,
37. K. M. Sunderland, Narayana, M., Putrus, G., Conlon, M. F., McDonald, S. The cost of energy associated with micro wind generation: International case studies of rural and urban installations. *Energy* **2016**, 109, doi:10.1016/j.energy.2016.05.045.
38. J. L. Acosta, K. Combe, Sasa Z. Djokic and I. Hernando-Gil. Performance Assessment of Micro and Small-Scale Wind Turbines in Urban Areas. *Ieee Systems Journal* **2012**, 6, doi:10.1109/jsyst.2011.2163025.
39. Yildiz Kalinci, Arif Hepbasli and Ibrahim Dincer. Techno-economic analysis of a stand-alone hybrid renewable energy system with hydrogen production and storage options. *International Journal of Hydrogen Energy* **2015**, 40, doi:<https://doi.org/10.1016/j.ijhydene.2014.10.147>.
40. Murat Gökçek. Hydrogen generation from small-scale wind-powered electrolysis system in different power matching modes. *International Journal of Hydrogen Energy* **2010**, 35, doi:<https://doi.org/10.1016/j.ijhydene.2010.07.149>.
41. Abdullah Al-Sharafi, Ahmet Z. Sahin, Tahir Ayar and Bekir S. Yilbas. Techno-economic analysis and optimization of solar and wind energy systems for power generation and hydrogen production in Saudi Arabia. *Renewable and Sustainable Energy Reviews* **2017**, 69, doi:<https://doi.org/10.1016/j.rser.2016.11.157>.

42. Wettenbank. (translated) Code of electricity rates/tariffs. Wettenbank, Ed. 2021.
43. Walter Packey Short, Daniel J.Holt, Thomas. *A Manual for the Economic Evaluation of Energy Efficiency and Renewable Energy Technologies*, NREL, 1995.<https://www.nrel.gov/analysis/tech-lcoe-documentation.html>
44. IEA. The cost of capital in clean energy transitions. Available online at: <https://www.iea.org/articles/the-cost-of-capital-in-clean-energy-transitions>
45. Sander Lensink and Koen Schoots. *Eindadvies Basisbedragen SDE++ 2022*, Planbureau voor de Leefomgeving (PBL), 2022.<https://www.pbl.nl/sites/default/files/downloads/pbl-2022-eindadvies-sde-plus-plus-2022-4403.pdf>
46. E. De Schepper, S. Van Passel, J. Manca and T. Thewys. Combining photovoltaics and sound barriers - A feasibility study. *Renewable Energy* **2012**, 46.
47. Alice C Orrell, Nikolas F Foster, Scott L Morris and Juliet S Homer. *2016 Distributed Wind Market Report*, Pacific Northwest National Laboratory, 2017.<https://www.pnnl.gov/publications/2016-distributed-wind-market-report>
48. Eric Lantz, Benjamin Sigrin, Michael Gleason, Robert Preus and Ian Baring-Gould. *Assessing the Future of Distributed Wind: Opportunities for Behind-the-Meter Projects*, United States, 2016; p Medium: ED; Size: 65 p.
<https://www.osti.gov/biblio/1333625>
<https://www.osti.gov/servlets/purl/1333625>
49. Nikolaos Chrysochoidis-Antsos, Andrea Vilarasau Amoros, Gerard J. W. van Bussel, Sander M. Mertens and Ad J. M. van Wijk. Wind resource characteristics and energy yield for micro wind turbines integrated on noise barriers – An experimental study. *Journal of Wind Engineering and Industrial Aerodynamics* **2020**, 203, doi:<https://doi.org/10.1016/j.jweia.2020.104206>.
50. KNMI. Uurgegevens van het weer in Nederland - Hourly Data of weather in the Netherlands. Available online at: <https://www.knmi.nl/nederland-nu/klimatologie/uurgegevens>
51. European Commission. Photovoltaic Geographic Information System - PVGIS. Available online at: https://joint-research-centre.ec.europa.eu/pvgis-photovoltaic-geographical-information-system_en
52. N.J.C.M. van der Borg and M.J. Jansen. *Photovoltaic noise barrier at the A9-highway in The Netherlands - Results of the monitoring programme*, ECN, 2001.<https://resolver.tudelft.nl/uuid:a746c334-1ae1-4ffb-a85e-1cdc7caf3426>

53. M. A. Gu, Y. S. Liu, J. J. Yang, et al. Estimation of environmental effect of PVNB installed along a metro line in China. *Renewable Energy* **2012**, 45, doi:10.1016/j.renene.2012.02.021.
54. * Makbul A.M. Ramli a, Eka Prasetyono b, Ragil W. Wicaksana b, Novie A. Windarko b, Khaled Sedraoui a, Yusuf A. Al-Turki On the investigation of photovoltaic output power reduction due to dust accumulation and weather conditions. *Renewable Energy* **2016**, 99.
55. Simona Villa and Minne de Jong. *Solar Highways Monitoring - End Report, 2020*.https://solarhighways.eu/sites/all/files/default/documents/Solar%20Highways%20-%20Monitoring%20End%20Report%20_2020.pdf
56. Selma Brynolf, Maria Taljegard, Maria Grahn and Julia Hansson. Electrofuels for the transport sector: A review of production costs. *Renewable and Sustainable Energy Reviews* **2018**, 81, doi:<https://doi.org/10.1016/j.rser.2017.05.288>.
57. Wettenbank. (*translated*) Regulation on the effectiveness of noise measures Noise Abatement Act - Appendix 1. **2022**.
58. CarbonTrustUK. *Small-scale wind energy - Policy Insights and practical guidance*, The Carbon Trust, UK, August 2008, **2008**.www.wind-power-program.com
59. Canadian Wind Energy Association. *CanWEA Small wind market survey - An overview of Canada's Small Wind Manufacturing Sector*, Canadian Wind Energy Association, 2010.<https://www.vindenergi.dtu.dk/english/-/media/Institutter/Vindenergi/Research/Current-projects/Smallwind/17-2010-CanWEA-small-wind-market-survey-An-overview.ashx?la=da&hash=AB8FF57B44B7F8ACD2FE45217E1057DE537FF028>
60. DWEA - Distributed Wind Energy Association. *DWEA Distributed Wind Vision – 2015-2030 Strategies to reach 30 GW of “behind-the-meter” wind generation by 2030*, 2015;
61. Trudy Forsyth, Tony Jimenez, Robert Preus, Suzanne Tegen and Ian Baring-Gould. *The Distributed Wind Cost Taxonomy*, NREL, 2017.<https://www.nrel.gov/docs/fy17osti/67992.pdf>
62. ISE Fraunhofer Institute for Solar Energy Systems. *Photovoltaics Report 2022, 2022*.<https://www.ise.fraunhofer.de/content/dam/ise/de/documents/publications/studies/Photovoltaics-Report.pdf>
63. ISE Fraunhofer Institute for Solar Energy Systems. *PHOTOVOLTAICS REPORT*, 2017;

64. Thomas Nordmann and Luzi Clavadetscher. PV on noise barriers. *Progress in Photovoltaics* **2004**, 12, doi:10.1002/pip.566.
65. OnyxSolar. Photovoltaic Glass for Acoustic Barriers - Feasibility Study for Los Angeles. Available online at: <https://www.onyxsolar.com/product-services/photovoltaic-glass-solutions/photovoltaic-acoustic-barrier>
66. Rijkswaterstaat. *Final Report - Solar Highways*, 2020. <https://solarhighways.eu/sites/all/files/default/documents/Solar%20Highways%20Final%20Report%202020.pdf>
67. David Feldman, Vignesh Ramasamy, Ran Fu, et al. *U.S. Solar Photovoltaic System and Energy Storage Cost Benchmark: Q1 2020*, 2021. <https://www.nrel.gov/docs/fy21osti/77324.pdf>
68. Wettenbank. (translated) Subsidy scheme for traffic noise remediation (Appendix C - Average costs of noise barriers). 2022.
69. STEDIN. Electricity Tariffs 2017. 2017.
70. Tyler Stehly, Philipp Beiter and Patrick Duffy. *2019 Cost of Wind Energy Review*, NREL - National Renewable Energy Laboratory, 2020. <https://www.nrel.gov/docs/fy21osti/78471.pdf>
71. Wettenbank. (translated) Electricity grid Code. 2021.
72. Maarten Afman, Sebastiaan Hers and Thijs Scholten. *Energy and electricity price scenarios 2020-2023-2030 - Input to Power to Ammonia value chains and business cases*, CE Delft, 2017. https://cedelft.eu/wp-content/uploads/sites/2/2021/04/CE_Delft_3H58_Energy_and_electricity_price_scenarios_DEF.pdf
73. S. Krishna Swamy, I. Gonzalez-Aparicio and N. Chrysochoidis-Antos. Developing a long-lasting offshore wind business case towards a Dutch decarbonised energy system by 2050. *Journal of Physics: Conference Series* **2022**, 2151, doi:10.1088/1742-6596/2151/1/012010.
74. IRENA. *Renewable Power Generation Costs 2022*, International Renewable Energy Agency, Abu Dhabi, 2023. <https://www.irena.org/Publications/2023/Aug/Renewable-Power-Generation-Costs-in-2022>

6

Technical potential of on-site wind powered hydrogen producing refueling station in the Netherlands

“When the wind of change blows, some build walls, while others build windmills.”

- Chinese Proverb

*This **chapter** provides a methodology to assess in a national scale the technical potential of wind turbines integrated with on-highway fuelling stations for the production and refuelling of hydrogen in the Netherlands. The method uses GIS databases, wind energy models and related policies related to onshore wind turbine installation*

*The **research question** that this chapter answers is:*

“Is there nationwide technical potential of wind turbines integrated with fuelling stations in the Netherlands for hydrogen production?”

This chapter is published as “Technical potential of on-site wind powered hydrogen producing refueling station in the Netherlands” by Nikolaos Chrysochoidis-Antsos, Miguel Rodríguez Escudé and Ad van Wijk, (2020) in “International Journal of Hydrogen Energy” published by © Elsevier

6.1 Introduction

This chapter expands the research on integrating wind turbines with highway infrastructures by assessing the potential of existing fuelling stations in the Netherlands to be converted to on-site wind powered hydrogen producing refuelling stations. The assessment is performed for the amount of fuelling stations, the annual hydrogen production potential, demand coverage and potential to connect to existing gas grids combining several GIS datasets and buffering zones based on current legislation and other criteria. Much of this work was based on the MSc Thesis work [1] and has been extended and detailed within this chapter.

6.1.1 *Hydrogen roadmaps worldwide and in the Netherlands*

Numerous countries have released reports giving pathways towards a green hydrogen transition. From Australia [2] to Japan [3] and from California [4] to Europe [5]. All those pathways have a common vision to produce green hydrogen coming from renewable energy resources (wind and solar energy) and utilise in transportation through hydrogen refuelling stations in order to achieve the climate targets. Many of the studies and plans of governments assessed in [6] indicated that, between 2030-2050 Fuel Cell Electric Vehicles (FCEVs) would be cheaper under several circumstances and one of them is the increasing number of refuelling stations.

In the Netherlands, the cabinet's vision on hydrogen was recently announced, where the roll out of hydrogen refuelling stations is addressed with a vision for 50 stations by 2025 [7]. Also, a roadmap with a vision to have a carbon emission free economy by 2050 with green hydrogen as a key ingredient is published [8]. This report vision lies into large cost reductions due to large upscaling of the whole sector coupling with hydrogen, utilizing most of the industrial facilities in the Northern part of the Netherlands. In addition, a report from the gas and electricity transmission operators [9] identifies the electrical grid capacity issues of the Netherlands and the flexibility that the hydrogen gas networks could provide by storing and transporting large amounts of potential energy. Large scale hydrogen production could also seasonally be stored in salt caverns, as Netherlands have large potential of 10.4 PWh [10]. Beside large-scale implementation, production closer to the demand and to distribution points of connection could play a significant role for the energy transition.

The study presented here is focussed on the small-scale distributed generation of hydrogen with Power-to-Gas technologies rather than large scale offshore implementation. This is a parallel step needed to bring about innovation, social acceptance and workforce training within the hydrogen transition targets and manage a successful hydrogen station deployment. The studied concept here has similarities with the deployment plans for hydrogen refuelling infrastructure in North-eastern United States described in [11], where on-site stations play a crucial role as hydrogen production factories for off-site stations by saving total investment costs.

6.1.2 *Hydrogen Refuelling stations in the Netherlands*

Globally, there are many initiatives that have studied the optimal sizing and design of a hydrogen fuelling station, safety aspects, distances and risks and many lessons have been learned [12-16]. In Germany, 84 stations are currently operating with a vision of 100 in the course of 2020 [17] from H2 Mobility initiative, while company H-TEC announced a 1MW electrolyser to be used for decentralised application at wind power plants and hydrogen refuelling stations [18, 19]. In California research institutions are already collecting and analysing operational data from nearly 40 hydrogen refuelling stations [20]. The role of hydrogen refuelling stations is also highlighted in [21] where the Chinese development goal of hydrogen FCEV development is to have over a 1000 stations with 50% renewable sourced hydrogen by 2030 for over a million FCEVs.

This trend starts picking up in the Netherlands as well. Since 2003, hydrogen refuelling stations are under-going operational and closing status [22]. However, with the hydrogen roadmaps mentioned above, more and more initiatives announce their commitment and will to open new hydrogen stations linked to mobility, following global trends. Recent examples are mentioned in [23-26] where: 20 fuel cell buses and hydrogen refuelling stations are envisioned for Provinces of Groningen and Drenthe by December 2020 and openings of hydrogen fuelling stations are announced, while Dutch government set financial incentives for 9 new public hydrogen stations. However, most are still relying on non-renewable hydrogen while having the ambition for green hydrogen. A green hydrogen concept in the Netherlands is from HyGro, where an on-site wind turbine is used for electrolysis for hydrogen production next to a fuelling station [27, 28]. A turbine on-site next to an existing fuelling station could contribute to cost reductions. This could be realized by coupling the wind turbine directly with an electrolyser next to where the demand is needed. This would lead in elimination the transportation costs, land reclamation costs, higher grid interconnection costs, behind-the-meter utilization of energy without administrative taxation and eliminating the need to build a new fuelling station from scratch.

In this study, the concept of on-site wind powered hydrogen producing refuelling stations (or hubs) is assumed. Initially wind turbines are producing green electricity. The electricity is then directly fed to a Proton Exchange Membrane (PEM) electrolysis hydrogen production unit and a compressor that stores hydrogen in a medium pressure storage or a pressure regulator that feeds in hydrogen to the local high pressure gas distribution grids (4-8 bars). Being connected to the local gas distribution grids provides benefits of blending hydrogen to the local natural gas networks and thus offsetting CO₂ emissions in the short-term, and in the long term providing greater flexibility to the fuelling station assuming that the networks' are converted to 100% hydrogen gas [29]. Blending hydrogen in natural gas networks is technically possible and although it is currently challenging and expensive [30] it is still an option towards the 100% hydrogen economy. Similar system's dynamic operation, excluding connection to gas grids, has been examined in [31] where it is mentioned that with

careful system sizing it is possible to have a self-sustainable fuelling station relying on renewable sources.

The refuelling equipment receives hydrogen either directly after the electrolyser or from the medium pressure storage (typically at 200 bars). In the future scenario of the 100% hydrogen infrastructure, it could also take hydrogen from the gas grid in case of low wind days. This equipment requires electricity to operate. As it was highlighted in [32], the operation of an H₂ station using combined energy from wind and the electricity grid is preferred as it can increase the number of cars served. Therefore, in current study, an assumption is made that the electrical energy for the refuelling processes (dispensing and high-pressure compression) is provided by the existing electrical grid nearby the stations. Currently in the Netherlands 80% of fuelling stations are connected to 3x63A to 3x80A while the rest 20% are connected to 3x152A up to 3x250A, offering fast charging for electric vehicles. Some concepts of fuelling stations have a high peak electrical consumption of ionic compressors (~105kW) and other equipment [33], while others are on the lower range of 30-50 kW [34]. Thereby it is commented that some of the stations might have to slightly upgrade their electrical connection to match those.

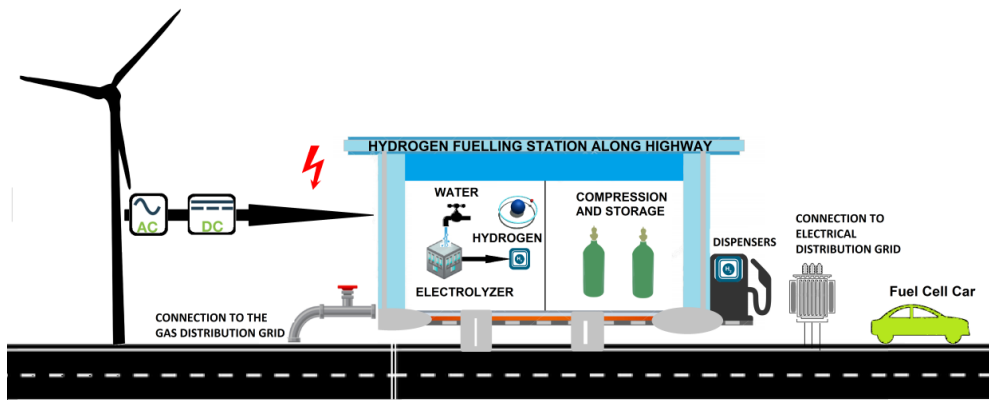


Figure 6 - 1: On-site wind powered hydrogen production and refuelling station

6.1.3 GIS and technical potential of hydrogen production

Wind turbines could not be retrofitted in existing fuelling stations which are inside cities and other built-up areas, ecological parks, airports and other infrastructures due to safety and risk concerns. These set of rules should be taken into account in order to define the technical potential of wind turbines installed in existing fuelling stations. GIS data are being used within GIS software to define all the necessary buffer zones around existing fuelling stations in order to estimate this potential according to the Dutch laws and other criteria.

GIS use in energy system modelling is part of the current energy systems challenges because these are usually considering topological relationships and disregard the geographic relationships. There is a challenge to link the spatial nature of energy systems with not considering only energy-related parameters but also geographic ones [35]. GIS can be used to design the future hydrogen infrastructure and can be an analytical tool at different spatial scales [36]. There are many notable studies that estimate the potential of hydrogen in combination with GIS that have inspired this study in many ways. In current study, a deeper dive is done by assessing existing locations and areas with constraints derived from legislations and guidelines, rather than optimizing a theoretical scenario which is common in literature.

In [37] the potential of wind-powered hydrogen production for the transportation sector is estimated using local wind resource characteristics, land use constraints with the exclusion of highly elevated areas or highly sloped areas and some constraints regarding infrastructures (such as road networks). The wind turbines are assumed to be installed in all areas available after all constraints with a 10-rotor diameter spacing criteria. In [38] a GIS-based scenario is made to calculate the investments necessary to envision a pipeline distribution and transmission network in Germany for hydrogen being produced by different scenarios (offshore wind, onshore wind, lignite gasification). Their conclusion is that a smooth transition is needed from the existing situation towards the successful adoption of energy systems. Relying on network of existing fuelling stations and existing infrastructure could facilitate this transformation towards hydrogen economy. This statement is in-line with the current study about retrofitting existing fuelling stations towards on-site wind powered hydrogen producing refuelling stations. GIS are also used in [39] to analyse hydrogen station roll-out strategy to introduce hydrogen vehicles in Andalusia. Mainly road networks, nodes and population datasets have been used in this study. Finally, an interesting study for Cordoba (Argentina) is presented using GIS for wind resource mapping, hydrogen production estimation, delivery time estimation through road networks and delivery in Cordoba city. This study is quite interesting because it combines as well economic aspects [40].

GIS are also a useful tool for other numerous potential hydrogen applications, such as in [41] for application of power-2-gas where investment screening was performed by synthesizing GIS data for different power plants for hydrogen production taking into account infrastructures. Also the hydrogen demand for transportation sector is assessed for Algeria in [42] together with analysis of production costs and environmental benefits. GIS are also used for the study in Germany [43], where a geospatial hydrogen demand-weight distribution is presented for several hydrogen mobility markets (bus, car, train etc.). The study in [44], makes a comparison of different alternative vehicle fuelling infrastructure scenario, where GIS is used to assess the time-related proximity and coverage of those stations to the user. Large GIS datasets in combination with wind turbines are used in [45] for decarbonizing heat with use of

hydrogen and inter-seasonal storage. In [46] energy systems are linked with GIS models for hydrogen infrastructure development. GIS can easily link so many energy system models with geospatial data in order to effectively design and quantify costs, infrastructural upgrades and other useful information for policymakers towards energy transition. A holistic approach is presented in [47] for all potential pathways for hydrogen refuelling infrastructure in Norway where several production technologies beside wind are considered in combination with supply/delivery scenarios.

Reading this literature, it is clear that GIS have a great potential to help designers, urban planners, energy planners and other stakeholders to effectively design the future energy systems with hydrogen being a key ingredient. Finding and synthesizing the appropriate datasets is key for a successful and understandable assessment.

6.1.4 *Outline*

In this chapter, a method is developed to assess the technical potential of existing fuelling stations to host a wind turbine within their vicinity and classify them based on wind availability, hydrogen production capability and proximity to gas distribution networks, with the vision for covering the fuel cell electric vehicle drivetrain for the future as well as providing flexibility with connection to the gas network.

As a first step, the barriers are identified for wind turbine installation and estimate the amount fuelling stations suitable for conversion to wind powered hydrogen producing refuelling station presented in Section 6.2. Then the wind production potential is estimated based on wind energy resource assessment and related this to the future hydrogen demand for the transportation sector. A case study is performed to identify the interconnection possibility with existing gas grids. The results are discussed derive conclusions are derived at the end of this Chapter.

6.2 Amount of suitable fuelling stations

6.2.1 *Methodology*

Here the amount and the location of the existing fuelling stations are found that could host a wind turbine within their vicinity for the future on-site hydrogen production. Laws/guidelines for getting a permit for installation are used as a basis to define which of the fuelling stations could to have a wind turbine next to them. Laws dedicated to hydrogen related installations are not considered in this study but are suggested to be included in further investigations.

The fuelling stations have been found through Open Street Maps shown in Figure 6 - 2 which might generate some uncertainty as the persons who are registering these data are individuals. Buffer zones are used to define the maximum distances stated by the guidelines.

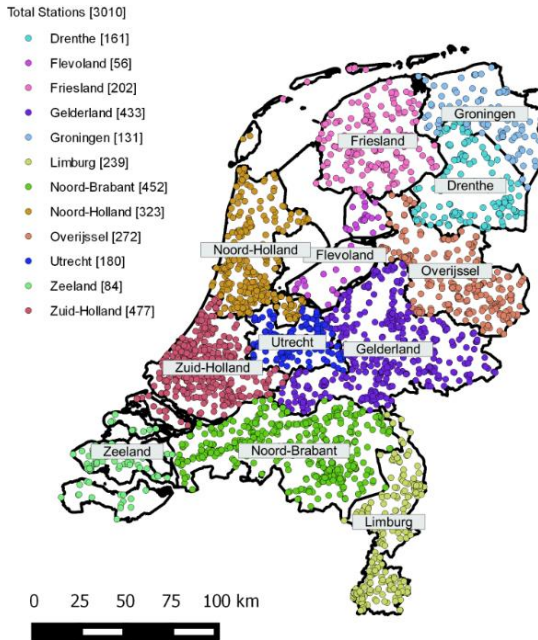


Figure 6 - 2: Map of all existing fuelling stations from Open Street Map dataset classified by Province

All the datasets were found online and converted (if needed) into a CRS (Coordinate Reference System) of (EPSG: 28992, Amersfoort / RD New) for further geoprocessing filtering. The filtering methodology was done with the Difference tool provided by QGIS software.

Below you can see the buffer zone descriptions. The physical notion behind most of those is the maximum throwing distance of an object from a wind turbine during normal operating conditions (for example ice or a detached blade) as has its background in the handbook for risk assessment for wind turbines [48]. There are also other buffer zones with respect to noise and turbulence which are based on environmental and aviation guidelines. The buffer zone description, distance and datasets used are summarized below in Table 6 -1.

Table 6 - 1: Datasets used

Buffer Zone Description	Buffer Distance	Dataset used
Proximity to existing wind turbines	200 m	[1]
Built-Up Areas	245m (based on the maximum throwing distance of a 3-5 MW wind turbine at normal operating conditions [2])	[3-5]
Silent Zone Areas	1250 m (based on maximum allowable noise level and a reference turbine)	[6,7]
Airports	2000m (based on turbulence coming from turbines)	[3]
Railtracks/Waterways/Motorways/Main Roads	80m (based on ½ rotor diameter of a 160m wind turbine [2])	[1,3]
Ecological Networks	600m (based on a median value of most species present in [8])	[9]
Winter Geese Resting Areas	3000m (based on criteria in [10])	[11]
High Voltage Lines and High-pressure pipelines	245m (based on maximum throwing distance of a 5MW wind turbine at normal operating conditions [2])	[12]

Proximity to existing wind turbines

At first, the fuelling stations where there are wind turbine(s) within proximity of 200m are removed from the dataset. These stations could also be envisioned as potential candidates for wind turbine installation for hydrogen production, but for now they are considered part of a different project connected to the electrical grid. The wind turbine data are found in the National GeoRegister of the Netherlands [60].

Built-Up Areas Zoning

This zoning covers vulnerable buildings such as houses, hospitals, schools, restaurants, hotel, office buildings, sport facilities as described in the handbook of risk zoning for wind turbines [48]. The datasets used for this zoning are from Open Street Maps, EuroGeographics and Land Cover and Land Use surveys from the Copernicus institutes. All these datasets were used to validate each other but also include areas that are not present in all datasets as with sport facilities which were not included in Open Street Maps. The buffer distance from all those buildings and areas is defined as the

maximum throwing distance in normal operating conditions for a 3-5MW wind turbine [48] and is 245 meters. In Figure 6 - 3, the suitable stations can be located when excluding the built-up areas.



Figure 6 - 3: Map near the city of Delft with Residential/Commercial/Retail areas, Sport Facilities, Industrial Areas and Roads with buffer zones.

Finally, another zoning restriction applies for the built environment and is the Silent Zone. It has its origin in the Noise Nuisance Act (Bulletin of Acts and Decrees, 1979). Silent areas were defined therein as areas in which the noise pollution caused by human activities is so low that the natural sounds prevailing in that area are not or hardly disturbed. In the governmental and legal pages in [54, 61], the zones and their maximum allowable limit of 40 dB is mentioned. For an example turbine of 5MW the limit of 40dB is found at a buffering distance of 1250m for wind speeds of 10 m/s as shown in [62, 63]. It is advised that a more thorough, detailed and site-specific noise assessment is needed for each fuelling station but for the purpose of this study this distance is assumed representative enough. The locations depicted from [53] with the 1250m buffer are shown in Figure 6 - 4 below.

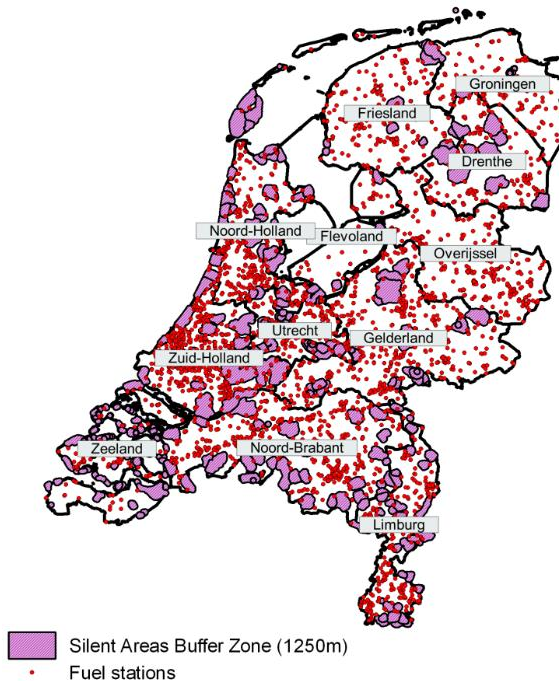


Figure 6 - 4: Map overview of existing petrol stations and Silent zone buffers of 1250m

Infrastructure Zoning

Infrastructure zoning covers railways, waterways, motorways, high voltage electrical lines and stations, airports and high-pressure gas networks. Around waterways, rail tracks and motorways the placement of wind turbines is permitted at a distance of at least 30m from the edge of the pavement or when a rotor diameter exceeds 60m, at least half the rotor diameter [48]. In this study, a rotor diameter of 160 meters is considered, looking in the future where larger rotors are used. Therefore, the buffer distance is 80m. A note is made for the motorways as they are not included because the motorways have a buffer of 80m while the station has a buffer of 150 meters around it, leaving potential space in the back of the station away from the road. However, further investigation is considered for complex road junctions. For overhead high voltage power lines and stations and high-pressure pipelines, a buffer distance of 245m is used based on the maximum throwing distance at normal operating conditions [48]. The same handbook of risk zoning advises for high-pressure gas pipelines above ground, to be in a maximum throwing distance at over speeding and asks for an expert assessment on this. Since not enough datasets are found for the placement of the pipelines and as most pipelines are installed underground [64] the buffer distance of 245m is assumed for those as well. It looks contradictory that the buffers are used for

the gas grids while hydrogen production and compression occur on-site, however it is assumed that the station is designed holistically taking all necessary risk mitigation strategies from combining wind powered electrolysis with close proximity. More research is definitely needed for this concept.

Finally for airports, [65] mentions that high objects should be considered by local authorities to determine effects on the airport operation and refers to the dimensions and slopes of obstacle limitations surfaces. But since this is very site specific, it is suggested that more specific studies should be conducted for stations near airports. However, the following study is considered as a baseline for the buffer distance of each airport in the Netherlands, with respect to turbulence effects being noticeable at 16 rotors distances [66], therefore a 2km setback distance shall be used as “rule-of-thumb” and further investigation is advised. Finally, Figure 6 - 5 shows the location of Schiphol (Amsterdam’s airport) and all the infrastructures around it. It is clear that the onshore infrastructure limitations in wind turbine placement are as well numerous like built-up zoning.

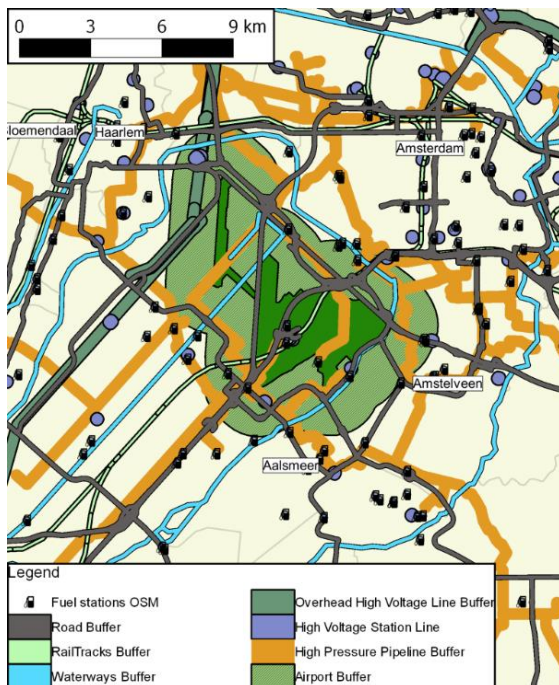


Figure 6 - 5: Map near Schiphol showing existing fuel stations with Infrastructure Zoning Areas (Airport, High Voltage Lines, Rail Tracks, Waterways, High Pressure Grid)

Environmental Zoning

This zoning covers important natural zones that need to be protected. Especially zones that are natural habitats for breeding or for migration paths. In practise, an environmental assessment is required for each specific installation site with respect to the natural habitat that surrounds the area and the particular species that reside there. This is needed since there are so many different species present which require different buffer distance from the wind turbine nuisance. This has been thoroughly examined in [55] where a review of several environmental articles has been made to define the setback distances for minimum natural habitat disturbance. Most of the results were in between 0-600 meters but as the authors indicate there can be great variations and for some cases there could be even greater distances (4.5km) depending on the flight path of certain species. For simplicity, the highest buffer distance of 600m is used for most species from all the ecological networks datasets used in this study. In that way an approximation is given of what can happen in a national level. But as explained, it is greatly advised that further investigation is needed and the results are just a rough qualitative estimation of the reduction of the fuelling station suitability. Finally, fuelling stations in proximity of 3000m (3km) from Winter Geese resting zones are removed from the final dataset. This is a special zoning advised in [57] and is included as an example for bird protection buffer zoning.

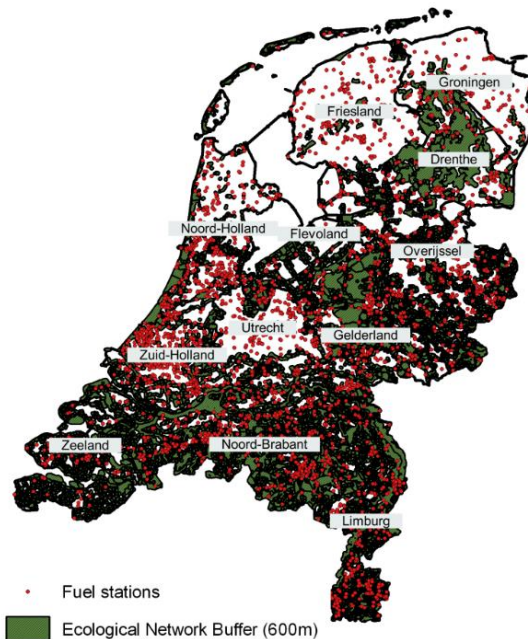


Figure 6 - 6: Map overview of existing fuelling stations and the ecological network buffers of 600m

6.2.2 Results

After applying all the zoning guidelines with the GIS software, the suitable existing fuelling stations are left that have the technical potential to become the future wind powered hydrogen production and refuelling station that will be part of the transition towards a hydrogen economy. In Table 6 – 2, below, it is observed that the Built-up area zoning regulations are the highest reduction factor, especially the residential/commercial/retail and Land Cover (discontinuous urban fabric) zoning, allows only 22%-28% from all stations. Environmental zoning allows in total only 59% while Infrastructure zoning allows 70% of the total. The intersection of all remaining stations is 4.35% (132) of the total 3021. This seems little but in fact these potential pilot projects could be one of the first adopters of this technology in order to act as hydrogen production hubs in order to test and start retrofitting all the equipment needed. Finally, the number of 4.35% could change if more site-specific studies are being performed. These studies might allow more than a single wind turbine to be installed. Most of the zonings applied are based on the handbook of risk zoning for wind turbines which provides guidance/advice and allowable distances for the legal procedure towards getting a permit for installation. To conclude, this study provides a number for planners to take into account towards further energy transition pathways towards hydrogen economy.

Chapter 6

Table 6 - 2: Effect of zoning regulations on the amount of fuelling stations suitable for wind turbine installation, for all fuelling station datasets

Filtering Steps	Station-difference in numbers and percentage from all	
All existing fuelling stations	3021	
Stations no closer than 200m to existing wind turbines	3011	
Built-Up Area Zoning (allowed stations)	465 (15.3% of total)	
Residential/Commercial/Retail	668	22.1%
Land Cover (discontinuous urban fabric)	851	28.2%
Land Cover (sport facilities)	2810	93.0%
Silent Zones	2781	92.1%
Infrastructure Zoning (allowed stations)	2122 (70% of total)	
Rail Tracks	2923	96.8%
Small Waterways	2959	97.9%
Large Waterways	3010	99.6%
High-Voltage Lines	2871	95.0%
High Voltage Stations	2948	97.6%
Airports	2940	97.3%
High Pressure Pipelines	2448	81%
Environmental Zoning (allowed stations)	1796 (59% of total)	
Natural Ecological Networks	1894	62.7%
Geese Winter Resting Areas	2864	94.8%
Total Results	132 (4.35% of total)	

Additionally, those are classified with respect to Province level. Table 6 - 3 presents the total number of feasible stations per Province of the Netherlands. The percentage of feasible fuelling stations with respect to the existing ones per Province ranges between 1-12%.

Table 6 - 3: Amount of suitable fuelling stations per Province

Province	Existing Fuelling Stations	Feasible Stations (% from total)
Friesland	202	25 (12%)
North-Holland	323	15 (4.6%)
Gelderland	433	19 (4.4%)
Groningen	131	9 (6.9%)
Overijssel	272	9 (3.3%)
Drenthe	161	10 (6.2%)
South-Holland	477	19 (4%)
Utrecht	180	9 (5%)
Flevoland	56	3 (5.3%)
North-Brabant	452	4 (0.8%)
Zeeland	84	6 (7.1%)
Limburg	239	4 (1.7%)

6.3 Wind powered hydrogen production potential at suitable fuelling stations

6.3.1 Methodology

Now that all the fuelling stations have been found that could potentially host a turbine, another important step is to identify which of those are worth in terms of available wind energy and their respective hydrogen production. Total Annual Hydrogen Production (AHP) potential is estimated from wind time series and the hydrogen production conversion efficiency. Meteorologists found that it takes at least 5 years for a site to have a typical average wind speed [67]. Therefore, the wind time series for each fuelling station from 5-year datasets from the closest weather station from KNMI are used [68]. The closest station is found through a Nearest Neighbour Analysis among the 47 weather stations of KNMI. The hourly time series of the weather station are translated to the hub height of the wind turbine to be installed at the fuelling station. This is done in 2 steps.

At first, for each time step i wind speed u_i (m/s) is translated to u_{blend} (m/s) at the blending height of 60 meters with a log-wind law [69], which is sampled with weighted averages of the surrounding local surface roughness lengths of the weather station for

each as seen in the equation 6.1 below. The roughness length z_0 (m) is estimated for 10° segments for each weather station from the CORINE Land Cover classes [70]. *Figure 6 - 7* shows the translated Land Cover map to an equivalent roughness length map with the weather station and the sampling points around it. A set of 4 fuel stations can also be found above the scale bar. These stations use the datasets from the station shown.

$$u_{blend} = u_{ref} \times \frac{\ln\left(\frac{h_{blend} - d}{z_0}\right)}{\ln\left(\frac{h_1 - d}{z_0}\right)} \quad (6.1)$$

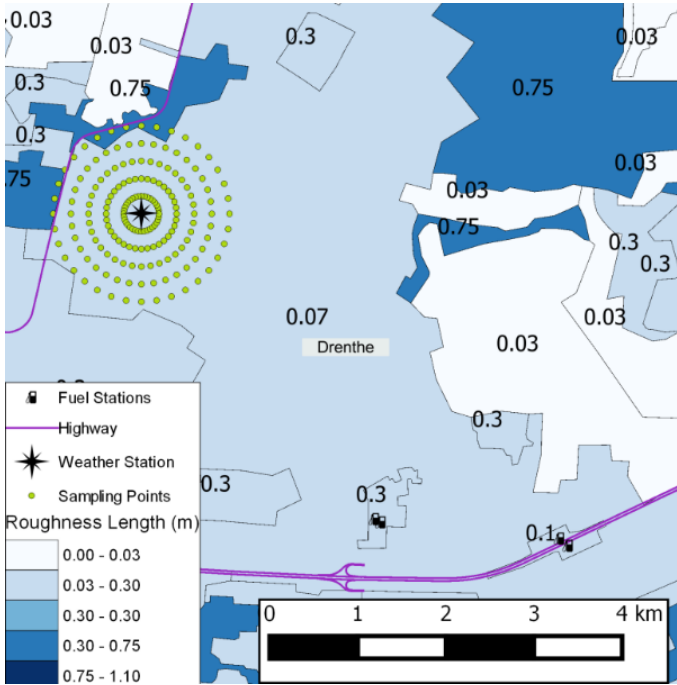


Figure 6 - 7: Roughness length map used for assessing the wind energy potential of the fuelling stations

In the second step, the wind speed time series are translated to u_{hub} (m/s) at the wind turbine's hub height h (m) with the wind power law equation in 6.2 with the Hellman power exponent $a=0.143$, which is applicable for open land surfaces, such as the common landscape in the Netherlands [69].

$$u_{hub} = u_{blend} \times \left(\frac{h}{h_{blend}} \right)^\alpha \quad (6.2)$$

Once these are found the Weibull fitting function is used to find the scale (λ), and shape (κ) parameter of the statistical curve. These parameters provide the frequency where a specific wind speed is occurring through a complete year with the equation 6.3.

$$f(u) = \frac{\kappa}{\lambda} \left(\frac{u}{\lambda} \right)^{\kappa-1} e^{-(u/\lambda)^\kappa} \quad (6.3)$$

Following, a non-dimensional power curve is used from a Vestas V136-3.45MW assumed to be installed at a hub height of 112m [71] in order to express the hydrogen produced per kW installed of wind energy with Power $P(u)$. This assumption is made for all Netherlands. In reality, for each location and wind characteristics an optimal wind turbine type and hub height would be needed for maximum energy production but is out of the scope of current work.

The Annual Electricity Production (AEP) is estimated with the Weibull probability for each wind speed and the non-dimensional wind power produced at each wind speed for a full year of 8760 hours in equation 6.4.

$$AEP \left(\frac{kWh}{kW_{installed}} \right) = 8760 \sum_{u=0}^{u=30} f(u)P(u) \quad (6.4)$$

For the hydrogen production a hydrogen conversion efficiency of 53.4 kWh per kg of hydrogen produced is assumed from the Near Future scenario 2030 in [72]. In reality, hydrogen production efficiency is dynamic and depends on many factors but this number gives a rough approximation of the capability of the station. The following equation is used for estimating the Annual Hydrogen Production (AHP) expressed in kg of hydrogen produced per kW of wind turbine installed in equation 6.5.

$$AHP \left(\frac{kgH_2}{kW_{installed}} \right) = AEP \left(\frac{kWh_e}{kW_{installed}} \right) \times \eta \left(\frac{kgH_2}{kWh_e} \right) \quad (6.5)$$

Further the total annual hydrogen production potential is classified per Province, by simply adding all potential production of each station in each Province. However, it

is interesting to observe it in relation with the passenger car fuel demand that it could potentially cover for the future. This is estimated based on the average figure of 13.200 kilometres per year for all cars in the Netherlands [73] and a fuel economy of 1 kgH₂ / 100km driven, as it has been published in several car brands that have brought fuel cell cars into market and is reported in [74] [21]. Finally for the number of vehicles it is assumed that in the Near Future there will be 30% FCEV for the drivetrain of Dutch car, which is an optimistic scenario. The number of cars per Province is assumed not change and car registrations and population statistics from CBS (Centrale Bureau voor de Statistiek) datasets from 2018 are used [75] in order to classify the results per Province.

Even though this approach is over-simplified, assuming an equal amount of hydrogen cars serviced by each station, it still can provide an indication of the possibilities of wind energy to cover a part of the hydrogen demand for mobility. The numbers used in this study are subject to change with future developments in the field. The method described provides national level key figures and numbers per Province which are useful for planners. Finally, it is strongly suggested for each individual station that a specific system design and sizing is performed taking into account refuelling behaviours and future predictions such as the study in [76].

6.3.2 Results

In Figure 6 - 8, the graduated green points are shown of the Annual Hydrogen Production (AHP) potential per station expressed in kilograms of hydrogen normalized per kW of wind turbine installed. The normalized representation is done so that someone could simply multiply the peak power of a turbine to get a rough estimation of the hydrogen produced for different turbine peak power. Regarding the results, as a logical consequence of the wind resource available near coastal areas of the Netherlands (West and North) the fuelling station with dark green have greater potential compared to the locations in the South-East of the country. For the locations in the South the lower production potential could be optimized by having wind turbines with higher hub heights which provide more energy. Nearly 100 stations can produce between 26-66 kgH₂ per kW of wind turbine installed capacity while the maximum of all 132 stations is 104kgH₂/kW.

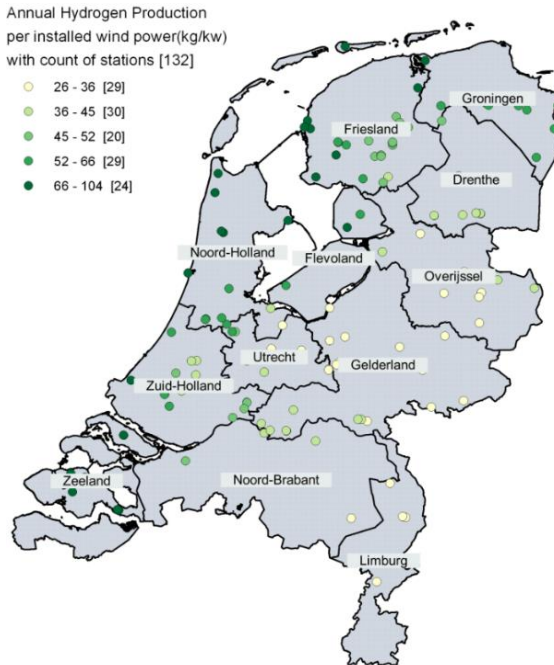


Figure 6 - 8: Map with the hydrogen production potential per suitable station in kilograms of hydrogen per kW of installed wind turbine capacity with a count of stations for different ranges of results. The greener the station the more production potential

In Figure 6 - 8, results are non-dimensional and as explained in the Methodology the example of the a 3.45MW wind turbine is used to calculate the potential for all Provinces. This amounts to an annual production range of 90-360 tonnes of hydrogen a year per station depending on the wind resource of each location. In Table 4 below results are presented in a Province level. The suitable fuelling stations could generate the annual hydrogen demand of 2.3% of the cars in a 30% FCEV national drivetrain scenario in a configuration with a V112-3.45MW turbine at each suitable station. This is subject to change depending on the future wind turbine peak power and the possibility to increase the amount of turbines installed next to the fuelling station.

Per Province level, the maximum coverage of the annual demand is observed in the Northern Provinces of Friesland (12%), Groningen (6%), Drenthe (5%) and the coastal Province of Zeeland (6%). For the most populated provinces the range of demand coverage is between 2-4% while for the most Southern Provinces is very low from 0.3-1%. The Northern areas are less densely populated and that is why there is greater demand coverage.

Table 6 - 4: Hydrogen production potential and coverage of all suitable stations for a 30% FCEV drivetrain scenario in the Netherlands

Province	Feasible Stations (%from total)	Total AHP Potential (tonnes)	FCEV Car Registrations in a 30% drivetrain scenario	Coverage of 30% FCEV drivetrain scenario	Cars Served in 30% FCEV plan
Friesland	25 (12%)	5034	303000	12%	37846
North-Holland	15 (4.6%)	3443	1100000	2%	25888
Gelderland	19 (4.4%)	2343	955000	2%	17613
Groningen	9 (6.9%)	1915	250000	6%	14397
Overijssel	9 (3.3%)	1142	530000	2%	8586
Drenthe	10 (6.2%)	1508	250000	5%	11336
South-Holland	19 (4%)	3771	1475000	2%	28352
Utrecht	9 (5%)	1208	585000	2%	9079
Flevoland	3 (5.3%)	635	175000	3%	4773
North-Brabant	4 (0.8%)	566	1235000	0.3%	4254
Zeeland	6 (7.1%)	1446	195000	6%	10869
Limburg	4 (1.7%)	397	555000	1%	2983
TOTALS	132 (4.35%)	~23400 tons	~2280000 cars	2.3%	~176000 cars

6.4 Case study to assess the possibility for Natural Gas Grid Interconnection

In the future, hydrogen gas grids will be a reality and on-site wind powered hydrogen fuelling stations could be an energy hub to deliver “green” hydrogen or receive from the gas grid. This could happen both in the transition phase where hydrogen could be admixed to the grid up to 20% concentrations [77] and in the future with a 100% hydrogen gas grid. Of course up until this future case, many other infrastructural changes would be required with respect to the machinery supporting the hydrogen economy, but this assessment investigates the possibilities with the existing infrastructures thus making the transition faster and more economical.

Fuelling stations are usually close to the distribution gas grid, which is divided into 2 levels in the Netherlands. These are the High Pressure grid (4-8 bars) where small industrial activities are made and the Low Pressure grid (0.03-0.10 bars) which is for residential consumers. Typically, the distribution high pressure grids are connected on one side with the regional gas transmission grid with a gas receiving station, and on the other side with the district stations of low pressure distribution grids going to the residential consumers [78].

For current assessment, the 4-8 bar grids are considered since the amounts of hydrogen produced could be sold directly to residential consumers and small industries beside the hydrogen vehicle demand present on-site. The Nearest Neighbour Analysis is used to define the proximity of the centroid that represents the fuelling station towards the closest present pipeline. In this way the needed pipeline extension is estimated to connect to current gas grids.

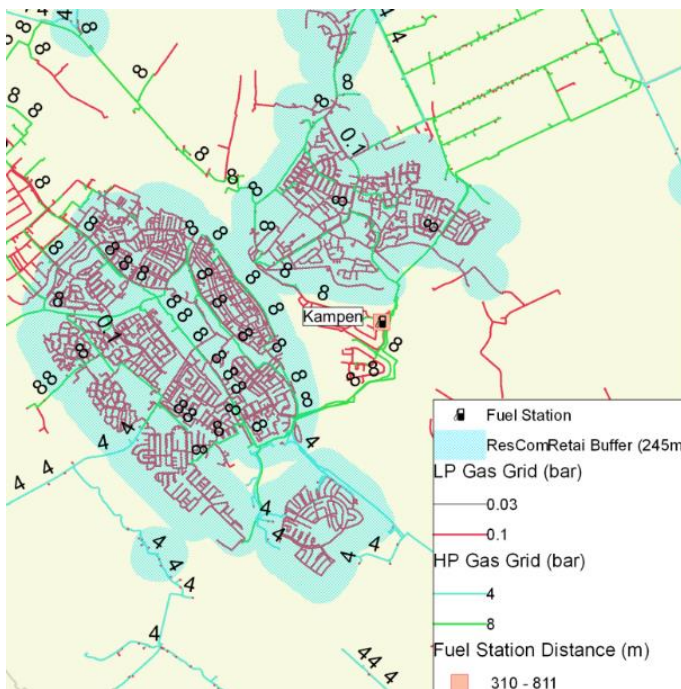


Figure 6 - 9: Suitable fuelling station for on-site wind powered hydrogen production next to a network of gas pipelines

The results should not be interpreted as representative for the whole country, as due to limited open data resources from gas distribution system operators (DSOs) in the Netherlands, only the ENEXIS distribution system operator's (DSO) domain for gas is assessed.

In Figure 6 - 9 above, the proximity of the point that represents the fuelling station to the nearest pipeline of 4-8 bars. This method could be used by any gas DSO to estimate how much extra pipeline they would need to manufacture and layout in order to connect to fuelling stations with on-site hydrogen production by wind turbines. For the particular operator, a total of 21.8 kilometres of extra pipeline would be needed for the 23 stations within this operating domain (17.5% of the total of 132 stations). This applies for 5 Provinces (Groningen, Drenthe, Overijssel, Limburg and Noord Brabant) in which 35% of Dutch population lives. For a more detailed view on the distance per station, see below in Figure 6 - 10.

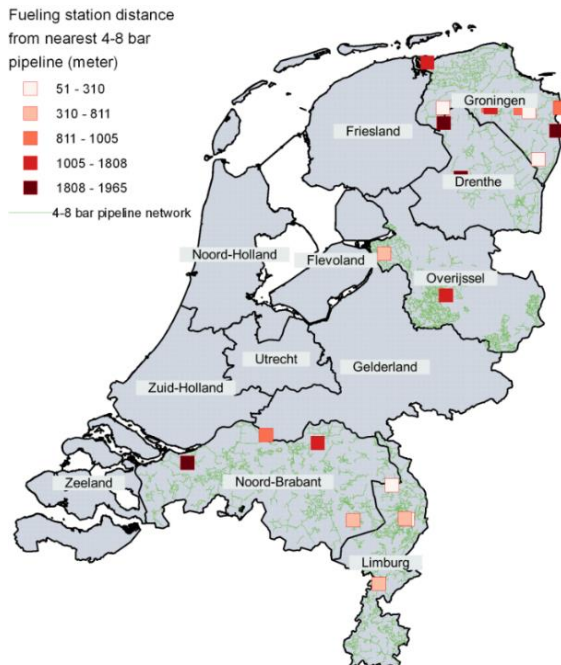


Figure 6 - 10: Distance of some fuelling stations from high pressure gas distribution grids (4-8 bars) grid

6.5 Discussion

This study shows the technical potential of existing fuelling stations to be converted to wind powered hydrogen producing refuelling station. The utilization of open source datasets was key in order to achieve such a study and it is highly encouraged although uncertainty could be an issue especially for the datasets arriving from Open Street Maps, which are based on individuals to fill in the data. It is an attempt to utilize and synthesize all these data in order to help engineers, scientists and policy makers to define new steps towards the hydrogen economy seen from this angle of

smaller scale projects. This study could be used as a basis for some Dutch system operators in order to assess their future planning activities of interconnecting these hubs with hydrogen pipeline infrastructure. For the ones not assessed, this chapter could be used as a guideline and method to estimate how much grid upgrades would be needed for these stations. Additionally, this study is valuable for future fuelling station retailers and designers who might want to invest in wind powered hydrogen production and could use this methodology as a guideline to assess the feasibility of their station. The results of hydrogen production potential per kW of wind turbine installed capacity presented *Figure 6 - 8* could be used as a preliminary rough estimation and first indication of hydrogen production per station per different province and for an assumed wind turbine peak power capacity, as results are normalized. Finally, this study provides useful input in a national level about onshore wind powered hydrogen production next to existing fuelling stations and also quantifies the hydrogen production potential in relation to the future demand of fuel cell electric vehicles. The results are quite promising, given the fact that these stations are only a few stations of all stations of the Netherlands placed mostly outside urban areas.

Finally, some roll-out scenarios are identified based on the infrastructural upgrades and the FCEV uptake for these stations. The infrastructural upgrades refer to whether the natural gas grids will need first to blend hydrogen with natural gas or will directly move to a 100% hydrogen utilization. In the first case, the wind powered refuelling station will be able to inject hydrogen gas in the distribution grid but will need some separation technologies in the case of getting hydrogen from the grid and an intermediate storage for the hydrogen. In the 100% hydrogen scenario, the installation is straightforward with possibilities of injecting when there's production surplus and receiving hydrogen gas when there's hydrogen production deficit by wind turbine and the station's intermediate storage is not sufficient.

6.6 Conclusions

This Chapter aimed to answer the research question "Is there nationwide technical potential of wind turbines integrated with fuelling stations in the Netherlands for hydrogen production?". A methodology was therefore presented to evaluate the technical potential of on-site wind powered hydrogen producing refuelling stations. The stations were filtered based on risk zoning guidelines that limit the installation of wind turbines. The main conclusions are:

- The combination of all buffers reduces the amount of suitable fuelling stations to 4.6% of all (132 out of 3021). These can have a wind turbine installation next to them for hydrogen production.
- Built-Up area buffers reduce the amount of the suitable stations to (15% of total), Environmental Zoning to 59% and Infrastructure zoning to 70%

- Then a wind resource model and energy estimation were made to identify the technical potential of wind-powered hydrogen production on each suitable station. The results were also classified per Province and related to an assumed 30% FCEV drivetrain in the future.
- The results were normalized for a 3.45MW wind turbine power curve and resulted in a range of hydrogen production potential 26-104 kgH₂/kW_{wind_installed} per year. This range is explained by the different wind resources available at different sites throughout the country of the Netherlands
- A 3.45MW turbine next to a suitable fuelling station has the potential to deliver 90-360 tonnes of hydrogen a year
- The aggregated results for the Netherlands indicate that these stations can produce 2.3% of the total annual hydrogen demand for FCEV in a 30% FCEV drivetrain scenario.
- The range of demand coverage for different Provinces in the Netherlands for those stations is 0.3%-12% of the future hydrogen demand for FCEV in a 30% FCEV drivetrain scenario
- Northern provinces of the Netherlands have the highest demand coverage from such stations due to their low population density and less zoning restriction for the fuelling stations.
- This study provided as well the length of gas grid expansion needed for the stations to be connected for one grid operator in the Netherlands. A total of 21.8 kilometres of pipeline was found needed to connect to those stations in order to export hydrogen in the grid.

6.7 References

1. Rodríguez Escude M, Chrysochoidis-Antos N, and van Wijk A. *Power-to-Gas for the Dutch transportation sector: Wind-powered hydrogen fueling stations with on-site hydrogen generation*. 2019, <http://resolver.tudelft.nl/uuid:2a5c0646-dd91-49f6-b604-7cd3843359e5>, Delft University of Technology
2. Bruce S, et al. *National Hydrogen Roadmap - Pathways to an economically sustainable hydrogen industry in Australia*, 2018,
3. *Basic Hydrogen Strategy*, 2017, Ministerial Council on Renewable Energy, Hydrogen and Related issues
4. Forrest M, et al. *The California Fuel Cell Revolution - A vision for advancing economic, social and environmental priorities*, 2018, California Fuel Cell Partnership (CFCP)
5. FCH-JU *Hydrogen Roadmap Europe - A sustainable pathway for the European Energy Transition*, 2019, Fuel Cells and Hydrogen Joint Undertaking

6. Tanc B, Arat H T, Baltacioglu E, and Aydin K *Overview of the next quarter century vision of hydrogen fuel cell electric vehicles*. International Journal of Hydrogen Energy, 2019. **44**(20): p. 10120-10128, DOI: 10.1016/j.ijhydene.2018.10.112.
7. Wiebes E *Cabinet Vision for hydrogen*, 2020, Ministry of Economic Affairs and Climate
8. Ad van Wijk, Hans Coenen, Jaco Reijerkerk, Maurits Alberda, Luuk Buit, and Kasova D *The Green Hydrogen Economy in the Northern Netherlands*, 2017, Northern Innovation Board
9. *Infrastructure Outlook 2050 - A joint study by Gasunie and TenneT on integrated energy infrastructure in the Netherlands and Germany*, 2019, Gasunie and TenneT
10. Caglayan D G, et al. *Technical potential of salt caverns for hydrogen storage in Europe*. International Journal of Hydrogen Energy, 2020. **45**(11): p. 6793-6805, DOI: 10.1016/j.ijhydene.2019.12.161.
11. Tsuda K, et al. *Design proposal for hydrogen refueling infrastructure deployment in the Northeastern United States*. International Journal of Hydrogen Energy, 2014. **39**(14): p. 7449-7459, DOI: 10.1016/j.ijhydene.2014.03.002.
12. Siyal S H, Mentis D, and Howells M *Economic analysis of standalone wind-powered hydrogen refueling stations for road transport at selected sites in Sweden*. International Journal of Hydrogen Energy, 2015. **40**(32): p. 9855-9865, DOI: 10.1016/j.ijhydene.2015.05.021.
13. Deng Z H and Jiang Y W *Optimal sizing of wind-hydrogen system considering hydrogen demand and trading modes*. International Journal of Hydrogen Energy, 2020. **45**(20): p. 11527-11537, DOI: 10.1016/j.ijhydene.2020.02.089.
14. Pan X M, Li Z Y, Zhang C M, Lv H, Liu S J, and Ma J X *Safety study of a wind-solar hybrid renewable hydrogen refuelling station in China*. International Journal of Hydrogen Energy, 2016. **41**(30): p. 13315-13321, DOI: 10.1016/j.ijhydene.2016.05.180.
15. Tsunemi K, Kihara T, Kato E, Kawamoto A, and Saburi T *Quantitative risk assessment of the interior of a hydrogen refueling station considering safety barrier systems*. International Journal of Hydrogen Energy, 2019. **44**(41): p. 23522-23531, DOI: 10.1016/j.ijhydene.2019.07.027.
16. Lipman T, Witt M, and Elke M *Lessons learned from the installation and operation of Northern California's first 70-MPa hydrogen fueling station*. International Journal of Hydrogen Energy, 2013. **38**(36): p. 15868-15877, DOI: 10.1016/j.ijhydene.2013.08.120.
17. *Hydrogen filling station network expansion updates*, 2020, Available from: <https://h2.live/en>, (Accessed 2020-34-05)
18. *H-TEC Systems 10 MW PEM electrolyser for hydrogen economy*. Fuel Cells Bulletin, 2019. Volume: **2019**, Page(s):9 DOI: [https://doi.org/10.1016/S1464-2859\(19\)30422-5](https://doi.org/10.1016/S1464-2859(19)30422-5).

19. *German wind park deploys H-TEC PEM electrolyser for fueling*. Fuel Cells Bulletin, 2018. Volume:2018, Page(s):11 DOI: [https://doi.org/10.1016/S1464-2859\(18\)30422-X](https://doi.org/10.1016/S1464-2859(18)30422-X).
20. Saur G, Sprik S, Kurtz J, Onorato S, Gilleon S, and Winkler E. *Hydrogen Station Data Collection and Analysis*, Editor. 2019,
21. *Hydrogen Fuel Cell Vehicle Technology Roadmap*, 2018, Strategic Advisory Committee of the Technology Roadmap for Energy Saving and New Energy Vehicles
22. Honselaar M, Pasaoglu G, and Martens A *Hydrogen refuelling stations in the Netherlands: An intercomparison of quantitative risk assessments used for permitting*. International Journal of Hydrogen Energy, 2018. **43**(27): p. 12278-12294, DOI: <https://doi.org/10.1016/j.ijhydene.2018.04.111>.
23. *Netherlands: 20 Fuel Cell Buses and hydrogen refuelling stations for Provinces of Groningen and Drenthe by December 2020*, 2019, Available from: <https://www.fuelcellbuses.eu/public-transport-hydrogen/netherlands-20-fuel-cell-buses-and-hydrogen-refuelling-station-provinces>, (Accessed 2020-04-25)
24. *The Netherlands to expand its H2 infrastructure with OrangeGas' first hydrogen stations*, 2019, Available from: <http://www.hydrogenfuelnews.com/the-netherlands-to-expand-its-h2-infrastructure-with-oranagegas-first-hydrogen-stations/8539111/>, (Accessed 2020-04-25)
25. *Dutch government sets its sights on hydrogen - Financial incentives for 9 new public hydrogen stations*, 2018, Available from: <https://www.pitpointcleanfuels.com/news/dutch-government-sets-sights-on-hydrogen/>, (Accessed 2020-04-25)
26. *KWR institute opens green hydrogen filling station for own car fleet*, 2019, Available from: <https://www.dutchwatersector.com/news/kwr-institute-opens-green-hydrogen-filling-station-for-own-car-fleet>, (Accessed 2020-04-25)
27. *Wind-to-Hydrogen (W2H2) - TKI System Integration Study*, HYGRO, ECN, Energy Valley
28. *First wind turbine for direct 'green' hydrogen planned in Netherlands*. Fuel Cells Bulletin, 2017. Volume:2017, Page(s):10 DOI: [https://doi.org/10.1016/S1464-2859\(17\)30392-9](https://doi.org/10.1016/S1464-2859(17)30392-9).
29. Mukherjee U, Walker S, Maroufmashat A, Fowler M, and Elkamel A *Development of a pricing mechanism for valuing ancillary, transportation and environmental services offered by a power to gas energy system*. Energy, 2017. **128**: p. 447-462, DOI: 10.1016/j.energy.2017.04.042.
30. Ogden J, Jaffe A M, Scheitrum D, McDonald Z, and Miller M *Natural gas as a bridge to hydrogen transportation fuel: Insights from the literature*. Energy Policy, 2018. **115**: p. 317-329, DOI: 10.1016/j.enpol.2017.12.049.

31. Zhao L and Brouwer J *Dynamic operation and feasibility study of a self-sustainable hydrogen fueling station using renewable energy sources*. International Journal of Hydrogen Energy, 2015. **40**(10): p. 3822-3837, DOI: 10.1016/j.ijhydene.2015.01.044.
32. Nistor S, Dave S, Fan Z, and Sooriyabandara M *Technical and economic analysis of hydrogen refuelling*. Applied Energy, 2016. **167**: p. 211-220, DOI: 10.1016/j.apenergy.2015.10.094.
33. Bauer A, Mayer T, Semmel M, Morales M A G, and Wind B J *Energetic evaluation of hydrogen refueling stations with liquid or gaseous stored hydrogen*. International Journal of Hydrogen Energy, 2019. **44**(13): p. 6795-6812, DOI: <https://doi.org/10.1016/j.ijhydene.2019.01.087>.
34. Brown T, Stephens-Romero S, and Samuelsen G S *Quantitative analysis of a successful public hydrogen station*. International Journal of Hydrogen Energy, 2012. **37**(17): p. 12731-12740, DOI: <http://dx.doi.org/10.1016/j.ijhydene.2012.06.008>.
35. Resch B, et al. *GIS-Based Planning and Modeling for Renewable Energy: Challenges and Future Research Avenues*. Ispr International Journal of Geo-Information, 2014. **3**(2): p. 662-692, DOI: 10.3390/ijgi3020662.
36. Agnolucci P and McDowall W *Designing future hydrogen infrastructure: Insights from analysis at different spatial scales*. International Journal of Hydrogen Energy, 2013. **38**(13): p. 5181-5191, DOI: 10.1016/j.ijhydene.2013.02.042.
37. Siyal S H, Mentis D, Mortberg U, Samo S R, and Howells M A *A preliminary assessment of wind generated hydrogen production potential to reduce the gasoline fuel used in road transport sector of Sweden*. International Journal of Hydrogen Energy, 2015. **40**(20): p. 6501-6511, DOI: <https://doi.org/10.1016/j.ijhydene.2015.03.108>.
38. Baufume S, et al. *GIS-based scenario calculations for a nationwide German hydrogen pipeline infrastructure*. International Journal of Hydrogen Energy, 2013. **38**(10): p. 3813-3829, DOI: 10.1016/j.ijhydene.2012.12.147.
39. Brey J J, Carazo A F, and Brey R *Analysis of a hydrogen station roll-out strategy to introduce hydrogen vehicles in Andalusia*. International Journal of Hydrogen Energy, 2014. **39**(8): p. 4123-4130, DOI: 10.1016/j.ijhydene.2013.06.087.
40. Sigal A, Cioccale M, Rodriguez C R, and Leiva E P M *Study of the natural resource and economic feasibility of the production and delivery of wind hydrogen in the province of Cordoba, Argentina*. International Journal of Hydrogen Energy, 2015. **40**(13): p. 4413-4425, DOI: 10.1016/j.ijhydene.2015.01.149.
41. Nielsen S and Skov I R *Investment screening model for spatial deployment of power-to-gas plants on a national scale - A Danish case*. International Journal of Hydrogen Energy, 2019. **44**(19): p. 9544-9557, DOI: 10.1016/j.ijhydene.2018.09.129.
42. Rahmouni S, Settou N, Negrou B, and Gouareh A *GIS-based method for future prospect of hydrogen demand in the Algerian road transport sector*.

- International Journal of Hydrogen Energy, 2016. **41**(4): p. 2128-2143, DOI: 10.1016/j.ijhydene.2015.11.156.
43. Cerniauskas S, Grube T, Praktijnjo A, Stolten D, and Robinius M *Future Hydrogen Markets for Transportation and Industry: The Impact of CO2 Taxes*. Energies, 2019. **12**(24)DOI: 10.3390/en12244707.
 44. Lane B, Shaffer B, and Samuelsen S *A comparison of alternative vehicle fueling infrastructure scenarios*. Applied Energy, 2020. **259**DOI: <https://doi.org/10.1016/j.apenergy.2019.114128>.
 45. Samsatli S and Samsatli N J *The role of renewable hydrogen and inter-seasonal storage in decarbonising heat - Comprehensive optimisation of future renewable energy value chains*. Applied Energy, 2019. **233**: p. 854-893, DOI: 10.1016/j.apenergy.2018.09.159.
 46. Strachan N, Balta-Ozkan N, Joffe D, McGeevor K, and Hughes N *Soft-linking energy systems and GIS models to investigate spatial hydrogen infrastructure development in a low-carbon UK energy system*. International Journal of Hydrogen Energy, 2009. **34**(2): p. 642-657, DOI: 10.1016/j.ijhydene.2008.10.083.
 47. Stiller C, Bungler U, Moller-Holst S, Svensson A M, Espegren K A, and Nowak M *Pathways to a hydrogen fuel infrastructure in Norway*. International Journal of Hydrogen Energy, 2010. **35**(7): p. 2597-2601, DOI:
 48. Faasen C J, Franck P A L, and Taris A M H W *Handboek Risicozonering Windturbines*, 2014, Rijksdienst voor Ondernemend Nederland
 49. *Geografische open-data GIS bestanden*, Available from: <https://www.imergis.nl/htm/opendata.htm>, (Accessed 01/04/2019)
 50. *EuroGeographics - Open Topographic Data*, Available from: <https://eurogeographics.org/products-and-services/open-data/topographic-data/>, (Accessed 08/08/2018)
 51. *OpenStreetMap data for the Netherlands*, Available from: <http://download.geofabrik.de/europe/netherlands.html>, (Accessed 01/03/2019)
 52. *Copernicus - Corine Land Cover 2018 (CLC)*, 2018, Available from: <https://land.copernicus.eu/pan-european/corine-land-cover/clc2018>, (Accessed 01/02/2019)
 53. *StilteGebieden - Protected Sites of Silent Zones*, Available from: <http://nationaalgeoregister.nl/geonetwork/srv/dut/catalog.search#/metadata/cc408b2d-09a6-4b2b-9aa3-b46bfe2f00a5>, (Accessed 01/04/2019)
 54. *Stiltegebieden - Silent Zoning in the Netherlands*, Available from: <https://www.atlasleefomgeving.nl/meer-weten/geluid/stiltegebieden>, (Accessed 2020-06-02)

55. Winkelman J E, Kistenkas F H, and Epe M J *Ecologische en natuurbeschermingsrechtelijke aspecten van windturbines op land*, 2008, Alterra, Wageningen
56. *NATURA 2000 Areas*, Available from: <http://nationalegeoregister.nl/geonetwork/srv/dut/catalog.search#/metadata/8829e5dd-c861-4639-a6c8-fdbb6e3440d2?tab=inspire>, (Accessed 15/03/2019)
57. *Recommendations for distances of wind turbines to important areas for birds as well as breeding sites of selected bird species (as at April 2015)*, 2015, Working Group of German State Bird Conservancies (LAG VSW)
58. *Geese Resting Areas*, Available from: http://nationalegeoregister.nl/geonetwork/srv/dut/catalog.search#/search?isChild='false'&resultType=details&fast=index&content_type=json&from=1&to=20&sortBy=relevance&any_OR_title=ganzen, (Accessed 14/03/2019)
59. *Basisregistraties - Kadaster*, Available from: <https://zakelijk.kadaster.nl/brt>, (Accessed 01/04/2019)
60. *Wind turbines in the Netherlands*, 2018, Available from: <http://nationalegeoregister.nl/geonetwork/srv/dut/catalog.search#/home>, (Accessed
61. *Scheme of Environmental Management Activities - Activiteitenregeling milieubeheer.2017.S.P.a.t.E.* Minister of Housing
62. Madsen H A *Low Frequency Noise from Wind Turbines Mechanisms of Generation and its Modelling*. *Journal of Low Frequency Noise Vibration and Active Control*, 2010. **29**(4): p. 239-251, DOI: <https://doi.org/10.1260/0263-0923.29.4.239>.
63. Barlas E, Zhu W J, Shen W Z, Dag K O, and Moriarty P *Consistent modelling of wind turbine noise propagation from source to receiver*. *Journal of the Acoustical Society of America*, 2017. **142**(5): p. 3297-3310, DOI: 10.1121/1.5012747.
64. *Open Datasets for Gas Pipelines in the Netherlands from Risicokaart.nl*, Available from: <https://flamingo.bij12.nl/risicokaart-viewer/app/Risicokaart-openbaar>, (Accessed 2020-04-24)
65. *ICAO Annex 14 - Aerodromes - Volume 1 : Aerodrome Design and Operations*, 2018, International Civil Aviation Organization
66. *CAA Policy and Guidelines on Wind Turbines*, 2016, Civil Aviation Authority
67. Manwell J F, McGowan J G, and Rogers A L. *Wind Energy Explained - Theory, Design and Application*. Second ed. 2009: John Wiley & Sons Ltd.
68. *Uurgegevens van het weer in Nederland - Hourly Data of weather in the Netherlands*, 2018-2019, Available from: <https://www.knmi.nl/nederland-nu/klimatologie/uurgegevens>, (Accessed 03/04/2019)

Chapter 6

69. Wieringa J *Roughness-dependent geographical interpolation of surface wind speed averages*. Quarterly Journal of the Royal Meteorological Society, 1986. **112**(473): p. 867-889, DOI: 10.1002/qj.49711247316.
70. Silva J, Ribeiro C, and Guedes R. *Roughness length classification of Corine Land Cover Classes*. in *Proceedings of EWEC*. 2007.
71. *Power Curve of Vestas V136-3.45MW*, Available from: <https://en.wind-turbine-models.com/turbines/1282-vestas-v136-3.45>, (Accessed 03/04/2019)
72. Vincent Oldenbroek , Leendert A. Verhoef, and Wijk A J M v *Fuel cell electric vehicle as a power plant: Fully renewable integrated transport and energy system design and analysis for smart city areas*. Journal of Hydrogen Energy, 2016DOI: <https://doi.org/10.1016/j.ijhydene.2017.01.155>
73. *CBS Trends in the Netherlands*, 2018, Central Bureau of Statistics
74. Jennifer Kurtz S S, Chris Ainscough, Genevieve Saur, Shaun Onorato *Fuel Cell Electric Vehicle Performance Composite Data Products: Spring 2018*, 2018, NREL
75. *Motorvoertuigenpark; inwoners, type, regio, 1 januari*, 2018, Available from: <https://statline.cbs.nl/StatWeb/publication/?DM=SLNL&PA=7374HVV>, (Accessed 06 June 2018)
76. Gruger F, Dylewski L, Robinius M, and Stoltren D *Carsharing with fuel cell vehicles: Sizing hydrogen refueling stations based on refueling behavior*. Applied Energy, 2018. **228**: p. 1540-1549, DOI: 10.1016/j.apenergy.2018.07.014.
77. Taminiau F *Hydrogen admixture in the Dutch gas grid*, 2017, TNO
78. Rob van Gerwen R B, Lucas Grond, Sebastiaan Hers, Benno Scherpers, Harry Croezen *System Integration - Hybrid Energy Infrastructure*, 2015, DNV GL/ CE Delft/ Dutch Ministry of Economic Affairs/ Netherlands Enterprise Agency (RVO)

7

Conclusions – Recommendations

“What doesn't kill you only makes your book longer.”

— Anthony Kiedis

The chapter distills all results into relevant conclusions and provide recommendations for further research.

This chapter discusses the main findings and conclusions of this thesis entitled “Integrating wind turbines with highway infrastructures”. The first part of this chapter answers the main research question and the sub-questions followed by the conclusions and a brief discussion. The second part of this chapter provides recommendations for further research

7.1 Answers to the Research Questions

The main research question that encompasses all this book is “*What is the technical and economic potential of integrating wind turbines with highway infrastructures?*”.

The answer to this question is given for 2 concepts. The first concept is structurally integrated micro wind turbines with noise barrier infrastructures along highways, while the second one is large scale wind turbine collocated with highway fuelling stations dedicated to hydrogen production and refuelling. For the first concept, it was found that micro wind turbines (kW scale) can be integrated on top of the 55% of the total noise barrier length of the highway infrastructures in the Netherlands. And for the second concept, MW-scale wind turbines can be collocated with 4.6% of the existing fuelling stations in the Netherlands. Micro wind turbines on top of noise barriers can benefit from the increased wind speeds (mostly when flows are perpendicular to noise barriers). Since wind speeds can also decrease in parallel flows, the total annual energy yield strongly depends on the orientation of the noise barrier and the local wind rose. The effect of the noise barrier on the annual energy yield ranges between 60 – 130% compared to a reference case without a noise barrier. Next to this, micro wind turbines exhibit poor performance (42% of an ideal performance) due to the turbine’s controller, the inefficient yaw alignment and other factors. When these micro wind turbines are implemented at a nationwide scale there is potential, but is relatively small when compared with the existing installed onshore wind capacities. The potential for the Netherlands is only 25 MW, while the existing installed onshore wind capacity is about 7000 MW. Regarding the economic potential, the levelised cost of electricity from micro wind turbines on top of noise barriers varies greatly, (0.25 – 2.5 €/kWh, depending on the site conditions, turbine performance and combination of noise barrier orientation and local wind rose. The levelised cost of electricity is lower when the system is combined with photovoltaic systems on the noise barrier (0.15 – 0.24 €/kWh).

MW wind turbines can be integrated at fuelling stations, to produce hydrogen for hydrogen refuelling of Fuel Cell Electric Vehicles (FCEV) integration. For a fuel cell electric vehicle market penetration scenario of 30%, the integrated MW wind turbines are capable of covering 2.3% of the hydrogen demand for FCEV in the Netherlands.

In each of the chapters a sub research question has been answered. The conclusions with regard to these sub questions are given below.

1. What is the wind resource that micro wind turbines will experience when integrated on top of noise barrier highway infrastructures?

To answer this question, an experimental measuring campaign using several sonic anemometers installed next to and on top of a noise barrier was carried out. The measurements were analysed statistically to understand the wind resource properties and the influence of the noise barrier on the wind flow. Finally, the results from the influence of the noise barrier were used in a sensitivity analysis of a theoretical wind turbine performance on top of that noise barrier.

The result is that the available wind resource on top of noise barriers for wind electricity generation varies greatly due to a number of factors that influence wind flows on top of the noise barrier. Wind speed is affected by the noise barrier. Wind speed was found to be increased when flows were perpendicular, while decreased when flows are parallel to the barrier, ranging between 50% (parallel) – 130% (perpendicular) of a reference measurement far from the noise barrier. Furthermore, it was found that wind flow is skewed by 5° to 25° on top of noise barrier thus influencing the energy yield especially for horizontal axis turbines as they would only harness the horizontal components of wind speed and not the skewed components. The total annual energy yield of micro wind turbines on top of the noise barrier depends on the height of installation from the top of the noise barrier and the orientation of the noise barrier with respect to the location's wind rose.

A 0.375kW micro wind turbine installed 1 up to 5 meters higher than a typical height of a noise barrier (~ meters) in the Netherlands for the location of the experiment could produce between 290 – 500 kWh. But when the influence of the noise barrier is included in the estimation this could range between 354 – 580 kWh. For this particular orientation of the noise barrier the result is positive. However, a sensitivity analysis was performed assuming that the noise barrier is rotated with respect to the wind time series in increments of 20°, this sensitivity shown that these results can greatly deviate between 150 – 600 kWh, therefore both positive and negative influence.

In some cases even this slight orientation change of 20° could lead to a great deviation in energy yield. This wide range is explained by the wind speed changes due to the noise barrier obstacle on the wind flow. Therefore, it is concluded that noise barriers can induce, depending on the orientation, increases in energy yield, Careful assessment of the annual energy yield predictions on top of noise barriers is necessary as these can be highly influenced by the noise barrier and its orientation.

2. What is the performance of a micro wind turbine integrated on top of a noise barrier?

To answer this question, an experiment was conducted in the wind tunnel to understand and measure parameters for the ideal performance of a micro wind turbine when exposed to skewed flows. This turbine was then integrated on a noise barrier near a highway and the same performance parameters were measured. It is concluded

that for the tested micro wind turbine in the field at the noise barrier, the energy yield was only 42% of the energy yield measured in a wind tunnel. The reasons for the energy losses in the field compared to the wind tunnel were analysed. It was found that the inverter and its standby losses can take up to 8% of the total loss. Additionally, the controller was poorly performing in the field far from the optimal point of operation which causes 32% of the total loss. Finally the turbine's passive yaw system failed to follow and track effectively the direction of the wind flow thus resulting in 18% of the total loss. Therefore, it was concluded that this micro wind turbine could not capture the highly turbulent wind speed and fast changing wind directions. It is concluded that it is necessary to improve the micro wind turbine's performance.

3. Is there nationwide technical potential of micro wind turbine noise barriers in the Netherlands?

To answer this question a GIS assessment was conducted by filtering the suitable noise barriers from GIS datasets. It was found that a considerable length of noise barriers is suitable (55% of total length) for micro wind turbine installation. The annual energy yield was estimated by correcting wind time series from weather stations in less than 20km proximity to the noise barrier together with adjustments for wind flow above noise barriers and micro wind turbine performance. A technical potential of 25MW of micro wind turbines (a total of 65,000 turbines of 0.375kW rated capacity) could be installed along 560km of noise barriers capable of producing 20GWh of electricity. The noise barriers were found to positively increase the total cumulative annual energy yield by 6.5% when comparing micro wind energy yield at the same locations but excluding the noise barrier influence. GIS analysis of those noise barriers showed that most of them are closely placed to grid infrastructures (between 30 - 200m distance). Therefore, the electricity produced from those noise barriers could be utilised in a number of nearby applications ranging from urban scooter mobility, highway lighting and others.

4. What is the levelised cost of electricity of noise barrier integrated wind turbines?

To answer this question, a techno-economic modelling and analysis was performed for an average noise barrier length of 150m capable of structurally integrating 9 kW of micro wind turbine systems. The cost breakdown of the integrated micro wind turbine system was analysed which identified 40% potential cost reductions due to savings in tower, foundation, installation and electrical infrastructure costs. The levelised cost of electricity from micro wind turbines was estimated for 3 locations with different average wind speed resulting in a wide range of LCOE values between 0.25 – 2.5 €/kWh. The noise barrier location, orientation and the performance of the micro wind turbine influences the LCOE values drastically. The levelised cost of electricity could be reduced when integrating also photovoltaic systems on the same 150m of noise barrier of

90kWp. This results in a LCOE between 0.15 – 0.24 €/kWh for with an annual energy yield between 60 – 130 MWh/year. This range is for different noise barrier orientations and locations in the Netherlands. Finally, a sensitivity analysis was conducted by varying the CAPEX, OPEX and WACC of the micro wind turbine system by 50%. This analysis resulted in a range of LCOE between 0.13 – 3.41 €/kWh with CAPEX having the greatest influence of all parameters. Finally, it was concluded that for all possible system configuration (wind, solar, hybrid) the LCOE remains above the global average of the LCOE for utility scale solar and onshore wind electricity. Therefore, the conclusion is that integrating solar and wind systems with noise barrier infrastructures using present day technology, does not yield economically feasible projects. However, it delivers the electricity nearby consumer's, which could have additional value.

5. Is there nationwide technical potential of wind turbines integrated with fuelling stations in the Netherlands for hydrogen production?

To answer this question, GIS datasets were analysed to find the suitable fuelling stations in the Netherlands on which a wind turbine can be collocated. Several criteria were used to define the suitability. The infrastructure zoning criteria limit a 70% of the total potential installations. The environmental zoning criteria limit a 59% of the total potential locations and the built-up areas criteria limit a 15.3% of the total potential locations. When combining those criteria only 4.6% of all Dutch fuelling stations are suitable for wind turbine installation. Installing a 3.5 MW wind turbine at the fuelling stations, results in an annual production potential between 90 – 360 tonnes hydrogen per year. In total, all wind turbines at these stations could produce 23400.... tonnes hydrogen per year. This results in 2.3% of the total annual hydrogen demand for a 30% fuel cell vehicle market penetration scenario in the Netherlands. This scenario was constructed according to certain assumption regarding the fuel use efficiency and km per year mileage. An analysis per Province was conducted to conclude that Northern Provinces have a higher demand coverage due to their low population density and less zoning restrictions. Furthermore, fuelling stations have as well potential to export and import hydrogen in the future by interconnecting to the gas grids. Therefore, it can be concluded that highway infrastructures like fuelling stations have a potential to produce hydrogen by co-located wind turbines at 4.6% of the total fuelling stations in the Netherlands and can cover a part of a future hydrogen demand for mobility.

7.2 Recommendations for Future Research

Research gaps were identified during the course of this PhD project which are analysed in this section with recommendations for future research. The gaps and recommendations are structured in the following manner:

1. Wind Resource Assessment on top of Noise Barriers

This dissertation provided insights on the influence of noise barrier structures on the incoming wind flow properties (wind speed, turbulence, wind direction etc.). A first recommendation is to further analyse the already published datasets from the measurements. More than a year's dataset of 8 measurement points in different locations on top of the noise barrier are available. The data could be used or analysed by designers and modellers of wind turbines or researchers in the field of wind engineering in general.

Additionally, this study focussed on a particular noise barrier design with a specific height of ~5m and a slope of ~80°. There are however a lot more noise barriers with different slopes, shapes or are placed in different locations, for example locations with high buildings, low building etc. Also, the surrounding landscape could differ per location as other highway features could be present thus affecting the localised roughness length factors. For that reason, additional measurements are recommended to more noise barriers with other shapes, angles, surroundings, highway speed limits. The additional datasets could help to correlate or validate the current findings from this research. Finally, energy yield prediction and estimation on top of noise barriers by applying correction factors related to the influence of a noise barrier on the wind flow provided a wide range of results depending on the noise barrier orientation and the localised wind rose. But making wind resource assessments is a rather expensive and demanding procedure. Therefore, it is recommended that further data collection and correction factors are depicted from other types of barriers, which could potentially lead to the development of standardized tables with correction factors for wind turbine applications.

2. Micro wind turbine technologies on top of noise barriers

This study highlighted the challenges of a particular type of micro wind turbine (downwind configuration) would face in a very turbulent environment on top of a noise barrier. The outcomes of this research present that this micro wind turbine cannot handle efficiently the localised wind resource on top of a noise barrier. It was found that different sub-systems need to work more effectively to make an efficient conversion of the wind energy to electrical energy. Therefore, it is recommended to investigate ways to improve the inefficiencies and losses of this particular system. For example, more research on the turbine controller, the power electronic units as well with the yaw mechanisms. Specifically, research could focus on more agile control systems which could follow and track more effectively the tip speed ratio and power performance curve (C_p - TSR). This research could be dedicated to more fundamental micro wind turbine design research.

Another recommendation is on considering more wind turbine technologies to be tested and compared. Even though there was motivation for this study to place different typed of micro wind turbines on top of the noise barrier, the installation complexities

presented limitations by restricting the work only to a downwind horizontal axis micro wind turbine for the experiment, while other technologies were not considered. Follow-up work could consider the assessment of the performance of other micro wind turbine technologies. For example, compare upwind and downwind turbine configurations with respect to the yaw alignment. Assess the performance of number of blades for the horizontal axis wind turbines. Another proposal is to consider testing vertical axis turbine rotor technologies (Savonius, Darrieus or other) as they would potentially not exhibit issues with respect to horizontal axis turbine's flow alignment with the turbine's rotor.

3. *Technical potential studies via GIS for integrated concepts*

Current research provided some methodologies on how to use GIS models to investigate the technical potential of integrated energy systems in a nationwide scale. It additionally provided analysis on a Provincial level. Several GIS layers were utilised in order to make quantitative estimations for a number of noise barriers and fuelling stations to calculate the technical potential of each technology to produce electricity or hydrogen. Even though the methodologies developed, aimed to identify as pragmatically possible, the technical potential of micro wind turbine electricity on top of noise barriers and hydrogen production of wind turbines collocated with fuelling stations, there are still gaps. Parameters related to installation, operation and maintenance per site were not considered in detail. Additionally, limitations on the grid availability were not taken into account. For the case of fuelling stations, the turbine's size was assumed the same for all stations. It is therefore recommended to extend the methodologies and analyses to include parameters related to the complexities around installation and maintenance of those turbines. Additionally, it is recommended to identify more critical grid related parameters per site and include in the analysis such as grid availability, both for electricity as well as for hydrogen. And finally, since each location could exhibit different localised electricity demand, scenarios could be tested to identify benefits for the local communities. The last recommendation is to extend the GIS layers with cost related parameters such as the capital expenditure required leading to metrics such as levelised cost of electricity and hydrogen. Most importantly though since highway infrastructures are usually publicly and privately financed, a financial analysis could quantify the additional investments required to upgrade those infrastructures.

4. *Other innovations in integrated wind turbine concepts*

This thesis assesses the concept of structurally integrating micro wind turbines with noise barrier infrastructures and collocating wind turbines with fuelling stations for hydrogen production. Complementary to the structural integration, the electrical integration is as well an interesting field that could reduce the number of power electronics and thus benefit from further cost reduction. It is therefore recommended to further test and demonstrate a DC coupling between micro wind turbines and PV

Conclusions – Recommendations

arrays on top of noise barriers. PV inherently produce DC power while wind turbine power controls typically rectify the alternating current (AC) power to direct current (DC) power and then back to AC power which follows the grid requirements of $220V_{AC}$ and 50Hz (as an example in Europe). Therefore, a common inverter could be designed which would accumulate the wind and PV power before the grid inverter. Additionally, other concepts for further exploration could be integrating DC battery storage, connections to local DC demand such as the street lighting mentioned in Chapter 6. Furthermore, for the concept of wind powered hydrogen production and refuelling stations, wind turbine could be directly coupled to the stacks of an electrolyser which require DC power, thus eliminating power electronics, power control and grid interconnection costs. Also, the wind turbines could also be used for charging Battery Electric Vehicles. Finally, researchers could focus on assessing the technical and economic feasibility and develop sizing algorithms which take into account the different localised parameters for each integration concepts and especially taking into account new system design in DC with integrating nearby demand. For example, assessments of better integration on fuelling stations to support both the battery electric charging infrastructure and also to produce hydrogen by applying reversible fuel cells, and thus benefit as well from localised electricity production.

LIST OF PUBLICATIONS

Academic Journal Publications

Nikolaos Chrysochoidis Antsos, Andrea Vilarasau Amoros, Gerard J. W. van Bussel, Sander M. Mertens and Ad J. M. van Wijk

“Wind Resource Characteristics and energy yield for micro wind turbines integrated on noise barrier – An Experimental Study”

Journal of Wind Engineering and Industrial Aerodynamics

August 2020

DOI: 10.1016/j.jweia.2020.104206

Nikolaos Chrysochoidis Antsos, Gerard J.W. van Bussel, Jan Bozelie, Sander M. Mertens and Ad J.M. van Wijk

“Performance Characteristics of A Micro Wind Turbine Integrated on A Noise Barrier”
Energies

February 2021

DOI: 10.3390/en14051288

Nikolaos Chrysochoidis Antsos, Miguel Rodríguez Escudé and Ad J. M. van Wijk.

“Technical potential of on-site wind powered hydrogen producing refuelling stations in the Netherlands”

International Journal of Hydrogen Energy

August 2020

DOI: 10.1016/j.ijhydene.2020.06.125

Simon van Overeem, Louis Alen, Yair Brouwer, Andre D. van Dam, Glenn M. Vandekken, Geoffrey Garrett, Sven Geboers, Jelle A. W. Poland, Harry W. S. Aldridge, Vinit V. Dighe and **Nikolaos Chrysochoidis Antsos**

“Wind assessment for micro wind turbines in an urban environment”

International Journal of Energy Production and Management

November 2017

DOI: 10.2495/EQ-V2-N4-327-338

Conference Proceedings

Nikolaos Chrysochoidis-Antsos, Ad van Wijk and Vincent D.W.M. Oldenbroek

“The wind energy potential along highways to fuel a sustainable transportation sector”

Conference Paper in European Wind Energy Association 2015 (Paris)

November 2015

Nikolaos Chrysochoidis Antsos and Ad van Wijk

“Wind flow potential above noise barriers for urban wind turbine applications near highways”

7th European and African Conference on Wind Engineering (Liege, Belgium)

October **2017**

Nikolaos Chrysochoidis-Antsos, Changzhi Liu and Ad van Wijk.

“On-site wind powered hydrogen refuelling stations – From national level to a case study in Germany”

In Proceedings of 2018 International Conference on Smart Energy Systems and Technologies

(SEST)

September **2018**

DOI: 10.1109/SEST.2018.8495693

Poster Presentations

Nikolaos Chrysochoidis-Antsos and Ad van Wijk

“Could wind turbines fuel up our future hydrogen refuelling stations? A GIS-based methodology”

Wind Europe – Wind Resource Assessment (Edinburgh, Scotland)

March **2017**

DOI: 10.13140/RG.2.2.25944.29443

Nikolaos Chrysochoidis-Antsos and Ad van Wijk

“Wind speed measurements above a noise barrier next to a highway for urban wind turbine

Installations”

Wind Europe – Wind Resource Assessment (Edinburgh, Scotland)

March **2017**

DOI: 10.13140/RG.2.2.19233.40806

Datasets

Nikolaos Chrysochoidis-Antsos

“Sonic anemometer wind speed field for urban wind flows around a noise barrier (acoustic screen) and weather station supplementary dataset (temperature, wind, solar)”

Dataset published in 4TU.Centre for Research Data

March **2019**

DOI: 10.4121/uuid:b878c00c-1c31-40bb-a3f4-0bed7aabb9ed

CURRICULUM VITAE



NIKOLAOS CHRYSOCHOIDIS ANTOSOS

Phone: +31 (0) 620749804

Email: chrisoconicko@hotmail.com

EDUCATION

2015 – 2024	PhD, Delft University of Technology, Delft, The Netherlands
2011 – 2014	MSc Sustainable Energy Technology, Technical University of Delft, The Netherlands
2005 – 2011	BSc and MSc Mechanical Engineering, University of Western Macedonia, Greece

WORK

EXPERIENCE

2024 – now	Hydrogen Engineer, Air Products, The Netherlands
2021 – 2024	Principal Hydrogen Consultant, Ricardo, United Kingdom
2019 – 2021	Researcher in Wind Energy Systems, TNO, The Netherlands
2015 – 2019	PhD Contract, TU Delft, The Netherlands
2014 – 2015	PV Project Engineer, LineSolar BV, The Netherlands
2014	Patent Reclassifier, European Patent Office, The Netherlands

ACKNOWLEDGEMENTS

This last part is to thank and acknowledge all the people that have played an important role during this long PhD journey both in academic, professional and personal terms.

I would like to start by thanking my promotors Ad van Wijk and Gerard van Bussel. Ad helped me to explore in numerous ways a lot of different innovative concepts and shape my “out of the box thinking”. I value your patience for this long journey to have ended. Gerard was my guiding and focusing power in times when experiments needed to be concluded and words needed to be finalized. Ad and Gerard, I value the unique combination of your two different worlds as it has boosted my personal development of skills as a researcher, an engineer and as an individual.

I continue with saluting the people that shaped the Future Energy Systems group, starting with Vincent who was the first person to have met during my PhD journey who kept me excited with discussions on all new developments in the Renewable and Hydrogen world. Carla Robledo thank you for the guidance, discussions, kindness and good times during all the hydrogen fuel cell scooter workshops and experiments we conducted. Samira Farahani thank you for helping me to rationalize. Finally, Rishabh Ghotge, your smile, laugh and relaxed discussions kept me really going in times of stress and hence deserved to be one of the paranymphs of this work. I will miss our fun Ping Pong battles, the unlimited jokes and teasing in the room.

This research work would not have been possible without the support of the people during the experiments. In particular, in the wind tunnel days lots of people played a role in the meticulous organization, preparation and finally experimentation in the Open Jet Facility. I would like to start by thanking Vinit Dighe and Juan Tang for their participation and sharing of sweat and thoughts to facilitate the experiments. Special thanks to Nico van Beek, the guardian of the Open Jet Facility and my Go-To guy in terms of Tech Support. A special recognition to Jan Bozelie and Alliander as a whole for providing me with unlimited support with the hardware for the wind tunnel experiments and sharing insightful work stories in the field of wind engineering. Francesco Avallone and Livia Brandetti for combining your acoustic experiments with my set-up to co-benefit with the limited availability of the wind tunnel. Finally, all the student groups (Wind Energy Practical and students from Twente) which participated and learned of course by gathering all the necessary datasets in the wind tunnel from sonic anemometer calibration to wind turbine testing.

Beside the wind tunnel, the complexity of field experiments both for the sonic anemometer set-up and the wind turbine tests would not have been untangled without the support of the following. First of all, great thanks to Province of South Holland (Sander van Vliet) for trusting this project and making sure that permits were in place to be able to experiment along the highway. Also, Jeroen de Jong for arranging a great

tech support during the experiments. But without the equipment, all this work would not be realized, therefore the kindest thank you to Sander Mertens (WindChallenge) for providing me with the turbine and insights on operational aspects. Regarding the sonic anemometer set-up, I was very very lucky to have been introduced by Wittich and Visser to TNO's Chris Geurts who had done some work with 10 sonic anemometers which were "*hopefully for me*" sitting in the shelf of TNO offices in Delft. Once this was arranged, the amazing Erik Slis made sure to give me 2 very large boxes of 500m of cables, measuring equipment and 10 high-end Gill Master sonic anemometers of high frequency (I really don't know where would this PhD would lead without this electrotechnical equipment). Now having all equipment, anemometers and turbines someone needed to guide a rookie engineer/researcher on how to place equipment in the complex highway environment. Therefore, a big salute to the Westland Infra's support where they provided me with 4 full days to commission all the equipment and bring all this amazing road works machinery (cherry picker, cranes, excavators) and all those amazing workers (whom I unfortunately forget all names) who both did the "dirty work" but also guided me to install all the sonic anemometers and the poles with safety and professionalism. Finally, KD Telematica who arranged a remote access at the location which would be very hard to access in cold nights and in general to record data whenever I needed so. Finally, I cannot forget prof. Herman Russchenberg who gave me a DAVIS weather station to install in the field.

All those setups needed the electrical and mechanical support from DEMO 3mE and EWI. Therefore, I deeply thank Jaap van Raamt and his team (especially Daniel van Baarle) who helped me to design the metal structures and retrofits to the adapted 12m light poles to install the sonic anemometers. Additionally, I want to thank EWI DEMO who helped me design, test, analyse with FEM of the flange necessary to be installed at the location to integrate the micro wind turbine on top of the noise barrier. Finally, a big thanks for the support and patience of Rajeev Bheemireddy who had to design and adapt instrumentation in a small wind turbine. It was a hard task with lots of iterations to minimize errors which in the end made both me and Rajeev surely more experienced in data acquisition system designs.

While all those experiments were happening, a lot of work was conducted in parallel with really motivated students whom I supervised in their System Integration Projects, Wind Energy Practicals and some with Master Theses. I am highlighting the curiosity and preciseness of Andrea Vilarasau Amoros helping to analyse important wind datasets. The devotion and commitment of Changzhi Liu to work with complex GIS datasets. The patience, will and kindness of Miguel and focus of Michael.

Beside the strong academic and research business though, fun times and social aspects are to be noted even more importantly. This amazing room and floor we had with all the take it easy coffee breaks, intense ping-pong sessions, happy lunches, Secret Santas, winning the PhD vs MSc football cup, numerous outings are unforgettable. A big thanks to all my dear friends and fellow PhD students and colleagues in the room, 3mE

and others. Gustavo (for all the serious and non-serious moments), Vilborg (for your loudness), Karsten (for your loudness as well), Noura (our office Queen), Hassan (for raising that football cup together after the come-back victory match against MSc students since the 80s), Reza (for our Greek-Persian musical fusion times), Uttiya (for the deep political talks), Fatma (for your biggest smile), Hakan (for your big laughs), Jelle, Johan, Luis, MengMeng (for your love in music), Seyid (for your unlimited kindness), Simone, Elyas (for the amazing shoulder dances) and so much more people we sure had great moments.

Outside the work and academic environment comes the most important supporters though which I will especially raise my glass and drink for you.

My most important supporter who I love and care for is my partner in life Eirini who has supported me. Your support in my rollercoaster of this long PhD journey just kept me going!! So thank you "My Love". You gave me also joy as well of having those 2 young souls, Iris and Melina, our 2 beloved daughters. I thank them too for your smiles that simply got me going. Finally, Marilou, our 4-legged friend.

I express my gratitude to my father Christos who has never stopped supporting in anything, anytime and anywhere. He has shaped myself in so many ways, from guiding me to become an engineer and researcher while also making me hungry for this amazing gift of music which we share together. Also, to my mother for whom I understood the power of boundaries, limits and insisting the ever-ending fight and struggle. Finally, my siblings Vangelis and Valentini, who helped me refocus in times of reluctance to finalise the work, with their love, sympathy, empathy.

One of the warmest special thanks goes to Stelios and Despoina the parents of Eirini (my partner) who have unconditionally supported our family regardless of effort and time letting me to have space and time to work into finalizing this PhD. I really appreciate this as it would not be possible without this support.

The final big thanks go to all the friends in Delft and Rotterdam that helped me get back on tracks by getting power from small moments. The great dinners with Katerina, Stavros and Yro. The musical journeys with Panos and the support from Sonia. George and Lazaros from the band Soup. And of course, Jorge Ortiz Gonzalez my beloved friend, no words can fill this space.

Finally, and very importantly, another special person who also is paranymp in this defence is Daniel Baldacchino. Daniel was my mentor during the MSc times while all the past contract years of the PhD he was my hidden motivational power to make up my mind to finish this. Thank you for that as well as thanks for your beloved Tina. Thanks Martina!

With all those acknowledgements this book is "Over and Out".

